Doctoral Dissertation
Doctoral Program in Material Science and Technology (30th Cycle)

Nanostructured Zinc Oxide as drug carrier for pharmaceutical applications

By

Federica Leone
******

Supervisor:
Prof. Barbara Onida

Doctoral Examination Committee:
Dr. Gloria Berlier, Referee, Universitá degli Studi di Torino
Dr. Francesca Bosco, Referee, Politecnico di Torino
Prof. Michela Signoretto, Referee, Università Ca' Foscari
Prof. Flaviano Testa, Referee, Universitá della Calabria
Prof. Enrica Verné, Referee, Politecnico di Torino

Politecnico di Torino
2018

Declaration

I hereby declare that, the contents and organization of this dissertation constitute my own original work and does not compromise in any way the rights of third parties, including those relating to the security of personal data.

Federica Leone
Turin, 2018

* This dissertation is presented in partial fulfillment of the requirements for **Ph.D. degree** in the Graduate School of Politecnico di Torino (ScuDo)

"'This here's a _re_-search laboratory. _Re_-search means _look again_, don't it? Means they're looking for something they found once and it got away somehow, and now they got to _re_-search for it? How come they got to build a building like this, with mayonnaise elevators and all, and fill it with all these crazy people? What is it they're trying to find again? Who lost what?"

from "Cat's Cradle" by Kurt Vonnegut, 1963

A mamma, papà e Francesca.

Acknowledgment

I would like to gratefully acknowledge my supervisor Prof. Barbara Onida, who gave me the possibility to challenge myself in the Material Science world. I sincerely thank her, for the kind support and patient teaching during these three years.

Moreover, I thank all the members of the SMAC groups, Prof. Mauro Banchero, Prof. Luigi Manna and Prof. Silvia Ronchetti, for helping and supporting me in carrying out my PhD project.

I would like to acknowledge Prof. Roberta Cavalli, who keeps supporting me, since my first steps in the research laboratories at the Pharmacy Department.

A special thanks to Dr John G. Hardy, who hosted me in his research group for six months within my PhD. He opened my mind to new scientific challenges and his enthusiasm for the research has been of inspiration. I also would like to thank Dr Karen Wright, who taught me a lot about the cells world in a very short period.

I warmly acknowledge Prof. Vivian Tullio and Dr. Janira Roana for their precious collaboration in the biological investigations.

In conclusion, I would like to specially acknowledge my PhD fellow Dr Andrea Gignone, who kindly supported and taught me, during my first year at the DISAT department.

Abstract

In this PhD thesis nanostructured ZnO (NsZnO) was studied to develop innovative drug carriers for future dermatological applications.

In particular the novelty of the research was the use of a green organic-solvent free route both for the production of the NsZnO and for the loading of of the Active Pharmaceutical Ingredients (API), by means of supercritical carbon dioxide ($scCO_2$) technology.

The first chapter deals with a general overview of the ZnO properties and applications in the biomedical field, offering a detailed description of the current state-of-art related to the use of ZnO nanostructures as drug delivery systems. Particular attention is focused on the existing studies of NsZnO in skin applications.

The second chapter presents the $scCO_2$ technology as an innovative and greener approach to perform the drug loading of a delivery system. The fundamental properties of the $scCO_2$ are described in order to understand the mechanism of $scCO_2$-mediated drug impregnation, since it is the drug loading method selected in this PhD research project.

The third chapter illustrates the development of a green organic-solvent-free route to prepare ZnO-based drug carriers. Two NsZnO materials with different morphologies were synthesized using wet organic-solvent-free processes and they were characterized to elucidate their morphological and physico-chemical properties. In this investigation, Clotrimazole (CTZ) and Ibuprofen (IBU) were selected as the drug models. For the first time, $scCO_2$-mediated drug impregnation was used in the loading of NsZnO materials.

The fourth chapter describes the study of a third ZnO nanostructure, which consists in mesoporous ZnO particles. A simple synthesis was carried out,

based on the on the hydrolysis of a zinc salt in basic alcoholic solutions. A material with a significant high surface area and a morphology suitable for the biomedical applications was obtained. Also in this case the $scCO_2$ technology was studied as a greener alternative technology to carry out the drug loading of the mesoporous NsZnO. CTZ was selected as the drug model.

The fifth chapter is focused on the study of the three developed NsZnOs from a biological point of view, in order to highlight their intrinsic biological properties. Particularly, their antimicrobial activity against different microbial strains were investigated, and the results were correlated with their physico-chemical parameters. Also the *in vitro* Zn^{2+} release profiles from the NsZnO matrices were evaluated, simulating a release to the skin.

The sixth chapter presents the research work carried out at the Lancaster University (UK). The main aim was the study of innovative materials for wound healing. Particularly, this section describes the development of biocompatible *in-situ*-forming composite hydrogels, based on natural polysaccharides, where one of the previously synthetized NsZnO was used as inorganic nanofiller. The crosslinking mechanism, structure, morphology and swelling behavior of the in situ forming composite hydrogels were studied. Moreover, *in vitro* release of $Zn^{2+}$from the formulations was simulated on synthetic skin and the cytotoxicity of the different component was carried out on a HaCat cell line.

The seventh chapter describes the main results of a parallel research project carried out within my PhD studies. In particular, the proof of concept of an innovative dermatological formulation containing ordered mesoporous silica (OMS) was successfully demonstrated. The possibility to obtain a drug reservoir system, combining API-loaded OMS with a saturated solution of the same API was investigated obtaining outstanding results from both a physical-chemical and biological point of view. The innovative formulation resulted in a sustained release of the drug lasting two times with respect to the commercial gel, which opens the possibility of reducing the daily number of administrations during a real treatment.

Contents

Chapter 1

Zinc Oxide nanomaterials as drug delivery systems

1.1. Introduction

In accordance with the European Commission, a "*nanomaterial* consists in *an insoluble or biopersistant and intentionally manufactured material with one or more external dimensions, or an internal structure, on the scale from 1 to 100 nm*" [1]. In the last decade, the use of nanomaterials has attracted much attention due to their small sizes and innovative structures that exhibit significantly improved physical, chemical, and biological properties compared to their bulk or molecular precursors [2]. Metal oxides have found several applications in various fields of nanotechnology due to their excellent optical, magnetic, electrical, and chemical properties. Nanostructured metal oxides are interesting materials, because they can be synthesized with a very high surface-to-volume ratio and with unusual morphologies that can be easily functionalized with different groups for the new applications. An increasing use of nanomaterials has been reported in biological- and medical-related applications such as imaging, sensing, target drug delivery, healthcare products, cosmetics, and food preservative agents due to better safety and stability compared to bulk precursors or their organic counterparts.

Zinc Oxide (ZnO) is a multifunctional material possessing unique physical and chemical properties, such as high chemical stability, high electrochemical coupling coefficient, broad range of radiation absorption and high photostability [3]. It is classified as a wurtzite-type semiconductor (group II-VI) and piezo-electrical material, and possesses a broad band-gap energy of 3.1–3.4 eV, a large excitation binding energy of 60 meV and a high thermal and mechanical stability at room temperature. Thanks to these outstanding properties ZnO is largely used in many attractive applications, ranging from electronic, optoelectronic, sensoristic and photocatalysis [4,5]. Moreover, ZnO is listed by the Food and Drug Administration (FDA) as a Generally Recognized as Safe (GRAS) substance, due to its low toxicity, biocompatibility and biodegradability. Consequently, ZnO materials are attracting growing attention also in the biomedical field.

ZnO exhibits three crystal structures named wurtzite, zinc-blende and an occasionally noticed rock-salt (Figure 1.1) [6].

The hexagonal wurtzite structure possesses lattice spacing a = 0.325 nm and c = 0.521 nm, the ratio c/a * 1.6 that is very close to the ideal value for hexagonal cell c/a = 1.633. Each tetrahedral Zn atom is surrounded by four oxygen atoms and vice versa [43]. The structure is thermodynamically stable in an ambient environment and usually illustrated schematically as a number of alternating planes of Zn and O ions stacked alongside the c-axis. On the other hand, zinc-blende structure is metastable and can be stabilized via growth techniques.

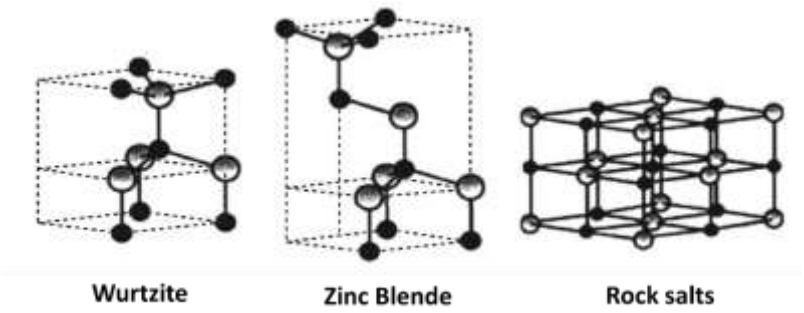

Figure 1.1 ZnO crystal structures. Adapted from [6]

The variety of available ZnO nanostructures make it an interesting material for nanotechnology applications [7–10]. In fact, in comparison to the bulk material, nanostructured ZnO has enhanced properties that can be exploited in many industrial area such as gas sensors, biosensors, semiconductors, piezoelectric

devices, field emission displays, photocatalytic degradation of pollutants, antimicrobial treatments and UV-blocker materials in cosmetics [11]. The nanostructures of ZnO can be classified in one- (1D), two- (2D), and three-dimensional (3D) structures (Figure 1.2) [3]. One-dimensional structures make up the largest group, including nanorods [12,13], nanoneedles [14], nanohelixes, nanosprings and nanorings [15], nanoribbons [16], nanotubes [17], nanobelts [18], nanowires [19] and nanocombs [20]. ZnO can be obtained in 2D structures, such as nanoplate/nanosheet and nanopellets [21]. 3D structures of ZnO include flower, dandelion, snowflakes, coniferous urchin-like [3]. This impressive assortment of ZnO particle structures plays a key role in making this material one of the most investigated metal oxides in the nanotechnology field.

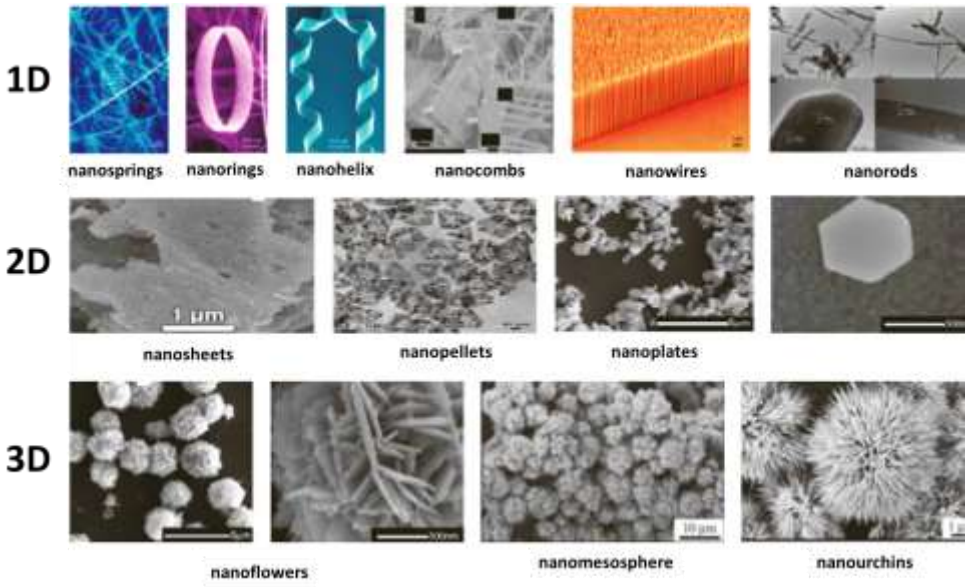

Figure 1.2 Different structures of ZnO, classified as one-dimensional (1D), two-dimensional (2D) and three-dimensional (3D). Image modified from [22].

Synthesis approaches of nanostructured ZnO

Nowadays, the environmental implications of a material synthesis are one of the most investigated issues in the material science field. The need of synthetizing nanoparticles using eco-friendly, cost-effective, biocompatible and safe techniques has been one of the major focuses of this last decade. A wide number of synthetic techniques have been explored for the synthesis of ZnO [10,23–26]. The choice of a suitable method mainly depends on the desired application, morphology and size. Here, a general overview of the most adopted approaches for the synthesis of nanostructured ZnO is reported. In accordance with a recent classification, it is possible to divide the synthetic routes to obtain ZnO nanomaterials as follows [22]:

i) *Chemical methods*

Liquid phase synthesis

Precipitation and coprecipitation methods are based on the reaction of a reducing agent (i.e. inorganic alkalis) with a zinc salt. The product typically consists in soluble or insoluble precipitate which is washed and calcined to obtain nanoparticles with the desired morphology and characteristics.

Sol-gel techniques belong to the colloidal chemistry approach. Sols are colloidal solution consisting in solid nanoparticles suspended in a liquid phase, while gels are mostly formed by polycondensation methods followed by aging to achieve phase transformations and Ostwald ripening. The gels are dehydrated at high temperature and finally densified to obtain metal oxide nanoparticles. Sol-gel approach assures the pure and uniform nanostructured ZnO [27] to be obtained.

In solvothermal and hydrothermal processes, precursors are dissolved in hot solvents or water under moderate to high pressure (1–10,000 atm) and moderately high to high temperature (100–1000°C). These processes are used to synthesize a variety of zinc nanostructures such as thin films, bulk powders, spheres (3D), rods (2D), and wires (1D).

The above-mentioned methods offer several advantages, such as simplicity, low cost, repeatability and relatively mild operative conditions, which make them particularly suitable for the synthesis of nanostructured

ZnO for biomedical applications, as in the synthesis of ZnO-based drug delivery systems. This aspect will be deepened in the paragraph 1.2.

Gas phase synthesis

In the *spray pyrolysis method*, a zinc salt precursor is formulated in aerosol droplets by flame heating. The droplets are dispersed in the gas and their sizes decreased by dehydration. *Inert gas condensation* methods are divided into physical vapor deposition (without catalytic interaction) and chemical vapor deposition (with catalytic interaction). Briefly, these techniques include evaporation of a zinc source inside a chamber by resistive heat. The vapors are forced to migrate into cooler chamber filled with inert gas, from where they are collected for further consolidation.

ii) *Biological methods*

The emerging trend of developing new green, more environmentally friendly and sustainable synthesis methods, have increasingly involved the metal oxides field, including ZnO. Green synthesis of ZnO have been attracted much attention due the possibility to use a reduced number of chemicals, resulting in more energy efficient and cost-effective [24,28] processes. It is possible to classify the biological methods in plant-source mediated synthesis and microorganism-mediated synthesis. Briefly, in the former case, the mechanism is dependent on the secondary metabolites of the plant, which play a significant role as reducing agents for the conversion of metal salts (precursors) into metal or metal oxide nanoparticles. In the latter case, microorganisms are able to transform metal ions to metal or metal oxide nanoparticles through enzymes generated by cell activities.

iii) *Physical methods*

Physical/mechanical processes are mostly used for the industrial processes. Physical methods for the synthesis of ZnO nanoparticles include high energy ball milling, melt mixing, physical vapor deposition,

laser ablation, sputter deposition, electric arc deposition, and ion implantation [24].

1.1.1 Biomedical applications of nanostructured ZnO

Because of its outstanding intrinsic properties, nanostructured ZnO fulfils a remarkable importance in many fields of applications. Many scientific reviews have been dedicated to list the main uses of ZnO, highlighting the remarkable versatility of this nanomaterial [3,24–26]. For instance, ZnO nanostructures play key roles as fillers in the rubbers industries [3], can be used as conventional wide band-gap semiconductors in microelectronic devices and or employed for accelerating the degradation of water pollutants by means of their photocatalytic activity [29]. Applications in energy storage and hydrogen storage have also been explored. Since this thesis is focused on the development of ZnO nanomaterials as drug delivery systems, this paragraph highlights the biological-related properties of ZnO and its consequent applications.

ZnO as antibaterial agent

Antibacterial activity is defined as *the action by which bacterial growth is destroyed or inhibited*. It is also described as a function of the surface area in contact with the microorganisms [30]. ZnO is an efficient antimicrobial agent and its activity is based on several mechanisms involving different chemical species. In the literature, three distinct mechanisms of action have been discriminated (Figure 1.3) [6,31–33]:

1. *Photocatalytic antibacterial mechanism.* Recognized as the predominant antimicrobial mechanism, it is based on the production of reactive oxygen species (ROS) because of the semiconductive properties of ZnO [32]. The production of hydroxyl radicals, singlet oxygen and superoxide radicals are toxic to the cells because they damage many cellular constituents such as DNA, lipids, and proteins. Basically, when the ZnO nanostructures are illuminated by light with a photoenergy equal to or greater than its band-gap energy, e^- are promoted across the band gap to the conduction band, generating a hole (h^+) in the valence band. The e^- in the conduction band exhibit strong reducing power, while the $h+$ in the valence band possess an oxidizing power. These configurations are able to generate three main types of ROS, which mainly contribute to the oxidative stress in biological systems:

i) superoxide anion radicals $O_2^{\bullet-}$: generated when the electron reacts with molecular oxygen through a reductive process;

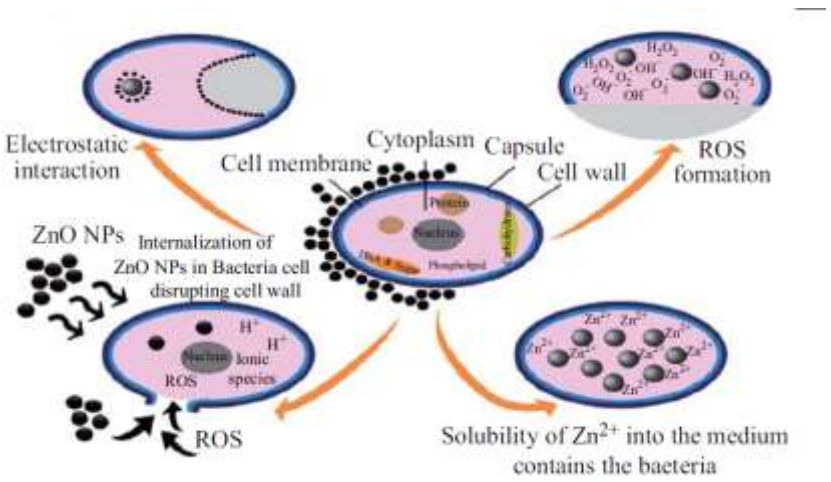

Figure 1.3 Different possible mechanisms of ZnO-NPs antibacterial activity [6]

ii) hydroxyl radicals $OH^{\bullet}$: generated through an oxidative process when h^+ can capture the e^- from water and/or hydroxyl ions. $OH^{\bullet}$ is known as the most reactive oxygen radical known because it rapidly reacts with a wide range of organic biomolecules, such as nucleic acids, lipids, carbohydrates, proteins, DNA and amino acids. The dominating recombination of two $OH^{\bullet}$ radicals produces hydrogen peroxide (H_2O_2), which chemically interacts with bacteria. This mechanism has been proposed as the predominant mechanism underlying the antibacterial activity of ZnO.

iii) singlet oxygen $^1O_2$: is mostly produced indirectly from aqueous reactions of superoxide anion radicals $O_2^{\bullet-}$. They are not as strong as $OH^{\bullet}$, but act as mediator of photocytoxicity by irreversibly damaging the tissues, through biomembrane oxidation and degradation.

2. Intrinsic antimicrobial properties of Zn^{2+} ions released by ZnO. Zinc is an essential element for microorganisms and higher organisms. It plays an important role in many vital cellular reactions at its low endogenous

concentrations (10^{-4} M in blood). Zn^{2+} ions are essentially nontoxic to higher organisms, because its concentration is physiologically regulated by several transporters. The antimicrobial properties of Zn^{2+} both against bacterial and fungal strains are well known. Briefly, increasing Zinc concentrations above the optimal levels, its homeostasis is perturbated, allowing Zn^{2+} to enter the cells. At this point, zinc becomes cytotoxic to prokaryotes (concentration $>10^{-4}$ M). The antimicrobial activity of Zn^{2+} depends on its concentration and contact duration. Nevertheless, the contribution of Zn^{2+} to the antimicrobial activity of ZnO has been reported as the less efficient mechanism because the too low dissolution rate of ZnO particles [31].

*3. Destabilization of microbial membranes upon direct contact of ZnO particles with the cell walls***.** The direct contact of ZnO particles with the bacterial membrane may lead to penetration and disorganization of its structure, causing the loss of membrane integrity and malfunction of the permeability barrier. Nanostructured ZnO possesses large specific surface area and high surface energy that is adsorbed by the bacteria, altering their metabolism due to the altered exchange of matter and energy with the environment.

The antibacterial response is significantly affected by various parameters, among which the morphology, size and concentration of ZnO nanostructures [6,30].The shape-dependent activity is explained in terms of the percent of active facets in the nanoparticles. ZnO with different morphologies possesses different active facets, which lead to enhanced antibacterial activity [34]. For instance, rod-structures of ZnO have (111) and (100) facets, while spherical nanostructures mainly have (100) facets. High-atom-density facets with (111) facets exhibit higher antibacterial activity. Moreover, the shape of ZnO nanostructures can influence their mechanism of internalization. Even though, rods and wires showed an enhanced penetration into the cell walls of bacteria with respect to spherical ZnO particles, rod-like structures possess a greater toxicity effect, because of their larger production of ROS in suspension, which cause disruption of cellular function and disorganization of membrane.
For instance, Talebian and colleagues, who evaluated different ZnO nanostructures, assessed that the flower-shaped ZnO possessed a higher antibacterial activity than the spherical and rod-shaped ZnO nanostructures [35].

This was explained by the fact that higher surface interstitial defects reduce the electron or hole recombination and consequently increase the antibacterial activities. As far as the contribution of the polar facets of ZnO nanostructured to the antibacterial activity is concerned and in addition to the enhancement of internalization, it has been suggested, that the higher number of polar surfaces possesses higher amount of oxygen vacancies. Oxygen vacancies are known to increase the generation of ROS and consequently affect the photocatalytic activity of ZnO [6,36].

Furthermore, the particle sizes and concentration of ZnO nanostructures play a key role in the antibacterial activity. Large surface area and high concentrations lead to an enhanced bactericidal response. ZnO particles with small sizes have been reported as the most active against bacteria, due to the high specific surface area exposed. Moreover, both the release of Zn^{2+} ions and the generation of H_2O_2, which are two of the main antibacterial mechanisms, were reported to be size and surface-dependent [37–40]. As for as the concentration of antibacterial agent is concerned, usually two different parameters are assessed: the *minimum bactericidal concentration* (MBC), which is defined as the lowest concentration of antibacterial agent that showed no bacteria growth in the medium, and the *minimum inhibitory concentration* (MIC), which is the lowest concentration at which colonies are observed on the surface of the medium. In other words, MIC is the concentration that prevents bacterial growth.

It is worth noticing that the same mechanisms involved in the antibacterial activity of ZnO make this material active also against fungal pathogens. This dual-antimicrobial activity is fundamental in the multi-tasking role of ZnO nanomaterials and many research works have been addressed to investigate of this material from a biological point of view [41–45] .

The antimicrobial properties of ZnO can be considered attractive for its use as an antimicrobial preservative of pharmaceutical or cosmetic formulations [46]. Nevertheless, few research works have been addressed to this application. Favet and collaborators investigated the antibacterial activity of ZnO in comparison with parabens, in a zinc gelatin-based ointment [47]. The role of ZnO as preservative in topical formulations was also investigated by Pasquet and colleagues, who studied the antibacterial activity of ZnO powders on five microrganisms strains used for the Challenge Tests [48]. Even though the use of

ZnO as an antimicrobial preservative for pharmaceutical and cosmetic formulations has been scarcely investigated, its role as antibacterial agent in the food industry has also been considered [6]. Particularly its application as antimicrobial agent in food active packaging against food-borne pathogens has been investigated [49].
Moreover, it is worth noticing that ZnO can be considered as a promising and low-cost alternative to silver and gold nanoparticles, which are also popular for their pronounced antibacterial activity, but the use of which on the industrial scale is limited by their high cost [50].

ZnO as antitumoral agent

Nowadays, nanomedicine represents a promising solution in the anticancer field due to its advanced imaging and therapeutic properties, which allow early detection of cancer and more efficient treatments to be achieved [51]. Many inorganic nanoparticles, such as iron oxide, titanium dioxide, cerium oxide, zinc oxide, copper oxide and silica have been being widely researched and used for anticancer therapy as-such or conjugated with anti-cancerous drugs or bio-active molecules (i.e proteins and DNA). These nanomaterials have unique features, among which intrinsic selective cytotoxicity towards cancer cells, which make them a novel and efficient tool for anticancer therapy. Among all these nanomaterials, zinc oxide nanostructures are showing promising application and efficacy in cancer therapy due to their highly selective nature and potency towards cancer cells [52]. The anti-cancerous activity of ZnO depends on its own properties, such as its biocompatibility and its selective cytotoxicity against cancerous cells in *in vitro* condition in comparison with other nanoparticles. Moreover, their surface can be furtherly engineered increasing this selectivity. One of the mechanisms of cytotoxicity of ZnO nanoparticles towards cancer cells is based on the unique ability of ZnO nanoparticles to induce oxidative stress. This property depends on the semiconductor nature of ZnO, which induces ROS generation, as described earlier, leading to oxidative stress and cell death. ZnO is a suitable anticancer agent also due to the wide range of synthesis approaches available. For instance, the possibility to significantly reduce its size allows the intra-tumour concentration of nanoparticles after administration to be increase (enhanced EPR effect).

Furthermore, the electrostatic characteristics of ZnO nanoparticles make this nanomaterial an attractive candidate for anticancer therapy [29]. At lower pH, protons from the environment are probably transferred to the ZnO particle surface, leading to a positive charge from surface $ZnOH^{2+}$groups. In aqueous medium and at high pH, the chemisorbed protons (H^+) move out from the particle surface leaving a negatively charged surface with partially bonded oxygen atoms (ZnO^-). The isoelectric point of 9-10 indicates that the ZnO nanoparticles have a strong positive surface charge under physiological conditions. Thanks to its electrostatic nature, ZnO would be able to interact with the anionic phospholipids on the outer membrane of cancer cells, so promoting cellular uptake, phagocytosis and ultimate cytotoxicity.
Significant examples of the application of ZnO-based drug delivery systems for anticancer purposes are given in Section 1.2.

ZnO as UV blocker

As a result of their ability to absorb UV radiation, ZnO nanoparticles are used in the cosmetic industry, typically in sunscreens and facial creams [53,54]. Sunscreens are used to protect the skin against the harmful effects of solar ultraviolet (UV) radiation. When UVB (290 - 320 nm) rays together with UVA (320 - 400 nm) rays reach our skin, they can cause biological and metabolic reactions. These can range from short-term effects, such as UVB-induced vitamin D synthesis and, at higher doses, the insurgence of erythema, to long-term effects which include different degenerative skin changes, such as actinic keratoses, skin cancer from epidermal cells and loss of the skin elasticity due to UVA producing reactive oxygen species (ROS). Nowadays, the combination of ZnO and titanium dioxide (TiO_2) is frequently used in sunscreen products. Their UV-blocking mechanism depends on their ability in reflecting and/or scattering most of the UV-rays, as well as absorbing UV radiation because of their semiconductive properties. As inorganic physical sun blockers, ZnO and TiO_2 assure the absence of skin irritation and sensitization, inertness of the ingredients, limited skin penetration and a broad-spectrum protection, against both UVA and UVB. ZnO is generally used in the

form of nanoparticles at the size of 30-200 nm. The surface of the nanoparticles can also be treated with inert coating materials to enhance their dispersion in sunscreen formulations (i.e. silicon oils) [55]. Current examples of the application of ZnO nanostructures as UV blocker are reported in section 1.3.2.

ZnO-based biosensor

A biosensor system aims at the quantitative detection of certain parameters during the occurrence of complex biochemical reactions through a transducer coupled with a biologically derived recognition entity [32]. The large surface-to-volume ratio, nontoxicity, chemical stability, high catalytic activity, electrochemical activity, and excellent electron-communication features make ZnO nanostructures the best candidates for biosensor applications. For instance, ZnO aligned one-dimensional (1D) nanostructures are suitable materials for this application. In fact, they offer a large area for enzyme immobilization and direct channels for electron transport from the redox enzymes to the current collector. Moreover, ZnO nanostructures are particularly suitable for the absorption of some proteins through electrostatic interaction, due to the high ZnO isoelectric point of about 9-10. Up to now, ZnO nanostructures have been applied in biosensors for the detection of several biomolecules, such as cytochrome C, uric acid, protein and glucose [56–59].

ZnO in Bioimaging

ZnO nanostructures, in particular in the form of Quantum Dots, are suitable candidates for the bioimaging applications, such as tracing live cells and real-time monitoring of target tissues. The possibility to use this nanomaterial in bioimaging derives from its improved properties, in comparison with traditional organic fluorescent dyes. These range from photoluminescent activity, including broad-band absorption, a narrow and symmetrical emission band, a tunable emission wavelength, high stability against photo-bleaching, and its semiconductor nature [32]. ZnO Quantum Dots are also characterized by excellent biocompatibility, good biodegradability, low cost and environment compatibility [60,61].

ZnO as drug delivery system

Since this PhD project aimed at the study of ZnO nanostructures as drug reservoirs for future skin applications, the following sections of this thesis describe the application of ZnO nanomaterial as drug delivery systems. First, the current state-of-the-art of ZnO nanomaterial as drug delivery system is carefully taken in consideration. Second, a major focus of the use of ZnO-based carriers on the skin and its application in wound healing is reported.

1.2 ZnO as drug carrier: the state-of-the-art

Despite Zinc Oxide (ZnO) is a widely investigated material in many research fields, its application as a drug delivery system has begun to attract attention only in this last decade and it is considered at its nascent stage (Figure 1.4). In particular, in the last couple of years many research works have been dedicated to the development of ZnO materials as drug carriers thanks to its outstanding biocompatibility, giving new light to this outstanding material. Therefore, from a careful analysis of the literature, it has emerged that it would be possible to classify the main studies of ZnO as a material for drug delivery into two main categories: i) studies dealing with pure ZnO carriers and ii) studies on ZnO-composites carriers (Figure 1.5).

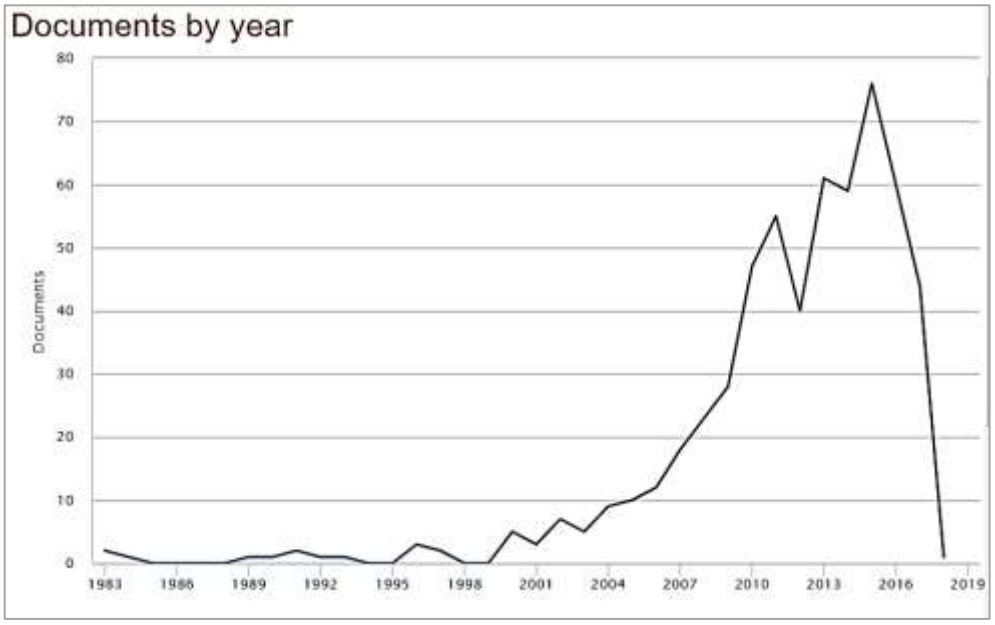

Figure 1.4 Analysis of the number of documents related to the use of Zinc Oxide as drug delivery system, in the range 1983 – 2018 [62].

1.2.1 Pure ZnO drug carriers

The possibility to synthetize a wide range of ZnO nanostructures tuning their morphology and properties, has played a significant key role in the study of pure ZnO as a drug carrier. It is a matter of fact that a high surface area,

significant pore volume and uniform pore size distribution remarkably influence the carrier capability of firstly hosting a drug molecule and then of releasing it.

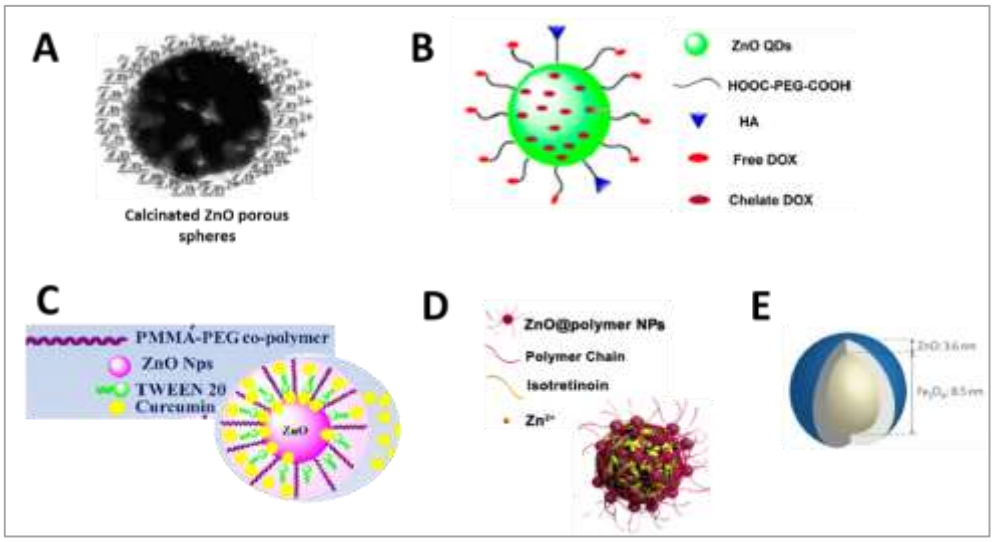

Figure 1.5 Schematic representations of pure ZnO drug carriers in comparison with ZnO-composite carriers. The images were adapted from: A [63], B [64], C [65], D [66] and E [60]

In these last 5 years, different research groups have investigated the possibility to obtain highly performant pure ZnO drug carriers. Going through the literature, it has emerged that nowadays the study of ZnO particles as drug delivery system is particularly focused on the anti-cancer field [52]. In fact, ZnO particles are being widely studied for their anti-cancerous properties, such as the selective cytotoxicity towards cancer cells. From the analysis of the published documents, it is evident that the development of pure ZnO carriers for the delivery of anti-cancerous molecules has been attracting large attention. In particular many researchers selected Doxorubicin as a drug model for their investigations. In 2017, for instance, some interesting results have been drawn by Tian and colleagues. Their study aimed at the development of a pure mesoporous ZnO carrier for the delivery of Doxorubicin Hydrochloride [67]. They were able to obtain ZnO nanospheres (150 nm) via decomposition of a precursor by thermal treatment. As expected, the material presented large specific surface area (43.4 m^2/g), narrow pore size distribution (6.2 nm) and good hydrophily. Tian performed the drug loading of the mesoporous ZnO by

a traditional soaking technique. Although any information related to the drug amount loaded into the ZnO nanospheres was provided in the paper, the *in vitro* release study reported a Doxorubicin release at pH 5 higher than that at 7.4, which confers a pH-triggered behaviour on the system.

A doxorubicin delivery system based on ZnO nanomaterials has also been the main object of investigation carried out by Liu and colleagues [68], who also obtained a pH-triggered drug release in acidic environment due to degradation of the carriers. In this second case the ZnO nanoparticles (about 50 nm) were prepared by reprecipitation method in ethanol, followed by an overnight drying step in vacuum. The drug loading was performed directly in the reaction vessel, just before the drying phase, by adding Doxorubicin in the ethanolic mixture. Also in this case, any information about the drug loading amount was provided.

Vimala and collaborators proposed the development of green synthesized ZnO nanosheets, functionalized with polyethylene glycol and folic acid for the delivery of Doxorubicin and photothermal therapy against breast tumour [69]. This research work has provided to remarkable results, since a functionalized ZnO material with an impressive BET surface area of 673.44 m^2/g, with regularly distributed pores of size around 1.56 nm. ZnO nanosheets had an average size of 100 nm, and a high drug loading efficiency of 89% was reported (0.57 mg of drug per mg of the functionalized ZnO). As in previous works, a pH-triggered release of Doxorubicin from the functionalized ZnO was demonstrated, with an enhanced release at acidic pH.

The same approach, was adopted by Cai and collaborators [64] who fabricated a ZnO quantum dots-based pH responsive drug delivery platform for intracellular controlled release of Doxorubicin. ZnO quantum dots (~3 nm) were synthesized using the precipitation method. They were not used as-synthetized, but modified with several functionalization groups, in order to improve the stability in physiological fluid. The Doxorubicin loading were performed through a traditional approach, incubating a drug solution with the carrier for a certain time. Doxorubicin loading of 30% into the modified ZnO QDs was calculated. Again, a higher drug release was achieved at low pH value, due to the the dissolution of the ZnO QDs and dissociation of drug−metal complex under acidic conditions. Similar results were presented in 2011 by Muhammad and his research group, who investigated the functionalized-ZnO quantum dots for the delivery of Doxorubicin [70].

Other functionalization approaches were also evaluated in order to enhance the anti-cancer treatments efficacy. The possibility to produce

PEGylated ZnO nanoparticles for drug delivery was investigated by Fakhar e Alam et al [71]. In this case the PEGylated ZnO nanoparticles were loaded with protoporphyrin IX, by a simple drug solution addition to the particles.

A different ZnO nanostructure was proposed by Kumar and collaborators, who reported the production of mesoporous self-assembled ZnO 'dandelions' with spherical shape, as delivery systems for anticancer drugs and DNAs [72]. Mesoporous self-assembled ZnO 'dandelion' capsules were synthesized by hydrolysis of a zinc precursor in the presence of a surfactant, followed by heat treatment of the hydrolysed dry powder. The results showed the formation of ZnO spheres, with a BET surface area of 230 m^2/g and an average pore size of 8.46-8.85 nm. Drug loading studies were performed through traditional soaking method, by using Doxorubicin and Rhodamine B, a fluorescent agent, as models. The loading efficiency of the two drugs in self-assembled ZnO 'dandelion' was found to be equal to 10 mg/10 mg and 6.5 mg/10 mg of sample, respectively. The release of both the molecules was successfully demonstrated.

In 2010, Mitra at collaborators investigated the development of porous ZnO nanorods, for the targeted delivery of Doxorubicin [73]. For the synthesis of the material, a precipitation method followed by a drying step in vacuum was adopted. To improve the *in vivo* performance of the system, a further multi-step chemical functionalization was performed. The drug loading procedure was carried out by traditional adsorption technique from an aqueous solution. The synthetized ZnO consisted in porous rod particles with an average size ranging from 30 to 70 nm. N_2 adsorption and desorption analysis revealed an incredible high surface area of 305.14 m^2/g with homogenously distributed pores of 5 nm. A remarkable high drug loading efficiency of 88% was observed, with 0.58 mg of Doxorubicin loaded per mg of functionalized ZnO.

Also Barick and colleagues studied highly mesoporous spherical three dimensional ZnO nano-assemblies as potential delivery systems for Doxorubicin [74]. They investigated a facile soft-chemical approach based on the ZnO nanocrystals precipitation from a precursor. The anticancer drug was loaded into the materials through traditional adsorption. The morphology of the ZnO particles resulted in discrete spherical shaped assemblies ranging from 100-600 nm composed by connected nanocrystals of 20 nm. The average pore diameter was found to be 28 nm, while the BJH surface area and pore volume were around 27.5 m^2/g and 0.22 cm^3/g, respectively. The Doxorubicin loading efficiency was about 80%. The investigation highlighted that the release of the

drug molecules was strongly dependent on the pH of the release medium, with the possibility to obtain a pH-triggered release, which is advantageous in treatment of cancerous target site, where the relatively low pH might specifically stimulate the doxorubicin release.

Danourobicin is another chemotherapy agent belonging to the same family as that of Doxorubicin. Its delivery from ZnO carrier was investigated by Haijun Zhang in its research work [75]. ZnO was synthetized by solid state reaction at room temperature, while the drug loading was performed by simple overnight incubation of a drug solution with the aqueous suspension of ZnO nanorods. The encapsulation efficiency and loading efficiency of Daunorubicin were about 75% and 20%, respectively. The drug release was dependent on the pH of the medium, as in the case of Doxorubicin, with a slow and sustained rate (19%) at pH 7.4 and a much faster rate (87%) at pH 5.0.

A further application of pure ZnO carrier in the antitumoural field was provided by the work of Kathun et al [76]. In their study, ZnO nanoparticles were conjugated with trans-Resveratrol, an anti-proliferative and chemopreventive agent, for treatment of ovarian cancers. ZnO nanoparticles of about 5 nm were obtained by the co-precipitation technique. Nano-conjugation between Resveratrol and ZnO was obtained by incubating the two components together.

Baskar et al conjugated L-asparaginase with zinc oxide nanoparticles, studying the cytotoxic effect on cancer cells [77]. The zinc oxide nanoparticles conjugated with L-asparaginase was produced by the fungus *Aspergillus terreus*, which is able to reduce zinc sulphate ions, to form ZnO, thanks to the proteins present in the fungal culture filtrate.

Another remarkable contribution to the research of innovative pure ZnO drug carrier derives from the work of Bakrudeen and collaborators. The most recent investigation was focused on spheroidal mesoporous auto-fluorescent ZnO nanospheres, which are potentially able to target specific sites and to deliver drug molecules especially in cancer treatments [78]. In this project, zinc oxide mesospheres were obtained by a multi-steps procedure, that involves the use of organic solvents. The BET specific surface area and the corresponding pore volume of the mesoporous ZnO were 16.56 m^2/g and 0.0861 cm^3/g, respectively. The average pore size was about 5 nm. Although any drug loading attempts were reported in this research work, the same author, Bakrudeen H. Bava, had published in 2013 a previous work, illustrating the fabrication of mesoporous ZnO nanospheres for the controlled delivery of Captopril, a drug used in the treatment of high blood pressure [63]. In this

investigation, the ZnO particles were obtained by a soft-template based synthesis, using starch as the templating agent. The Captopril loading was performed through a traditional incubation method. The porous spherical-shaped particles presented a diameter in the range of 200–500 nm. Each sphere resulted composed by smaller nanoparticles of about 20 nm-35 nm. The porosity of the system was confirmed by Nitrogen adsorption analysis, that revealed a BET surface area of 15.53 m^2/g and a pore volume of 0.118 cm^3/g. The average pore size was about 10 nm, which was enough to accommodate the captopril molecule, in fact the storage capacity was found to about 28%. The drug-loaded system showed the *in vitro* capability to control the release of molecules in different fluids over at least 24 h.

In 2013 Palanikumar and coworkers synthetized different ZnO nanoparticles to study their behavior as drug delivery carrier for Amoxicillin, an antibiotic molecule with a broad spectrum of bactericidal activity [79]. Traditional methods were applied for both the synthesis of the particles (low-temperature approach) and the Amoxicillin loading (incubation from a solution). The particle sizes of the as-prepared ZnO were about 38 nm. A maximum drug loading of 87% was achieved after 120 minutes of incubation under stirring. The release of Amoxicillin was found to be controlled by the carrier, and to gradually increase over time.

1.2.2 ZnO-composite drug carriers.

In these last 5 years, a new research branch related to the use of ZnO materials as drug delivery systems has attracted increasing attention. It consists in the development of drug carriers based on the combination of ZnO and other materials, such as polymers, in order to enhance the properties of the overall system. For sake of completeness, some examples of these ZnO-based composite carriers are reported in this paragraph.

In this last year much work has been addressed to study composite drug delivery systems, that contain ZnO. Zhao and collaborators proposed ZnO@polymer core−shell nanoparticles for the delivery of anti-cancerous molecules [80]. In particular they investigated the loading of Isotreonin. ZnO@polymer core−shell nanoparticles were obtained through a multi-steps procedure that involve the use of several organic solvents. The particles sizes

were found to be equal to 100 nm and presented a drug storage capability of about 35 wt%.

Another recent work took in consideration the development of ZnO-based core-shell nanoparticles for the pH-responsive drug delivery of Doxorubicin [81]. In this case, mesoporous ZnO particles were used as core of the system for the Doxorubicin storage, while the shell, which was composed by zeolitic imidazolate frameworks (ZIFs), was tuned up to prevent premature drug release in the physiological environment. Results showed that the obtained ZnO nanoparticles presented a diameter of 240 nm, which increased to 270 nm after the formation of composites core-shell nanoparticles. Also the specific surface area dramatically increased from 34.8 m^2/g to 637.4 m^2/g after the composite formation. As desired, the release of Doxorubicin was pH responsive with a higher amount and faster rate at lower pH.

In their research work, Lin and collaborators fabricated fluorescein isothiocyanate (FITC)-loaded zinc oxide nanotubes onto indium tin oxide (ITO) -coated polyethylene terephthalate substrate as a smart electrically responsive drug release device [82]. In this investigation a traditional precipitation synthesis of the ZnO nanotubes directly onto the ITO/PET substrates was adopted and the FITC molecules were loaded into the material by a soaking approach from a solution. This study demonstrated that the *in vitro* controlled drug release under an alternative electrical field of the FITC loaded onto the ZnO-based device was possible.

A similar approach was also investigated by Yang and colleagues, who prepared a drug delivery device by electrodeposition of a glucose responsive bioinorganic composite onto the nanostructured ZnO on ITO substrate [83]. Yang's drug delivery device was thought for the delivery of Insulin and its release was triggered by the level of glucose, instead of an electrical field. The role of ZnO nanoparticles was to immobilize the glucose responsive bioinorganic composite due to their high isoelectric point (IEP ~ 9.5) and biocompatibility.

In order to address the issue of the poorly-soluble drug administration, a novel composite material composed by biocompatible polymers and ZnO nanoparticles as a delivery carrier for Curcumin, has been proposed by Dhivya and collaborators [65]. The ZnO nanoparticles were synthetized through a traditional precipitation method. The preparation of the curcumin-loaded PMMA-PEG/ZnO bionanocomposite was carried out in free radical polymerisation by linking the PMMA-PEG copolymer with the ZnO

nanoparticles with the addition of surfactant agents. The average size of the bionanocomposite particles was found to be equal to 87 nm. This drug carrier was able to load a large amount of curcumin, that could be rapidly released at low pH, so increasing the bioavailability of curcumin and enhancing its anticancer efficacy.

Another biocompatible polymer, the poly(lactic-co-glycolic acid) (PLGA), was instead proposed in combination with ZnO in the investigation of Stankovic [84]. She studied PLGA nanocomposite spheres with immobilized nano-ZnO to obtain an innovative drug carrier for infectious diseases. ZnO nanoparticles were prepared via microwave assisted synthesis method and the composite material was produced by physicochemical solvent/nonsolvent approaches. Nanostructured ZnO powder resulted composed of uniform, spherical particles with an average diameter of approximately 63 nm.

Moreover, Wei and collaborators also evaluated the possibility to combine PLGA and mesoporous ZnO [85]. Their innovative idea consisted in creating a single carrier for multi-drug delivery in order to overcome the drug resistance and maximize the antitumor activity. For this purpose, ZnO/PLGA/gelatin electrospun composite fibers were fabricated, which were able to simultaneously encapsulate a hydrophilic (doxorubicin hydrochloride) and a hydrophobic drug (camptothecin). Mesoporous ZnO was synthetized by a traditional method, and spherical particles of about 300 nm were obtained. The BET surface area was calculated to be equal to 84.78 m^2/g and the pore size was about 6.75 nm. Particularly, the Doxorubicin was loaded into the mesoporous ZnO by a traditional method, which consisted in incubating a drug solution with the material for 24 hours. The drug loading resulted in around 9.09 %. The Camptotecin was directly loaded into the polymeric fibers. In this way, the release of the two drugs was enabled with distinct rates: Camptotecin was released in a rapid rate while Doxorubicin showed a sustained and longterm release behavior because of the hindrance of mesoporous ZnO and PLGA/gelatin matrixes.

Maiti and colleagues reported the drug loading and release profiles of a multifunctional composite material, which was based on magnetically active γ-Fe_2O_3 nanoparticles and optically active mesoporous ZnO nanoparticles [86]. Daunorubicin hydrochloride, an anti-cancer drug, was selected as the drug model for their study. The composite was characterized by a BET surface area and the total pore volume of about 47 m^2/g and 0.432 cm^3/g, respectively. The average pore diameter was equal to 35 nm. The porous structure of ZnO

assured a high drug storage. In fact, the drug loading was around 76% after 60 minutes of exposure of the composite to the drug solution. The larger amount of drug was released at pH~5.5, which is the intracellular pH of the cancer cells.

Qiu and collaborators produced a Fe_3O_4@ZnO@Gd_2O_3:Eu multifunction composite nanoparticles [87]. The role of each component was accurately evaluated: in this case upon irradiation the ZnO shells act in absorbing and converting microwaves to heat, so triggering the release of the loaded Etoposide drug.

The possibility of combining ZnO and SiO_2 is described in the work of Vijay B. Kumar [88]. This investigation dealt with innovative mesoporous SiO_2–ZnO composite nanocapsules (90–150 nm) for the storage of biomolecules. The BET surface area and the pore diameter of the composite resulted in 230 m^2/g and ca. 2–8 nm, respectively. In order to test the loading efficiency of the SiO_2-ZnO composite nanocapsules three different molecules were loaded into the materials: Rhodamine 6G, a fluorescent dye, Doxorubicin and DNA molecules. The study highlighted the functionality of this promising mesoporous SiO_2–ZnO nanoparticles as drug carrier.

The above reported analysis of the literature, clearly highlights that the design of stimuli-responsive controlled drug delivery systems in cancer therapy is the most investigated challenge in the field of ZnO-containing composite materials, as it was already pointed out in the case of pure ZnO carriers.

1.3 ZnO nanomaterials for skin applications

1.3.1 Skin structure and skin-particles interaction

The skin is the largest organ of the human body and accomplishes different important roles, such as the body protection from external factors [89]. Due to its high surface area (about 2 m^2), the skin is constantly exposed to several pathogenic agents, which commonly cause cutaneous infections [90]. Nevertheless, the skin impermeability to the drugs, which is mainly caused by the lipidic nature and cohesive structure of the *stratum corneum*, is a significant limitation in the treatment of these altered dermatological conditions [91]. In the last years, drug delivery systems for topical administration have been proposed as possible solutions to overcome the skin route barrier. Several advantages result from the application of drug carriers onto the skin: for instance, they can enhance the dermatological formulations, so delivering both hydrophobic and hydrophilic drugs and allowing a controlled release for a prolonged time to be achieved.

If the skin is to be considered a possible route of exposure to drug delivery systems, some aspects about its structure and composition have to be described. Briefly, the skin consists of two main layers: the epidermis and the dermis.

The epidermis is the outermost part and is composed mostly (95%) by layers of stratified keratinocytes, which represent the predominant cell type in this layer. Keratinocytes undergo a differentiation process, keratinization, during which they move upward from the basal layer of the epidermis, *stratum basale*, to the outermost, *stratum corneum*. Here, the keratinocytes become anucleated with a flat shape, corneocytes, and are prevalently surrounded by an extracellular lipid matrix, enriched of proteins. The structure of this extracellular matrix is usually defined as "*brick and mortar*" [92,93], where the corneocytes represent the *brick* and the intercellular lipids represent the *mortar*. The epidermis lies on a basement membrane, which separates it from the dermis (0.1-0.4 cm).

The dermis is composed of a network of dense and irregular connective tissue (collagen, elastic and reticular fibres) and different cell types, such as nerves, blood vessels and lymphatics. Vascular networks are absent in the

epidermis, which means that, to achieve a systemic drug delivery, penetrating the epidermis and reaching the dermis, is mandatory. In the viable epidermis there are also other cells with different roles, such as the melanocytes, which are melanin producers, the Merkel cells, which provide the sensory perception and the Langerhans cells, which possess an immunological function. In addition to the cellular components, there are appendages in the skin which include the pilosebaceous units (10–70 μm), such as the hair follicles and associated sebaceous glands, and the apocrine and eccrine sweat glands (60–80 μm)[92,94].

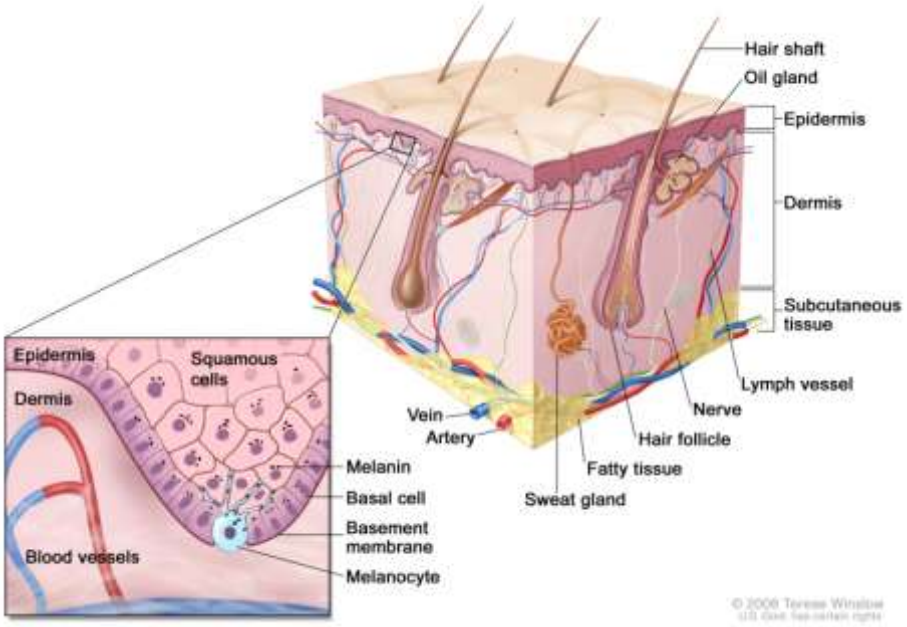

Figure 1.6 Schematic representation of normal skin. This image has been taken by *The web site of the National Cancer Institute (*http://www.cancer.gov*)*

When the diffusion of a molecule across the skin is considered, the *stratum corneum* (SC) represents the main physical barrier. Typically, SC has a thickness of about 10-20 μm [93] which depends on the body site, and is in direct contact with the outside environment. It is largely responsible for the physical barrier function of the skin and regulates the diffusion of water out of the skin. As previously described, the SC is a lipophilic medium, that is covered by an irregular and discontinuous layer of sebum secreted by the sebaceous glands, along with sweat, bacteria and dead skin cells. Obviously, this composition

favors the absorption of non-polar molecules through the skin. Moreover, the surface of the skin is characterized by the presence of furrows, which provide a reservoir for topically applied particles [93]and where the large particles can also aggregate.

Transport of substances across the SC occurs mainly by passive diffusion may be interrupted by appendages. Three possible routes may occur: i) the transcellular, ii) the intercellular and iii) the appendageal route (Figure 1.7).

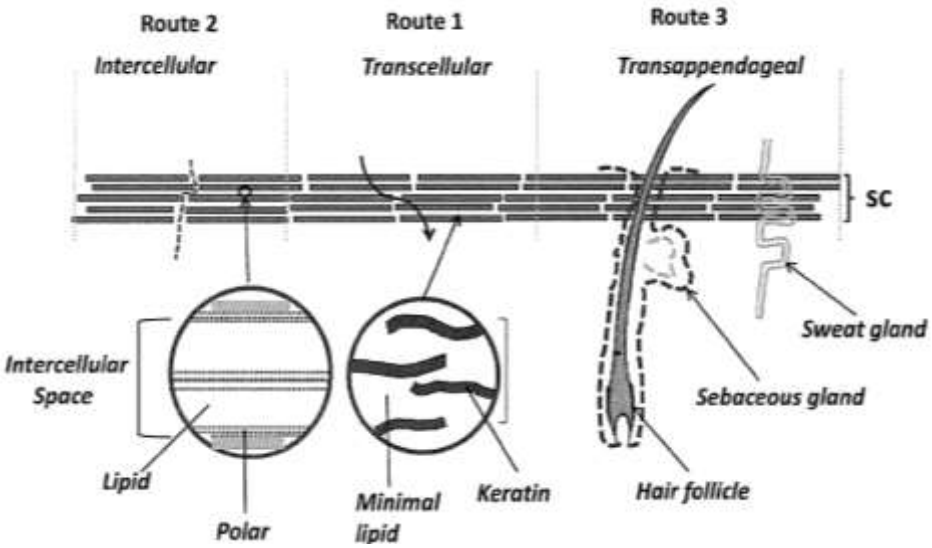

Figure 1.7 Transport routes of substances across the SC [93]

The transcellular pathway is currently considered as unlikely for most compounds, due to the repeated partitioning between lipophilic and hydrophilic compartments that a molecule should meet, including the almost impenetrable corneocytes intracellular matrix [93]. The intercellular route is generally supported by penetrants, like small molecules, able to move freely within the intercellular spaces. In this case diffusion rates depend mostly by their lipophilicity, molecular weight or volume, solubility and hydrogen bonding ability [92]. Despite the free movement of larger molecules or particles results to be physically restricted within the lipid matrix of the SC, the diffusion through intercellular lipids is more likely to occur for most solutes. The trans-appendages pathway consists in a promising alternative mechanism to cross the SC despite the relative low density of these structures on the skin surface (ranging from about 50 follicles/cm^2 in the majority of the body sites to about

290 follicles/cm^2 in the forehead [95]). Structural parameters such as the shape, the complex vascularization and the deep invagination of hair follicles transform them in suitable place for the mechanical accumulation and storage of substances. The hair follicles are based in the dermis, where blood and lymphatic vessels are located, so representing a possible approach to achieve a systemic effect.

Despite the considerable interest in the use of particles as topical drug delivery carriers, there is a significant concern about the toxic consequences of their unwanted penetration. When a drug delivery system is administered to the skin, several factors affect this interaction (Figure 1.8).

♦ *Size*. Dimensions are considered the most important parameter governing the interaction between a carrier and the skin. Skin penetration and transport route are strongly dependent on the size of the particles. Penetration of particles through the skin is an open debate and many investigations have been addressed on this topic, aiming at obtaining standard conclusions. Important rules have been set by the Scientific Committee on Consumer Products (SCCP) who concluded that only very small particles (<10 nm) could penetrate the skin and that there is no evidence for skin penetration into viable tissue for particles >20 nm, even if they can penetrate deeply into viable tissues [92]. The same assumptions were drawn by Liang and coworkers, who brilliantly summarized the size effect on skin penetration. What emerges from their work is that only very small particles (4-6 nm), as Quantum Dots and TiO_2 nanoparticles, penetrated in the deeper layer of epidermis after skin administration. Most of the evaluated cases showed no penetration into viable epidermis, reaching only the superficial layers of SC, due to aggregation phenomena on the skin surface or penetration into the hair follicles [93]. Nevertheless, as suggested by Roberts and colleagues in their remarkable work, it is important to carefully consider the experimental conditions under which the skin penetration experiments were performed [96]. A significative example has been given by Roberts, who compared the penetration of gold base nanoparticles through the skin of different species. For instance, rat and pig skin was more permeable than human skin due to different thickness and permeability.

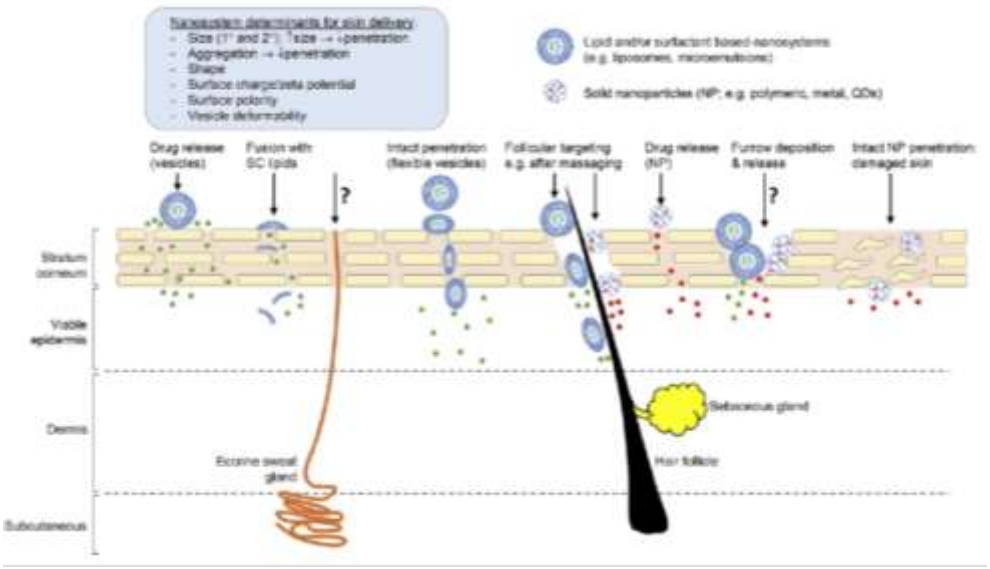

Figure 1.8 Schematic representation of the drug carriers properties affecting the interaction with skin. The image has been taken from [96].

♦ *Shape.* Different morphologies can also affect the interaction between carrier and skin. A cornerstone example is represented by the flexible nanovesicles, which are particles able to deform in shape thanks to their structural composition [96,97]. Briefly, these vesicles can elongate their starting spherical shape and squeeze through narrow channels. The enhanced skin penetration ability of the flexible vesicles, can be exploited to improve the permeation of many compounds. Another aspect related to the shape of the particles is the toxicity associated with some morphology. For instance it has been recently reported that a rod shape could involve more toxicity issues than other morphologies [30].

♦ *Surface properties*. The surface charge can influence the carrier penetration, but its role is still unclear [98]. However, since the skin is negatively charged on its surface under physiological conditions, consequently an enhanced electrostatic interaction with positively charged particles has been reported [93].

Another crucial aspect to be considered, it is that the skin is generally used as a route of administration for both local and systemic drugs. The former case is defined “topical administration” and consists in the administration of a drug to a particular spot on the outer surface of the body; the latter is defined “transdermal administration” and involves the administration through the dermal layer of the skin to the systemic circulation by diffusion. These definitions are given accordingly to the Food and Drug Administration monographs.

As in other fields, drug delivery systems have reached significant improvements in the topical and transdermal administration of compounds [99]. For instance, the use of skin drug carriers can reduce systemic side effects, being it an alternative to the oral route, and can allow a controlled or prolonged drug delivery to be achieved. On one hand, a topical formulation can be improved by the addition of a drug delivery system for innovative treatment of skin disorders, such as infective conditions (i.e. acne) so enhancing the drug penetration through the skin layers, where its effect is expected. On the other hand, transdermal formulations can help the drug permeation through the skin and enter the systemic circulation.

Among the two above reported routes of skin administration, the possibility to enhance the local delivery of a drug through innovative drug delivery systems has been the driven force of this PhD thesis project. The next section deals with the state of the art related to the current studies of ZnO nanostructures on the skin.

1.3.2. ZnO nanomaterials and skin: the state-of-the-art

For millennia Zinc oxide has been used in skin care applications, due to its intrinsic properties, such as its non-toxicity, biocompatibility and antimicrobial activity. The oldest reference about the use of this material could be dated back to 500 BC, when a ZnO-based healing salve, called Pushpanjan, was indicated in an Indian Medical Text for the treatment of the eyes and open wounds. Nowadays, ZnO is generally used to address several skin conditions, like burns, scars and irritations. ZnO is able to act as soothing and protecting agent, so creating a protective barrier on the skin. Thanks to this property, a ZnO is traditionally used as the main component of many baby-care products, such as powders and pastes, to treat diaper rash. In this case a ZnO film reduces the effects of bacteria and other irritants, which are present in urine and excrements, so protecting the delicate baby skin. Other popular uses of ZnO include its application as an active ingredient in anti-dandruff shampoos and in antiseptic ointments, due to its antibacterial properties. It is also used in rectal haemorrhoid creams to relieve itchiness and protect irritated tissues. Moreover, there is a growing attention on the topical use of ZnO to prevent acne through sebum reduction and anti-inflammatory action.

As a result of the wide spread of nanotechnology, also cosmetics and pharmaceuticals have been revolutionised. Nanomaterials play a key role in the cosmetic and dermatological fields due to their nanometric size and potential applications. Among all the materials, also ZnO has been developed in different nanostructures to enhance its interaction with the skin and to improve the existing products. A careful analysis of the literature has been carried out aiming at determining the main studied roles of nanosized ZnO in topical application. Table 1.1 summarizes these findings.

ZnO as a drug carrier for the skin

Going through the literature, it has emerged that few research works have been dedicated to the evaluation of ZnO as a material for drug delivery to the skin. During the *International Conference and Exhibition on Nanomedicine and Drug Delivery* (May 29-31, 2017 Osaka, Japan) Markus and colleagues presented a poster focused on the development of a drug carrier for topical delivery composed by ZnO nanocomposites functionalized by hyaluronic acid

or carboxymethyl chitosan. The resulting flower-shaped nanocomposites were further loaded with a vegetal extract and functionalized with ginsenoside Rh2. The properties of the drug delivery system were deeply characterized, which resulted a promising carrier for the topical delivery of active substances to treat skin disorders and prevent skin cancer [100].

The study of Huang and collaborators is a unique example of the use of ZnO nanoparticles as drug carrier on the skin [101]. They developed a UV and dark-triggered drug delivery system for skin protection, that was based on ZnO nanoparticles as carrier for benzophenone-3, a UV-absorption molecule. The ZnO particles sizes were found to be 30-40 nm and were assembled into larger aggregates ranging from 500 to 1400 nm. The encapsulation efficiency and loading capacity of benzophenone-3 were about 53.68% and 133.61%. The benzophenone-3 was released almost completely released from the carrier, under 2 hours of UV. The drug loaded system reported low cytotoxicity to human keratinocyte cells and human skin fibroblasts.

Nayak and collaborators developed ZnO nanorods for non-destructive drug delivery, to enhance the penetration of Albumin-Fluorescein isothiocyanate (FITC) across the skin. ZnO nanorods (lengths of 30–35 μm and diameters of of 200–300 nm) successfully facilitated FITC penetration through the skin along the channels formed by the nanorods. This work is a clear example of non-invasive and painless intradermal drug delivery achieved through the use of ZnO nanorods [12].

ZnO as antibacterial additive in skin formulations

Recently Sonia and colleagues proposed colloidal ZnO nanoparticles, which were obtained through an eco-friendly synthesis, as innovative additives for a cosmeceutical formulation. The nanocosmeceutical formulation was tested against clinical skin pathogens and significant inhibitory action was observed against *Candida sp*., which showed resistance against a commercial antifungal cream (2%) [102]. Also, Raij and collaborators investigated the topical anti-infective properties of ZnO nanoparticles against *Propionibacterium acnes*, a gram positive bacillus normally present on human skin and that causes acne. The antibacterial effects of ZnO nanoparticles were tested as-such and after incorporation into cold cream. Results showed an effective and promising role of ZnO for topical applications in treating acne vulgaris [54].

Wiegand and coworkers investigated the role of ZnO as a smart additive to functionalize textile fibers, in order to improve the control of oxidative stress in atopic dermatitis, which is a chronic inflammatory disease characterized by the impairment of the skin-barrier function, the increase in the oxidative cellular stress and bacterial colonization [103]. The antibacterial effect and biocompatibility of the Zn textile was evaluated in vitro, so demonstrating that the ZnO textiles possess very good biocompatibility and were well tolerated by the patients.

The successful role of ZnO nanoparticles as a topical anti-infective agent was confirmed by Patil and colleagues in their research work. They showed that the administration of ZnO significantly reduced the skin infection caused by *S. aureus*. in mice; this resulted in improved skin structure, with a reduced bacterial load and a reduced tissues inflammation [50].

ZnO in wound dressings

As far as the applications of ZnO nanomaterials on the skin are concerned, a nascent application that is worth mention, consists in the addition of ZnO in wound dressing. A wound is defined as *a disruption in the continuity of the epithelial lining of the skin or mucosa resulting from physical or thermal damage* [104,105]. A wound is generally classified as acute or chronic depending on the duration. An acute skin injury commonly heals at a predictable and fixed time (8-12 weeks), which depends on the extent of the damage in the epidermis and dermis layers of the skin. For instance, acute wounds can occur due to an accident or surgical injury. On the contrary, a chronic wound is an injury that fails to progress through the normal stages of healing and cannot be repaired in a prefixed time. Examples of chronic wounds are ulcers and burns. Wound healing is *a dynamic and complex process of tissue regeneration and growth progress* which is traditionally divided in different phases i) *inflammation*, ii) *proliferation*, and ii) *remodeling* [106].

Nowadays, much research works have been focused on the development of innovative wound dressings, which are able to interact with the wounded skin, promoting its healing. A suitable material for wound dressing application should possess antimicrobial properties, should be biodegradable, biocompatible, non-toxic and non-allergenic. Moreover, an ideal wound dressing should also be able to preserve a moist environment at the wound

surface, to permit gaseous exchange, to defend the wound against microorganisms, to absorb the excess of exudates avoiding maceration and to reduce scar formation. Among the different types of wound dressing materials, synthetic and natural polymers, such as polyurethane, poly(vinyl alcohol), poly(lactic acid) and alginate, chitin, chitosan and collagen are the most investigated [32]. During the wound healing process, the possible insurgence of infections represents one of the major issue, because of the negative consequences, such as exudate formation, improper collagen deposition and prolonged healing time. Furthermore, microorganisms can reach the deeper tissues through the wounded skin, causing internal infections. For instance, *S. aureus* and *E. coli* have been listed among the major infection-causing bacteria [32,107]. Moreover, it is worth to note that also wound dressing as such can cause an infection, if the material is not be able to absorb wound exudate or guarantee sterility. To overcome these issues, the need of innovative wound dressings is compelling.

In Material Science, bionanocomposites represent an emerging group of advanced materials that resulting from the combination of biopolymers with inorganic component [108]. Particularly, the addition of ZnO nanostructures in the polymeric matrix has been investigated in order to impart novel functionality, such as antibacterial activity [6]. Moreover, it has been demonstrated that topically applied ZnO act as a source of Zinc ions and this would improve, improving wound healing [109,110]. In fact, zinc is an essential trace element in the human body. Among its functions, it acts as a cofactor in zinc-dependent matrix metalloproteinases that augment auto debridement and keratinocyte migration during wound repair. Zinc confers cytoprotection against reactive oxygen species and bacterial toxins. Zinc deficiency can lead to pathological conditions and delayed wound healing.

Recently, many research works have been dedicated to the study of ZnO nanomaterials as inorganic fillers for bionanocomposite wound dressings. Several biocompatible materials have been studied; among all chitin and its derivatives are of particular interest for their capability of accelerating the healing processes. Going through the literature, it is evident that the combination of ZnO nanomaterials and chitosan represents one of the most promising solution in the field of innovative wound dressings [26,107,111–115]. Furthermore, a wide range of polymeric matrices have also been evaluated, such as carboxymethyl cellulose hydrogels [116], poly (vinyl alcohol)[117–119],

chitosan-gelatin [120], collagen and dextran hydrogels [121], cross linked sodium alginate-gum acacia hydrogels [122].

ZnO as Skin penetration enhancer

The role of ZnO as a skin penetration enhancer has also been studied. This application consists in the simultaneous skin administration of ZnO with another compound (i.e. drug) and not in its direct use as a drug carrier. Shokri N. has been one of the pioneering scientist in this field. He dedicated significant research works to the study of ZnO as a skin enhancer in topical formulations. In 2014, ZnO and ZnO nanoparticles were compared as absorption enhancers for Ibuprofen, so demonstrating that both compounds could act as enhancers for transdermal delivery of Ibuprofen, with a higher efficiency for the ZnO nanoparticles [123]. In the same year, Shokri and coworkers also investigated the enhanced skin permeation of solvents and surfactants due to the co-utilization of ZnO nanoparticles in topical products. ZnO resulted able to increase the permeation of hydrophobic, oily and hydrophilic solvents and surfactants, which indicated a potential role in the co-enhancement of drug absorption [124]. The aim of the research work that was published two years ago by the same authors consisted in the evaluation of the skin permeation of albumin when co-administered with ZnO nanoparticles in comparison with Calcium Phosphate. In their work, the nanoparticles were not used as drug carriers, but were simultaneously administered separetely with the Albumin, but separated from it. Their enhancer effect depended on their position and stay in the skin layers, which helped the drug to cross the skin. Results showed that the enhancer effect of Calcium Phosphate nanoparticles was weaker than that of ZnO, because of the different skin distribution and solubility of the particles [125].

ZnO as UV- Blocker in sun-screen formulations

Doubtless, the most popular use of ZnO on skin applications is its addition in sunscreen products as a UV-blocker agent [53]. In fact, ZnO is a broad spectrum UVA and UVB reflector, completely photo-stable. Due to its ability in blocking UVA (320–400 nm) and UVB (280–320 nm) rays of ultraviolet illumination it is often used as associate degree ingredient in sunscreen

products. Due to the frequent use of ZnO in commercial sunscreen formulations, many research works have been addressed to the study of the human epidermal skin penetration of ZnO and its zinc ion dissolution products, after the application of ZnO nanoparticles to human epidermis [53,126–131]. Moreover, it is worthy of note that the European Commission has added ZnO, in both its nano and non-nano forms, to Annex VI of the EU Cosmetics Regulation only in 2016, thus allowing its use as a UV filter in cosmetic products. Different is the case of USA, where the Food and Drug Administration approved the use of nanoparticles in sunscreens in 1999. Nanosized ZnO particles are generally preferred by consumers because of the less opaque effect when they are dermally applied.

Table 1.1 Recently proposed applications of nanosized ZnO on skin

	Applications of nanosized ZnO on skin	**Ref.**
Drug carrier	UV and dark-triggered drug delivery system for skin protection based on ZnO nanoparticles as carriers for benzophenone-3	101
	ZnO nanocomposites functionalized by hyaluronic acid or carboxymethyl chitosan, loaded with a vegetal extract and functionalized with ginsenoside Rh2	100
	ZnO nanorods for non-destructive transdermal drug delivery	12
Antibacterial additive	ZnO is added to cosmeceutical formulation against clinical skin pathogens	132
	ZnO is added to cold cream against *Propionibacterium acnes*, normally present on human skin and causes acne	54
	ZnO is added to textile fibers to reduced oxidative stress in atopic dermatitis; good antibacterial effect and biocompatibility	103
Wound Dressing	ZnO as inorganic nanofiller to impart novel functionality, such as antibacterial activity and to accelerate the wound healing process	6,109,110
	Different bionanocomposite materials developed i.e. chitosan, polymers, polysaccharides etc	26,107,111–114,116–122,133
Penetration enhancer	ZnO nanoparticles as absorption enhancer of Ibuprofen, when co-administered	123
	ZnO nanoparticles enhanced skin permeation of solvents and surfactants, when co-administered	124
	ZnO nanoparticles enhanced skin permeation of albumin when co-administered with ZnO nanoparticles	125
Sun blocker	study of the human epidermal skin penetration of ZnO and its zinc ion dissolution products, after the application of ZnO nanoparticles to human epidermis	53,126–131

Toxicity of ZnO on the skin

Due to the active role of ZnO particles in many dermatological applications and its large use in sunscreen products, in this last decade an increasingly attention has been focused on whether the nanoparticles could penetrate the skin barrier and access the viable epidermis [53]. Notwithstanding the prompted concern about this issue,"*it is commonly accepted that passive penetration of ZnO nanoparticles into intact human skin is limited to the surface and upper layers of the stratum corneum*" [96]. Many research works support this affirmation and a huge mole of investigations have been addressed to this purpose [55,130,134–136]. Moreover, also ZnO and TiO_2 nanoparticles penetration through UVB-damaged skin was investigated, observing only a slightly enhancement of the penetration; however transdermal absorption was not detected [131].

Also the penetration of Zinc Ions released from topically applied ZnO has been deeply studied. One of the most interesting and recent work concerning this topic, is represented by the investigation of Holmes and colleagues. In order to figure out the level of penetration of ZnO particles in the skin and their toxicity, Holmes investigated different ZnO nanoparticle formulations commonly used in commercially available sunscreen products. Results showed that the ZnO in the formulations did not penetrate into the intact viable epidermis, but displayed an enhanced increase of zinc ions in both the *stratum corneum* and the viable epidermis [137].

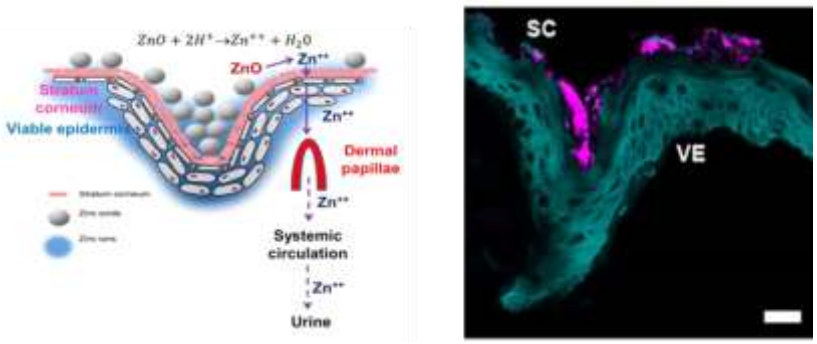

Figure 1.9 Schematic representation of the postulated fate of the zinc ions absorbed by the skin after ZnO hydrolysis [137].

The penetration of Zn through human skin after the application of sunscreens containing ZnO, was also reported in other investigations [138,139].

The proposed mechanism would be based on the hydrolysis of ZnO on the skin surface, due to its acidic pH, which is followed by Zn^{2+} ions penetration.
On one hand safety of the topical applied ZnO nanoparticles results well-established in the literature. On the other hand, some research works suggested a sort of toxicity of ZnO nanoparticles, due to their internalization by cultured human keratinocytes, which caused cytotoxic and genotoxic responses [140]. Also Kokbec and colleagues reported the *in vitro* toxicity of ZnO and TiO_2 nanoparticles on keratinocytes over short- and long-term applications. They mainly demonstrated intracellular formation of radicals and alterations in cell morphology [141].
Notwithstanding these isolated research works, carried out between the 2010 and 2011, the investigation of Ryu and colleagues in 2014 assessed no evidence of toxicity after a 90-day repeated dermal application of ZnO in rats [129]. Moreover, the same conclusion was drawn by Virnardell and colleague, who dedicated their efforts in the study of nanosized ZnO potential cause of acute cutaneous irritation. In their investigation cultured HaCaT keratinocytes and a human skin equivalent were used, both with nano- and non-nano sized materials. In conclusion, they observed a non-irritation condition of the skin with both the nanosized ZnO and non-nano ZnO [142].

1.4 Conclusions

This chapter dealt with a general overview of the ZnO properties and applications in the biomedical field, offering a detailed description of the current state-of-art related to the use of ZnO nanostructures as drug delivery system. Particular attention was focused on the existing studies of NsZnO on skin applications.
In conclusion, it emerged that despite of the growing attention focused on ZnO nanostructures (NsZnO), the study of NsZnO as drug delivery system is still in its nascent stage, particularly considering the administration to the skin. In order to fill this gap, this PhD thesis has been dedicated to the study of nanostructured ZnO as material to develop innovative drug carriers for future dermatological applications.

1.5 References

(1) European Commission. Regulation (EC) No 1223/2009 of the European Parliament and of the Council of 30 November 2009 on Cosmetic Products. *Off. J. Eur. Union* **2009**, No. 1223, 342–359.

(2) Cossio, M. L. T.; Giesen, L. F.; Araya, G.; Pérez-Cotapos, M. L. S.; VERGARA, R. L.; Manca, M.; Tohme, R. A.; Holmberg, S. D.; Bressmann, T.; Lirio, D. R.; Román, J. S.; Solís, R. G.; Thakur, S.; Rao, S. N.; Modelado, E. L.; La, A. D. E.; Durante, C.; Tradición, U. N. A.; En, M.; Espejo, E. L.; Fuentes, D. E. L. A. S.; Yucatán, U. A. De; Lenin, C. M.; Cian, L. F.; Douglas, M. J.; Plata, L.; Héritier, F. *Nano-Antimicrobials*; 2012; Vol. XXXIII.

(3) Kołodziejczak-Radzimska, A.; Jesionowski, T. Zinc Oxide—From Synthesis to Application: A Review. *Materials (Basel).* **2014**, *7* (4), 2833–2881.

(4) Wang, Z. L.; Kong, X. Y.; Ding, Y.; Gao, P.; Hughes, W. L.; Yang, R.; Zhang, Y. Semiconducting and Piezoelectric Oxide Nanostructures Induced by Polar Surfaces. *Adv. Funct. Mater.* **2004**, *14* (10), 943–956.

(5) Wang, Z. L. Novel Nanostructures of ZnO for Nanoscale Photonics, Optoelectronics, Piezoelectricity, and Sensing. *Appl. Phys. A Mater. Sci. Process.* **2007**, *88* (1), 7–15.

(6) Sirelkhatim, A.; Mahmud, S.; Seeni, A. Review on Zinc Oxide Nanoparticles : Antibacterial Activity and Toxicity Mechanism. *Nano-Micro Lett.* **2015**, *7*, 219–242.

(7) Wang, Z. L. Zinc Oxide Nanostructures: Growth, Properties and Applications. *J. Phys. Condens. Matter* **2004**, *16*, R829–R858.

(8) Wang, Z. L. Nanostructures of Zinc Oxide. *Mater. Today* **2004**, *7* (6), 26–33.

(9) Sahu, D. R.; Liu, C. P.; Wang, R. C.; Kuo, C. L.; Huang, J. L. Growth and Application of ZnO Nanostructures. *Int. J. Appl. Ceram. Technol.* **2013**, *10* (5), 814–838.

(10) Gomez, J. L.; Tigli, O. Zinc Oxide Nanostructures: From Growth to Application. *J. Mater. Sci.* **2013**, *48* (2), 612–624.

(11) Mirzaei, H.; Darroudi, M. Zinc Oxide Nanoparticles: Biological Synthesis and Biomedical Applications. *Ceram. Int.* **2017**, *43* (1), 907–914.

(12) Nayak, T.; Wang, H.; Pant, A.; Zheng, M.; Junginger, H.; Goh, W.; Lee, C.; Zou, S.; Alonso, S.; Czarny, B.; Storm, G.; Sow, C.; Lee, C.; Pastorin, G. ZnO Nano-Rod Devices for Intradermal Delivery and Immunization. *Nanomaterials* **2017**, *7* (6), 147.

(13) Marimuthu, T.; Anandhan, N.; Thangamuthu, R. Electrochemical Synthesis of One-Dimensional ZnO Nanostructures on ZnO Seed Layer

for DSSC Applications. *Appl. Surf. Sci.* **2018**, *428*, 385–394.
(14) Ma, H.; Qin, Z.; Wang, Z.; Ahmad, M.; Sun, H. Enhanced Field Emission of ZnO Nanoneedle Arrays via Solution Etching at Room Temperature. *Mater. Lett.* **2017**, *206*, 162–165.
(15) Kashif, M.; Akhtar, M. N.; Nasir, N.; Yahya, N. Versatility of ZnO Nanostructures. In *Carbon and Oxide Nanostructures. Advanced Structured Materials, vol.5*; Springer, Berlin, Heidelberg, 2010.
(16) Gui, Z.; Liu, J.; Wang, Z. .; Song, L.; Hu, Y. .; Fan, W.; Chen, D. From Muticomponent Precursor to Nanoparticle Nanoribbons of ZnO. *J. Phys. Chem. B* **2005**, *27* (3), 1113–1117.
(17) Martinson, A. B. F.; Elam, J. W.; Hupp, J. T.; Pellin, M. J. ZnO Nanotube Based Dye-Sensitized Solar Cells. *Nano* **2007**, *7* (June), 2183–2187.
(18) Wang, Z. L. ZnO Nanowire and Nanobelt Platform for Nanotechnology. *Mater. Sci. Eng. R Reports* **2009**, *64* (3–4), 33–71.
(19) Singh, D. . Synthesis and Growth of ZnO Nanowires. *Sci. Adv. Mater.* **2010**, *2* (3), 245–272.
(20) Umar, A. Growth of Comb-like ZnO Nanostructures for Dye-Sensitized Solar Cells Applications. *Nanoscale Res. Lett.* **2009**, *4* (9), 1004–1008.
(21) Hu, J. Q.; Bando, Y.; Zhan, J. H.; Li, Y. B.; Sekiguchi, T. Two-Dimensional Micrometer-Sized Single-Crystalline ZnO Thin Nanosheets. *Appl. Phys. Lett.* **2003**, *83* (21), 4414–4416.
(22) Naveed Ul Haq, A.; Nadhman, A.; Ullah, I.; Mustafa, G.; Yasinzai, M.; Khan, I. Synthesis Approaches of Zinc Oxide Nanoparticles: The Dilemma of Ecotoxicity. *J. Nanomater.* **2017**, *2017* (Table 1).
(23) Djurišić, A. B.; Chen, X.; Leung, Y. H.; Man Ching Ng, A. ZnO Nanostructures: Growth, Properties and Applications. *J. Mater. Chem.* **2012**, *22* (14), 6526.
(24) Madhumitha, G.; Elango, G.; Roopan, S. M. Biotechnological Aspects of ZnO Nanoparticles: Overview on Synthesis and Its Applications. *Appl. Microbiol. Biotechnol.* **2016**, *100* (2), 571–581.
(25) Moezzi, A.; McDonagh, A. M.; Cortie, M. B. Zinc Oxide Particles: Synthesis, Properties and Applications. *Chem. Eng. J.* **2012**, *185–186*, 1–22.
(26) Vasile, B. S.; Oprea, O.; Voicu, G.; Ficai, A.; Andronescu, E.; Teodorescu, A.; Holban, A. Synthesis and Characterization of a Novel Controlled Release Zinc Oxide/gentamicin-Chitosan Composite with Potential Applications in Wounds Care. *Int. J. Pharm.* **2014**, *463* (2), 161–169.
(27) Owens, G. J.; Singh, R. K.; Foroutan, F.; Alqays, M.; Han, C.-M.; Mahapatra, C.; Kim, H.-W.; Knowles, J. C. Sol–gel Based Materials for Biomedical Applications. *Prog. Mater. Sci.* **2016**, *77*, 1–79.

(28) Agarwal, H.; Venkat Kumar, S.; Rajeshkumar, S. A Review on Green Synthesis of Zinc Oxide Nanoparticles – An Eco-Friendly Approach. *Resour. Technol.* **2017**.

(29) Rasmussen, J. W.; Martinez, E.; Louka, P.; Wingett, D. G. Zinc Oxide Nanoparticles for Selective Destruction of Tumor Cells and Potential for Drug Delivery Applications. *Expert Opin. Drug Deliv.* **2010**, *7* (9), 1063–1077.

(30) Ann, L. C.; Mahmud, S.; Seeni, A.; Bakhori, S. K. M.; Sirelkhatim, A.; Mohamad, D.; Hasan, H. Structural Morphology and in Vitro Toxicity Studies of Nano- and Micro-Sized Zinc Oxide Structures. *J. Environ. Chem. Eng.* **2015**, *3* (1), 436–444.

(31) Pasquet, J.; Chevalier, Y.; Pelletier, J.; Couval, E.; Bouvier, D.; Bolzinger, M. A. The Contribution of Zinc Ions to the Antimicrobial Activity of Zinc Oxide. *Colloids Surfaces A Physicochem. Eng. Asp.* **2014**, *457*, 263–274.

(32) Zhu, P.; Weng, Z.; Li, X.; Liu, X.; Wu, S.; Yeung, K. W. K.; Wang, X.; Cui, Z.; Yang, X.; Chu, P. K. Biomedical Applications of Functionalized ZnO Nanomaterials: From Biosensors to Bioimaging. *Adv. Mater. Interfaces* **2016**, *3* (1), 1–30.

(33) Kumar, R.; Umar, A.; Kumar, G.; Nalwa, H. S. Antimicrobial Properties of ZnO Nanomaterials: A Review. *Ceram. Int.* **2017**, *43* (5), 3940–3961.

(34) Ramani, M.; Ponnusamy, S.; Muthamizhchelvan, C.; Marsili, E. Amino Acid-Mediated Synthesis of Zinc Oxide Nanostructures and Evaluation of Their Facet-Dependent Antimicrobial Activity. *Colloids Surfaces B Biointerfaces* **2014**, *117*, 233–239.

(35) Talebian, N.; Amininezhad, S. M.; Doudi, M. Controllable Synthesis of ZnO Nanoparticles and Their Morphology-Dependent Antibacterial and Optical Properties. *J. Photochem. Photobiol. B Biol.* **2013**, *120*, 66–73.

(36) Li, G. R.; Hu, T.; Pan, G. L.; Yan, T. Y.; Gao, X. P.; Zhu, H. Y. Morphology-Function Relationship of ZnO: Polar Planes, Oxygen Vacancies, and Activity. *J. Phys. Chem. C* **2008**, *112* (31), 11859–11864.

(37) Yamamoto, O. Influence of Particle Size on the Antibacterial Activity of Zinc Oxide. *Int. J. Inorg. Mater.* **2001**, *3* (7), 643–646.

(38) Zhang, L.; Jiang, Y.; Ding, Y.; Povey, M.; York, D. Investigation into the Antibacterial Behaviour of Suspensions of ZnO Nanoparticles (ZnO Nanofluids). *J. Nanoparticle Res.* **2007**, *9* (3), 479–489.

(39) Padmavathy, N.; Vijayaraghavan, R. Enhanced Bioactivity of ZnO Nanoparticles—an Antimicrobial Study. *Sci. Technol. Adv. Mater.* **2008**, *9* (3), 35004.

(40) Xie, Y.; He, Y.; Irwin, P. L.; Jin, T.; Shi, X. Antibacterial Activity and Mechanism of Action of Zinc Oxide Nanoparticles against

Campylobacter Jejuni. *Appl. Environ. Microbiol.* **2011**, *77* (7), 2325–2331.

(41) Gunalan, S.; Sivaraj, R.; Rajendran, V. Progress in Natural Science : Materials International Green Synthesized ZnO Nanoparticles against Bacterial and Fungal Pathogens. *Prog. Nat. Sci. Mater. Int.* **2013**, *22* (6), 693–700.

(42) He, L.; Liu, Y.; Mustapha, A.; Lin, M. Antifungal Activity of Zinc Oxide Nanoparticles against Botrytis Cinerea and Penicillium Expansum. *Microbiol. Res.* **2011**, *166* (3), 207–215.

(43) Kumar, R.; Umar, A. Antimicrobial Properties of ZnO Nanomaterials : A Review. **2017**, *43* (November 2016), 3940–3961.

(44) Sharma, D.; Rajput, J.; Kaith, B. S.; Kaur, M.; Sharma, S. Synthesis of ZnO Nanoparticles and Study of Their Antibacterial and Antifungal Properties. *Thin Solid Films* **2010**, *519* (3), 1224–1229.

(45) Esteban-tejeda, L.; Prado, C.; Cabal, B.; Sanz, J. Antibacterial and Antifungal Activity of ZnO Containing Glasses. **2015**.

(46) Pasquet, J.; Chevalier, Y.; Couval, E.; Bouvier, D.; Bolzinger, M. A. Zinc Oxide as a New Antimicrobial Preservative of Topical Products: Interactions with Common Formulation Ingredients. *Int. J. Pharm.* **2015**, *479* (1), 88–95.

(47) Favet, J.; Chappuis, M. L.; Doelker, E. A Case Study of Preservation of Semi-Solid Preparations Using the European Pharmacopoeia Test: Comparative Efficacy of Antimicrobial Agents in Zinc Gelatin. *Eur. J. Pharm. Biopharm.* **2001**, *52* (2), 255–259.

(48) Pasquet, J.; Chevalier, Y.; Couval, E.; Bouvier, D.; Noizet, G.; Morli??re, C.; Bolzinger, M. A. Antimicrobial Activity of Zinc Oxide Particles on Five Micro-Organisms of the Challenge Tests Related to Their Physicochemical Properties. *Int. J. Pharm.* **2014**, *460* (1–2), 92–100.

(49) Espitia, P. J. P.; Soares, N. de F. F.; Coimbra, J. S. dos R.; de Andrade, N. J.; Cruz, R. S.; Medeiros, E. A. A. Zinc Oxide Nanoparticles: Synthesis, Antimicrobial Activity and Food Packaging Applications. *Food Bioprocess Technol.* **2012**, *5* (5), 1447–1464.

(50) Pati, R.; Mehta, R. K.; Mohanty, S.; Padhi, A.; Sengupta, M.; Vaseeharan, B.; Goswami, C.; Sonawane, A. Topical Application of Zinc Oxide Nanoparticles Reduces Bacterial Skin Infection in Mice and Exhibits Antibacterial Activity by Inducing Oxidative Stress Response and Cell Membrane Disintegration in Macrophages. *Nanomedicine Nanotechnology, Biol. Med.* **2014**, *10* (6), 1195–1208.

(51) Walker, M.; Kublin, J. G.; Zunt, J. R. NIH Public Access. **2009**, *42* (1), 115–125.

(52) Bisht, G.; Rayamajhi, S. ZnO Nanoparticles: A Promising Anticancer

Agent. *Nanobiomedicine* **2016**, *3*, 9.
(53) Smijs, T. G.; Pavel, S. Titanium Dioxide and Zinc Oxide Nanoparticles in Sunscreens: Focus on Their Safety and Effectiveness. *Nanotechnol. Sci. Appl.* **2011**, *4* (1), 95–112.
(54) Raj, M. S.; Roselin, P. The Antibacterial Activity of ZnO Nanoparticles against Propionibacterium Acnes. *Int. J. Pharma Bio Sci.* **2012**, *3* (1), 267–276.
(55) Nohynek, G. J.; Dufour, E. K.; Roberts, M. S. Nanotechnology, Cosmetics and the Skin: Is There a Health Risk? *Skin Pharmacol. Physiol.* **2008**, *21* (3), 136–149.
(56) Wei, A.; Pan, L.; Huang, W. Recent Progress in the ZnO Nanostructure-Based Sensors. *Mater. Sci. Eng. B Solid-State Mater. Adv. Technol.* **2011**, *176* (18), 1409–1421.
(57) Ozgür, M.; Hofstetter, D.; Morkoç, H. ZnO Devices and Applications: A Review of Current Status and Future Prospects. *Proc. IEEE* **2010**, *98*, 1255–1268.
(58) Arya, S. K.; Saha, S.; Ramirez-Vick, J. E.; Gupta, V.; Bhansali, S.; Singh, S. P. Recent Advances in ZnO Nanostructures and Thin Films for Biosensor Applications: Review. *Anal. Chim. Acta* **2012**, *737*, 1–21.
(59) Wang, J. X.; Sun, X. W.; Wei, A.; Lei, Y.; Cai, X. P.; Li, C. M.; Dong, Z. L. Zinc Oxide Nanocomb Biosensor for Glucose Detection. *Appl. Phys. Lett.* **2006**, *88* (23), 2004–2007.
(60) Xiong, H. M. ZnO Nanoparticles Applied to Bioimaging and Drug Delivery. *Adv. Mater.* **2013**, *25* (37), 5329–5335.
(61) Wu, Y. L.; Lim, C. S.; Fu, S.; Tok, a I. Y.; Lau, H. M.; Boey, F. Y. C.; Zeng, X. T. Surface Modifications of ZnO Quantum Dots for Bio-Imaging. *Nanotechnology* **2007**, *18* (21), 215604.
(62) Elsevier. Scopus.
(63) Bakrudeen, H. B.; Tsibouklis, J.; Reddy, B. S. R. Facile Fabrication of Mesoporous ZnO Nanospheres for the Controlled Delivery of Captopril. *J. Nanoparticle Res.* **2013**, *15* (3), 1505.
(64) Cai, X.; Luo, Y.; Zhang, W.; Du, D.; Lin, Y. PH-Sensitive ZnO Quantum Dots-Doxorubicin Nanoparticles for Lung Cancer Targeted Drug Delivery. *ACS Appl. Mater. Interfaces* **2016**, *8* (34), 22442–22450.
(65) Dhivya, R.; Ranjani, J.; Bowen, P. K.; Rajendhran, J.; Mayandi, J.; Annaraj, J. Biocompatible Curcumin Loaded PMMA-PEG / ZnO Nanocomposite Induce Apoptosis and Cytotoxicity in Human Gastric Cancer Cells. *Mater. Sci. Eng. C* **2017**, *80*, 59–68.
(66) Zheng, C.; Wang, Y.; Phua, S. Z. F.; Lim, W. Q.; Zhao, Y. ZnO–DOX@ZIF-8 Core–Shell Nanoparticles for pH-Responsive Drug Delivery. *ACS Biomater. Sci. Eng.* **2017**, acsbiomaterials.7b00435.
(67) Tian, B.; Liu, S.; Zhang, Y.; Li, C.; Wang, Z. Hydrophilic, Mesoporous

Structural ZnO Nanospheres for pH-Triggered Release of Drug. *Mater. Lett.* **2017**, *188* (August 2016), 165–168.

(68) Li, M.; Lv, S.; Tang, Z.; Song, W.; Yu, H.; Sun, H.; Liu, H.; Chen, X. Polypeptide/Doxorubicin Hydrochloride Polymersomes Prepared Through Organic Solvent-Free Technique as a Smart Drug Delivery Platform. *Macromol. Biosci.* **2013**, *13* (9), 1150–1162.

(69) Vimala, K.; Shanthi, K.; Sundarraj, S.; Kannan, S. Synergistic Effect of Chemo-Photothermal for Breast Cancer Therapy Using Folic Acid (FA) Modified Zinc Oxide Nanosheet. *J. Colloid Interface Sci.* **2017**, *488*, 92–108.

(70) Muhammad, F.; Guo, M.; Guo, Y.; Qi, W.; Qu, F.; Sun, F.; Zhao, H.; Zhu, G. Acid Degradable ZnO Quantum Dots as a Platform for Targeted Delivery of an Anticancer Drug. *J. Mater. Chem.* **2011**, *21* (35), 13406.

(71) Fakhar-e-Alam, M.; Rahim, S.; Atif, M.; Hammad Aziz, M.; Imran Malick, M.; Zaidi, S. S. Z.; Suleman, R.; Majid, a. Corrigendum: ZnO Nanoparticles as Drug Delivery Agent for Photodynamic Therapy (2014 Laser Phys. Lett. 11 025601). *Laser Phys. Lett.* **2014**, *11* (3), 39501.

(72) Kumar, V. B.; Kumar, K.; Gedanken, A.; Paik, P. Facile Synthesis of Self-Assembled Spherical and Mesoporous Dandelion Capsules of ZnO: Efficient Carrier for DNA and Anti-Cancer Drugs. *J. Mater. Chem. B* **2014**, *2* (25), 3956.

(73) Mitra, S.; B., S.; Patra, P.; Chandra, S.; Debnath, N.; Das, S.; Banerjee, R.; Kundu, S. C.; Pramanik, P.; Goswami, A. Porous ZnO Nanorod for Targeted Delivery of Doxorubicin: In Vitro and in Vivo Response for Therapeutic Applications. *J. Mater. Chem.* **2012**, *22* (45), 24145.

(74) Barick, K. C.; Nigam, S.; Bahadur, D. Nanoscale Assembly of Mesoporous ZnO: A Potential Drug Carrier. *J. Mater. Chem.* **2010**, *20* (31), 6446.

(75) Zhang, H.; Chen, B.; Jiang, H.; Wang, C.; Wang, H.; Wang, X. A Strategy for ZnO Nanorod Mediated Multi-Mode Cancer Treatment. *Biomaterials* **2011**, *32* (7), 1906–1914.

(76) Khatun, M.; Choudhury, S.; Liu, B.; Lemmens, P.; Pal, S. K.; Mazumder, S. Resveratrol–ZnO Nanohybrid Enhanced Anti-Cancerous Effect in Ovarian Cancer Cells through ROS. *RSC Adv.* **2016**, *6* (107), 105607–105617.

(77) Baskar, G.; Chandhuru, J.; Sheraz Fahad, K.; Praveen, A. S.; Chamundeeswari, M.; Muthukumar, T. Anticancer Activity of Fungal L-Asparaginase Conjugated with Zinc Oxide Nanoparticles. *J. Mater. Sci. Mater. Med.* **2015**, *26* (1), 1–7.

(78) Bakrudeen, H. B.; Sugunalakshmi, M.; Reddy, B. S. R. Auto-Fluorescent Mesoporous ZnO Nanospheres for Drug Delivery Carrier Application. *Mater. Sci. Eng. C* **2015**, *56*, 335–340.

(79) Palanikumar, L.; Ramasamy, S.; Hariharan, G.; Balachandran, C. Influence of Particle Size of Nano Zinc Oxide on the Controlled Delivery of Amoxicillin. *Appl. Nanosci.* **2013**, *3* (5), 441–451.
(80) Zhao, W.; Wei, J. S.; Zhang, P.; Chen, J.; Kong, J. L.; Sun, L. H.; Xiong, H. M.; Möhwald, H. Self-Assembled ZnO Nanoparticle Capsules for Carrying and Delivering Isotretinoin to Cancer Cells. *ACS Appl. Mater. Interfaces* **2017**, *9* (22), 18474–18481.
(81) Zheng, C.; Wang, Y.; Phua, S. Z. F.; Lim, W. Q.; Zhao, Y. ZnO–DOX@ZIF-8 Core–Shell Nanoparticles for pH-Responsive Drug Delivery. *ACS Biomater. Sci. Eng.* **2017**, acsbiomaterials.7b00435.
(82) Lin, C. C.; Chen, Y. W.; Hsiao, C. S.; Chen, S. Y. Electrically Responsive ZnO Nanotubes for Controlled Release of Biomolecules. *Ceram. Int.* **2017**, *43* (May), S802–S806.
(83) Yang, C.; Zhang, D.; Wu, J.; Pan, W.; Cai, R. Electrodeposition of Biocomposite Film Onto ZnO Nanoparticles Modified Electrode for Closed-Loop Insulin Delivery Electrodeposition of Biocomposite Film Onto ZnO Nanoparticles Modified Electrode for Closed-Loop Insulin Delivery. *J. Nanosci. Nanotechnol.* **2016**, *15* (3), 1–6.
(84) Stankovic, A.; Sezen, M.; Marina, M.; Kaišarevic, S.; Andric, N.; Stevanovic, M. PLGA / Nano-ZnO Composite Particles for Use in Biomedical Applications : Preparation , Characterization , and Antimicrobial Activity. *J. Nanomater.* **2016**, *2016*, Article ID 9425289, 10 pages http://dx.doi.org/10.
(85) Wei, J.; Hu, J.; Li, M.; Chen, Y.; Chen, Y. Multiple Drug-Loaded Electrospun PLGA/gelatin Composite Nanofibers Encapsulated with Mesoporous ZnO Nanospheres for Potential Postsurgical Cancer Treatment. *Rsc Adv.* **2014**, *4* (53), 28011–28019.
(86) Maiti, D.; Mukhopadhyay, S.; Chandra Mohanta, S.; Saha, A.; Sujatha Devi, P. A Multifunctional Nanocomposite of Magnetic γ-Fe<inf>2</inf>O<inf>3</inf> and Mesoporous Fluorescent ZnO. *J. Alloys Compd.* **2015**, *653*, 187–194.
(87) Qiu, H.; Cui, B.; Zhao, W.; Chen, P.; Peng, H.; Wang, Y. A Novel Microwave Stimulus Remote Controlled Anticancer Drug Release System Based on Fe_3O_4@ZnO@mGd_2O_3:Eu@P(NIPAm-Co-MAA) Multifunctional Nanocarriers. *J. Mater. Chem. B* **2015**, *3* (34), 6919–6927.
(88) Kumar, V. B.; Annamanedi, M.; Prashad, M. D.; Arunasree, K. M.; Mastai, Y.; Gedanken, A.; Paik, P. Synthesis of Mesoporous SiO2-ZnO Nanocapsules: Encapsulation of Small Biomolecules for Drugs and "SiOZO-Plex" for Gene Delivery. *J. Nanoparticle Res.* **2013**, *15* (9).
(89) Goyal, R.; Macri, L. K.; Kaplan, H. M.; Kohn, J. Nanoparticles and Nanofibers for Topical Drug Delivery. *J Control Release* **2016**, *240*, 77–

92.
(90) Tull, T.; Morris Jones, R. Common Cutaneous Infections. *Med. (United Kingdom)* **2017**, *45* (6), 390–395.
(91) Gupta, M.; Agrawal, U.; Vyas, S. P. Nanocarrier-Based Topical Drug Delivery for the Treatment of Skin Diseases. *Expert Opin. Drug Deliv.* **2012**, *9* (7), 783–804.
(92) Prow, T. W.; Grice, J. E.; Lin, L. L.; Faye, R.; Butler, M.; Becker, W.; Wurm, E. M. T.; Yoong, C.; Robertson, T. A.; Soyer, H. P.; Roberts, M. S. Nanoparticles and Microparticles for Skin Drug Delivery. *Adv. Drug Deliv. Rev.* **2011**, *63* (6), 470–491.
(93) Liang, X. W.; Xu, Z. P.; Grice, J.; Zvyagin, A.; Roberts, M.; Liu, X. Penetration of Nanoparticles into Human Skin. *Curret Pharm. Des.* **2013**, *19*, 6353–6366.
(94) Baroli, B.; Ennas, M. G.; Loffredo, F.; Isola, M.; Pinna, R.; Arturo López-Quintela, M. Penetration of Metallic Nanoparticles in Human Full-Thickness Skin. *J. Invest. Dermatol.* **2007**, *127* (7), 1701–1712.
(95) Otberg, N.; Richter, H.; Schaefer, H.; Blume-Peytavi, U.; Sterry, W.; Lademann, J. Variations of Hair Follicle Size and Distribution in Different Body Sites. *J. Invest. Dermatol.* **2004**, *122* (1), 14–19.
(96) Roberts, M. S.; Mohammed, Y.; Pastore, M. N.; Namjoshi, S.; Yousef, S.; Alinaghi, A.; Haridass, I. N.; Abd, E.; Leite-Silva, V. R.; Benson, H. A. E.; Grice, J. E. Topical and Cutaneous Delivery Using Nanosystems. *J. Control. Release* **2017**, *247*, 86–105.
(97) Romero, E. L.; Morilla, M. J. Highly Deformable and Highly Fluid Vesicles as Potential Drug Delivery Systems: Theoretical and Practical Considerations. *Int. J. Nanomedicine* **2013**, *8*, 3171–3186.
(98) Larese Filon, F.; Mauro, M.; Adami, G.; Bovenzi, M.; Crosera, M. Nanoparticles Skin Absorption: New Aspects for a Safety Profile Evaluation. *Regul. Toxicol. Pharmacol.* **2015**, *72*, 310–322.
(99) Ruela, A. L. M.; Perissinato, A. G.; Lino, M. E. de S.; Mudrik, P. S.; Pereira, G. R. Evaluation of Skin Absorption of Drugs from Topical and Transdermal Formulations. *Brazilian J. Pharm. Sci.* **2016**, *52* (3), 527–544.
(100) Markus, J.; Yaxi, H.; Soshnikova, V.; Perez, E. Z. J.; Mathiyalagan, R.; Kim, Y.-J.; Yang, D. C. Applications of Flower-Shaped Polymer-ZnO Nanocomposites for Topical Delivery of Dendropanax Morbifera Extract and Ginsenoside Rh2. In *International Conference and Exhibition on Nanomedicine and Drug Delivery*; Osaka, Japan, 2017.
(101) Huang, X.; Wang, X.; Wang, S.; Yang, J.; Zhong, L.; Pan, J. UV and Dark-Triggered Repetitive Release and Encapsulation of Benzophenone-3 from Biocompatible ZnO Nanoparticles Potential for Skin Protection. *Nanoscale* **2013**, *5*, 5596–5601.

(102) Sonia, S. S.; Linda Jeeva Kumari, L. J. K. H.; Ruckmani, R. K.; Sivakumar, S. M. Antimicrobial and Antioxidant Potentials of Biosynthesized Colloidal Zinc Oxide Nanoparticles for a Fortified Cold Cream Formulation: A Potent Nanocosmeceutical Application. *Mater. Sci. Eng. C* **2017**, *79*, 581–589.
(103) Wiegand, C.; Hipler, U.; Boldt, S.; Strehle, J. Skin-Protective Effects of a Zinc Oxide- Functionalized Textile and Its Relevance for Atopic Dermatitis. **2013**, 115–121.
(104) Boateng, G.; Matthews, J.; Stevens, K.; Eccleston, H. Wound Healing Dressings and Drug Delivery Systems: A Review. *J. Pharm. Sci.* **2010**, *99* (10), 4215–4227.
(105) Dhivyaa, S.; Padma, V. V.; Santhini, E. Wound Dressings – a Review. *Biomedicine* **2015**, *5* (4), 24–28.
(106) Martin, P. Wound Healing--Aiming for Perfect Skin Regeneration. *Science (80-.).* **1997**, *276* (5309), 75–81.
(107) Ueno, H. Topical Formulations and Wound Healing Applications of Chitosan 2 . Topical Findings of Healing with Chitosan at Early Phase of Experimental Open Skin Wound. **2001**, *52*, 105–115.
(108) Zafar, R.; Zia, K. M.; Tabasum, S.; Jabeen, F.; Noreen, A.; Zuber, M. Polysaccharide Based Bionanocomposites, Properties and Applications: A Review. *Int. J. Biol. Macromol.* **2016**, *92*, 1012–1024.
(109) Agren, M. S.; Mirastschijski, U. The Release of Zinc Ions from and Cytocompatibility of Two Zinc Oxide Dressings. *J. Wound Care* **2004**, *13* (9), 367–369.
(110) Lansdown, A. B. G.; Mirastschijski, U.; Stubbs, N.; Scanlon, E.; Ågren, M. S. Zinc in Wound Healing: Theoretical, Experimental, and Clinical Aspects. *Wound Repair Regen.* **2007**, *15* (1), 2–16.
(111) Díez-Pascual, A. M.; Díez-Vicente, A. L. Wound Healing Bionanocomposites Based on Castor Oil Polymeric Films Reinforced with Chitosan-Modified ZnO Nanoparticles. *Biomacromolecules* **2015**, *16* (9), 2631–2644.
(112) Jayakumar, R.; Prabaharan, M.; Sudheesh Kumar, P. T.; Nair, S. V.; Tamura, H. Biomaterials Based on Chitin and Chitosan in Wound Dressing Applications. *Biotechnol. Adv.* **2011**, *29* (3), 322–337.
(113) Vicentini, D. S.; Smania, A.; Laranjeira, M. C. M. Chitosan/poly (Vinyl Alcohol) Films Containing ZnO Nanoparticles and Plasticizers. *Mater. Sci. Eng. C* **2010**, *30* (4), 503–508.
(114) Kumar, P. T. S. Flexible and Microporous Chitosan Hydrogel/Nano ZnO Composite Bandages for Wound Dressing: In Vitro and In Vivo Evaluation. *ACS Appl. Mater. Interfaces* **2012**, *4* (5), 2618–2629.
(115) Kumar, P. T. S. Synthesis and Biological Evaluation of Chitin Hydrogel/Nano ZnO Composite Bandage as Antibacterial Wound

Dressing. *J. Biomed. Nanotechnol.* **2012**, *8* (6), 891–900.
(116) Yadollahi, M.; Gholamali, I.; Namazi, H.; Aghazadeh, M. Synthesis and Characterization of Antibacterial Carboxymethyl cellulose/ZnO Nanocomposite Hydrogels. *Int. J. Biol. Macromol.* **2015**, *74*, 136–141.
(117) Shalumon, K. T.; Anulekha, K. H.; Nair, S. V; Nair, S. V; Chennazhi, K. P.; Jayakumar, R. Sodium Alginate/poly(vinyl Alcohol)/nano ZnO Composite Nanofibers for Antibacterial Wound Dressings. *Int. J. Biol. Macromol.* **2011**, *49* (3), 247–254.
(118) Liu, Y.; Kim, H. Il. Characterization and Antibacterial Properties of Genipin-Crosslinked Chitosan/poly(ethylene glycol)/ZnO/Ag Nanocomposites. *Carbohydr. Polym.* **2012**, *89* (1), 111–116.
(119) Staneva, D.; Atanasova, D.; Vasileva-tonkova, E.; Lukanova, V.; Grabchev, I. Applied Surface Science A Cotton Fabric Modified with a Hydrogel Containing ZnO Nanoparticles . Preparation and Properties Study. *Appl. Surf. Sci.* **2015**, *345*, 72–80.
(120) Meshram, J. V.; Pawar, S. H. Immobilization of Zinc Oxide Nanoparticles in Chitosan-Gelatin Composite Membrane for Antibacterial Activity. *Int. J. Pharma Bio Sci.* **2015**, *6* (3), P152–P161.
(121) Păunica-Panea, G. New Collagen-Dextran-Zinc Oxide Composites for Wound Dressing. *J. Nanomater.* **2016**, *2016*.
(122) Raguvaran, R.; Manuja, B. K.; Chopra, M.; Thakur, R.; Anand, T.; Kalia, A.; Manuja, A. Sodium Alginate and Gum Acacia Hydrogels of ZnO Nanoparticles Show Wound Healing Effect on Fibroblast Cells. *Int. J. Biol. Macromol.* **2017**, *96*, 185–191.
(123) Shokri, N.; Goodarzi, M. T.; Javar, H. A.; Soltani, Y. Zinc Oxide Nanoparticles as Skin Permeation Enhancer for Solvents and Surfactants. **2014**, *13* (2), 40–44.
(124) Shokri, N.; Javar, H. A. Zinc Oxide Nanoparticles as Skin Permeation Enhancer for Solvents and Surfactants. **2014**, *13* (3), 85–91.
(125) N., S.; H.A., J. Comparison of Calcium Phosphate and Zinc Oxide Nanoparticles as Dermal Penetration Enhancers for Albumin. *Indian J. Pharm. Sci.* **2015**, *77* (6), 694–704.
(126) Gutiérrez-Hernández, J. M.; Escalante, A.; Murillo-Vázquez, R. N.; Delgado, E.; González, F. J.; Toríz, G. Use of Agave Tequilana-Lignin and Zinc Oxide Nanoparticles for Skin Photoprotection. *J. Photochem. Photobiol. B Biol.* **2016**, *163*, 156–161.
(127) Kathawala, M. H.; Ng, K. W.; Loo, S. C. J. TiO2 Nanoparticles Alleviate Toxicity by Reducing Free Zn2+ Ion in Human Primary Epidermal Keratinocytes Exposed to ZnO Nanoparticles. *J. Nanoparticle Res.* **2015**, *17* (6), 1–17.
(128) Detoni, C. B.; Coradini, K.; Back, P.; Oliveira, C. M.; Andrade, D. F.; Beck, R. C. R.; Pohlmann, A. R.; Guterres, S. S. Penetration, Photo-

Reactivity and Photoprotective Properties of Nanosized ZnO. *Photochem. Photobiol. Sci.* **2014**, *13* (9), 1253–1260.

(129) Ryu, H. J.; Seo, M. Y.; Jung, S. K.; Maeng, E. H.; Lee, S.-Y.; Jang, D.-H.; Lee, T.-J.; Jo, K.-Y.; Kim, Y.-R.; Cho, K.-B.; Kim, M.-K.; Lee, B. J.; Son, S. W. Zinc Oxide Nanoparticles: A 90-Day Repeated-Dose Dermal Toxicity Study in Rats. *Int J Nanomedicine* **2014**, *9* (2), 137–144.

(130) Darvin, M. E.; König, K.; Kellner-Hoefer, M.; Breunig, H. G.; Werncke, W.; Meinke, M. C.; Patzelt, A.; Sterry, W.; Lademann, J. Safety Assessment by Multiphoton Fluorescence/second Harmonic Generation/hyper-Rayleigh Scattering Tomography of ZnO Nanoparticles Used in Cosmetic Products. *Skin Pharmacol. Physiol.* **2012**, *25* (4), 219–226.

(131) Monteiro-Riviere, N. A.; Wiench, K.; Landsiedel, R.; Schulte, S.; Inman, A. O.; Riviere, J. E. Safety Evaluation of Sunscreen Formulations Containing Titanium Dioxide and Zinc Oxide Nanoparticles in UVB Sunburned Skin: An In Vitro and in Vivo Study. *Toxicol. Sci.* **2011**, *123* (1), 264–280.

(132) Sonia, S. S.; Linda Jeeva Kumari, L. J. K. H.; Ruckmani, R. K.; Sivakumar, S. M. Antimicrobial and Antioxidant Potentials of Biosynthesized Colloidal Zinc Oxide Nanoparticles for a Fortified Cold Cream Formulation: A Potent Nanocosmeceutical Application. *Mater. Sci. Eng. C* **2017**, *79*, 581–589.

(133) Georgeta, P.; Ficai, A.; Marin, M. M.; Albu, G.; Constantin, V. D.; Dinu-pîrvu, C.; Vuluga, Z.; Corobea, M. C.; Ghica, M. V. New Collagen-Dextran-Zinc Oxide Composites for. **2016**, *2016*.

(134) Cross, S. E.; Innes, B.; Roberts, M. S.; Tsuzuki, T.; Robertson, T. A.; McCormick, P. Human Skin Penetration of Sunscreen Nanoparticles: In-Vitro Assessment of a Novel Micronized Zinc Oxide Formulation. *Skin Pharmacol. Physiol.* **2007**, *20* (3), 148–154.

(135) Kim, S. Y.; Jeong, S. H.; Lee, E. Y.; Park, Y. H.; Bae, H. C.; Jang, Y. S.; Maeng, E. H.; Kim, M. K.; Son, S. W. Skin Absorption Potential of ZnO Nanoparticles. *Toxicol. Environ. Health Sci.* **2011**, *3* (4), 258–261.

(136) Leite-Silva, V. R.; Lamer, M. Le; Sanchez, W. Y.; Liu, D. C.; Sanchez, W. H.; Morrow, I.; Martin, D.; Silva, H. D. T.; Prow, T. W.; Grice, J. E.; Roberts, M. S. The Effect of Formulation on the Penetration of Coated and Uncoated Zinc Oxide Nanoparticles into the Viable Epidermis of Human Skin in Vivo. *Eur. J. Pharm. Biopharm.* **2013**, *84* (2), 297–308.

(137) Holmes, A. M.; Song, Z.; Moghimi, H. R.; Roberts, M. S. Relative Penetration of Zinc Oxide and Zinc Ions into Human Skin after Application of Different Zinc Oxide Formulations. *ACS Nano* **2016**, *10*

(2), 1810–1819.
(138) Gulson, B.; Mccall, M.; Korsch, M.; Gomez, L.; Casey, P.; Oytam, Y.; Taylor, A.; Mcculloch, M.; Trotter, J.; Kinsley, L.; Greenoak, G. Small Amounts of Zinc from Zinc Oxide Particles in Sunscreens Applied Outdoors Are Absorbed through Human Skin. *Toxicol. Sci.* **2010**, *118* (1), 140–149.
(139) Wang, S.; Zhang, G.; Meng, H.; Li, L. Effect of Exercise-Induced Sweating on Facial Sebum, Stratum Corneum Hydration, and Skin Surface Ph in Normal Population. *Ski. Res. Technol.* **2013**, *19* (1), 1–6.
(140) Ng, C. T.; Yong, L. Q.; Hande, M. P.; Ong, C. N.; Yu, L. E.; Bay, B. H.; Baeg, G. H. Zinc Oxide Nanoparticles Exhibit Cytotoxicity and Genotoxicity through Oxidative Stress Responses in Human Lung Fibroblasts and Drosophila Melanogaster. *Int. J. Nanomedicine* **2017**, *12*, 1621–1637.
(141) Kocbek, P.; Teskač, K.; Kreft, M. E.; Kristl, J. Toxicological Aspects of Long-Term Treatment of Keratinocytes with ZnO and TiO2 Nanoparticles. *Small* **2010**, *6* (17), 1908–1917.
(142) Vinardell, M.; Llanas, H.; Marics, L.; Mitjans, M. In Vitro Comparative Skin Irritation Induced by Nano and Non-Nano Zinc Oxide. *Nanomaterials* **2017**, *7* (3), 56.

Chapter 2

Drug delivery goes supercritical

Part of the information reported in this chapter has been previously published in Leone *et al*. **2018**, *Journal of Cleaner Production, 172, 1433-1439* [1].

2.1 Introduction

Nowadays the huge consumption of organic solvents by the pharmaceutical industries is becoming a well-known issue [2] and each year a high amount of waste is produced [3]. Two main issues derive from the use of organic solvents in pharmaceutical technologies: (i) the toxicity of residual solvents in the final products and (ii) the environmental impact [3]. Therefore, in the last years even Life Cycle Assessment, which has been traditionally reserved to large scale continuous chemical and petrolchemical processes, has started to be applied to small scale batch pharmaceutical processes [4].

The synthesis of Active Pharmaceutical Ingredients (APIs) is commonly considered the main step in which organic solvents are employed. Nevertheless, other sources of organic solvent wastes occur in the production of drug delivery systems, such as the synthesis of the carrier and the API loading [5]. Green and sustainable chemical processes are then highly desired to develop organic-solvent-free production of drug-delivery devices.

In the last decade, supercritical fluid technology has been emerging as an alternative to conventional drug loading techniques, such as the adsorption or impregnation from an organic solvent solution [6]. Supercritical carbon dioxide ($scCO_2$) is the most used supercritical solvent because of its unique chemical and physical properties.

Since in this PhD research project, the $scCO_2$ technology has been studied as an innovative approach to perform the drug impregnation of ZnO nanostructures, this chapter aims at highlighting the fundamental properties of the $scCO_2$ in order to understand the mechanism at the basis of the $scCO_2$-mediated drug impregnation.

2.2 Supercritical carbon dioxide: generalities and properties

Supercritical fluids are defined *as substances the pressure and temperature of which are raised above their critical values* [7]. *Once above this critical point, they exist as a single phase with unique properties such as liquid-like densities and, hence, solvating characteristics that are similar to those of liquids, yet with mass transfer properties similar to gases.*

$ScCO_2$ is the most commonly used supercritical fluid in drug delivery applications for a number of reasons. CO_2 is an odorless, colorless, highly pure, safe, cost effective, nontoxic, nonflammable and recyclable gas with a relatively low critical point (T_c = 31°C; Pc = 74 bar). Above the critical point, CO_2 is considered to be in its supercritical state. In Figure 2.1 the different phases of carbon dioxide are plotted in a pressure–temperature phase diagram. CO_2 can exist under solid, liquid or gaseous phases and any modification of state can occur by changing pressure and temperature. Following the liquid–gas phase boundary, if the pressure and temperature are increased, the density of the liquid phase is reduced and the density of the vapor is rised. At a point named the "*critical point*", the two densities become equal and the liquid and vapor phases combine into a single phase.

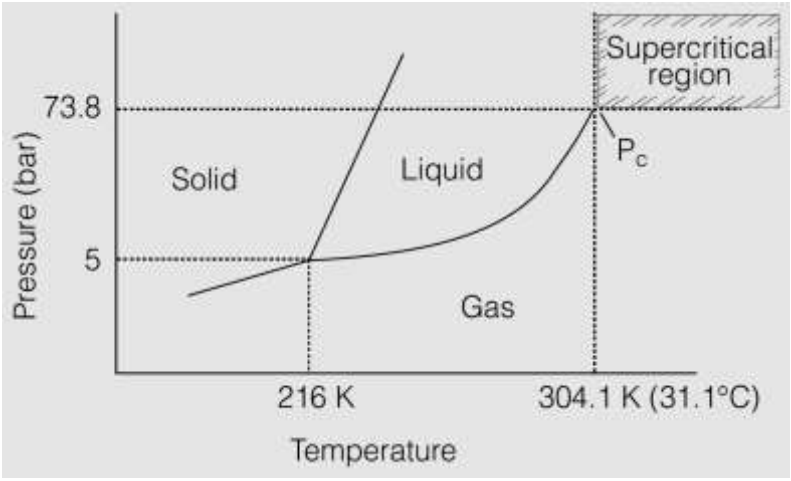

Figure 2.1 Phase diagram of carbon dioxide[7].

As all supercritical fluids, $scCO_2$ has physical properties (density, diffusivity, viscosity) in between those of a gas and a liquid; in particular, it has a liquid-like solvent power and gas-like diffusivity [8]. The density of $scCO_2$ is close to that at its liquid state, which is in between 0.2 and 1.5 g/cm^3, and its transport properties are close to those at its gas state [9]. $ScCO_2$ is generally considered as a "tunable" solvent. In fact, at pressures and temperatures not too far from its critical point, it has a high compressibility; therefore its density and hence its solvent power are easily adjustable over a wide range with a minimal change in temperature or pressure. For instance, at temperatures in the range from 25 to 60 °C, the density evolves largely with a slight change of pressure [9].
For the above-cited reasons, CO_2 can then be considered an ideal substitute for many organic solvents thanks to its tunable solvent power and also because it simplifies the problem of solvent residues since it is gaseous at ambient conditions [10].

Advantages and drawbacks

On one hand, $scCO_2$ offers remarkable advantages, such as its being readily available, cheap, non-flammable and non-toxic. Moreover, it is considered a green and highly versatile technology, that can potentially be used for the production of consumables, such as pharmaceutical and food products, as well

as for numerous processes, such as extractions, nanoparticle production and modification and polymer processing [6,11].

The $scCO_2$ technology offers advantageous operating conditions, such as rapid one step processing and moderate operating temperature, which is useful in case of thermo-sensitive materials. At the end of the supercritical technology process, no residual organic solvent is present, compared to the conventional techniques.

On the other hand, the $scCO_2$ presents some drawbacks, related to its physicochemical properties and to the required experimental set up. For instance, one of the most limiting factor is represented by the scarce ability of $scCO_2$ in dissolving polar and ionic species, because it is a linear molecule with no net dipole moment. Consequently, it is not applicable for processing of all compounds [6,9]. However, the addition of a cosolvent can increase the polarity of CO_2 , so overcoming this drawback. For this purpose, ethanol is one of the most used cosolvents [9].

Furthermore, the elevated pressure required and high maintenance costs can represent a limitation in the use of the $scCO_2$ technology [6].

Applications of the $scCO_2$ technology

Traditional applications of $scCO_2$ include extraction, drying and cleaning [12]. Currently, the large-scale extraction through $scCO_2$ is widely used in the food industry for the decaffeination of coffee or extraction of hops. Briefly, the material to be extracted is placed in a high pressure vessel, where temperature and pressure are regulated above the critical point. The circulating $scCO_2$ can extract the desired compounds from the solid material, which are collected in another vessel, where they can be separated from the gas CO_2 by reducing the pressure. Furthermore, $scCO_2$ is also used in drying and cleaning from organic residuals. Due to the zero surface tension of $scCO_2$, it can reach the valley of the narrow gaps of the material to be cleaned, and completely remove the organic residuals by dissolving them [13]. The $scCO_2$ technology is also widely used in the materials processing [12,14]. For instance, it can be used in the micronization of powder materials (i.e. drugs) [15], processing of 3D aerogels [16] and coatings [17,18], and exfoliation and intercalation of layered materials [12]. As far as the applications of $scCO_2$ technology in the pharmaceutical field are concerned, it plays a key role in a wide range of production and processing

processes. Particularly, $scCO_2$ has been investigated in the design of micro/nanosized drug delivery systems, in the development of many techniques to achieved the enhancement of drug solubilization and as an innovative method to perform the drug impregnation of different materials [8,19]. The mechanism at the basis of the $scCO_2$-mediated drug impregnation is discussed in the following paragraph.

2.3 Drug impregnation through supercritical Carbon Dioxide

In the pharmaceutical field, $scCO_2$ finds application in many processes, among which the most investigated are the drug micronization and particle formation and the incorporation of drug in matrices. In particular, the $scCO_2$ - based technology can represent an alternative and innovative method to load an Active Pharmaceutical Ingredient (API) into a support, in order to obtain a drug delivery system

The impregnation process is generally considered as a batch process. Figure 2.2 reports a schematic representation of a possible experimental apparatus required to perform the drug impregnation through $scCO_2$.

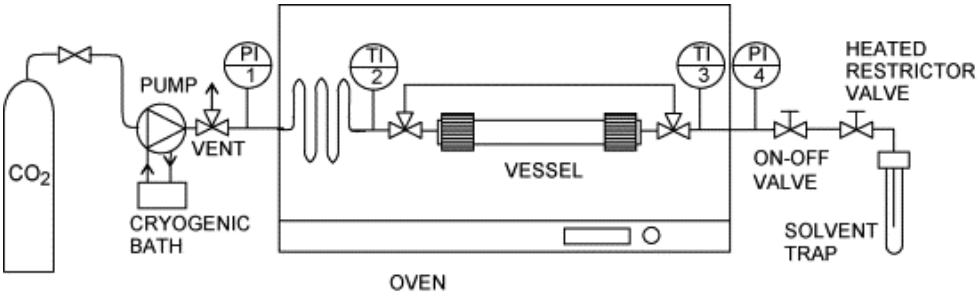

Figure 2.2 Schematic representation of the experimental apparatus in which the $scCO_2$ – mediated drug impregnation can be performed [20].

Traditionally, the experimental set-up consists in a vessel, in which the API and the material are simultaneously placed. The temperature is controlled and the CO_2 is pumped into the vessel until the desired pressure is reached. The impregnation can be carried on in static or stirring mode. The basic mechanism of $scCO_2$-mediated drug impregnation process is based on the density and diffusivity properties of $scCO_2$. In fact, thanks to their combination, it is possible to achieve the impregnation of a material with a solute (i.e. the drug), when placed in the same vessel and subjected to $scCO_2$. In particular, due to its high density, $scCO_2$ possesses a *good solvent power*, which allows the solubilization of several compounds to be achieved. Moreover, the high diffusivity of the $scCO_2$ results in a *high diffusion* rate of the supercritical solution into any support placed in the vessel.

Briefly, the impregnation process involves three components, the CO_2 as the solvent, the API and the material, and can be summarized in three different phases [9], as schematically represented in Figure 2.3:

1. The dissolution of the solute into $scCO_2$;

2. The contact between the [CO_2 + solute] solution and the material;

3. The depressurization stage.

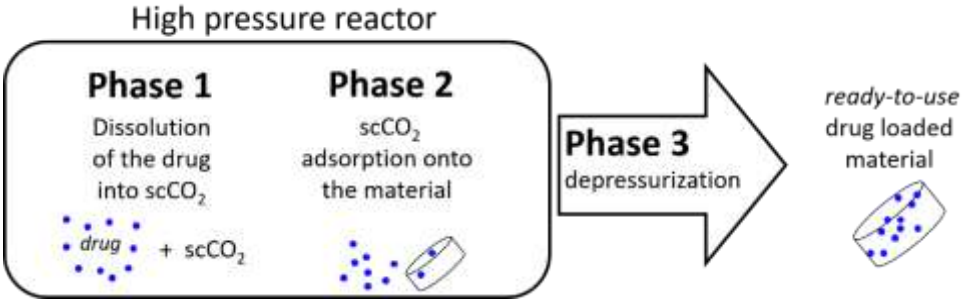

Figure 2.3 Schematic representation of the three steps of the $scCO_2$ mediated drug loading process. Adapted from [9]

When the $scCO_2$ is selected as the solvent to perform the loading of a drug into a material, it is fundamental to consider some crucial aspects. Since CO_2 is a not- polar molecule [11], $scCO_2$ represents a good solvent for nonpolar and low molecular weight solutes, while a poor one for the hydrophilic, polar molecules or compounds that have a high molecular weight [21]. After the drug solubilization in $scCO_2$, the loading of the drug into the material begins, through the diffusion of the solution into the material matrix. The dissolution of the API (Fig. 2.3, phase 1) and the impregnation of the matrix (Fig. 2.3, phase 1) are performed simultaneously, at the same conditions of temperature and pressure. At the end of the process, the system is depressurized and the CO_2 return gaseous. At the end of the $scCO_2$-mediated impregnation process, the drug-loaded material is recovered. It is worth noticing that the obtained drug loaded material results free of any solvent, so being it a ready-to-use drug delivery system, that does not require any other purification process.

The API-material interaction after the $scCO_2$ impregnation can be classified into two opposite types. The former consists in a simple deposition mechanism, that is caused by the scarce interaction between the API and the material. It can also lead to crystallization of the API phenomena. The latter is

based on a stronger affinity between the API and the material, which occurs through Van der Waals or H-bonding interactions and can lead to high drug loading [9,22].

The $scCO_2$-mediated drug impregnation is regulated by both thermodynamic and kinetic parameters. Among the most influencing thermodynamic properties, temperature and pressure play a key role in the loading of an API into a material by mean of $scCO_2$ [23]. Particularly, it has been demonstrated that temperature and pressure can increase, decrease or not affect the drug loading, which depends on the API and material that are being considered [9]. Nevertheless, the analysis of the literature suggests that increasing the temperature in isobaric condition is a good strategy to enhance the drug loading [24–27]. Similarly, the increase of the pressure was observed to improve the drug loading in isothermal conditions through the increase of the solubility of the drug in CO_2 and the CO_2 sorption in the material [26,28–30]. Other parameters such as contact time and diffusivity have also to be taken into account [9]. For instance, it has been demonstrated that the $scCO_2$ can improve the diffusion of the drug into a polymer matrix through the "molecular lubricant" effect. The facilitation of the drug diffusion into the matrix, results in a possible enhancement of the impregnation process, with respect to traditional soaking techniques.

Advantages of the $scCO_2$ drug impregnation compared to conventional drug loading techniques

As far as the advantages of the $scCO_2$-mediated drug impregnation are concerned, interesting observations can be drawn in comparison it with the other drug loading techniques, i.e. the adsorption from solution. Going through the literature, the adsorption from solution method results to be the most used drug impregnation strategy. This method consists in incubating the carrier with a concentrated drug solution [31]. Briefly, the drug is dissolved in a suitable solvent and the material is then dispersed in this solution. The adsorption from solution method can last several hours, during which the drug molecules are absorbed into the inner structure of the material. At the end of the process, the impregnated material requires several separation and purification steps to be recovered from the not-entrapped drug solution. These stages normally consist in several centrifugation processes, during which the drug-loaded carrier has

to be repeatedly washed with fresh solvent, followed by a filtration and drying phase to remove the remaining solvent.

On one hand, the adsorption from solution method results easy-to-perform, reproducible and does not require any particular experimental set up. Furthermore, it is usually performed at room temperature, which is suitable for the loading of thermo-sensitive molecules. On the other hand, several drawbacks emerge from the applications of this approach. First, relatively high concentrations of drug in the initial solution are needed to achieve high loading percentages into the carrier. Second, the repeated purification and separation steps result to be time-consuming, and lead to high amounts of wasted drug in the filtration/centrifugation process. In addition, the most challenging issue results to be the huge amount of solvent that is required to perform the adsorption from solution method. This is particularly alarming if we consider the high number of existing poorly-water soluble drugs, which require to be dissolved in organic solvents [32]. As mentioned above, the use of organic solvents in pharmaceutical technologies leads to both health issues, which are related to the toxicity of residual solvents in the final products, and of course to a negative environmental impact.

The $scCO_2$ technology can be an innovative alternative to overcome all these disadvantages:

- it is considered a green drug impregnation method; $scCO_2$ is readily available, cheap, non-flammable and recyclable. All these properties make the $scCO_2$ technology an environment-friendly approach. Moreover, $scCO_2$ is not-toxic, thus it is particularly suitable for the processing of pharmaceuticals products, such as innovative drug delivery system, without any health issue;
- $scCO_2$ possesses a not polar profile, so resulting a good solvent for poorly-water soluble drugs. This represents an outstanding advantage, because of the possibility to completely replace the use of organic solvents in the processing of these not polar molecules;
- at the end of the $scCO_2$ - mediated drug impregnation a ready-to-use drug loaded material is obtained that does not require any purification process and is free from any organic solvents. This allows the operator to save time and avoid producing huge amounts of waste solvents;
- $scCO_2$ - mediated drug impregnation offers the possibility to tailor the operating parameters, such as temperature, pressure and time, on the basis of the selected API [9]. This permits a better API-material

interaction to be obtained, with the API in amorphous state, which improves its dissolution profile and, consequently, its bioavailability.

Notwithstanding the above reported remarkable advantages, some drawbacks in the use of this innovative technology could emerge. As aforementioned, for instance, one of the most limiting factor is represented by the scarce ability of $scCO_2$ to dissolve polar and ionic species, since it is a linear molecule with no net dipole moment. Nevertheless, this limit can be overcome using a cosolvent, such as the ethanol, to increase the polarity of CO_2 [6,9]. Furthermore, the elevated pressure required and the high maintenance cost can represent a limitation in the use of $scCO_2$ technology [6].

2.4 ZnO and $scCO_2$-assisted drug impregnation

Due to its unique features, drug incorporation through $scCO_2$ was proposed in different research areas, which involve several materials. The drug loading of polymers by $scCO_2$ assisted impregnation was widely reviewed [9]. Furthermore the use of the $scCO_2$ processing has been investigated in the preparation of drug-cyclodextrin inclusion complexes [33,34]. A few works can also be found in the field of porous materials, such as the inclusion of active pharmaceutical ingredients in ordered mesoporous silica by $scCO_2$ impregnation [35–38]. Nevertheless, from a careful analysis of the literature, it has emerged that any research work was focused on the use of the $scCO_2$ technology to load APIs into ZnO based drug delivery systems, despite the growing importance of this material in this field.

As aforementioned, this PhD thesis aimed at studying nanostructured ZnO (NsZnO) to develop innovative drug carriers for future dermatological applications. In this framework, the $scCO_2$ technology was selected as an innovative approach to perform the drug impregnation into NsZnO. To the best of our knowledge, the scientific investigation described in this thesis represents the first study about the loading of drugs on NsZnO by means of $scCO_2$ [1]. In fact, even though a few research works report the combination of $scCO_2$ and ZnO-based materials, this involves applications that are different from the API loading into delivery systems. For instance, supercritical CO_2-assisted deposition processes [39–43] and synthesis processes are among the most investigated $scCO_2$ applications that involve ZnO [44–50].

2.4.1 Models drugs

The aim of this section is to offer a general overview about the two model drugs used in this PhD thesis. The drug properties as well as previous experiments with the $scCO_2$ are briefly reported.

Clotrimazole

Clotrimazole (CTZ) is a broad-spectrum antimycotic drug that is in widespread use for the treatment of *Candida albicans* and other fungal infections [51].

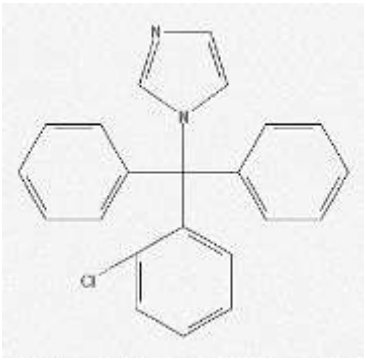

Figure 2.4 Clotrimazole chemical structure (1-[(2-chlorophenyl) diphenylmethyl]-1H-imidazole). Molecular formula: $C_{22}H_{17}ClN_2$. Molecular weight: 344,8 g/mol [52]

It possesses a peculiar chemical structure (Figure. 1), since it contains four aromatic rings bonded to a tetrahedral (sp^3 hybridized) carbon atom, causing a highly steric encumbrance on this atom. One of the aromatic groups is an imidazole ring, principally involved in many biological reactions. CTZ is a typical choice for the treatment of several skin infections caused by fungi, such as *tinea pedis*, that is well known as athlete's foot condition. Doubtless, the most known use of CTZ is in the topical treatment of vulvovaginal and oropharyngeal candidiasis, mainly caused by *Candida albicans*. In Europe CTZ is available in topical cream and pessary formulations, under a variety of trade names. For the treatment of fungal skin infections, CTZ is usually formulated as a 1% cream, lotion, spray or solution. When addressed to the vaginal area, the CTZ concentration can increase up to 2 or 10% [51]. According

to its traditional use in conventional topical formulations, CTZ was chosen for future skin administration within this PhD project as a good model drug to be loaded into the NsZnO.

In the last decade, the use of CTZ in the pharmaceutical field has become increasingly important, due to its broad range of antimycotic activity. For this reason, the development of new approaches to formulate and deliver CTZ is playing a key role [51]. Despite different studies of innovative greener approaches to load many API molecules into a wide amount of carriers have been reported [5], scarce research has been focused on new organic-solvent-free routes for the loading of CTZ. Since the most significant limitation in the CTZ utilization is represented by its low water solubility (29.84 mg/mL)[52], CTZ is often used in association with a wide range of organic solvents, which are generally employed during the drug loading step of pharmaceutical delivery systems. It is worth noting and somehow alarming that dangerous solvents, such as methanol [53] and chloroform [54,55], are still considered in the CTZ loading step for the development of new delivery systems. According to the "ICH guideline Q3C (R6) on impurities: guideline for residual solvents", which has been emended by the European Medicines Agency [56], both chloroform and methanol are solvents that should be limited in the pharmaceutical products because of their inherent toxicity (class 2 of this classification). Moreover, methanol has also been classified as one of the top four solvents used in the pharmaceutical sector with a dangerous impact on the environment and on health [3].

For all the mentioned above reasons, CTZ represents a good drug candidate for the $scCO_2$ assisted impregnation. Previous studies of Gignone and colleagues [38,57] reported its incorporation by means of $scCO_2$ into ordered mesoporous silica, and focused their research on the effect of the process conditions, such as time and pressure, on the incorporated amount. To the best of our knowledge no other examples of incorporation of CTZ into a porous solid matrix through $scCO_2$ is available in the literature.

Ibuprofen

Ibuprofen (IBU) is one of the most commonly used and most frequently prescribed not steroidal anti-inflammatory drug (NSAID) due to its prominent analgesic and antipyretic role [58].

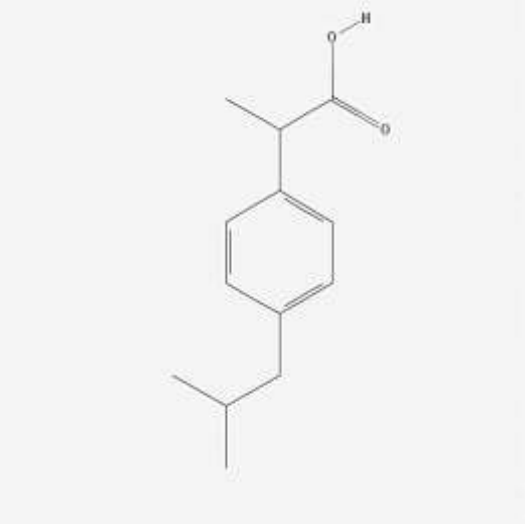

Figure 2.5 Ibuprofen chemical structure ((2RS)-1[4-(2-methyl propyl) phenyl] propionic acid). Molecular formula: $C_{13}H_{18}O_2$. Molecular weight: 206.131 g/mol. [59]

Among the conventional routes of IBU administration, the oral one in the form of tablets, capsules, suspensions and solutions is the most common. Moreover, the topical application of IBU offers many alternative dosage forms (cream, gels, foam, spray solutions) for the management of musculoskeletal, joint and soft tissue injury pain. [60].

In the last years, an alternative use of IBU that involves its application in the treatment of wounds has attracted attention in the biomedical field. In material science, several research works have been addressed to the development of innovative wound dressings, able to deliver IBU to the wound, which overcomes the main issues related to the wound healing process [61]. For instance, it has been demonstrated that painful wounds could take longer time to heal, so leading to a lack of compliance by the patients. IBU and other NSAIDs are excellent pain-reducing agents and very small doses of IBU can

have an excellent local effect on the superficial wound compartment, without detectable systemic levels [62].

This alternative use of IBU has been considered within this PhD thesis, where the IBU loading into ZnO nanostructures has been studied. Future applications of the IBU-loaded NsZnO developed in this research work could involve the combination of these drug delivery systems into composite dressings for wound healing treatment.

A second crucial aspect considered in the choice of IBU as model drug in this thesis, concerns its solubility. It is worth noting that IBU, as the above described CTZ, displays a low solubility in water (0.021 mg/ml) [59]. Due to its higher affinity for alcohols, the development of IBU delivery systems has often required the use of organic solvents, such as ethanol [63–65], methanol [66,67] and pentane [68]. It has already been highlighted how this choice can lead to a dangerous impact on the environment and on health, due to the possible presence of organic solvents residuals in the final drug carrier [56].

To overcome this limitation, the use of $scCO_2$ technology has been widely investigated to load IBU into several materials. Cyclodextrins [69–72], silica [73,74] and polymers [75–78] resulted to be among the most evaluated supports, which evidences the versatile role of this green solvent. To the best of our knowledge, the IBU loading into ZnO nanostructures by means of $scCO_2$ have not been reported yet.

The work of Shokri and colleagues is the only one that reports the combination between IBU and ZnO. Nevertheless, the aim of their research work was not the loading of the API inside the material, but the use of ZnO nanostructures as skin penetration enhancers in topical formulations [79]. In that case IBU and ZnO were simultaneously administered to the skin, but not combined in a drug delivery system.

2.5 Conclusions

Thanks to its outstanding properties, the $scCO_2$ technology has attracted growing attention in many fields of application. In the formulation of innovative drug delivery systems, the $scCO_2$ assisted drug impregnation is considered a valid alternative to the conventional drug loading methods. In fact, the $scCO_2$ technology offers several advantages, such as its being a green drug impregnation approach, safe for both environment and the consumer health. Moreover, it represents a good solvent for poorly-water soluble drugs, so replacing the use of organic solvents. Through the $scCO_2$ - mediated drug impregnation ready-to-use drug delivery systems can be produced, without any further purification process and free from organic solvents residues. The API loading mediated by $scCO_2$ technology has been investigated with different materials, from polymers to cyclodextrins, which demonstrates the versatility of this approach. Nevertheless, the supercritical impregnation of nanostructured ZnO has never been studied, despite the growing importance of this material as a drug delivery system. This PhD thesis is going to present the results obtained during the first investigations on the use of the $scCO_2$ assisted drug impregnation into different ZnO nanostructures, using clotrimazole and ibuprofen as model drugs.

2.6 References

(1) Leone, F.; Gignone, A.; Ronchetti, S.; Cavalli, R.; Manna, L.; Banchero, M.; Onida, B. A Green Organic-Solvent-Free Route to Prepare Nanostructured Zinc Oxide Carriers of Clotrimazole for Pharmaceutical Applications. *J. Clean. Prod.* **2018**, *172*, 1433–1439.

(2) Grodowska, K.; Parczewski, a. Organic Solvents in the Pharmaceutical Industry. *Acta Pol. Pharm.* **2010**, *67* (1), 3–12.

(3) Amado Alviz, P. L.; Alvarez, A. J. Comparative Life Cycle Assessment of the Use of an Ionic Liquid ([Bmim]Br) versus a Volatile Organic Solvent in the Production of Acetylsalicylic Acid. *J. Clean. Prod.* **2016**.

(4) Brunet, R.; Guillén-Gosálbez, G.; Jiménez, L. Combined Simulation-Optimization Methodology to Reduce the Environmental Impact of Pharmaceutical Processes: Application to the Production of Penicillin v. *J. Clean. Prod.* **2014**, *76*, 55–63.

(5) Li, M.; Lv, S.; Tang, Z.; Song, W.; Yu, H.; Sun, H.; Liu, H.; Chen, X. Polypeptide/Doxorubicin Hydrochloride Polymersomes Prepared Through Organic Solvent-Free Technique as a Smart Drug Delivery Platform. *Macromol. Biosci.* **2013**, *13* (9), 1150–1162.

(6) Girotra, P.; Singh, S. K.; Nagpal, K. Supercritical Fluid Technology : A Promising Approach in Pharmaceutical Research. *Pharm. Dev. Technol.* **2012**, *18* (1), 22–38.

(7) Ginty, P. J.; Whitaker, M. J.; Shakesheff, K. M.; Howdle, S. M. Drug Delivery Goes Supercritical. *Mater. Today* **2005**, *8* (8 SUPPL.), 42–48.

(8) Deshpande, P. B.; Kumar, G. Aravind Kumar, Averineni Ranjith Shavi, G. V.; Karthik, A.; Reddy, M. S.; Nayanabhirama, U. Supercritical Fluid Technology: Concepts and Pharmaceutical Applications. *PDA J Pharm Sci Technol* **2011**, *65* (3), 333–344.

(9) Champeau, M.; Thomassin, J.; Tassaing, T.; Jérôme, C. Drug Loading of Polymer Implants by Supercritical CO 2 Assisted Impregnation : A Review. *J. Control. Release* **2015**, *209*, 248–259.

(10) Pasquali, I.; Bettini, R. Are Pharmaceutics Really Going Supercritical? *Int. J. Pharm.* **2008**, *364* (2), 176–187.

(11) Peach, J.; Eastoe, J. Supercritical Carbon Dioxide : A Solvent like No Other. **2014**, 1878–1895.

(12) Zhang, X.; Heinonen, S.; Levänen, E. Applications of Supercritical Carbon Dioxide in Materials Processing and Synthesis. *RSC Adv.* **2014**, *4* (105), 61137–61152.

(13) Zhang, J.; Neoh, K. G.; Hu, X.; Kang, E. T. Mechanistic Insights into Response of Staphylococcus Aureus to Bioelectric Effect on Polypyrrole/chitosan Film. *Biomaterials* **2014**, *35* (27), 7690–7698.

(14) Cooper, A. I. Recent Developments in Materials Synthesis and Processing Using Supercritical CO2. *Adv. Mater.* **2001**, *13* (14), 1111–1114.
(15) Kerc, J.; Srcic, S.; Knez, Z.; Sencar-Bozic, P. Micronization of Drugs Using Supercritical Carbon Dioxide. *Int. J. Pharm.* **1999**, *182* (1), 33–39.
(16) Smirnova, I.; Gurikov, P. Aerogels in Chemical Engineering: Strategies toward Tailor-Made Aerogels. *Annu. Rev. Chem. Biomol. Eng.* **2017**, *8* (7), 307–334.
(17) Hay, J. N.; Khan, a. Review - Environmentally Friendly Coatings Using Carbon Dioxide as the Carrier Medium. *J. Mater. Sci.* **2002**, *37* (22), 4743–4752.
(18) Bose, S.; Bogner, R. H. Solventless Pharmaceutical Coating Processes: A Review. *Pharm. Dev. Technol.* **2007**, *12* (2), 115–131.
(19) Sekhon, B. S. Supercritical Fluid Technology: An Overview of Pharmaceutical Applications. *Int. J. PharmTech Res.* **2010**, *2* (1), 810–826.
(20) Banchero, M.; Manna, L.; Ronchetti, S.; Campanelli, P.; Ferri, A. Supercritical Solvent Impregnation of Piroxicam on PVP at Various Polymer Molecular Weights. *J. Supercrit. Fluids* **2009**, *49* (2), 271–278.
(21) Škerget, M.; Knez, Z.; Knez-Hrncic, M. Solubility of Solids in Sub-and Supercritical Fluids: A Review. *J. Chem. Eng. Data* **2011**, *56* (4), 694–719.
(22) Kazarian, S. G.; Martirosyan, G. G. Spectroscopy of Polymer/drug Formulations Processed with Supercritical Fluids: In Situ ATR-IR and Raman Study of Impregnation of Ibuprofen into PVP. *Int. J. Pharm.* **2002**, *232* (1–2), 81–90.
(23) Marizza, P.; Pontoni, L.; Rindzevicius, T.; Alopaeus, J. F.; Su, K.; Zeitler, J. A.; Keller, S. S.; Kikic, I.; Moneghini, M.; De Zordi, N.; Solinas, D.; Cortesi, A.; Boisen, A. Supercritical Impregnation of Polymer Matrices Spatially Confined in Microcontainers for Oral Drug Delivery: Effect of Temperature, Pressure and Time. *J. Supercrit. Fluids* **2016**, *107*, 145–152.
(24) Yoganathan, R.; Mammucari, R.; Foster, N. R. Impregnation of Ibuprofen into Polycaprolactone Using Supercritical Carbon Dioxide. *J. Phys. Conf. Ser.* **2010**, *215*.
(25) Masmoudi, Y.; Ben Azzouk, L.; Forzano, O.; Andre, J. M.; Badens, E. Supercritical Impregnation of Intraocular Lenses. *J. Supercrit. Fluids* **2011**, *60*, 98–105.
(26) Hussain, Y. A.; Grant, C. S. Ibuprofen Impregnation into Submicron Polymeric Films in Supercritical Carbon Dioxide. *J. Supercrit. Fluids* **2012**, *71*, 127–135.

(27) Guney, O.; Akgerman, A. Synthesis of Controlled-Release Products in Supercritical Medium. *AIChE J.* **2002**, *48* (4), 856–866.
(28) Braga, M. E. M.; Pato, M. T. V.; Silva, H. S. R. C.; Ferreira, E. I.; Gil, M. H.; Duarte, C. M. M.; de Sousa, H. C. Supercritical Solvent Impregnation of Ophthalmic Drugs on Chitosan Derivatives. *J. Supercrit. Fluids* **2008**, *44* (2), 245–257.
(29) Weinstein, R. D.; Muske, K. R.; Martin, S. A.; Schaeber, D. D. Liquid and Supercritical Carbon Dioxide-Assisted Implantation of Ketoprofen into Biodegradable Sutures. *Ind. Eng. Chem. Res.* **2010**, *49* (16), 7281–7286.
(30) Yu, J. P.; Guan, Y. X.; Yao, S. J.; Zhu, Z. Q. Preparation of Roxithromycin-Loaded Poly(l-Lactic Acid) Films with Supercritical Solution Impregnation. *Ind. Eng. Chem. Res.* **2011**, *50* (24), 13813–13818.
(31) Singh, D. . Synthesis and Growth of ZnO Nanowires. *Sci. Adv. Mater.* **2010**, *2* (3), 245–272.
(32) Kalepu, S.; Nekkanti, V. Insoluble Drug Delivery Strategies: Review of Recent Advances and Business Prospects. *Acta Pharm. Sin. B* **2015**, *5* (5), 442–453.
(33) Banchero, M.; Ronchetti, S.; Manna, L. Characterization of Ketoprofen / Methyl-Beta-Cyclodextrin Complexes Prepared Using Supercritical Carbon Dioxide. *J. Chem.* **2013**, *2013*, 8.
(34) Ravi, S.; Rudrangi, S.; Trivedi, V.; Mitchell, J. C.; Wicks, S. R.; Alexander, B. D. Preparation of Olanzapine and Methyl- B -Cyclodextrin Complexes Using a Single-Step , Organic Solvent-Free Supercritical Fl Uid Process : An Approach to Enhance the Solubility and Dissolution Properties. *Int. J. Pharm.* **2015**, *494* (1), 408–416.
(35) Patil, A.; Chirmade, U. N.; Trivedi, V.; Lamprou, D. A.; Urquhart, A.; Douroumis, D. Encapsulation of Water Insoluble Drugs in Mesoporous Silica Nanoparticles Using Supercritical Carbon Dioxide. *J. Nanomed. Nanotechnol.* **2011**, *2* (3), 1000111.
(36) Bouledjouidja, A.; Masmoudi, Y.; Van Speybroeck, M.; Schueller, L.; Badens, E. Impregnation of Fenofibrate on Mesoporous Silica Using Supercritical Carbon Dioxide. *Int. J. Pharm.* **2016**, *499* (1–2), 1–9.
(37) Gignone, A.; Manna, L.; Ronchetti, S.; Banchero, M.; Onida, B. Microporous and Mesoporous Materials Incorporation of Clotrimazole in Ordered Mesoporous Silica by Supercritical CO 2. *Microporous Mesoporous Mater.* **2014**, *200*, 291–296.
(38) Gignone, A.; Piane, M. D.; Corno, M.; Ugliengo, P.; Onida, B. Simulation and Experiment Reveal a Complex Scenario for the Adsorption of an Antifungal Drug in Ordered Mesoporous Silica. *J. Phys. Chem. C* **2015**, *119*, 13068−13079.

(39) Ivanovic, J.; Rezwan, K.; Kroll, S. Supercritical CO2 Deposition and Foaming Process for Fabrication of biopolyester–ZnO Bone Scaffolds. 2018.
(40) Chiu, W.-T.; Chen, C.-Y.; Chang, T.-F. M.; Tahara, Y.; Hashimoto, T.; Kurosu, H.; Sone, M. Fabrication and Photocatalytic Performance of Au/ZnO Layered Structure on Silk Textile for Flexible Device Applications. 2017, pp 39–46.
(41) Kondoh, E.; Sasaki, K.; Nabetani, Y. Deposition of Zinc Oxide Thin Films in Supercritical Carbon Dioxide Solutions. 2008, pp 612011–612013.
(42) Lin, W. H.; Chang, T. F. M.; Lu, Y. H.; Sato, T.; Sone, M.; Wei, K. H.; Hsu, Y. J. Supercritical CO2-Assisted Electrochemical Deposition of ZnO Mesocrystals for Practical Photoelectrochemical Applications. *J. Phys. Chem. C* **2013**, *117* (48), 25596–25603.
(43) Mauricio, M. R.; Manso, F. C. G.; Kunita, M. H.; Velasco, D. S.; Bento, A. C.; Muniz, E. C.; De Carvalho, G. M.; Rubira, A. F. Synthesis and Characterization of ZnO/PET Composite Using Supercritical Carbon Dioxide Impregnation Technology. 2011, pp 757–761.
(44) Hjiri, M.; Zahmouli, N.; Dhahri, R.; Leonardi, S. G.; Mir, L. E.; Neri, G. Doped-ZnO Nanoparticles for Selective Gas Sensors. 2017, pp 9667–9674.
(45) Haldorai, Y.; Shim, J.-J. Supercritical Fluid Mediated Synthesis of Highly Exfoliated graphene/ZnO Composite for Photocatalytic Hydrogen Production. 2014, pp 24–27.
(46) Haldorai, Y.; Voit, W.; Shim, J.-J. Nano ZnO@reduced Graphene Oxide Composite for High Performance Supercapacitor: Green Synthesis in Supercritical Fluid. 2014, pp 65–72.
(47) Meng, F.; Li, X.; Meng, M.; Ishizaka, Y.; Tsubaki, N. Effect of Supercritical Fluid of CO2 Drying during Cu/ZnO Catalyst Preparation on Methanol Synthesis from Syngas at Low Temperature. 2011, pp 397–403.
(48) Byrappa, K.; Ohara, S.; Adschiri, T. Nanoparticles Synthesis Using Supercritical Fluid Technology - towards Biomedical Applications. 2008, pp 299–327.
(49) Matsuyama, K.; Mishima, K.; Kato, T.; Ohara, K. Preparation of Hollow ZnO Microspheres Using Poly (Methyl Methacrylate) as a Template with Supercritical CO 2 -Ethanol Solution. *Society* **2010**, *333*, 8510–8517.
(50) Vostrikov, A. A.; Fedyaeva, O. N.; Shishkin, A. V; Sokol, M. Y. Synthesis of Nanostructured ZnO at Oxidation of Liquid Zn by Supercritical CO2. 2008, pp 231–234.
(51) Crowley, P. D.; Gallagher, H. C. Clotrimazole as a Pharmaceutical:

Past, Present and Future. *J. Appl. Microbiol.* **2014**, *117* (3), 611–617.
(52) PubChem. Clotrimazole https://pubchem.ncbi.nlm.nih.gov/compound/clotrimazole#section=Chemical-and-Physical-Properties (accessed Jan 1, 2017).
(53) Jøraholmen, M. W.; Vanić, Ž.; Tho, I.; Škalko-Basnet, N. Chitosan-Coated Liposomes for Topical Vaginal Therapy: Assuring Localized Drug Effect. *Int. J. Pharm.* **2014**, *472* (1–2).
(54) Rai, S. Y.; Ravikumar, P. Development and Evaluation of Microsphere Based Topical Formulation Using Design of Experiments. *Indian J. Pharm. Sci.* **2016**, *78* (2).
(55) Verma, P.; Ahuja, M. Optimization, Characterization and Evaluation of Chitosan-Tailored Cubic Nanoparticles of Clotrimazole. *Int. J. Biol. Macromol.* **2015**, *73* (1).
(56) ICH Q3C Guideline, Impurities: Residual solvents. https://www.ich.org/fileadmin/Public_Web_Site/ICH_Products/Guidelines/Quality/Q3C/Q3C_R6__Step_4.pdf (accessed Jun 26, 2017).
(57) Gignone, A. Ordered Mesoporous Silica for Drug Delivery in Topical Applications. PhD Thesis, 2016.
(58) Bushra, R.; Aslam, N. An Overview of Clinical Pharmacology of Ibuprofen. *Oman Med. J.* **2010**, *25* (3), 155–1661.
(59) PubChem. Ibuprofen https://pubchem.ncbi.nlm.nih.gov/compound/3672 (accessed Jan 1, 2017).
(60) Irvine, J.; Afrose, A.; Islam, N. Formulation and Delivery Strategies of Ibuprofen: Challenges and Opportunities. *Drug Dev. Ind. Pharm.* **2017**, *9045* (October), 1–11.
(61) Morgado, P. I.; Miguel, S. P.; Correia, I. J.; Aguiar-Ricardo, A. Ibuprofen Loaded PVA/chitosan Membranes: A Highly Efficient Strategy towards an Improved Skin Wound Healing. *Carbohydr. Polym.* **2017**, *159*, 136–145.
(62) Price, P.; Fogh, K.; Glynn, C.; Krasner, D. L.; Osterbrink, J.; Sibbald, R. G. Why Combine a Foam Dressing with Ibuprofen for Wound Pain and Moist Wound Healing? *Int. Wound J.* **2007**, *4* (SUPPL.1), 1–3.
(63) Kumar, R.; Singh, A.; Garg, N.; Siril, P. F. Solid Lipid Nanoparticles for the Controlled Delivery of Poorly Water Soluble Non-Steroidal Anti-Inflammatory Drugs. *Ultrason. Sonochem.* **2018**, *40* (Part A), 686–696.
(64) Wang, Q.; Jin, X. Q.; Sun, J. H.; Bai, S. Y.; Wu, X.; Panezai, H. Facile Synthesis and Fractal Feature of pH-Responsive Poly(acrylic Acid) Hollow Microspheres for Ibuprofen Delivery. *Int. J. Polym. Mater. Polym. Biomater.* **2017**, 1–9.
(65) Guo, Y.; Sun, J.; Bai, S.; Wu, X. pH-Sensitive Performance of Dextran–

poly(acrylic Acid) Copolymer and Its Application in Controlled in Vitro Release of Ibuprofen. *Int. J. Polym. Mater. Polym. Biomater.* **2017**, *66* (17), 900–906.

(66) Coviello, T.; Matricardi, P.; Marianecci, C.; Alhaique, F. Polysaccharide Hydrogels for Modified Release Formulations. *J. Control. Release* **2007**, *119* (1), 5–24.

(67) Hillerström, A.; Andersson, M.; Samuelsson, J.; van Stam, J. Solvent Strategies for Loading and Release in Mesoporous Silica. *Colloids Interface Sci. Commun.* **2014**, *3* (2014), 5–8.

(68) Mortera, R.; Fiorilli, S.; Garrone, E.; Verné, E.; Onida, B. Pores Occlusion in MCM-41 Spheres Immersed in SBF and the Effect on Ibuprofen Delivery Kinetics: A Quantitative Model. *Chem. Eng. J.* **2010**, *156* (1), 184–192.

(69) Charoenchaitrakool, M.; Dehghani, F.; Foster, N. R. Utilization of Supercritical Carbon Dioxide for Complex Formation of Ibuprofen and Methyl-β-Cyclodextrin. *Int. J. Pharm.* **2002**, *239* (1–2), 103–112.

(70) Temtem, M.; Pompeu, D.; Jaraquemada, G.; Cabrita, E. J.; Casimiro, T.; Aguiar-Ricardo, A. Development of PMMA Membranes Functionalized with Hydroxypropyl-β-Cyclodextrins for Controlled Drug Delivery Using a Supercritical CO<inf>2</inf>-Assisted Technology. *Int. J. Pharm.* **2009**, *376* (1–2), 110–115.

(71) Hussein, K.; Türk, M.; Wahl, M. A. Comparative Evaluation of Ibuprofen/β-Cyclodextrin Complexes Obtained by Supercritical Carbon Dioxide and Other Conventional Methods. *Pharm. Res.* **2007**, *24* (3), 585–592.

(72) Tozuka, Y.; Fujito, T.; Moribe, K.; Yamamoto, K. Ibuprofen-Cyclodextrin Inclusion Complex Formation Using Supercritical Carbon Dioxide. *J. Incl. Phenom. Macrocycl. Chem.* **2006**, *56* (1–2), 33–37.

(73) Ni, M.; Xu, Q.-Q.; Yin, J.-Z. Preparation of Controlled Release Nanodrug Ibuprofen Supported on Mesoporous Silica Using Supercritical Carbon Dioxide. *J. Mater. Res.* **2012**, *27* (22), 2902–2910.

(74) Alnaief, M.; Antonyuk, S.; Hentzschel, C. M.; Leopold, C. S.; Heinrich, S.; Smirnova, I. A Novel Process for Coating of Silica Aerogel Microspheres for Controlled Drug Release Applications. *Microporous Mesoporous Mater.* **2012**, *160*, 167–173.

(75) Rossmann, M.; Braeuer, A.; Schluecker, E. Supercritical Antisolvent Micronization of PVP and Ibuprofen Sodium towards Tailored Solid Dispersions. *J. Supercrit. Fluids* **2014**, *89*, 16–27.

(76) Hussain, Y. A.; Grant, C. S. Ibuprofen Impregnation into Submicron Polymeric Films in Supercritical Carbon Dioxide. *J. Supercrit. Fluids* **2012**, *71*, 127–135.

(77) Davies, O. R.; Lewis, A. L.; Whitaker, M. J.; Tai, H.; Shakesheff, K.

M.; Howdle, S. M. Applications of Supercritical CO2 in the Fabrication of Polymer Systems for Drug Delivery and Tissue Engineering. *Adv. Drug Deliv. Rev.* **2008**, *60* (3), 373–387.

(78) Kazarian, S. G.; Martirosyan, G. G. Spectroscopy of Polymer/drug Formulations Processed with Supercritical Fluids: In Situ ATR-IR and Raman Study of Impregnation of Ibuprofen into PVP. *Int. J. Pharm.* **2002**, *232* (1–2), 81–90.

(79) Shokri, N.; Javar, H. A. Zinc Oxide Nanoparticles as Skin Permeation Enhancer for Solvents and Surfactants. **2014**, *13* (3), 85–91

.

Chapter 3

Green organic-solvent-free routes to prepare nanostructured zinc oxide carriers for pharmaceutical applications.

"Part of the work described in this chapter has been previously published in Leone *et al*., **2018**, *Journal of Cleaner Production, 172, 1433-1439* [1].

3.1 Introduction

This chapter deals with the development of a green organic-solvent-free route to prepare ZnO-based drug carriers. As mentioned above, ZnO was selected due to its intrinsic biological properties and its well-established use in dermatological and cosmetic products [2]. Due to its low toxicity and high biocompatibility, ZnO has also been listed as a safe substance by Food and Drug Administration (21CFR182.8991). A large variety of methods were reported in the literature for the production of ZnO nanostructures with particles differing in shape, size and spatial structure [2]. However, these methods result in many drawbacks, which include the use of toxic solvents,

generation of hazardous by-products and the imperfection of the surface structure. To the best of our knowledge the loading of drugs on NsZnO by means of $scCO_2$ has not been reported yet. In order to fill this gap, the main objective of this work has been the development of an innovative organic-solvent-free process which combines both the production of the NsZnO carrier and the drug loading phase of the Active Pharmaceutical Ingredients (API) (Figure 3.1). Two NsZnO materials with different morphologies were synthesized using wet organic-solvent-free processes and they were characterized to elucidate their morphological and physico-chemical properties. In this investigation, Clotrimazole (CTZ) and Ibuprofen (IBU) were selected as drug models.

A $scCO_2$ drug loading technique was used to load the two different API's on the NsZnO so allowing the final material to be recovered without any solvent residue. Moreover preliminary *in vitro* dissolution studies were performed to verify the capability of the obtained materials to release the CTZ and IBU in view of future drug delivery applications.

Eventually it must be pointed that, in the perspective of the industrial development of the supercritical fluid technology [3], the preparation route here proposed can be easily transferred to real pharmaceutical industry, which traditionally involves small-scale batch processes. However**,** the limitation of the present study is the lack of *in vitro* studies mimicking the biological environment and conditions envisaged for the applications of these systems, which will be investigated in future work.

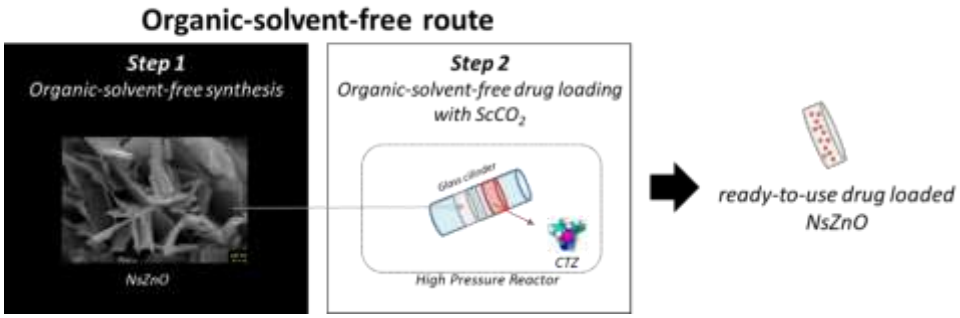

Figure 3.1 Schematic representation of the main steps involved in the organic- solvent-free route developed in [1].

3.2 Experimental

3.2.1. Materials

All the reagents for chemical synthesis were purchased from Sigma-Aldrich and used as received without further purification. Carbon dioxide with a purity of 99.998% was supplied by SIAD (Italy). Bidistilled water was used throughout this study.

3.2.2. Synthesis of nanostructured ZnO

Two different NsZnO materials were synthesized. For this purpose two wet chemical processes without any organic solvent were selected: chemical bath deposition and a soft-template sol-gel method.

Chemical bath deposition

The key mechanism of the chemical bath deposition (CBD) approach is based on the growth of layered inorganic materials, which contain Zn^{2+} ions, as precursors of ZnO. Many CBD processes that employ basic aqueous solvents and zinc salts for the fabrication of ZnO nanostructures have been reported in the literature due to several advantages, such as the easiness in preparation, cheap equipment, low deposition temperature (< 100 °C) and versatility [4–8].

The CBD procedure here investigated was previously described by Kakiuchi and co-workers [9]. $ZnCl_2$ and urea were used as starting reagents in order to obtain zinc carbonate hydroxide hydrate ($Zn_4CO_3(OH)\cdot 6H_2O$) with a nanosheet-like morphology, which is the precursor of ZnO. However, some changes have been here introduced in the recovery of the ZnO precursor before calcination.

Zinc chloride and urea were dissolved in bidistilled water in order to achieve a final concentration of 0.05 M of Zn^{2+} and 1.0 M of urea. The pH value of the solution was adjusted to 4 by using hydrochloric acid. At the end of these preliminary operation steps a transparent and precipitate-free solution was obtained. The solution was kept under magnetic stirring at 80°C for 24 hours using the reflux technique until the deposition of a white dense precipitate of $Zn_4CO_3(OH)_6\cdot H_2O$ was obtained. The suspension with the nanosheet-shaped ZnO precursor was carefully filtered allowing the precipitate to be separated on the surface of a cellulose filter (Whatman® qualitative filter

paper, Grade 3): a powder was then obtained instead of a film. Finally the precipitate was thermally treated by heating it at 300°C for 0.5 hour in a static oven to be transformed into zinc oxide. In the following sections the material obtained with the above described procedure is referred as NsZnO-1.

Soft-template sol-gel method

The use of a soft template in the synthesis of NsZnO materials has been scarcely investigated in the literature. Zinc acetate was selected as the zinc source and Pluronic F127 as the templating agent. A solution of Pluronic F127 (10% v/v) in water was prepared. Zinc acetate was then added until a concentration equal to 0.8 M was obtained. An opalescent suspension was immediately formed and was left under magnetic stirring at room temperature for 2 hours. Finally the suspension was dried under vacuum and the dried residue was calcinated at 500°C for about 2 hours and 45 minutes with a heating rate of 3°C/min in order to remove the template and obtain zinc oxide. In the following sections the material obtained with the above described procedure is referred as NsZnO-2.

3.2.3. Clotrimazole-loaded NsZnO materials

Drug loading through supercritical carbon dioxide

The supercritical impregnation process was carried out by contacting the drug and each of the two NsZnO materials in a static atmosphere of $scCO_2$ at constant temperature and pressure. The apparatus and the experimental procedure adopted to achieve the incorporation of the drug into the NsZnO are described in a previous work [10]. A tailored set-up, which was already used in a previous work [11], was applied to place the samples inside the supercritical impregnation vessel. First a pellet of the drug (100 mg) and a pellet of the NsZnO (100 mg) were prepared and introduced into a glass cylinder of 1 cm diameter. A disc of filter paper was placed between the two pellets to prevent their contact and guarantee an efficient recovery of the samples at the end of the drug loading process (Figure 3.2). Both the NsZnO and the drug were accurately pelletized using a manual hydraulic press to obtain small cylindrical pellets with a 9 mm diameter and a height ranging from 1 to 2 mm. Each glass device was supposed to contain one single combination of a NsZnO pellet and a drug pellet. The sample-loaded glass devices were placed inside a stainless steel vessel, which was put in an oven that kept all the system at constant temperature. To assure reproducibility the vessel can hold up to 5 homemade

glass cylinders and this endows different batches of the same sample to be obtained at the end of the impregnation process. To load the CTZ into the NsZnO materials, liquid CO_2 was used to fill the vessel, then the temperature was increased to 100°C and additional CO_2 was pumped to reach the target pressure (25.0 MPa): these operative conditions did not not affect the CTZ stability [12]. The system was maintained at the above-reported conditions for several hours (around 12) to allow the drug to be dissolved in the $scCO_2$ and diffuse into the NsZnO. At the end of the drug loading process, the apparatus was brought back to atmospheric pressure and cooled to room temperature.

Figure 3.2 Schematic representation of the homemade device used to perform the incorporation of the drug by means of $scCO_2$ (left side); picture showing the filled glass cylinder, ready for the incorporation process (right side. This images has been adapted from [1].

Drug loading through traditional approach

For comparison, incorporation of CTZ was also performed by traditional adsorption from ethanol solution [11]. For this purpose, 50 mg of NsZnO were incubated with an ethanolic solution of drug (CTZ 60 mg/ml), under stirring for 24 hours, at room temperature. Then, in order to separate the drug loaded ZnO, the suspensions were centrifugated at 4000 rpm for 30 minutes. The quantitative analysis of drug hosted into NsZnO samples was performed by using TG analyses, between 20°C and 800°C in air (flow rate 100 mL/min with a heating rate of 10 °C /min) using a SETARAM 92 instrument.

Preliminary in vitro drug release study

A preliminary in vitro release study was performed to assess the ability of the drug-loaded NsZnO to release the drug. Multicompartment rotating cells, equipped with a hydrophilic dialysis membrane (Spectra/Por, Spectrum®, cut-off 12000-14000 Da), were used to perform the in vitro release tests. The release profiles of CTZ-loaded NsZnO-1 sample was compared with that of

pure crystalline CTZ. A HCl 0.1 M solution was used as the receiving phase [13]. After fixed time intervals, the receiving phase was completely replaced by a fresh solution. The release study took approximately 2 hours. A quantitative analysis by UV spectroscopy at 254 nm was carried out in order to determine the amount of released drug on each withdrawn sample.

3.2.4 Ibuprofen-loaded NsZnO materials

Drug loading through supercritical carbon dioxide

The impregnation of the NsZnO with IBU was performed following the same procedure of CTZ, but the final temperature and pressure were 35°C and 10 MPa, respectively 14–17.

Drug loading through traditional approach

The adsorption from solution was also carried out in order to compare the supercritical impregnation of IBU into NsZnO with a conventional method. For this purpose, 50 mg of NsZnO were incubated with an ethanolic solution of IBU (30 mg/ml), under stirring for 24 hours, at room temperature [11]. Then, a separation process was carried out in order to separate the drug loaded NsZnO from the not-entrapped drug solution (4000 rpm for 30 minutes). A quantitative analysis of the IBU in the supernatant phase was performed by using TG analyses, between 20°C and 800°C in air (flow rate 100 mL/min with a heating rate of 10 °C /min) using a SETARAM 92 instrument.

Preliminary in vitro drug release study

The ability of the drug-loaded NsZnO to release IBU was also tested by using the multicompartment rotating cells, equipped with a hydrophilic dialysis membrane (Spectra/Por, Spectrum®, cut-off 12000-14000 Da). The release profiles from the NsZnO-1 and NsZnO-2 samples loaded with IBU through $scCO_2$ technique were compared. Phosphate buffered solution (pH 7.4) was used as the receiving medium. At predetermined time intervals, the receiving phase was completely replaced by a fresh solution, and analyzed for IBU content at 263 nm, using a Beckam-Coulter DU 730 spectrophotometer.

3.2.5 Characterization

The physico-chemical characterization of the NsZnO samples was performed before and after the drug loading step, adopting a wide range of techniques, among which X-ray diffraction (XRD), thermogravimetry (TG),

differential scanning calorimetry (DSC), nitrogen adsorption isotherms, and field emission scanning microscopy (FESEM) coupled with EDS.

XRD patterns were obtained using a PANalytical X'Pert (Cu Kα radiation) diffractometer. Data were collected with a 2D solid state detector (PIXcel) from 20 to 70 2θ with a step size of 0.001 2θ and a wavelength of 1.54187 Å. Crystallites size was determined according to Scherrer equation [18] by comparing the profile width of a standard profile with the sample profile. The Scherrer equation relates the width of a powder diffraction peak to the average dimensions of crystallites in a polycrystalline powder:

Eq. 3.2: $$D = K\lambda / \beta_{(2\theta)hkl} \cos\theta$$

where β is the crystallite size contribution to the peak width (full width at half maximum) in radians, K (shape factor) is a constant near unit and D is the average thickness of the crystal in a direction normal to the diffracting plane hkl.

Profile fits were performed using X'Pert High Score Plus, using Pseudo-Voigt peak function with Kα1 and Kα2 fitting on a background stripped pattern. The sample-induced peak broadening β was determined by subtracting the instrumental peak width from the measured peak width.

The instrumental broadening was determined using LaB6 powder (NIST SRM®660a, size of crystallites in the 2 μm to 5 μm range).

TG analyses were carried out between 20°C and 800°C in air (flow rate 100 mL/min with a heating rate of 10 °C /min) using a SETARAM 92 instrument while the DSC measurements were performed under nitrogen flux (60 ml/min), in the range between 50° C and 200° C, with a DSCQ 1000 by TA Instrument.

Nitrogen adsorption isotherms were measured using a Quantachrome AUTOSORB-1 instrument. Before the adsorption measurements, samples were outgassed for 2 h at 100° C. BET specific surface areas (SSA_{BET}) were calculated in the relative pressure range of 0.04–0.1.

Infrared spectroscopy was carried out on a Thermo Scientific FTIR Spectrometer (Thermo Fisher Scientific Inc., USA). Spectra were recorded for 16 scans in ATR mode at room temperature, with a 1 cm^{-1} resolution in the wavelength range of 4000 - 400 cm^{-1}. Spectra were corrected for background and atmosphere using OMNIC software provided with the spectrometer.

FESEM images were recorded with a FESEM ZEISS MERLIN instrument, equipped with an EDS detector (OXFORD).

For the measurement of CTZ concentration in the release tests a UV-Vis Beckman-Coulter spectrophotometer was used.

3.3. Results and Discussion

3.3.1. Characterization of the NsZnO materials as such.

Figure 3.3 reports the FESEM images, at low and high magnification, of the NsZnO-1 sample. NsZnO-1 appears as aggregates of nanosheets with thickness of about 20 nm that are formed by the self-assembling of ovoid nanoparticles (around 15-20 nm). This morphology is in agreement with the mechanism growth proposed by Kakiuchi et al. [9].

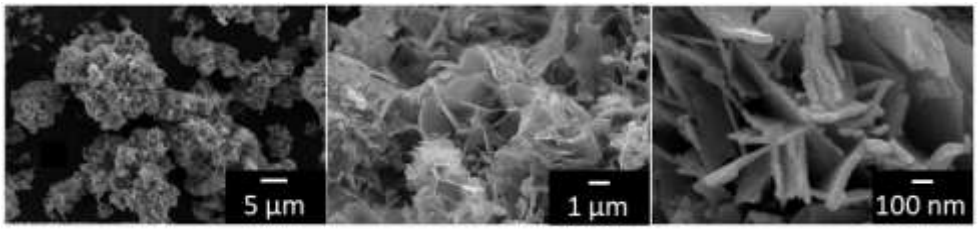

Figure 3.3 FESEM images of NsZnO-1 (magnification: 5.00 K X, 25.00 K X, 250.00 K X)

The morphology of NsZnO-2 is visible in Figure 3.4 at different magnification. The material appears in form of micrometric and sub-micrometric aggregates of interconnected nanoparticles with heterogeneous size of tens nanometers.

The presence of the nanometric particles might be explained considering a mechanism where the Pluronic F127 molecules would restrict the growth of the ZnO precursor [19].

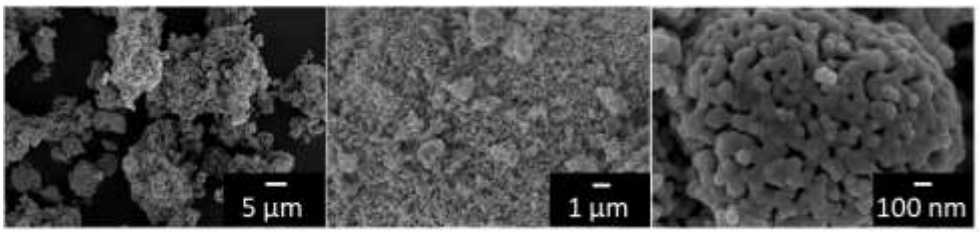

Figure 3.4 FESEM images of NsZnO-2 (magnification: 5.00 K X, 25.00 K X, 250.00 K X)

EDS analysis (data not shown) confirmed the presence of Zn and O at the surface in both samples. No occurrence of chloride is observed for NsZnO-1, from which the complete transformation of the $ZnCl_2$ precursor can be inferred.

Figure 3.5 reports the XRD patterns of both NsZnO materials, which reveal the occurrence of a highly crystalline single hexagonal phase of wurtzite structure. The five main reflection peaks (100), (002), (101), (102) and (110) and the intensity distribution of the peaks are consistent with those of the standard card for the hexagonal phase ZnO (JCPDS ICDD 36-1451). In both the XRD patterns reported in Figure 3.5 the characteristic peaks of the precursors cannot be detected: this means that pure ZnO can be obtained through the above-described synthetic methods. Comparing the XRD patterns of the two samples, it is evident that NsZnO-1 shows broader peaks than NsZnO-2.

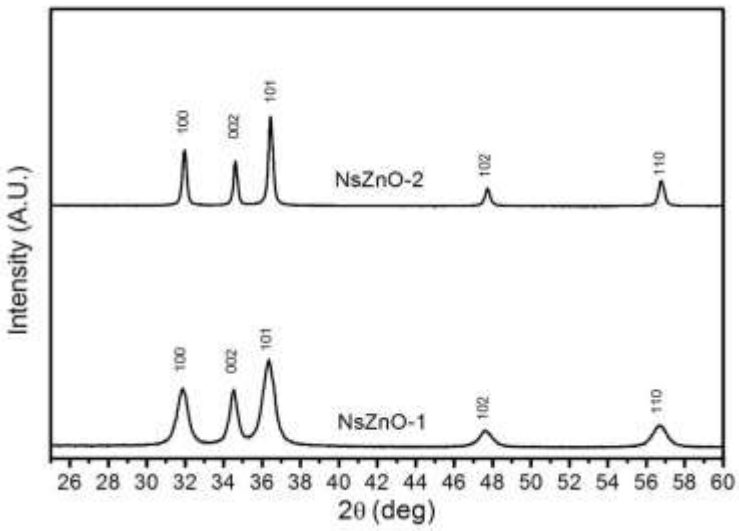

Figure 3.5 XRD patterns of NsZnO-1 e NsZnO-2

Both materials show the typical hexagonal wurtzite structure. The crystallites size determined using the Scherrer equation (Eq. 3.2) are similar to values reported in Table 3.1.

Table 3.1 Crystallite dimensions (nm) determined from application of the Scherrer equation to selected hkl reflections of NsZnO-1 and NsZnO-2

hkl	***NsZnO-1***	***NsZnO-2***
100	15	38
101	15	33
102	16	24
110	14	24

N_2 physisorption measurements were used to evaluate the specific surface area (m^2/g) and the pore volume (m^3/g) of the two samples. NsZnO-1 shows values of both parameters higher than those of NsZnO-2 (Table 3.2). These results are in agreement with the smaller particles size revealed for the former sample by FESEM and XRD data.

3.3.2 Characterization of the CTZ-loaded NsZnO materials

$ScCO_2$ was used to load CTZ inside the two NsZnO materials, TG analyses of the NsZnO materials loaded with CTZ (CZT@NsZnO) allowed the amount of CTZ to be evaluated, which corresponds to 17% w/w for CZT@NsZnO-1 and 14% w/w for CZT@NsZnO-2, respectively (Table 3.2).

Table 3.2 Surface area and pore volume values before and after the CTZ loading, together with the amount of CTZ adsorbed into NsZnO materials by $scCO_2$ process

	Before drug incorporation		*After drug incorporation*		*Amount of CTZ incorporated*
	Surface Area (m^2/g)	*Pore Volume* (cm^3/g)	*Surface Area* (m^2/g)	*Pore Volume* (cm^3/g)	*W/W %*
NsZnO-1	66	0.230	22	0.110	17
NsZnO-2	19	0.050	6.7	0.003	14

Figure 3.6 shows the isotherms of both the NsZnO materials before and after the loading of CTZ through $scCO_2$. The values of the surface area and pore volume values are reported in Table 3.2. As far as NsZnO-1 is concerned, the BET specific surface area decreased from 66 m^2/g, for the as-synthetized material, to 22 m^2/g, after CTZ loading, whereas the pore volume decreased from 0.230 cm^3/g to 0.110 cm^3/g. The BET specific surface area of NsZnO-2, instead, decreased from 19 m^2/g to 6.7 m^2/g and the pore volume decreased from 0.050 cm^3/g to 0.003 cm^3/g. The BET specific surface area of NsZnO-1 is lower than the value reported in literature for the nanostructured ZnO deposited in the film form on a glass substrate (88.5 m^2/g) [9]. As far as the sample NsZNO-2 is concerned, no comparison with the value reported in literature is possible because of the lack of this datum [19].

The decrease of BET specific surface area and pore volume upon CTZ loading for both samples is ascribed to the adsorption of CTZ molecules on the surface of NsZnO materials. This confirms the feasibility of using the NsZnO as CTZ carrier.

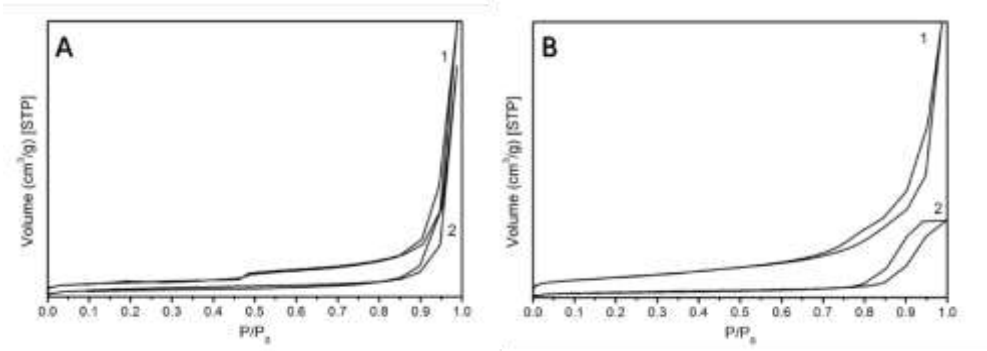

Figure 3.6 Section A: N_2 adsorption-desorption isotherms of NsZnO-1 before (1) and after (2) CTZ loading. Section B: N_2 adsorption-desorption isotherms of NsZnO-2 before (1) and after (2) CTZ loading

XRD and DSC analyses were performed to investigate the form of the drug inside the NsZnO materials pores. Figure 3.7A reports the XRD patterns of CTZ@NsZnO-1 and CTZ@NsZnO-2.

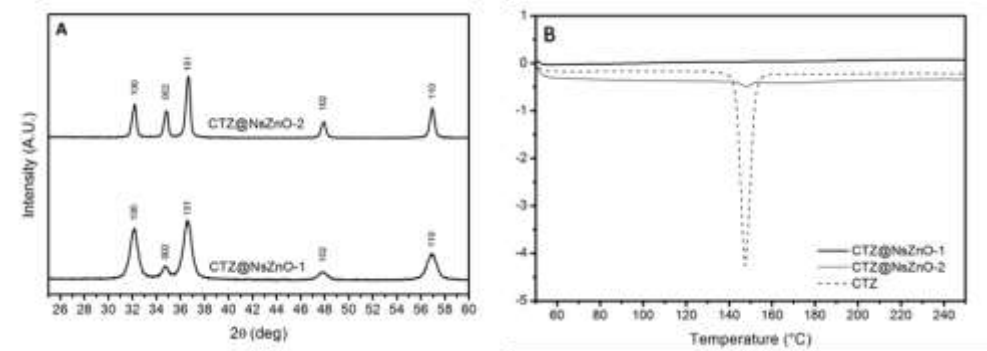

Figure 3.7 XRD patterns and DSC analyses of CTZ-loaded NsZnO materials after $scCO_2$ impregnation process. Figure 6A shows the XRD patterns of CTZ@NsZnO-1 and CTZ@NsZnO-2. Figure 6B reports the DSC curves of pure crystalline CTZ, CTZ@NsZnO-1 and CTZ@NsZnO-2.

No additional diffraction peaks of the crystalline CTZ are observed in both cases. This evidences that the loaded drug molecules are not assembled in the crystalline structure. The same result was also confirmed by the DSC analysis. DSC curves for pure CTZ, CTZ@NsZnO-1 and CTZ@NsZnO-2 are shown in Figure 3.7B. Pure CTZ showed a sharp melting endotherm peak at 147 °C, in

agreement with what reported in the product data sheet. No evidence of this peak was observed in the DSC curve of CTZ@NsZnO-1 (curve A), suggesting a complete amorphization of the drug in the carrier. The DSC curve of CTZ@NsZnO-2 (curve B) showed a dramatic decrease in the intensity of the drug melting peak, being only a very weak signal discernible. The disappearance or decrease in intensity of the drug endothermic peak is generally related to drug–material interactions and/or loss of drug crystallinity. The presence of a residual weak melting endotherm peak in the case of CTZ@NsZnO-2 is in agreement with the lower SSA (19 m^2/g) with respect to CTZ@NsZnO-1 (66 m^2/g). In fact, despite the higher amount of loaded CTZ in the latter sample (17 % w/w), complete amorphization is ascribed to the interaction between the drug molecules and the ZnO surface. From the content of CTZ (% w/w) the number of molecules of CTZ per gram of ZnO was evaluated and, using the SSA value, this was transformed into the number of molecules per nm^2, which resulted to be equal to 5.4 for NsZnO-1. The significantly lower SSA value of NsZnO-2 accounts for its lower capacity to form CTZ-surface interactions, favouring partial CTZ self-aggregation in crystalline form. Indeed, the amount of molecules/nm^2 in CTZ@NsZnO-2 resulted to be equal to 15.

FTIR spectroscopy was performed to *i)* confirm the successful loading of CTZ into NsZnO-1, selected as the sample with the higher CTZ content in amorphous form, and *ii)* to study the effect of the supercritical carbon dioxide on the NsZnO-1 surface. Figure 3.8 reports the FTIR spectra of NsZnO-1 as such, CTZ@NsZnO-1, NsZnO-1 as-such after a $scCO_2$ treatment and clotrimazole. The as-prepared NsZnO shows several IR bands between 1700 cm^{-1} and 1000 cm^{-1}, corresponding to C=O stretching (1561 cm^{-1}), C–O stretching (1155 cm^{-1}) and C–H vibrations [20]. The presence of these species could be ascribed to partially decomposed ZnO precursors (Zinc Carbonate Hydroxide Hydrate) originating from reaction intermediates. The broad band around 3400 cm^{-1} is attributed to O–H stretching, while the peak at 1641 cm^{-1} corresponds to O–H bending [21].
In order to evaluate the effect of the supercritical carbon dioxide on the NsZnO-1 surface, FTIR analysis was also performed on the sample as-such after a treatment in $scCO_2$ for 12 hours, at 100°C and 25 MPa. The spectrum displays an intensity growth of the absorption region between the 1600 and

1100 cm^{-1} caused by the adsorption of CO_2 on ZnO surface. This region can be mainly ascribed to carbonate-like species[22].

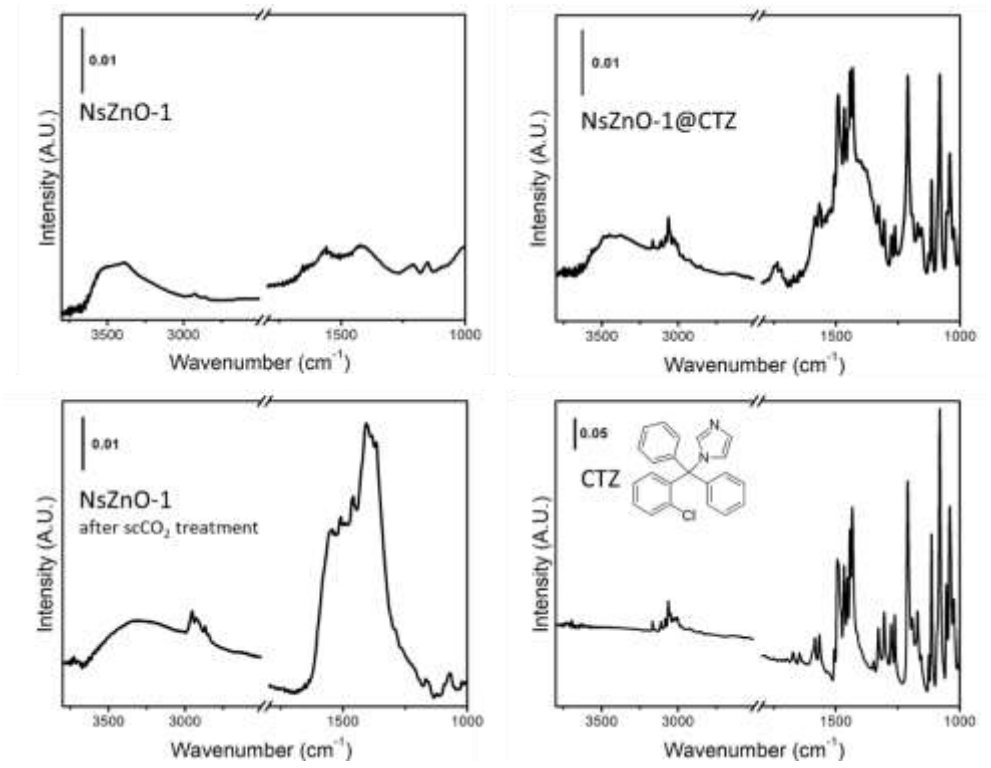

Figure 3.8 FT-IR spectra of: NsZnO-1, CTZ@NsZnO-1($scCO_2$ loading), NsZnO-1 after a $scCO_2$ treatment and crystalline clotrimazole

.

The characteristic bands displayed in the FTIR spectrum of clotrimazole are consistent with the literature [11,23–25]. The vibration bonds in an aromatic ring (Ar-H) are ascribed at 3050 cm^{-1}, which is characteristic of bonds C-H, the peak at 1580 cm^{-1} conforms to the group C=N and the bands at 1480 cm^{-1} and 1440 cm^{-1} are specific for the group C=C. At 1300 cm^{-1} and 1200 cm^{-1} are visible peaks respond the vibration of bonds C-H. Another characteristic peak of CTZ corresponds to the functional group C-Cl at 750 cm^{-1} (region not shown). Notwithstanding the evident CO_2 adsorption on the surface of the NsZnO-1 as -such after the treatment in $scCO_2$, the FTIR spectrum of the CTZ@NsZnO-1, impregnated through $scCO_2$ process, shows clearly the characteristic peaks of the drug. Moreover, the growth of the absorption region between the 1600 and 1100 cm^{-1} caused by the adsorption of CO_2 on CTZ@NsZnO-1 surface results less intense than the NsZnO-1 as-such. From these experimental evidences, it is possible to draw significative conclusions: *i)* a successful loading of CTZ into NsZnO-1 was achieved by supercritical process; *ii)* during the drug impregnation by means of the $scCO_2$, the drug played a protective function towards the NsZnO-1 surface, reducing the adsorption of CO_2.

For the sake of comparison, NsZnO-1 was also loaded with CTZ through a traditional approach, consisting in the adsorption of the drug from an ethanolic solution. Briefly the materials were incubated for 24 hours under magnetic stirring with a CTZ ethanolic solution. At end of the process, the drug loaded NsZnO-1 was separated from the not-encapsulated CTZ solution through a centrifugation process. The precipitate, consisting in the CTZ loaded material, was used to determine its drug content. In order to evaluate the amount of CTZ, TG analyses of the NsZnO materials loaded with CTZ (CTZ@NsZnO-1) were performed both after $scCO_2$ impregnation and after traditional adsorption loading from ethanolic solution. The characteristic curves are shown in Figure 3.9. The percentages calculated as loss of weight after TG analysis indicated that the drug loading corresponded to 17% w/w and 11%, after $scCO_2$ technique and traditional adsorption, respectively. In conclusion, it is worth of noting that a significant advantage in term of CTZ amount was gained using the supercritical approach in comparison with the traditional one. This advantage combined to the possibility to avoid organic solvents during the drug loading step makes the use of $scCO_2$ a promising route to develop ZnO-based reservoir of drug.

Considering the drug loading amount of the sample CTZ@NsZnO-1 loaded with supercritical technology, it is important to underline that the loss of weight (≈ 7%) obtained from the TG analysis of the sample NsZnO-1 as-such after $scCO_2$ treatment (Fig.3.9, red curve) could be ascribed to the loss of CO_2 adsorbed onto the material surface. This result confirmed the evidence collected by FTIR analysis (Fig. 3.8), from which the adsorption of CO_2 on the NsZnO-1 surface after the supercritical treatment was clearly displayed by the spectrum. Nevertheless, notwithstanding this evidence, it is important to take into consideration that the drug plays a protective role towards the NsZnOs surfaces, decreasing the adsorption of CO_2. This assessment clearly emerged from the FTIR analyses of the drug loaded samples and was also reported in other research works [15]. Consequently, it is reasonable to consider that the loss of weight of the sample CTZ@NsZnO-1 is mostly related to the amount of CTZ hosted inside the NsZnO-1 nanostructure and only in a small part to the contribution of CO_2.

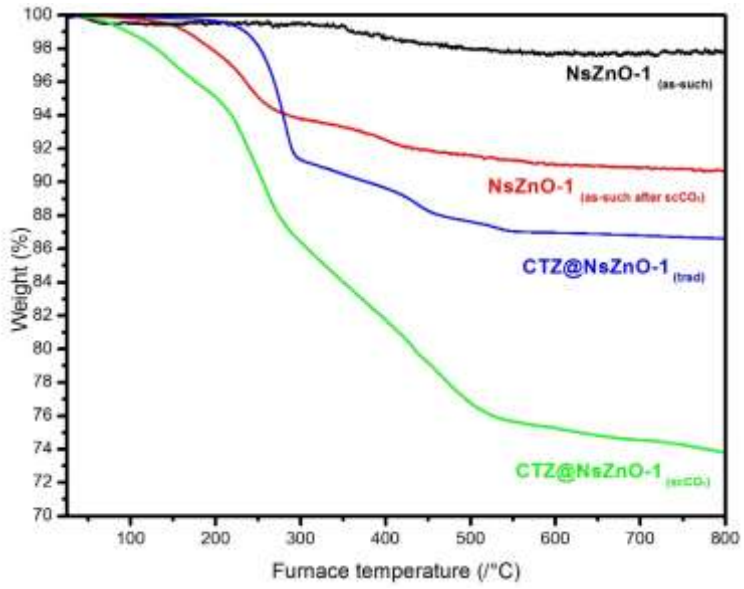

Figure 3.9 TG analyses of NsZnO-1 as-such (black curve), NsZnO-1 as-such after $scCO_2$ treatment (red curve), NsZnO-1 loaded with CTZ after $scCO_2$ (green curve) and after traditional approach (blue curve)

Preliminary in vitro drug release study

Previous results showed the possibility to load CTZ molecules into NsZnO materials by means of $scCO_2$. The capability of releasing the loaded CTZ was also investigated. For this purpose, an *in vitro* release study of CTZ from NsZnO-1, i e. the sample showing the higher CTZ content in amorphous form, was carried out using a multi-compartmental rotating cell. Figure 3.10 reports the cumulative percentage release curves of CTZ both from CTZ@NsZnO-1 and unsupported pure CTZ. The release profile of CTZ from CTZ@NsZnO-1 shows a fast release in the first 10 minutes of the test, where the amount of CTZ released by CTZ@NsZnO-1 was about 15 µg. Then the quantity of released drug kept slightly increasing over time until it was approximately doubled. This trend was significantly different from the release profile of unsupported CTZ. In fact, in this case the quantity released after 10 minutes was less than the half of that released by CTZ@NsZnO in the same time. At the end of experiment, the final quantity of released CTZ was about 25 % of that released by CTZ@NsZnO-1. These results show that CTZ is not irreversibly confined in the NsZnO material and that NsZnO can act as a drug delivery carrier, ensuring a fast release of a larger CTZ amount in comparison with the unsupported crystalline drug. This might play a key role in several biological applications where the bioavailability of poorly-water-soluble drugs is still a challenging issue. A possible explanation of this behaviour is the amorphous nature of CTZ hosted in the NsZnO sample. Amorphization of drugs on carriers has been already reported in literature. Several matrices were investigated such as mesoporous silica [11,26,27], cyclodextrins [16,28–30] and polymers [10]. It is widely accepted that the amorphization of the drug molecules plays a key role in increasing their dissolution rate and solubility, which are two fundamental parameters that affect the subministration of poorly-water-soluble active ingredients, such as CTZ.

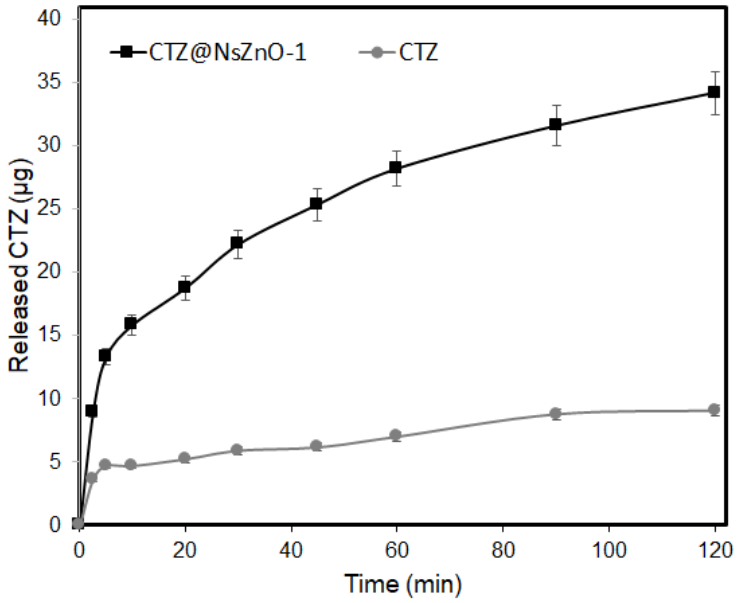

Figure 3.10 *In vitro* drug-release profiles of clotrimazole from pure crystalline clotrimazole and CTZ@NsZnO-1.

3.3.3 Characterization of the IBU-loaded NsZnO materials

The development of a green organic-solvent-free route to prepare ZnO-based drug carriers has been successfully demonstrated using CTZ as drug model [1]. In order to demonstrate the robustness of this approach, the same study was carried out selecting a different API molecule. In particular, IBU was used as drug candidate for this further investigation. A $scCO_2$ process was performed to load IBU inside the two NsZnO materials and the samples were carefully characterized.

Table 3.3 Surface area and pore volume values before and after the IBU loading, together with the amount of IBU adsorbed into NsZnO materials by $scCO_2$ process

	Before drug incorporation		*After drug incorporation*	
	Surface Area (m^2/g)	*Pore Volume (cm^3/g)*	*Surface Area (m^2/g)*	*Pore Volume (cm^3/g)*
NsZnO-1	68	0.230	8	0.04
NsZnO-2	12	0.050	~ 0	~ 0

Figure 3.11 shows the isotherms of both the NsZnO materials before and after the loading of IBU through $scCO_2$. The values of the surface area and pore volume values are reported in Table 3.3. As already observed in the case of Clotrimazole, a reduction of the values of BET specific surface area and pore volume after $scCO_2$ process was determined. Particularly, as far as NsZnO-1 is concerned, the BET specific surface area hugely decreased from 68 m^2/g, for the as-synthetized material, to 8 m^2/g, after IBU loading, whereas the pore volume steeply decreased from 0.230 cm^3/g to 0.04 cm^3/g. The BET specific surface area of NsZnO-2, instead, decreased from 12 m^2/g to a value minor that 2 m^2/g, with an almost total occlusion of the pore volume ($\approx$ 0 cm^3/g). As mentioned above, the decrease of BET specific surface area and pore volume upon IBU loading for both samples is ascribed to the adsorption of IBU molecules on the surface of NsZnO materials. As in the case of CTZ, the feasibility of using the synthetized NsZnO as carriers of IBU was confirmed. Moreover, the use of these ZnO nanostructures resulted versatile and potentially usable with different types of molecules.

As further demonstration, XRD analyses were performed to investigate the form of the IBU inside the NsZnO materials pores, after both the drug loading approaches. Figure 3.12 reports the XRD patterns of IBU@NsZnO-1 and IBU@NsZnO-2, compared with the materials as-such and with the pure crystalline drug. From the results, it is possible to draw some important observations: firstly, both materials keep showing the typical hexagonal wurtzite structure after the drug loading procedures. Secondly, no additional diffraction peaks of the crystalline IBU are observed in both cases, evidencing that the loaded drug molecules are not assembled in the crystalline structure.

This represents a further proof that $scCO_2$ can be considered as much efficient as the traditional drug loading methods, with the advantage of being a greener and cleaner approach. It is widely accepted that the amorphization of the drug molecules plays a key role in increasing their dissolution rate and solubility [1]. Moreover, since the same conclusions were drawn in the case of CTZ, also the versatile role of $scCO_2$ in acting as solvent for the drug loading of different molecules into ZnO-based carrier has been confirmed. These represent outstanding findings, considering that, to the best of our knowledge, this is the first time that the loading of drugs on NsZnO by means of $scCO_2$ has been studied. Particularly, it is worth of noting that the XRD patterns confirmed the lack of reactivity between ZnO and the CO_2 used as solvent in the drug loading phase. This result has not been taken for granted, considering that the reaction between ZnO and CO_2, to give $ZnCO_3$ as final product, is a well-known phenomenon [31,32]. To deepen this evidence, XRD analysis was performed on both the ZnO nanostructures after a treatment with $scCO_2$, carried out for 12 hours, at 35°C and 10 MPa. Figure 3.13 shows that in both cases the hexagonal wurzite pattern of ZnO was preserved, and any new peaks were detected, demonstrating the missed phase transformation of ZnO in $ZnCO_3$.

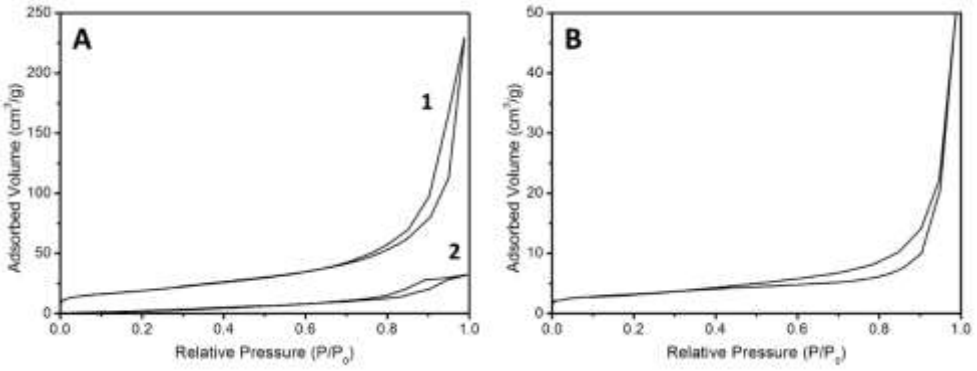

Figure 3.11 Section A: N_2 adsorption-desorption isotherms of NsZnO-1 before (1) and after (2) IBU loading. Section B: N_2 adsorption-desorption isotherms of NsZnO-\2 before IBU loading.

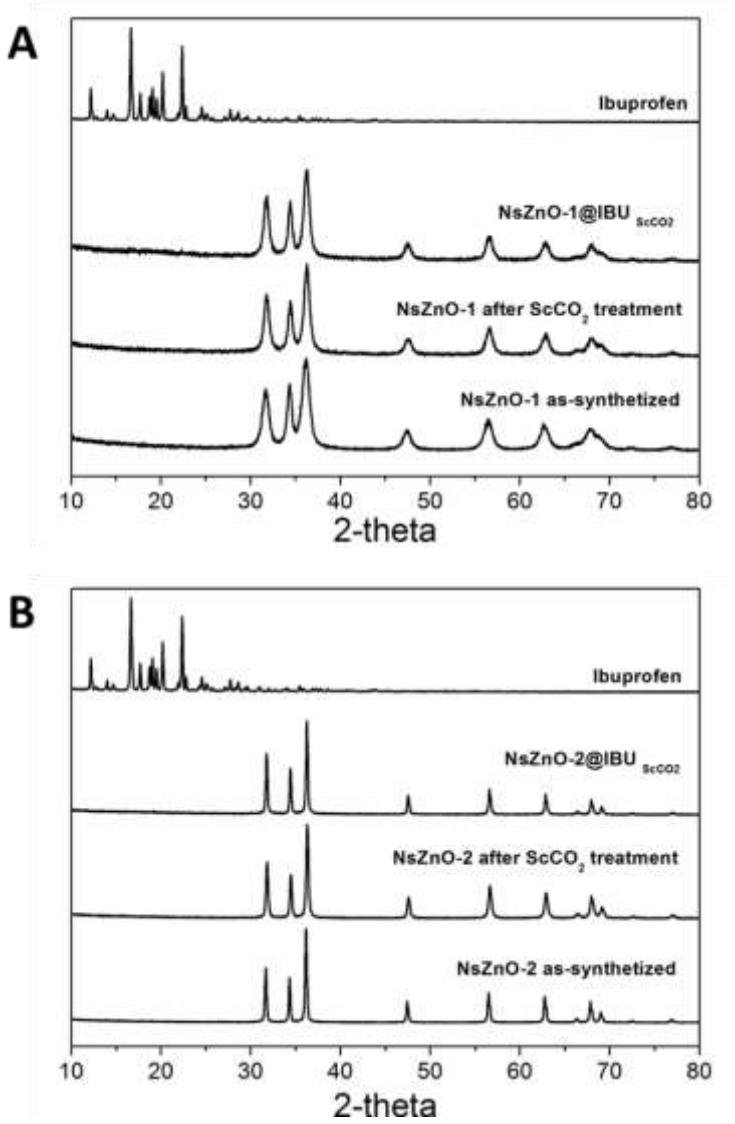

Figure 3.12 Panel A: XRD patterns of: NsZnO-1 after synthesis, IBU@NsZnO-1 after $scCO_2$ drug loading, IBU@NsZnO-1 after traditional drug adsorption and pure IBU. Panel |B: XRD patterns of: NsZnO-2 after synthesis, IBU@NsZnO-2 after $scCO_2$ drug loading, IBU@NsZnO-2 after traditional drug adsorption and pure IBU.

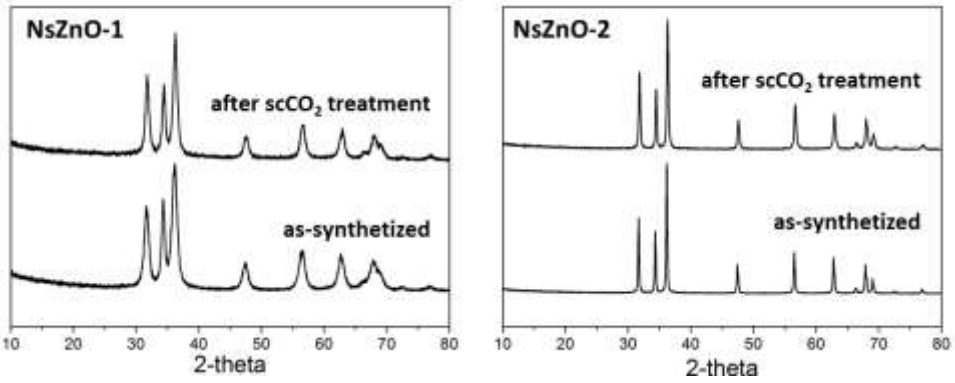

Figure 3.13 XRD spectra of NsZnO-1 and NsZnO-2 before and after a treatment in $scCO_2$ (12 hours, 40° C, 10 Mpa).

FTIR spectroscopy was performed to confirm the successful loading of IBU into both the ZnO nanostructures, after the $scCO_2$-mediated impregnation. Figure 3.14 reports the FTIR spectra of NsZnO-1 and NsZnO-2, before and after IBU loading (IBU@NsZnO-1 and IBU@NsZnO-2), in comparison with the spectrum of ibuprofen. Both the as-prepared NsZnO show a series of IR peaks between 1650 cm^{-1} and 1400 cm^{-1}, corresponding to C=O stretching, while at lower wavelength C–O stretching and C–H vibrations are present [20]. The presence of these species could be ascribed to the partially decomposition of ZnO precursors originating during the calcination treatment. This interpretation is coherent considering that the spectrum of NsZnO-1 displays a less intense peaks in the carbonate region in comparison with NsZnO-2: in fact, in the latter case the amount of organic template (Pluronic F127), modelling the ZnO particles formation, is much higher than the ZnO precursors (Zinc Carbonate Hydroxide Hydrate) from which NsZnO-1 is originated. The broad peak around 3400 cm^{-1} is attributed to O–H stretching, while the peak at about 1650 cm^{-1} corresponds to O–H bending [21]. The FTIR spectrum of pure ibuprofen clearly shows an intense peak at around 1710 cm^{-1}, ascribed to carbonyl-stretching of isopropionic acid group, while the bands at around 2900-2800 cm^{-1} correspond to hydroxyl group of carboxylic acid. As is evident from the graphs, in both the spectra of IBU@NsZnO-1 and IBU@NsZnO-2, the characteristic bands of ibuprofen at around 2900-2800 cm^{-1} are present, while the strong carbonyl stretching at 1710 cm^{-1} steeply decreases in the IBU@NsZnO-1 spectrum and disappears in that of IBU@NsZnO-2. This

change in the ν(C=O) spectral region could be attributed to a successful IBU incorporation into NsZnO samples [33]. Moreover, from the IBU@NsZnO-1 spectrum is evident that the ν(C=O) of IBU loaded into the material results shifted to high wavenumber region at 1738 cm^{-1} compared to the corresponding band of pure IBU (at 1710 cm^{-1}). This phenomenon is consistent with other results in the literature and could be ascribed to the breakage of the ibuprofen–ibuprofen interactions that are intrinsic in the solid form of this drug [15,34]. This evidence confirms the results obtained with the XRD analysis, emphasising the lack of solid crystallinity of the IBU after supercritical fluid impregnation.

As previously observed with CTZ, the IBU case study confirmed the possible protective function of the drug towards the NsZnO surfaces in reducing the adsorption of CO_2, since also in this case the carbonates region is not predominant, and the CO_2 did not react with ZnO to originate $ZnCO_3$.

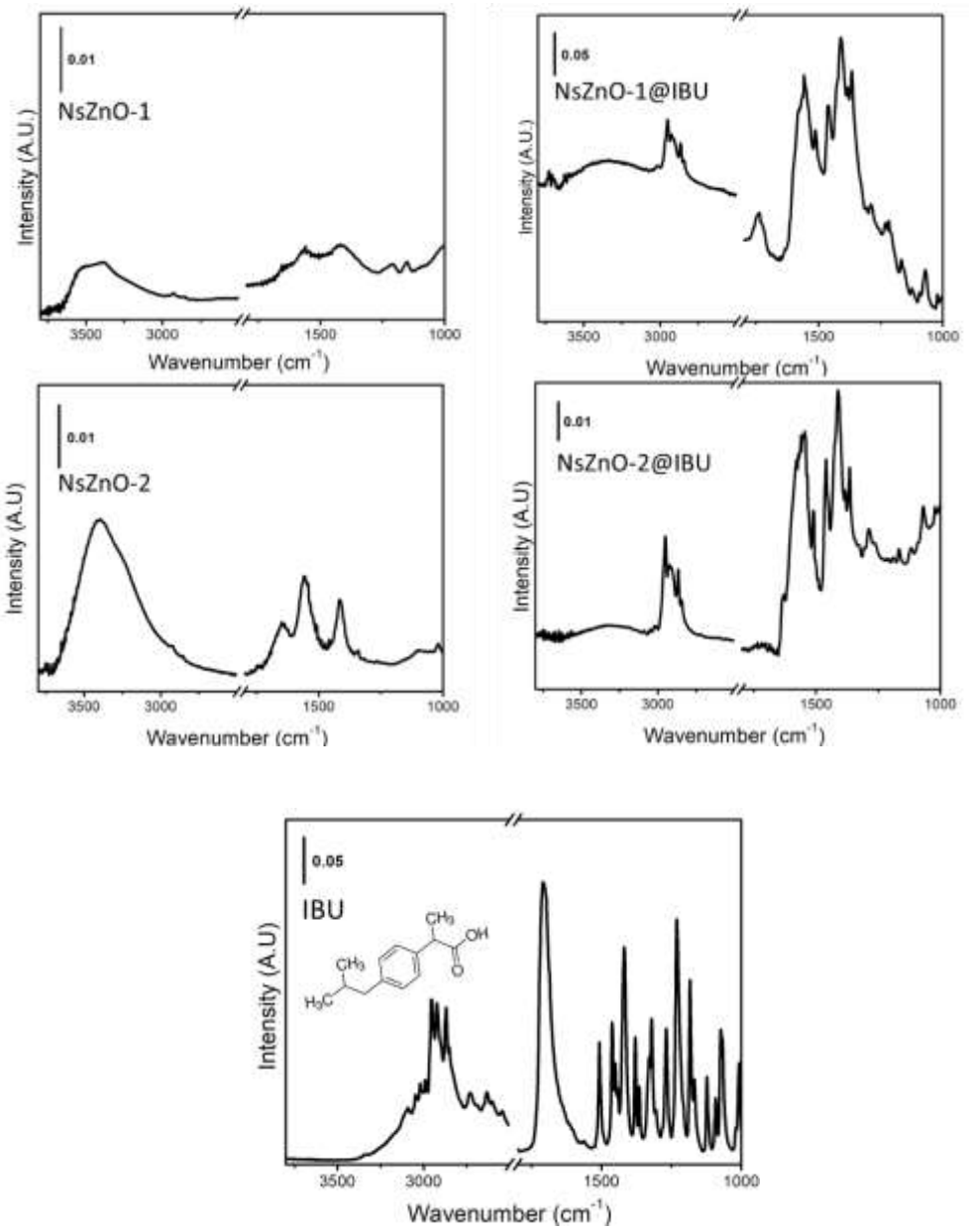

Figure 3.14 FT-IR spectra of: NsZnO-1 and NsZnO-2 before and after $scCO_2$-mediated drug loading (IBU@NsZnO-1 and IBU@NsZnO-2) in comparison with the pure ibuprofen.

NsZnO-1 and NsZnO-2 were also loaded of IBU through a traditional approach, consisting in the adsorption of the drug from an ethanolic solution. Briefly the materials were incubated for 24 hours under magnetic stirring with an IBU ethanolic solution. At end of the process, the drug loaded NsZnOs were separated from the not-encapsulated IBU solution through a centrifugation process. In order to evaluate the amount of IBU, TG analyses of the NsZnO materials loaded with IBU (IBU@NsZnO) were performed both after $scCO_2$ impregnation and after traditional adsorption loading from ethanolic solution. The characteristic curves are shown in Figure 3.15. The percentages calculated as loss of weight after TG analysis indicated that after $scCO_2$ technique the drug loading corresponded to 7% w/w for IBU@NsZnO-1 and 9% w/w for IBU@NsZnO-2, respectively, while after traditional adsorption the drug loading was found to be 9% w/w for IBU@NsZnO-$1_{(trad)}$ and 3% w/w for IBU@NsZnO-$2_{(trad)}$ (Table 3.4). Considering the drug loading amount of the sample IBU@NsZnO-1 loaded with supercritical technology, it is important to underline some considerations. As mentioned above, the loss of weight (≈ 7%) obtained from the TG analysis of the sample NsZnO-1 as-such after $scCO_2$ treatment (Fig. 3.15, panel A, red curve) could be ascribed to the loss of CO_2 adsorbed onto the material surface. This result confirmed the evidence collected by FTIR analysis (Fig. 3.8), from which the adsorption of CO_2 on the NsZnO-1 surface after the supercritical treatment was clearly displayed by the spectrum. Nevertheless, notwithstanding this evidence, it is important to take into consideration that the drug plays a protective role towards the NsZnOs surfaces, decreasing the adsorption of CO_2. This assessment clearly emerged from the FTIR analyses of the drug loaded samples and was also reported in other research works [15]. Consequently, it is reasonable to consider that the loss of weight of the sample IBU@NsZnO-1 is mostly related to the amount of IBU hosted inside the NsZnO-1 nanostructure and only in a small part to the contribution of CO_2. In conclusion, from the previous considerations it is possible to assess that the amount of IBU impregnated inside the sample NsZnO-1 after supercritical process, ranges from 14% (Fig. 3.15, panel A, green curve) to 7% (Fig. 3.15, panel A, red curve) not considering the CO_2 adsorption or considering the CO_2 adsorption, respectively.

Similar conclusions can be drawn for the sample IBU@NsZnO-2, even if the extent of CO_2 adsorbed on the material as-such (Fig.3. 15, panel B, red curve A) resulted to be minor than the sample NsZnO-1 (about 1.4%).

Consequently, the amount of IBU impregnated inside the sample NsZnO-2 after supercritical process, ranges from 10% (Fig. 3.15, panel A, green curve) to 9% (Fig. 3.15, panel A, red curve) not considering the CO_2 adsorption or considering the CO_2 adsorption, respectively.

Furthermore, it is worth of noting that a remarkable advantage in term of IBU amount hosted into both the NsZnO samples emerged using the supercritical approach in comparison with the traditional one. This advantage combined to the possibility to avoid organic solvents during the drug loading step makes the use of $scCO_2$ a promising route to develop ZnO-based reservoir of drug.

	Amount of ibuprofen incorporated	
	$scCO_2$ impregnation (%w/w)	Traditional adsorption loading (%w/w)
IBU@NsZnO-1	7-14	9
IBU@NsZnO-2	9	3

Table 3.4. Comparison between the amount of IBU incorporated in NsZnO-1 and NsZnO-2 after $scCO_2$ techniques and traditional absorption.

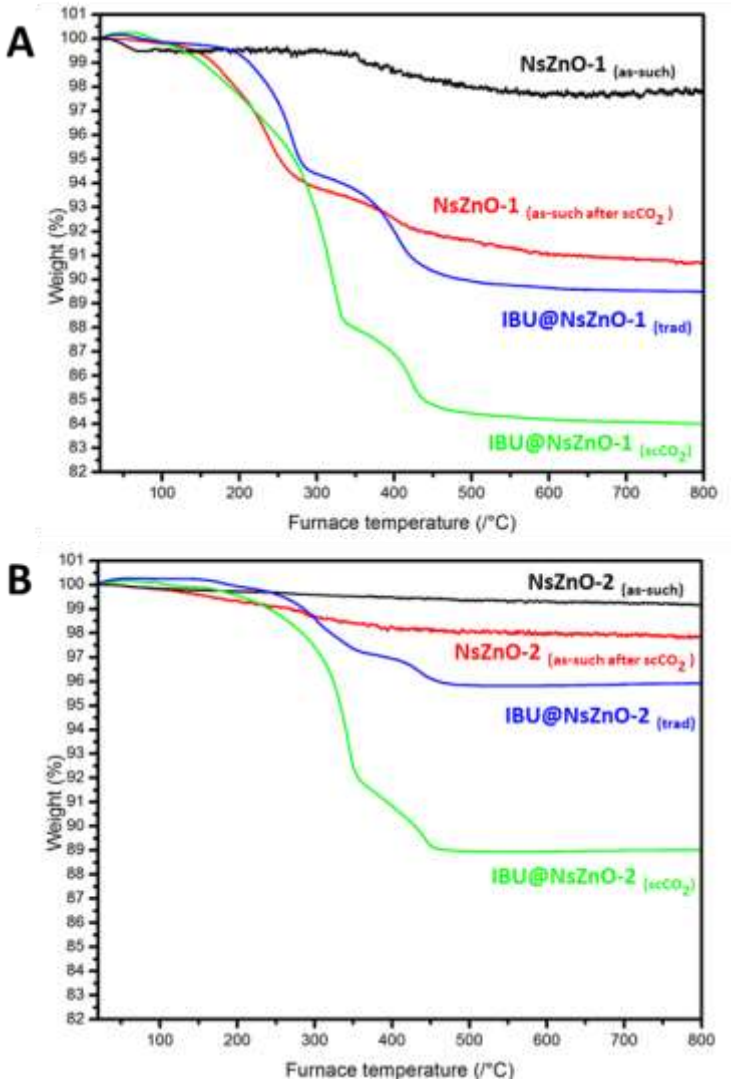

Figure **3.15** Panel A: TGA curves of: NsZnO-1 as-such, NsZnO-1 as-such after treatment in $scCO_2$, IBU@NsZnO-1 after $scCO_2$ drug loading and IBU@NsZnO-1 after traditional drug loading. Panel B: TGA curves of: NsZnO-2 as-such, NsZnO-2 as-such after treatment in $scCO_2$, IBU@NsZnO-2 after $scCO_2$ drug loading and IBU@NsZnO-2 after traditional drug loading

Preliminary in vitro drug release study

The *in vitro* release study was aimed simply at verifying the possibility of release the drug from the NsZnO carriers, assessing the lack of irreversible adsorption or occlusion of IBU molecules in the material. For this purpose, the ability of NsZnO-1 and NsZnO-2 in releasing the loaded IBU was investigated using a multi-compartmental rotating cell. Figure 3.16 displays the cumulative release curves of IBU from IBU@NsZnO-1 and IBU@NsZnO-2. As it is evident from the overall trend, the two ZnO-based carriers were able to release the same amount of drug in 6 hours. Nevertheless, the release profile of IBU from IBU@NsZnO-1 results lower during the first intervals investigated. A possible explanation for the different drug release profiles emerged from the two ZnO nanostructures, could be attributed to their different morphology affecting the delivery of the drug molecules. In fact, NsZnO-2 possess a simpler structure, based on spherical aggregates of nano-ovoidal particles. The total pore volume included among these nanoparticles is significantly lower than that of NsZnO-1 (Table 3.3), which could indicate an outer arrangement of the drug molecules on its surface. On the contrary, NsZnO-1 is characterized by a well-structured overlapping of nanosheets, which create a larger pore volume in between. The diffusion of drug molecules from this structure could require longer time than in the case of NsZnO-2.

As the total percentage of IBU released in respect to the loading is concerned, the results indicated that over than the 50% of the drug was released from both the NsZnOs in 6 hours (data not shown).

In conclusion, this preliminary *in vitro* release study clearly showed that IBU is not irreversibly confined in the NsZnO materials, confirming the role of NsZnO as drug delivery carrier, as previously demonstrated in the CTZ case study [1].

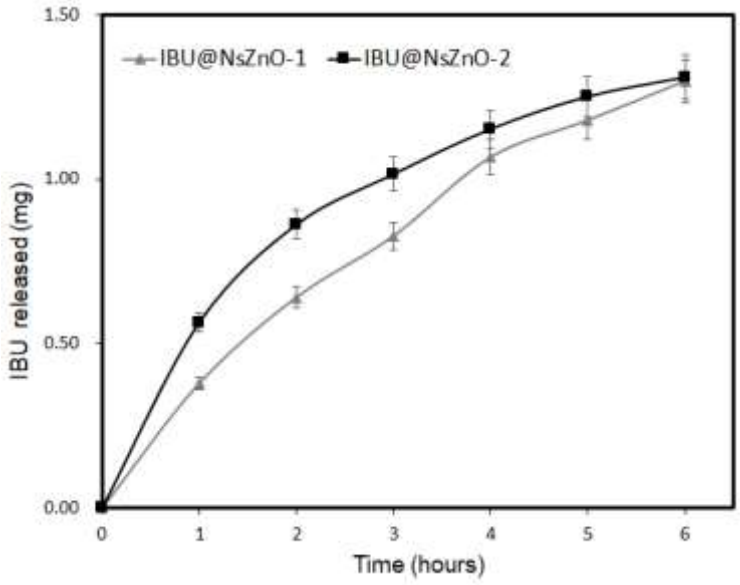

Figure 3.16 *In vitro* drug-release profiles of Ibuprofen from IBU@NsZnO-1 (light grey curve), IBU@NsZnO-2 (black curve)

3.4 Conclusions

An organic-solvent-free route to obtain a NsZnO reservoir of API was studied.

Two NsZnO materials with the hexagonal wurtzite structure and different morphologies were synthesized using wet organic-solvent-free processes. In particular, existing approaches reported in the literature for the synthesis of nanostructured ZnO films or nanosheets were properly modified to prepare novel NsZnO particles.

CTZ and IBU were loaded into NsZnO through $scCO_2$ impregnation and, at the best of our knowledge, this is the first time that a technology employing supercritical carbon dioxide was used for the drug loading of ZnO-based carriers, in order to obtain ready-to-use drug loaded materials.

The physico-chemical characterization of NsZnO before and after the loading of the APIs revealed that the $scCO_2$ process does not significantly affect the structure of the materials. A protective role of the drug molecules towards the NsZnO surface during the supercritical process was highlighted. The CTZ and IBU loading for the two NsZnO materials was significantly high, in comparison with those obtained through traditional absorption method. XRD and DSC analysis revealed that the APIs are distributed in the NsZnO carrier in amorphous form.

The capability of the materials in releasing the APIs was investigated. Results revealed that both CTZ and IBU are not irreversibly confined in the NsZnO support and that NsZnO can act as a drug delivery carrier. This might play a key role in several biological applications where the bioavailability of poorly-water-soluble drugs is still a challenging issue.

The reported results support the idea that the novel production routes here proposed to obtain NsZnO drug delivery carriers are feasible and can be a promising solvent-free alternative to the conventional ones since they are easily adabtable to batch small-scale pharmaceutical industrial process.

3.5 References

(1) Leone, F.; Gignone, A.; Ronchetti, S.; Cavalli, R.; Manna, L.; Banchero, M.; Onida, B. A Green Organic-Solvent-Free Route to Prepare Nanostructured Zinc Oxide Carriers of Clotrimazole for Pharmaceutical Applications. *J. Clean. Prod.* **2018**, *172*, 1433–1439.

(2) Kołodziejczak-Radzimska, A.; Jesionowski, T. Zinc Oxide—From Synthesis to Application: A Review. *Materials (Basel).* **2014**, *7* (4), 2833–2881.

(3) Perrut, M. Supercritical Fluid Applications: Industrial Developments and Economic Issues. *Ind. Eng. Chem. Res.* **2000**, *39* (12), 4531–4535.

(4) Kawano, T.; Imai, H. Nanoscale Morphological Design of ZnO Crystals Grown in Aqueous Solutions. *J. Ceram. Soc. Japan* **2010**, *118* (1383), 969–976.

(5) Khayatian, A.; Kashi, M. A.; Azimirad, R.; Safa, S.; Akhtarian, S. F. A. Effect of Annealing Process in Tuning of Defects in ZnO Nanorods and Their Application in UV Photodetectors. *Opt. - Int. J. Light Electron Opt.* **2016**, *127* (11), 4675–4681.

(6) Koao, L. F.; Dejene, F. B.; Swart, H. C. Properties of Flower-like ZnO Nanostructures Synthesized Using the Chemical Bath Deposition. *Mater. Sci. Semicond. Process.* **2014**, *27* (1), 33–40.

(7) Shaikh, S. K.; Inamdar, S. I.; Ganbavle, V. V.; Rajpure, K. Y. Chemical Bath Deposited ZnO Thin Film Based UV Photoconductive Detector. *J. Alloys Compd.* **2016**, *664*, 242–249.

(8) Shi, Y.; Truong, V. X.; Kulkarni, K.; Qu, Y.; Simon, G. P.; Boyd, R. L.; Perlmutter, P.; Lithgow, T.; Forsythe, J. S. Light-Triggered Release of Ciprofloxacin from an in Situ Forming Click Hydrogel for Antibacterial Wound Dressings. *J. Mater. Chem. B* **2015**, 3–6.

(9) Kakiuchi, K.; Hosono, E.; Kimura, T.; Imai, H.; Fujihara, S. Fabrication of Mesoporous ZnO Nanosheets from Precursor Templates Grown in Aqueous Solutions. *J. Sol-Gel Sci. Technol.* **2006**, *39* (1), 63–72.

(10) Banchero, M.; Manna, L.; Ronchetti, S.; Campanelli, P.; Ferri, A. Supercritical Solvent Impregnation of Piroxicam on PVP at Various Polymer Molecular Weights. *J. Supercrit. Fluids* **2009**, *49* (2), 271–278.

(11) Gignone, A.; Manna, L.; Ronchetti, S.; Banchero, M.; Onida, B. Microporous and Mesoporous Materials Incorporation of Clotrimazole in Ordered Mesoporous Silica by Supercritical CO 2. *Microporous Mesoporous Mater.* **2014**, *200*, 291–296.

(12) Hoogerheide, J. G.; Wyka, B. E. Clotrimazole. *Anal. Profiles Drug Subst.* **1982**, *11*, 225–255.

(13) Szymańska, E.; Winnicka, K.; Amelian, A.; Cwalina, U. Vaginal Chitosan Tablets with Clotrimazole — Design and Evaluation of Mucoadhesive Properties Using Porcine Vaginal Mucosa , Mucin and

Gelatine. *Chem. Pharm. Bull.* **2014**, *62* (2), 160–167.
(14) Tozuka, Y.; Fujito, T.; Moribe, K.; Yamamoto, K. Ibuprofen-Cyclodextrin Inclusion Complex Formation Using Supercritical Carbon Dioxide. *J. Incl. Phenom. Macrocycl. Chem.* **2006**, *56* (1–2), 33–37.
(15) Kazarian, S. G.; Martirosyan, G. G. Spectroscopy of Polymer/drug Formulations Processed with Supercritical Fluids: In Situ ATR-IR and Raman Study of Impregnation of Ibuprofen into PVP. *Int. J. Pharm.* **2002**, *232* (1–2), 81–90.
(16) Hussein, K.; Türk, M.; Wahl, M. A. Comparative Evaluation of Ibuprofen/β-Cyclodextrin Complexes Obtained by Supercritical Carbon Dioxide and Other Conventional Methods. *Pharm. Res.* **2007**, *24* (3), 585–592.
(17) Charoenchaitrakool, M.; Dehghani, F.; Foster, N. R. Utilization of Supercritical Carbon Dioxide for Complex Formation of Ibuprofen and Methyl-Beta-Cyclodextrin. *Int. J. Pharm.* **2002**, *239*, 103–112.
(18) Scherrer, P. Bestimmung Der Grösse Und Der Inneren Struktur Internal, Kolloidteilchen Mittels Röntgensrahlen [Determination of the Size and Goettingen, Structure of Colloidal Particles Using X-Rays]. *Nachr Ges Wiss Germa, Math-Phys Kl.* **1918**, 98–100.
(19) Ueno, N.; Dwijaya, B.; Uchida, Y.; Egashira, Y.; Nishiyama, N. Synthesis of Mesoporous ZnO, AZO, and BZO Transparent Conducting Films Using Nonionic Triblock Copolymer as Template. *Mater. Lett.* **2013**, *100*, 111–114.
(20) Sowri Babu, K.; Ramachandra Reddy, A.; Sujatha, C.; Venugopal Reddy, K.; Mallika, A. N. Synthesis and Optical Characterization of Porous ZnO. *J. Adv. Ceram.* **2013**, *2* (3), 260–265.
(21) Mitra, S.; B., S.; Patra, P.; Chandra, S.; Debnath, N.; Das, S.; Banerjee, R.; Kundu, S. C.; Pramanik, P.; Goswami, A. Porous ZnO Nanorod for Targeted Delivery of Doxorubicin: In Vitro and in Vivo Response for Therapeutic Applications. *J. Mater. Chem.* **2012**, *22* (45), 24145.
(22) Galhotra, P. Carbon Dioxide Adsorption on Nanomaterials. *Theses Diss.* **2010**.
(23) Pradines, B.; Gallard, J. F.; Iorga, B. I.; Gueutin, C.; Ponchel, G.; Loiseau, P. M.; Bouchemal, K. The Unexpected Increase of Clotrimazole Apparent Solubility Using Randomly Methylated β-Cyclodextrin. *J. Mol. Recognit.* **2015**, *28* (2), 96–102.
(24) Ravikumar, P. HONEY BASED CLOTRIMAZOLE. **2017**, No. January.
(25) Ismail, N. B. S.; Narayana, B. Spectrophotometric and Spectroscopic Studies on Charge Transfer Complexes of the Antifungal Drug Clotrimazole. *J. Taibah Univ. Sci.* **2017**, *11* (5), 710–717.
(26) Gignone, A.; Piane, M. D.; Corno, M.; Ugliengo, P.; Onida, B.

Simulation and Experiment Reveal a Complex Scenario for the Adsorption of an Antifungal Drug in Ordered Mesoporous Silica. *J. Phys. Chem. C* **2015**, *119*, 13068−13079.

(27) McCarthy, C. A.; Ahern, R. J.; Dontireddy, R.; Ryan, K. B.; Crean, A. M. Mesoporous Silica Formulation Strategies for Drug Dissolution Enhancement: A Review. *Expert Opin. Drug Deliv.* **2016**, *13* (1), 93–108.

(28) Al-Marzouqi, A. H.; Elwy, H. M.; Shehadi, I.; Adem, A. Physicochemical Properties of Antifungal Drug-Cyclodextrin Complexes Prepared by Supercritical Carbon Dioxide and by Conventional Techniques. *J. Pharm. Biomed. Anal.* **2009**, *49* (2), 227–233.

(29) Banchero, M.; Ronchetti, S.; Manna, L. Characterization of Ketoprofen / Methyl-Beta-Cyclodextrin Complexes Prepared Using Supercritical Carbon Dioxide. *J. Chem.* **2013**, *2013*, 8.

(30) Ravi, S.; Rudrangi, S.; Trivedi, V.; Mitchell, J. C.; Wicks, S. R.; Alexander, B. D. Preparation of Olanzapine and Methyl- B -Cyclodextrin Complexes Using a Single-Step , Organic Solvent-Free Supercritical Fl Uid Process : An Approach to Enhance the Solubility and Dissolution Properties. *Int. J. Pharm.* **2015**, *494* (1), 408–416.

(31) Anas, M.; Gönel, A. G.; Bozbag, S. E.; Erkey, C. Thermodynamics of Adsorption of Carbon Dioxide on Various Aerogels. *J. CO2 Util.* **2017**, *21* (1), 82–88.

(32) Graedel, T. E. Corrosion Mechanisms for Zinc Exposed to the Atmosphere. *J Electrochem Soc* **1989**, *136* (4).

(33) Morgado, P. I.; Miguel, S. P.; Correia, I. J.; Aguiar-Ricardo, A. Ibuprofen Loaded PVA/chitosan Membranes: A Highly Efficient Strategy towards an Improved Skin Wound Healing. *Carbohydr. Polym.* **2017**, *159*, 136–145.

(34) Shakhtshneider, T. P.; Vasiltchenko, M. A.; Politov, A. A.; Boldyrev, V. V. The Mechanochemical Preparation of Solid Disperse Systems of Ibuprofen-Polyethylene Glycol. *Int. J. Pharm.* **1996**, *130* (1), 25–32.

Chapter 4

Mesoporous ZnO as drug reservoir of clotrimazole: synthesis, drug loading and characterization

4.1 Introduction

As previously described, the different nanostructured ZnO materials investigated in this thesis have been thought for a dermatological application. The fundamental idea is focused on the development of a *multitasking ZnO based drug delivery carrier*, biologically active on the skin for its intrinsic properties, and able to deliver a pharmaceutical molecule.

This chapter deals with a research work addressed to the study of a third type of nanostructured ZnO material (NsZnO-3). Despite of NsZnO-1 and NsZnO-2 have been obtained with organic solvent-free synthesis methods [1], the approach adopted in this investigation consisted in a widely adopted precipitation synthesis, based on the hydrolysis of a zinc salt in basic alcoholic solutions. Since this method is based on difference mechanisms for the ZnO synthesis from the previously described materials, possible differences in terms of morphology, crystalline structure, porosity and capability in releasing

the drug were evaluated. Clotrimazole (CTZ) was selected as drug model in this investigation. Two different techniques were adopted for the incorporation of the drug, consisting in supercritical CO_2 ($scCO_2$) and impregnation from solution. A careful characterization of the physical-chemical profile of the material was performed, as-such and after the drug incorporation, using a wide range of techniques, such as X-ray diffractometry (XRD), Nitrogen adsorption (BET), Fourier transformed infrared spectroscopy (FT-IR), Field electronically-scanned microscopy (FESEM) and Ultraviolet-Visible Spectroscopy. Furthermore, a preliminary evaluation of the biological profile of this material was defined, performing an *in vitro* CTZ release study.

4.2 Experimental

4.2.1 Materials

All the chemicals were purchased from Sigma Aldrich (Italy) and were of analytical grade, used as received. Carbon dioxide with a purity of 99.998% was supplied by SIAD (Italy). Bidistilled water was used throughout this study.

4.2.2. Synthesis of nanostructured ZnO using the precipitation method

In order to synthetize NsZnO-3, a traditional precipitation approach was selected. The procedure was adopted from [2] and modified. Firstly, two separate suspensions were prepared, dissolving 14.75 g of Zinc Acetate Dihydrate ($(CH_3COO)_2$ $Zn{\cdot}2H_2O$) in 60 ml of methanol and 7,4 g of Potassium Hydroxide in (KOH) in 32 ml of methanol. Then the two suspensions were mixed, under magnetic stirring, at room temperature. Secondly, the reaction was run at 60° C for 3 days, in reflux. At the end of this procedure, in order to separate the ZnO white precipitate, the suspension was centrifugated for 15 minutes at 4000 rpm and subsequently washed three times, to eliminate the KOH excess. Finally, the white precipitate was dried in oven at 40°C for 24 hours.

4.2.3. Drug loading of NsZnO-3

CTZ was selected as drug model in this investigation. The drug loading phase was performed using two different techniques: incorporation with supercritical CO_2 and traditional impregnation from solution.

Drug loading through supercritical carbon dioxide

The supercritical impregnation process adopted in this research work for the loading of clotrimazole into NsZnO-3, was the same described in the Chapter 3 of this thesis (*for further details see Chapter 3, paragraph 3.2.3*).

Drug loading through traditional impregnation

The drug loading of NsZnO-3 was also carried out through a traditional impregnation method, as described in [3]. For this purpose, 50 mg of NsZnO

were incubated with an ethanolic solution of clotrimazole (60 mg/ml), under stirring for 24 hours, at room temperature. Then, in order to separate the drug loaded ZnO, the suspension was centrifugated at 4000 rpm for 30 minutes. The supernatant solution was then analyzed and the amount of entrapped clotrimazole was determined with the Equation 2.1 and the loading capacity of the material was determined by the Equation 2.2.

$$\text{Eq. 2.1. Entrapment efficiency \%} = \frac{\text{CTZ added} - \text{Free CTZ}}{\text{CTZ added}} * 100$$

The quantitative analysis of clotrimazole was performed by using a UV-VIS spectrophotometer (PerkinElmer Lambda 5) detecting the absorbance value at 254 nm.

4.2.4 Preliminary *in vitro* drug release study

The ability of the drug-loaded NsZnO-3 to release clotrimazole was demonstrated with an *in vitro* released study, based on the use of a multicompartment rotating cell. Three different samples were tested. Particularly, the release profiles of the NsZnO-3 loaded with CTZ through $scCO_2$ process (CTZ@NsZnO-3 $_{scCO2}$) and that of NsZnO-3 impregnated with CTZ by traditional approach (CTZ@NsZnO-3 $_{trad}$) was compared with pure crystalline CTZ. A hydrophilic dialysis membrane (Spectra/Por, Spectrum®, cut-off 12000-14000 Da) was used to separate the samples from the receiving phase, consisting in a citrate/buffer/ Tween 80 solution [4]. After fixed time intervals, the receiving phase was completely replaced by a fresh solution. The experiment was performed for 8 hours. A quantitative analysis by UV spectroscopy (*PerkinElmer Lambda 5*) at 264 nm was carried out in order to determine the amount of released drug on each withdrawn sample.

4.2.5. Characterization

The characterization of NsZnO-3 was carefully performed before and after the drug loading phase. Particularly, a wide range of techniques were adopted in order to define both the physical-chemical properties of the material and its biological behavior. The structure and morphology of the samples were investigated using a field emission scanning electron microscope (FESEM) *ZEISS MERLIN*. XRD patterns were obtained using a *PANalytical X'Pert* (Cu Kα radiation) diffractometer. Data were collected with a 2D solid state detector (PIXcel) from 20 to 70 2θ with a step size of 0.001 2θ and a wavelength of 1.54187 Å. Crystallites size was determined according to Scherrer equation [5] by comparing the profile width of a standard profile with the sample profile. The Scherrer equation relates the width of a powder diffraction peak to the average dimensions of crystallites in a polycrystalline powder:

$$D = K\lambda / \beta_{(2\theta)hkl} \cos\theta$$

where β is the crystallite size contribution to the peak width (full width at half maximum) in radians, K (shape factor) is a constant near unit and D is the average thickness of the crystal in a direction normal to the diffracting plane hkl.

Profile fits were performed using X'Pert High Score Plus, using Pseudo-Voigt peak function with Kα1 and Kα2 fitting on a background stripped pattern. The sample-induced peak broadening β was determined by subtracting the instrumental peak width from the measured peak width. In order to perform the FTIR analysis, the materials were pelletized as such, without KBr. The auto-supported pellets were analyzed using a *Bruker Equinox 55* in the wavelength range of 4000 - 400 cm^{-1}. Spectra were recorded in different conditions: at room temperature and atmospheric pressure and after an *outgassing* step at room temperature after high vacuum (10^{-3} Pa) treatment for 1 hour.

Thermal gravimetric analysis TG analyses were carried out between 20°C and 800°C in air (flow rate 100 mL/min with a heating rate of 10 °C /min) using a SETARAM 92 instrument.

4.3. Results and discussion

4.3.1. Characterization of NsZnO-3 as such

The aim of this investigation was to synthesize and characterize a nanostructured ZnO material able to act as drug reservoir. A traditional precipitation method was adopted and NsZnO-3 was obtained starting from Zinc acetate dehydrate ($Zn(CH_3COO)_2 \cdot 2\ H_2O$) as a precursor and a solution of Potassium Hydroxide (KOH) in methanol (CH_3OH) as solvent. Generally, methanol is selected in this type of synthesis for two main reasons. Firstly, it has a high dielectric constant and low ligand affinity [6], which make it an excellent solvent for Zinc acetate dehydrate, an electrolytic salt commonly used for synthesizing colloidal ZnO nanoparticles. Secondly, methanol can act as ligands to help to control the morphology of ZnO. For instance, it is reported that methanol is a better solvent than other alcohols for growing spherical ZnO crystals [6], which is an important parameter in biological applications. During the precipitation synthesis in basic conditions, a sequence of different chemical reactions take place. Briefly, the complete hydrolysis of zinc acetate in equilibrium with condensation reactions endows to the formation of a colloidal suspension of ZnO particles. The hydrolysis of Zinc Acetate in solution produces acetate ions and zinc ions, helped by the heating. The abundance of electrons in the oxygen atoms makes the hydroxyl gr$oups (-OH) of alcohol molecules bond with the zinc ions. The overall chemical reaction to form ZnO nanopowder as follow:

$$(Zn(CH_3COO)_2 \cdot 2H_2O) + 2KOH \rightarrow ZnO + 2CH_3CO_2K + H_2O$$

During the hydrolysis reaction, also the intermediate Zinc hydroxide acetate is formed in the presence of H_2O and OH ions, that is transformed into ZnO during the reaction [7]. After the synthesis, the sample was washed and then dried in an oven. At the end of this treatment, a white powder was obtained. NsZnO-3 as such was carefully characterized, before the loading with CTZ.

Figure 4.1 displays pictures of the as-prepared NsZnO-3, collected through FESEM analysis. At lower magnification, the material appears in form of micrometric platforms ($\approx$ 10 μm) without any precise shape. However, increasing the magnification, it is possible to observe a sub-micrometric organization of this larger aggregates in smaller spherical nanoparticles with

homogenous size (≈ 20 nm). The morphology obtained in this investigation can be considered suitable for a biological application, not including any rod-like particles, often related to toxicological issues..

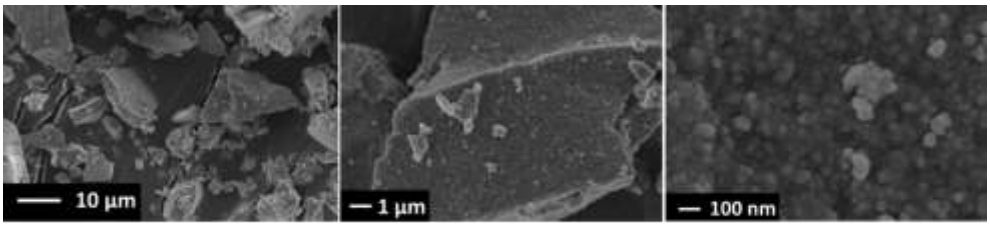

Figure 4.1. FESEM images of NsZnO-3 as synthesized, at different magnification (from the left to the right 5.0, 25.0 and 250.00 K X)

Figure 4.2 reports the XRD patterns of NsZnO-3 as such. A highly crystalline single hexagonal phase of wurtzite structure was confirmed. The five main reflection peaks (100), (002), (101), (102) and (110) and the intensity distribution of the peaks are consistent with those of the standard card for the hexagonal phase ZnO (JCPDS ICDD 36-1451). The characteristic peaks of the synthesis precursors do not appear in the XRD pattern of NsZnO-3, meaning that pure ZnO can be obtained through the above-described synthetic method. Moreover, the crystallites size determined using the Scherrer equation are was about 18 nm (Table 2.1).

Table 4.1 Crystallite dimensions (nm) determined from application of the Scherrer equation to selected peaks position of NsZnO-3

Peak position [°2Th]	***NsZnO-3***
36.32	18
47.64	22
56.73	17
63.04	18

FTIR spectroscopy was performed on the as-prepared NsZnO-3 after a treatment in vacuum at room temperature for 1 hour. Panel B of the Figure 4.2 reports the FTIR spectrum obtained. The main peaks displayed are consistent with the literature [2]. In particular, the presence of O–H and C=O groups on the surface is evident. The broad peak around 3400 cm^{-1} is ascribed to the O–H

stretching, while the narrower peak at 1413 cm^{-1} can be assigned to O–H bending [8]. The peaks at 1583 cm^{-1} and at 1334 cm^{-1} can be related to carbonate-like species.

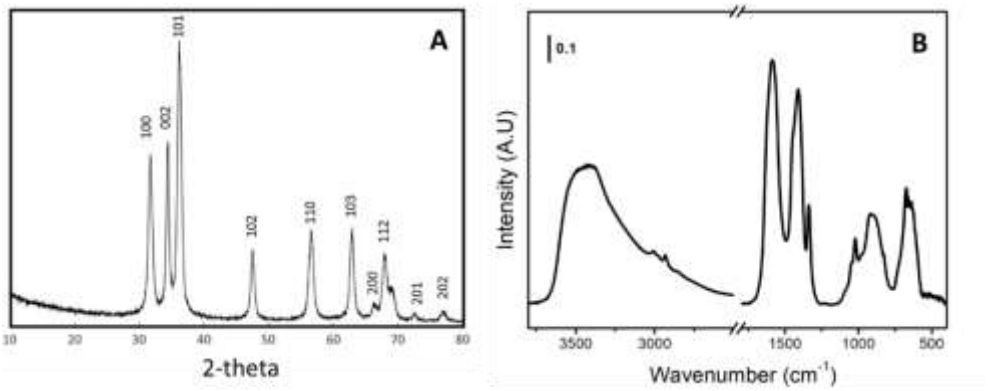

Figure 4.2. X-ray diffraction pattern (panel A) and FTIR spectrum of NsZnO-3 as-synthesized (panel B)

In order to develop a good drug reservoir material, a porous structure with a high surface area is desirable. For this purpose, N_2 adsorption–desorption analysis was carried out on NsZnO-3 as-synthetized to evaluate its surface area (SSA_{BET}), pore volume and pore size distribution before the drug loading steps. Figure 4.3 shows the isotherm of NsZnO-3, which is characterized by a regular IV type hysteresis, which is associated with capillary condensation taking place in mesopores. The specific surface area (m^2/g) and the pore volume (m^3/g) of the sample were found to be 57 m^2/g and 0.135 m^3/g, as reported in Table 4.2.The pore size distribution resulted homogenous at 10.5 nm, confirming the mesoporous nature of the NsZnO-3 material.

4.3.2 Characterization of the CTZ-loaded NsZnO-3

Two different techniques were used to load CTZ inside the NsZnO-3, in order to compare the innovative supercritical fluid technology to a traditional approach, investigating advantages and drawbacks. After the $ScCO_2$ process a ready-to-use drug loaded material was obtained, without any further purification process. TG analyses of the NsZnO-3 material loaded with CTZ (CZT@NsZnO-3) allowed the amount of CTZ to be evaluated, which corresponds to 7% w/w (Table 4.2). As far the N_2 adsorption analysis is

concerned, Figure 4.3 shows the isotherms of NsZnO-3 materials before and after the loading of CTZ through $scCO_2$ and the values of surface area, pore volume and pore sizes are reported in Table 4.2.

Table 4.2 Surface area, pore volume and pore sizes values before and after the CTZ loading, together with the amount of CTZ adsorbed into NsZnO-3 by scCO2 process

CTZ@NsZnO-3$_{scCO_2}$

	Before drug incorporation	*After drug incorporation*
Surface Area (m^2/g)	57	18
Pore Volume (cm^3/g)	0.135	0.040
Pore sizes (Å)	105	68
Amount of CTZ incorporated (W/W%)	-	4-7

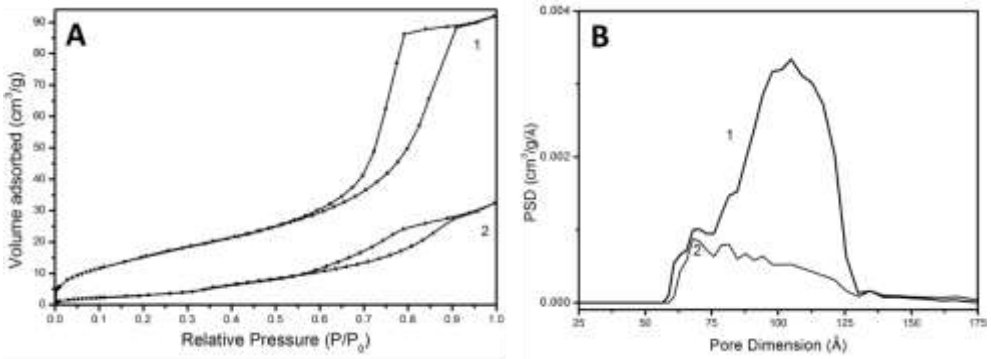

Figure 4.2. Panel A: N_2 adsorption - desorption isotherm of NsZnO-3, before (curve 1) and after (curve 2) supercritical impregnation. Panel B: pore size distribution of NsZnO NsZnO-3, before (curve 1) and after (curve 2) supercritical impregnation.

As illustrated in Table 4.2, the BET specific surface area decreased from 57 m^2/g, for the as-synthetized material, to 18 m^2/g, after CTZ loading, whereas the pore volume decreased from 0.135 cm^3/g to 0.040 cm^3/g. Moreover, the pore sizes value decreased from 10.5 to 6.8 nm. The decrease of BET specific surface area and pore volume upon CTZ loading for both samples is ascribed to the adsorption of CTZ molecules on the surface of NsZnO-3 material. These remarkable results confirmed the feasibility of using the $scCO_2$ technology as drug loading approach to obtain ZnO-based CTZ carrier, as already emerged for the other materials considered in this thesis. For the sake of comparison, NsZnO-3 was also loaded with CTZ through a

traditional approach, consisting in the adsorption of the drug from an ethanolic solution. Briefly the material was incubated for 24 hours under magnetic stirring with a CTZ ethanolic solution. After 24 hours, a separation process by centrifuge was carried out, in order to divide the drug loaded material (CTZ@NsZnO-3 $_{trad}$) from the solution of not entrapped CTZ. The entrapment efficiency (%) of the NsZnO-3 resulted 33%. The precipitate, consisting in the CTZ loaded material, was used to determine its drug content by TG analysis, as described later.

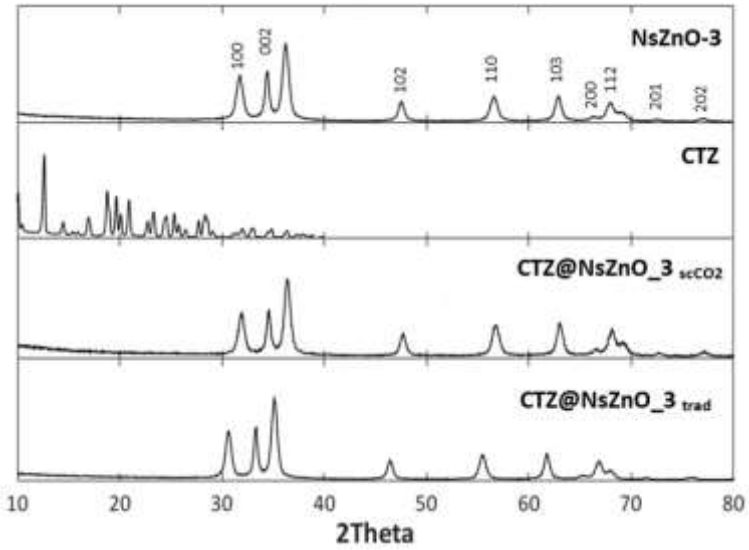

Figure 4.3 XRD patterns of the samples NsZnO-3 after supercritical drug impregnation and after traditional drug loading, in comparison with the material as such and the plane Clotrimazole (CTZ).

XRD analyses were performed to investigate the form of the drug inside the NsZnO-3 material pores. Figure 4.3 reports the XRD patterns of the samples NsZnO-3 after supercritical drug impregnation and after traditional drug loading, in comparison with the material as-such and the plane CTZ. In both cases, the drug loaded materials show the typical hexagonal wurtzite structure. The crystallites size determined using the Scherrer equation are similar to values reported in Table 4.1. No additional diffraction peaks of the crystalline CTZ are observed in both cases. This evidences that the loaded drug molecules are not assembled in the crystalline structure. Despite of the two

different drug loading approaches, the complete amorphization of CTZ was observed in both cases. As underlined in the previous chapter, this behavior is ascribed to the interaction between the drug molecules and the ZnO surface. It is widely accepted that the amorphization of the drug molecules plays a key role in increasing their dissolution rate and solubility [1]. This represents a further proof that $scCO_2$ can be considered as much efficient as the traditional drug loading methods, with the advantage of being a greener and cleaner approach. Morevoer, it is worth of noting that the XRD patterns confirmed again the lack of reactivity between ZnO and the CO_2 used as solvent in the drug loading phase. As highlighted in the previous chapter, this result has not been taken for granted, considering that the well-known reaction between ZnO and CO_2, to give $ZnCO_3$ as final product [10,11]. Since the same conclusions were achieved study the CTZ incorporation into NsZnO-1 and NsZnO-2 samples, it is possible to affirm that $scCO_2$ can be equal effective in the drug loading of different ZnO nanostructures, not causing any structure modification of the starting nanostructured ZnO and proven the feasibility in using this technology with ZnO-based materials. This represents an outstanding conclusion, considering that, to the best of our knowledge, this is the first time that the loading of drugs on NsZnO by means of $scCO_2$ has been studied.

After the supercritical-mediated drug loading step, FTIR spectroscopy was performed to i) confirm the successful loading of CTZ into NsZnO-3 and ii) to study the effect of the supercritical carbon dioxide on the NsZnO-1 surface. Figure 4.4 reports the FTIR spectra of NsZnO-3 as such, CTZ@NsZnO-3, NsZnO-3 as-such after a $scCO_2$ treatment and pure clotrimazole. FTIR spectra of the as-prepared NsZnO-3 and of pure clotrimazole has been previously reported and discussed, respectively in Figure 4.2 and Figure 3.8. In order to evaluate the effect of the supercritical carbon dioxide on the mesoporous NsZnO-3 surface, FTIR analysis was also performed on the sample as-such after a treatment in $scCO_2$ for 12 hours, at 100°C and 25 MPa. As emerged in the cases of NsZnO-1 and NsZnO-2, the spectrum shows an intensity growth of the absorption between the 1600 and 1000 cm^{-1} due to carbonate-like species caused by the adsorption of CO_2 on ZnO surface [9]. Notwithstanding the evident CO_2 adsorption on the surface of the sample NsZnO-3 as -such after the treatment in $scCO_2$, the FTIR spectrum of the CTZ@NsZnO-3, impregnated through $scCO_2$ process, shows clearly the characteristic peaks of the drug. Moreover, the growth of the absorption region between the 1600 and 1100 cm-1 caused by the adsorption of CO_2 on CTZ@NsZnO-3 surface results less

intense than the NsZnO-3 as-such. In summary, the evidences drawn from the FTIR spectroscopy studies endow to confirm the same conclusions highlighted for the other ZnO nanostructures: *i)* a successful loading of CTZ into NsZnO-3 was achieved by supercritical process; *ii)* the presence of the drug reduces the chemisorption of CO_2.

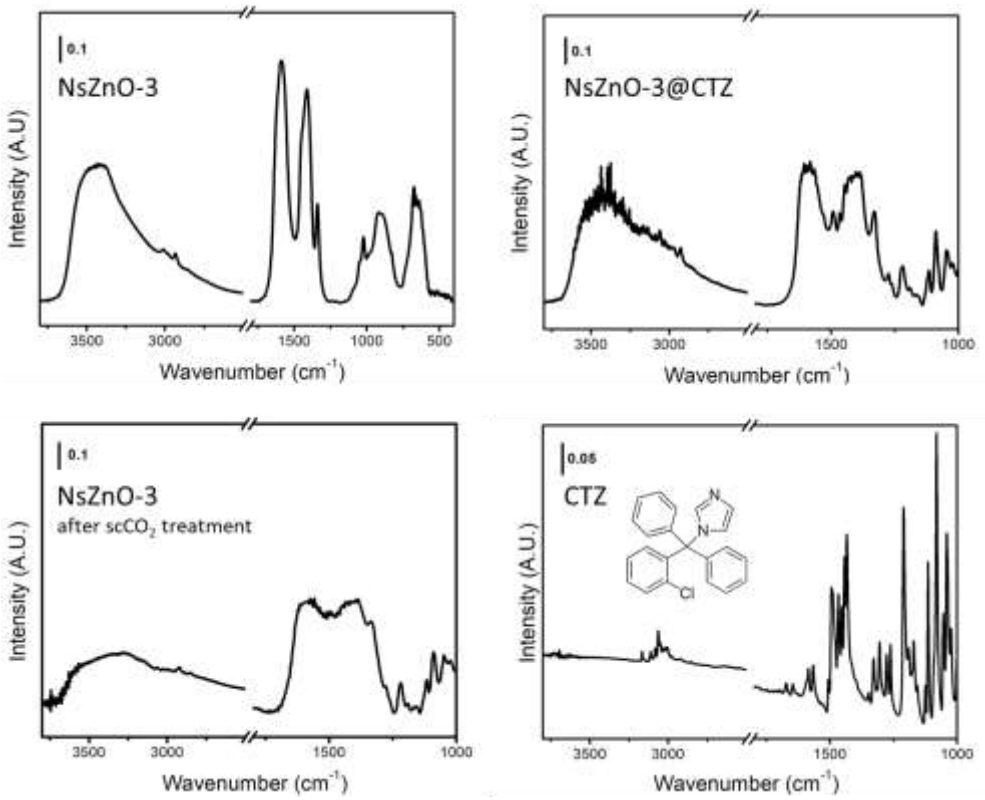

Figure 4.4 FTIR spectra of the samples NsZnO-3 as-synthetized, NsZnO-3 after a $scCO_2$ treatment, CTZ@NsZnO-3 and crystalline clotrimazole (CTZ).

In order to evaluate the amount of CTZ, TG analyses of the NsZnO-3 samples loaded with CTZ (CTZ@NsZnO-3) were performed both after $scCO_2$ impregnation and after traditional adsorption loading from ethanolic solution. The characteristic curves are shown in Figure 4.5. The percentages calculated as loss of weight after TG analysis indicated that after $scCO_2$ technique the drug loading corresponded to about 7% w/w for CTZ@NsZnO-3 while after traditional adsorption the drug loading was found to be 8% w/w for CTZ@NsZnO-$3_{(trad)}$. Considering the drug loading amount of the sample CTZ@NsZnO-3 loaded with supercritical technology, it is important to

underline some considerations. As mentioned above, the loss of weight (≈ 3%) obtained from the TG analysis of the sample NsZnO-3 as-such after $scCO_2$ treatment (Fig.4.5, red curve) could be ascribed to the loss of CO_2 adsorbed onto the material surface. Also in this case, this result confirmed the evidence collected by FTIR analysis (Fig. 4.4), from which the adsorption of CO_2 on the NsZnO-3 surface after the supercritical treatment was clearly displayed by the spectrum. Nevertheless, notwithstanding this evidence, it is important to take into consideration that the drug plays a protective role towards the NsZnOs surfaces, decreasing the adsorption of CO_2. This assessment clearly emerged from the FTIR analyses of the drug loaded samples and was also reported in other research works [12]. Consequently, it is reasonable to consider that the loss of weight of the sample CTZ@NsZnO-3 is mostly related to the amount of CTZ hosted inside the NsZnO-3 nanostructure and only in a small part to the contribution of CO_2. In conclusion, from the previous considerations it is possible to assess that the amount of CTZ impregnated inside the sample NsZnO-3 after supercritical process, ranges from 4% (Fig. 4.5, red curve) to 7% (Fig. 4.5, green curve) considering the CO_2 adsorption or not considering the CO_2 adsorption, respectively.

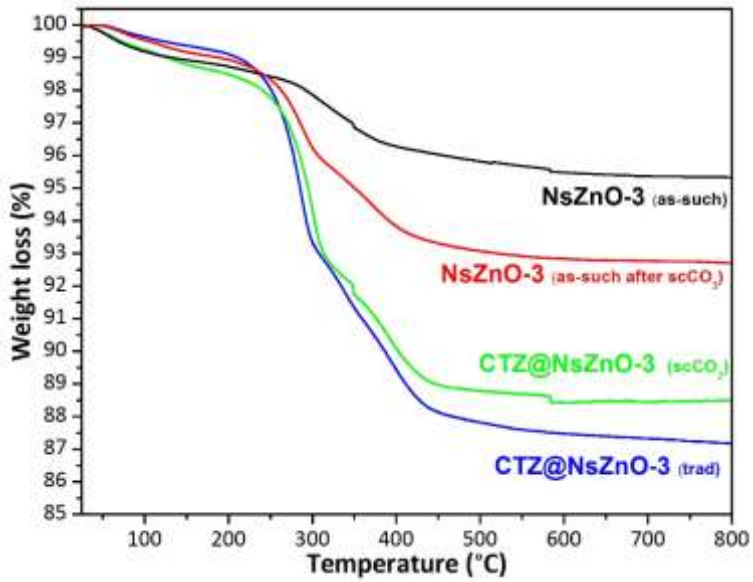

Figure 4.5 TG analyses of NsZnO-1 as-such (black curve), NsZnO-1 as-such after $scCO_2$ treatment (red curve), NsZnO-1 loaded with CTZ after $scCO_2$ (green curve) and after traditional approach (blue curve)

In term of CTZ amount hosted into the mesoporous NsZnO-3 material emerged that using traditional approach a slight higher amount of drug was impregnated, equal to about 8% (Fig. 4.5, blu curve).

The comparison between the $scCO_2$-based drug loading with the traditional absorption method leads to some interesting conclusions, which highlight the remarkable advantages of using $scCO_2$ technology. Firstly, as mentioned above, after the $scCO_2$ process a ready-to-use drug loaded material was obtained, without any further purification process. The possibility to skip the purification step results in a more time-effective drug loading procedure. Secondly, the $scCO_2$ is a green solvent, which allows to dissolve many poorly-water soluble molecules. This represents a great advantage, considering that huge amounts of organic solvent are usually required in the traditional drug loading method to incorporate poorly-soluble drug into carriers. Particularly, the use of organic solvents could remarkably affect the scale-up of a drug carriers production, when toxic solvents are required.

4.3.3 Preliminary *in vitro* drug release study

The lack of irreversible adsorption or occlusion of CTZ molecules in the NsZnO-3 material was evaluated by a preliminary *in vitro* drug release study. For this purpose, the ability of NsZnO-3 in releasing the loaded CTZ was investigated using a multi-compartmental rotating cell, equipped by semisynthetic membrane. Figure 4.6 displays the cumulative release curves of CTZ from CTZ@NsZnO-3_{scCO_2} loaded through $scCO_2$ (black curve) in comparison with CTZ@NsZnO-3_{trad} loaded by traditional incubation method. From the evaluation of the two clotrimazole release curves, it emerged that the sample CTZ@NsZnO-3_{trad} displayed a slower drug release kinetic than CTZ@NsZnO-3_{scCO_2}. For instance, at 30 minutes from the beginning of the experiment, the amount of CTZ released from CTZ@NsZnO-3_{scCO_2} was more than double the quantity released from CTZ@NsZnO-3_{trad} , 51% and 19%, respectively. This behaviour could be ascribed to aggregations phenomena that may occur between the ZnO particles during the traditional drug loading in solution, during which the drug may be "trapped" inside the material. On the contrary, after $scCO_2$-mediated drug incorporation a faster release may be obtained due to the presence of drug on the surface of the nanomaterial. In conclusion, this preliminary *in vitro* release study clearly showed that CTZ is not irreversibly confined in the NsZnO-3, confirming the role of NsZnO as drug delivery carrier, as previously demonstrated in the CTZ case study [1]. Moreover, a more efficient drug distribution inside the carrier was gained through $scCO_2$ technology.

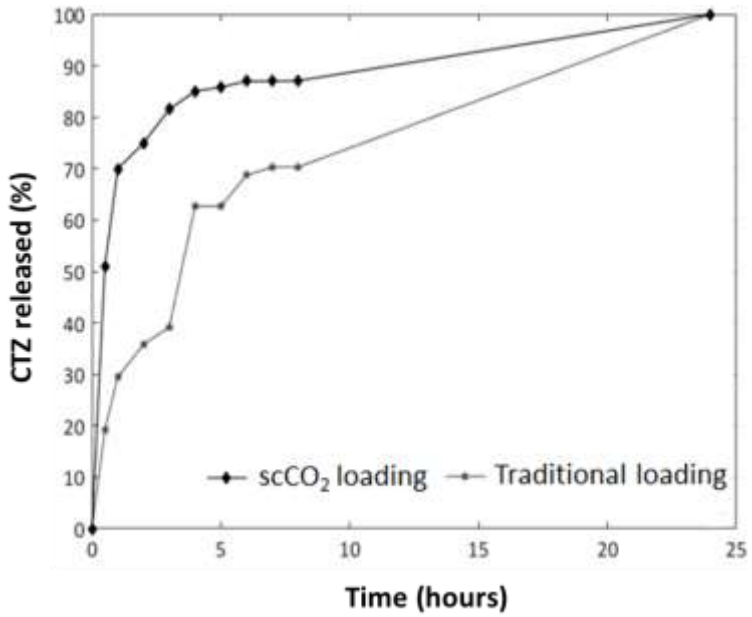

Figure 4.6 *In vitro* drug-release profiles of CTZ from CTZ@NsZnO-3 loaded through supercritical technology (black curve) a9nd after traditional loading (grey curve)

4. 4 Conclusions

In summary, the possibility to develop mesoporous ZnO particles as reservoir of drugs was investigated. A simple synthesis was carried out obtaining a material with significant high surface area (56 m^2/g) and suitable morphology for the biomedical applications (NsZnO-3). Clotrimazole (CTZ) was selected as drug model, because of its hydrophobic profile, which usually requires the utilizations of organic solvents, and the possibility to enhance its topical therapeutic activity in combination with ZnO. The $scCO_2$ technology was studied as greener alternative technology to carry out the drug loading step of the mesoporous NsZnO-3. A traditional drug loading method was also performed, adopting the absorption from ethanolic solution approach, for sake of comparison. The physico-chemical characterization of NsZnO-3 before and after the loading of CTZ confirmed that the $scCO_2$ process does not significantly affect the structure of the materials. XRD analysis revealed that CTZ was distributed in the NsZnO-3 carrier in amorphous form and that the wurtiztic phase of ZnO was preserved after $scCO_2$ process, without any

structural modification after the contact with CO_2. FTIR analysis confirmed the successful interaction between the material and the drug and highlighted a protective role of the drug molecules towards the NsZnO surface during the supercritical process. A similar CTZ amount was hosted in the mesoporous NsZnO-3 by $scCO_2$-mediated approach and by traditional absorption method. Furthermore, the capability of the materials in releasing CTZ was investigated. Results revealed that CTZ is not irreversibly confined in the NsZnO-3 support, that can act as a drug delivery carrier. This might play a key role in several biological applications where the bioavailability of poorly-water-soluble drugs is still a challenging issue. Different CTZ release profiles were obtained comparing NsZnO-3 loaded with the two different methods, underlining a possible better dispersion of the drug in the material after $scCO_2$ process. In addition to this, the comparison between the $scCO_2$-based drug loading with the traditional absorption method leads to some interesting conclusions, which highlight the remarkable advantages of using $scCO_2$ technology. Firstly, as mentioned above, after the $scCO_2$ process a ready-to-use drug loaded material was obtained, without any further purification process. The possibility to skip the purification step results in a more time-effective drug loading procedure. Secondly, the $scCO_2$ is a green solvent, which allows to dissolve many poorly-water soluble molecules. This represents a great advantage, considering that huge amounts of organic solvent are usually required in the traditional drug loading method to incorporate poorly-soluble drug into carriers. Particularly, the use of organic solvents could remarkably affect the scale-up of a drug carriers production, when toxic solvents are required.

The investigation described in this chapter was a further proof that innovative procedures to obtain nanostructured ZnO-based drug carriers with the support of $scCO_2$ technology can be considered as a promising route.

4.5 References

(1) Leone, F.; Gignone, A.; Ronchetti, S.; Cavalli, R.; Manna, L.; Banchero, M.; Onida, B. A Green Organic-Solvent-Free Route to Prepare Nanostructured Zinc Oxide Carriers of Clotrimazole for Pharmaceutical Applications. *J. Clean. Prod.* **2018**, *172*, 1433–1439.

(2) Mitra, S.; B., S.; Patra, P.; Chandra, S.; Debnath, N.; Das, S.; Banerjee, R.; Kundu, S. C.; Pramanik, P.; Goswami, A. Porous ZnO Nanorod for Targeted Delivery of Doxorubicin: In Vitro and in Vivo Response for Therapeutic Applications. *J. Mater. Chem.* **2012**, *22* (45), 24145.

(3) Gignone, A.; Manna, L.; Ronchetti, S.; Banchero, M.; Onida, B. Microporous and Mesoporous Materials Incorporation of Clotrimazole in Ordered Mesoporous Silica by Supercritical CO 2. *Microporous Mesoporous Mater.* **2014**, *200*, 291–296.

(4) Ning, M.; Gu, Z.; Pan, H.; Yu, H.; Xiao, K. Preparation and in Vitro Evaluation of Liposomal/niosomal Delivery Systems for Antifungal Drug Clotrimazole. *Indian J. Exp. Biol.* **2005**, *43* (2), 150–157.

(5) Scherrer, P. Bestimmung Der Grösse Und Der Inneren Struktur Internal, Kolloidteilchen Mittels Röntgensrahlen [Determination of the Size and Goettingen, Structure of Colloidal Particles Using X-Rays]. *Nachr Ges Wiss Germa, Math-Phys Kl.* **1918**, 98–100.

(6) Sun, D.; Wong, M.; Sun, L.; Li, Y.; Miyatake, N.; Sue, H. J. Purification and Stabilization of Colloidal ZnO Nanoparticles in Methanol. *J. Sol-Gel Sci. Technol.* **2007**, *43* (2), 237–243.

(7) Hasnidawani, J. N.; Azlina, H. N.; Norita, H.; Bonnia, N. N.; Ratim, S.; Ali, E. S. Synthesis of ZnO Nanostructures Using Sol-Gel Method. *Procedia Chem.* **2016**, *19*, 211–216.

(8) Sowri Babu, K.; Ramachandra Reddy, A.; Sujatha, C.; Venugopal Reddy, K.; Mallika, A. N. Synthesis and Optical Characterization of Porous ZnO. *J. Adv. Ceram.* **2013**, *2* (3), 260–265.

(9) Galhotra, P. Carbon Dioxide Adsorption on Nanomaterials. *Theses Diss.* **2010**.

(10) Anas, M.; Gönel, A. G.; Bozbag, S. E.; Erkey, C. Thermodynamics of Adsorption of Carbon Dioxide on Various Aerogels. *J. CO2 Util.* **2017**, *21* (1), 82–88.

(11) Graedel, T. E. Corrosion Mechanisms for Zinc Exposed to the Atmosphere. *J Electrochem Soc* **1989**, *136* (4).

(12) Kazarian, S. G.; Martirosyan, G. G. Spectroscopy of Polymer/drug Formulations Processed with Supercritical Fluids: In Situ ATR-IR and Raman Study of Impregnation of Ibuprofen into PVP. *Int. J. Pharm.* **2002**, *232* (1–2), 81–90.

Chapter 5

Antimicrobial activity of NsZnO-1, NsZnO-2 and NsZnO-3 related to their physicochemical properties

5.1 Introduction

As mentioned previously in this PhD thesis, the choice of ZnO as material was driven by several factors, which can be summarized as follow:

i) in Material Science, ZnO is recognised as a multifunctional material possessing unique physical and chemical properties (i.e. a band gap of 3.28 eV, high exciton binding energy of 60 meV), which make it suitable for many attractive applications (i.e electronic, optoelectonic, sensoristic, photocatalysis, biomedical etc)[1,2];

ii) from a biological point of view, ZnO is an outstanding material, due to its intrinsic properties, such as low toxicity, biocompatibility and biodegradability[3,4].

Therefore, the fundamental idea of this research project was based on the possibility to combine these two different aspects to develop *multitasking ZnO-based drug delivery systems*. ZnO is particularly suitable for this role, because its nanostructure can be tailored to host drug molecules and because it can offer several biological advantages deriving from its intrinsic properties, such as its antimicrobial activity [5]. It is well-established in the literature, that ZnO displays significant bactericidal properties over a broad range of Gram-positive as well as Gram-negative bacteria [6]. As already described, several mechanisms such as generation of reactive oxygen species (ROS), Zinc ion release, membrane dysfunction and nanoparticles penetration are involved in the generation of this antibacterial activity. Moreover, it is worth of noting, that physicochemical parameters of the ZnO nanomaterials, such as size, morphology and specific surface area, remarkably affect the antibacterial properties [5]. For instance, high surface area and small crystallite sizes of the ZnO nanomaterials can greatly enhance their antibacterial properties [7].

These intrinsic characteristics added to the therapeutic activity of the hosted molecule make ZnO a promising material to build powerful drug delivery system for many biological applications [8]. In fact, as mentioned above, the antimicrobial properties of ZnO can be attractive for its use as an antimicrobial preservative of pharmaceutical or cosmetic formulations [9].

In the previous chapters, three nanostructured ZnO powders with different morphologies and physico-chemical parameters were synthetized and characterized. This chapter is focused on the study of the three developed NsZnOs from a biological point of view, in order to highlight their intrinsic properties. Particularly, their antimicrobial activity against different microbial strains were investigated, and the results were correlated to their physico-chemical parameters. Also the *in vitro* Zn^{2+} release profiles from the NsZnO matrices was evaluated, due to the important role of the Zinc in several physiological mechanisms, such as acting as cofactor in enzymatic reactions and being cytotoxic to microbial agents [10–12].

The antimicrobial tests were performed by the research group of Prof. Vivian Tullio at the Department of Public Health and Pediatrics of the University of Turin. I gratefully acknowledge Dr. Janira Roana for her precious collaboration.

5.2 Experimental

5.2.1 Microbial strains and culture conditions

The antibacterial activity of NsZnO-1, NsZnO-2 and NsZnO-3 samples was tested against two bacterial strains. In particular, *Staphylococcus aureus* (ATCC 29213) and *Klebsiella pneumoniae* (ATCC 700603) were selected as Gram-positive and as Gram-negative bacteria, respectively. Moreover, the antifungal activity of NsZnO-1, NsZnO-2 and NsZnO-3 samples was investigated against *Candida albicans* (ATCC 90023), the most common opportunistic *fungal* pathogen of humans. The strains were purchased from American Type Culture Collection (ATCC) (Manassas,Virginia, USA)**.**

5.2.2 Inocula preparation

Microorganism inocula were prepared by picking two to three colonies from an overnight culture of *S.aureus/K.pneumoniae* on Brain Hearth Infusion Agar (BHA,Merck KGaA, Darmstadt, Germany) or of *C. albicans* on Sabouraud dextrose agar (SABA, Merck KGaA) at 37 °C, and suspending them in 5 mL of 0.85 % normal saline, to yield a stock suspension of$\approx 5\times10^{8}$cells/mL for bacteria or 5×10^{6}cells/mL for yeast by 0.5 McFarland standard. A working suspension was made by a 1:10 dilution of the stock suspension in RPMI-1640 without sodium bicarbonate and with L-glutamine (Invitrogen, San Giuliano Milanese, Milano, Italy), buffered to pH 7.0 with 0.165 M morpholinepropanesulfonic acid (MOPS) (Sigma-Aldrich, Milan, Italy) at a concentration of 0.165 mol 1^{-1} and supplemented with glucose 18 g/L, for yeast or by a 1:1000 dilution for bacteria in Mueller Hinton broth (MHB,Merck KGaA). The microbial concentration of S. aureus and K. pneumoniae suspensions resulted in 105 CFU mL^{-1} while *C. albicans* suspension was prepared at a concentration of 103 CFU mL^{-1}, confirmed by colony counts in duplicate.

5.2.3 *In vitro* antimicrobial assays

Broth microdilution method

The antimicrobial activity of NsZnO-1, NsZnO-2 and NsZnO-3 was determined using a broth microdilution method susceptibility assay, according to CLSI document M27-A3 for yeasts [13]. The aim of the broth dilution method is to determine the lowest concentration of the assayed antimicrobial that

inhibits the visible growth of the microrganism being tested (MIC, expressed in μg/ml). In this investigation, MIC determination was performed by serial dilution using 96-well microtitre plates (Sarstedt, Milan,Italy). Stock suspensions of NsZnO prepared at 30000 μg/ml (w/v) in PBS were dispersed for 1 h using an ultrasonic bath, in order to minimize sedimentation of NsZnO particles. Doubling dilutions of the ZnO ranging from 15000 to 30 μg/ml were prepared in 96-well microtitre trays in MHB for bacteria or in RPMI-1640 with MOPS for yeasts. After inoculum addition (0.1 mL), the trays were incubated under normal atmospheric conditions at 37 °C for 24 h. A sterile medium incubated under the same conditions was used as a blank, while the medium inoculated with the target microorganisms (without NsZnO) was used as a positive control of growth. All determinations were performed in duplicate. The lowest concentration of the NsZnO showing complete inhibition of visible growth was defined as MIC. The absence of visible growth was determined under a binocular microscope.

The minimal bactericidal (MBC) or fungicidal (MFC) concentration of NsZnO, was determined by subculturing 10 μL of broth taken from all the wells without visible growth onto SAB agar plates that do not contain the test agents. After incubation for 24 h at 37 °C, MFC was defined as the lowest concentration of ZnO resulting in the death of 99.9 % of the inoculum in no growth on subculture.

Enumeration of viable organisms

The antibacterial experiments were also performed by the enumeration of viable organisms using a method described in the literature [14]. Briefly, the bacterial cells were grown overnight in Brain Heart Infusion broth (BHI,Merck KGaA) or Sabouraud Dextrose Broth (SABB,Merck KGaA) at T = 37°C. The cells were harvested by centrifugation, washed, resuspended in a PBS buffer solution, suspended in 5 mL of 0.85 % normal saline and diluted to yield a stock suspension of $\approx 5\times10^5$cells/mL for bacteria and for yeast. All the NsZnO samples with concentration of 13000 μg/ml, suspended in a sterilized PBS, were incubated with bacterial or yeasts suspension in a shaker incubator at T = 37◦C for 24 h. PBS solution was used as negative control. All samples were serially diluted and 100 μL of bacterial/yeasts suspension was drawn from each sample tube, spread on the BHA or SAB agar plate in duplicate and finally

incubated at T = 37°C for 24 h for colony forming. The viable colonies were counted and reported as colony forming units (CFU) per ml.

5.2.4. *In vitro* Zinc Ions release

Zinc ion release from NsZnO-1, NsZnO-2 and NsZnO-3 was studied using vertical Franz diffusion cells and synthetic skin (Dow Corning, 7-4107, Silicone Elastomer Membrane). Each NsZnO was singualarly employed as a donor phases. The receiving phase consisted of PBS buffer, at pH 7.4. The apparatus was maintained at 33°C with stirring, and at scheduled times the receiving phase was withdrawn and entirely substituted with fresh receiving phase. Zinc ion quantification was performed for each sample using inductively coupled plasma mass spectrometry (ICP-MS).

5.3. Results and discussion

In order to investigate the antimicrobial activities of the NsZnO samples, two different experimental techniques were adopted: broth microdilution method and the enumeration of viable organisms' method. Through the former approach, the minimum inhibitory concentration (MIC) and the minimum bactericidal concentration (MBC) were determined, as indicated in Table 5.1. The MIC is defined as the lowest concentration of NsZnO that leads to full inhibition of bacterial growth after 24 hours of contact and is expressed in μg/ml (Table 1.1). The minimum bactericidal concentration (MBC) is complementary to the MIC, and it expresses the lowest concentration of an antibacterial agent required to kill a particular bacterium. It indicates the lowest concentration of antibacterial agent that reduces the viability of the initial bacterial inoculum by ≥99.9%.

The latter method allowed the determination of the antimicrobial activity of the NsZnOs expressed as CFU/ml of each strain, by counting the viable microbial colonies after 24 h of incubation with the NsZnOs (Fig. 5.1 and Table 5.2).

Table 5.1 Minimum Inhibitory Concentration (MIC) and Minimal Bactericidal Concentration (MBC) of NsZnO-1, NsZnO-2 and NsZnO-3 determined for the *S. aureus*, *K. pneumoniae* and *C. albicans* expressed in μg/ml.

Microbial strain	***S. aureus***		***K. pneumoniae***		***C.albicans***
	MIC (μg/ml)	*MBC* (μg/ml)	*MIC* (μg/ml)	*MBC* (μg/ml)	*MIC* (μg/ml)
NsZnO-1	**120**	**> 470**	**470**	**1875**	**>15000**
NsZnO-2	**230**	**> 470**	**930**	**> 3750**	**>15000**
NsZnO-3	**930**	**> 3750**	**930**	**1875**	**>15000**

Table 5.2 Comparison of antibacterial activities of NsZnO-1, NsZnO-2 and NsZnO-3 against *S. aureus*, *K. pneumoniae* and *C.albicans* determined with the enumeration of viable microorganism assay and expressed in CFU/ml.

Microbial strain	***S. aureus***	***K. pneumoniae***	***C.albicans***
NsZnO-1	**10** UFC/ml	**$1.62x10^7$** UFC/ml	**$1.85x10^5$** UFC/ml
NsZnO-2	**$1.65x10^4$** UFC/ml	**$2.66x10^8$** UFC/ml	**$1.43x10^6$** UFC/ml
NsZnO-3	**$2.03x10^4$** UFC/ml	**$5.12x10^8$** UFC/ml	**$2.19x10^5$** UFC/ml

As emerges from Table 5.1, the broth dilution method clearly revealed that the three ZnO nanostructures exhibited a stronger bactericidal activity on the Gram-positive *S. aureus* than the Gram-negative *K. pneumoniae*. Since ZnO suspensions appeared cloudy in the case of *C.albicans*, it was not possible to determine the MIC from the visual appearance of the medium.

Figure 5.1 reports the results of the enumeration of viable organisms assessed through CFU assay. As emerges from Fig. 5.1 - A, the bactericidal activity of NsZnO-1 against *S. aureus* (expressed in Log CFU/ml) was greater than that achieved by NsZnO-2 and NsZnO-3 (1 *vs* 4,22 and 4,31, respectively). The same trend is evident from Figure 5.1- B, where the Log CFU/ml of bacterial load reduction against *K. pneumoniae* was 7,21, 8,42 and 8,71 for NsZn0-1, NsZnO-2 and NsZnO-3, respectively. Despite the failure of the broth dilution technique, the enumeration of viable organisms' method resulted efficient in the determination of the antifungal activity. The results are displayed in Figure 5.1-C. No significant difference was found between the NsZnO-1 and NsZnO-3 log counts recovered for *C.albicans* (5,27 *vs* 5,34), while NsZnO-2 was able to slow down the bacterial growth only of 6.15 log. In conclusion, the CFU assay confirmed the results obtained through the broth dilution method, revealing that the three ZnO nanostructures exhibited a stronger microbicidal activity towards the Gram-positive *S. aureus* than the Gram-negative *K. pneumoniae* and yeast *C. albicans* (Figure 5.1).

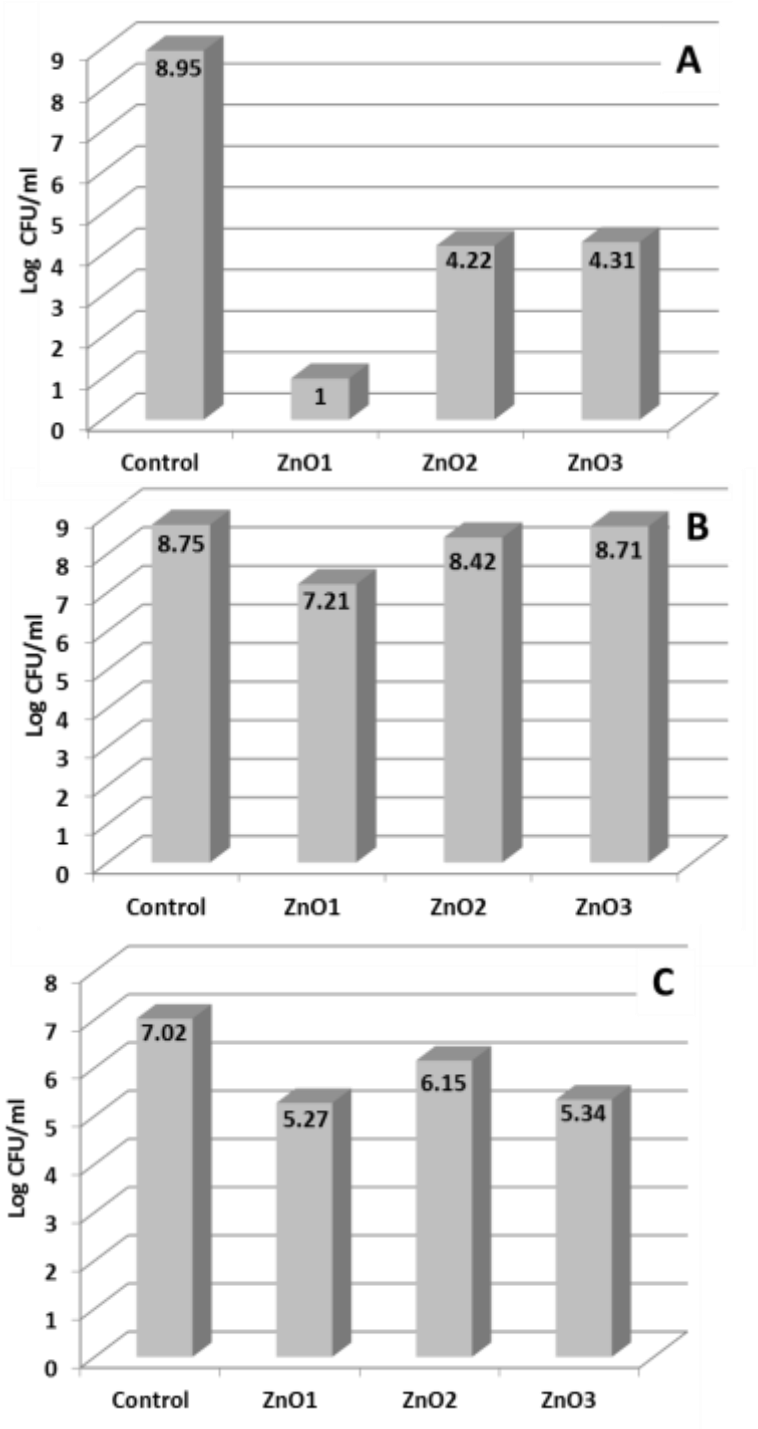

Figure 5.1 Comparison of antibacterial activities of NsZnO-1, NsZnO-2 and NsZnO-3 against *S. aureus* (A), *K.Pneumoniae* (B) and *C.albicans* (C) expressed in Log CFU/ml

These experimental evidences agree with the conclusions of Reddy et al. [15] and Tayel et al. [16] and dismisse the conclusions of Pasquet et al. [7] and Applerot et al. [16]. In detail, Tayel and Reddy explained that the peptidoglycan envelope of Gram-positive bacteria may promote ZnO attachment onto the cell wall whereas components of Gram-negative bacteria may oppose this attachment.

Among the NsZnOs investigated, the sample NsZnO-1 showed the higher antimicrobial activity compared to NsZnO-2 and NsZnO-3. This trend was confirmed by both the *in vitro* tests carried out. This phenomenon could be ascribed to the crystallite sizes of the nanoparticles, which has been reported to greatly impact their antimicrobial activity, probably because of a greater accumulation of the nanoparticles inside the cell membrane and cytoplasm [6]. In fact, from the previous characterization, the crystallite sizes were found to be 15 nm for NsZnO-1, 30 nm for NsZnO-2 and 18 nm for NsZnO-3. This observation can be reinforced by the results obtained against *C. Albicans*, against which NsZnO-1 and NsZnO-3 possessed a higher antifungal activity than NsZnO-2. This is clearly showed in Figure 5.2, where the result of the CFU assay, expressed in CFU/ml was used to correlate the crystallite sizes of NsZnOs with the antifungal activity against *C.albicans*. These conclusions are consistent with the study of Lipovsky et al. [17], who suggested that ZnO nanoparticles display a marked activity against *C. albicans* and that the cytotoxic effect is size dependent. In fact, NsZnO-1 and NsZnO-3 are characterized by lower crystallite sizes than NsZnO-2.

Figure 5.3 shows a comparison of the antibacterial activities of the three NsZnOs against *S. aureus* and *K. pneumoniae*, while the physico-chemical parameters of the three materials are summarized in Table 5.3. It worth noticing that the sample NsZnO-1, characterized by the smallest crystallite sizes, the highest SSA and pore volume and by the largest pore sizes possessed the best antimicrobial activity against all the investigated strains, *S. aureus*, *K. pneumoniae* and *C.albicans.* This result is in agreement with what reported in the literature, where it is well assessed that an enhanced antimicrobial activity depends on small crystal size, large pore size and high porosity [7].

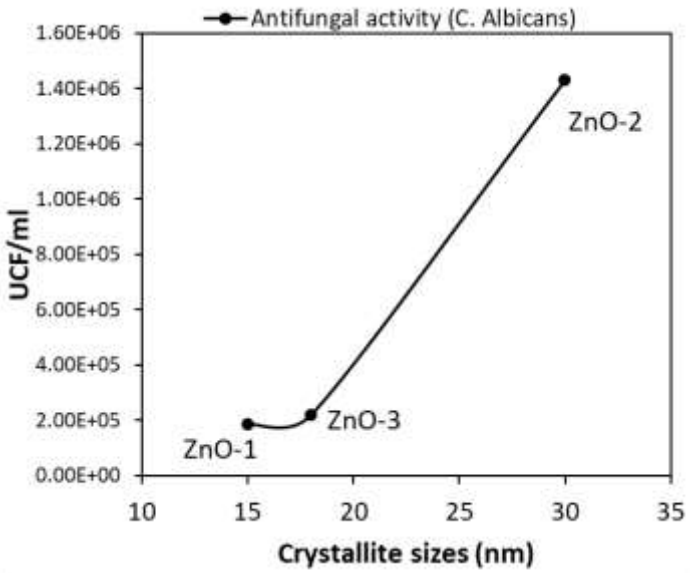

Figure 5.2 Influence of the crystallite sizes on the antifungal activity of NsZnO-1, NsZnO-2 and NsZnO-3. The plot reports the viable colonies (CFU/ml) of *C.albicans* after 24 hours of incubation with NsZnOs correlated to the crystallite sizes of NsZnOs.

Table 5.3 Summary of the main physicochemical parameters of NsZnO-1, NsZnO-2 and NsZnO-3.

	NsZnO-1	**NsZnO-2**	**NsZnO-3**
Specific area (m^2/g)	66	19	56
Mean pore size (nm)	27	5	10
Volume of pores (cm^3/g)	0.230	0.050	0.140
Crystallite size (nm)	15	30	18
Particle shape from FESEM observations	Aggregates of nanosheets	Spherical aggregates of ovoidal nanoparticles	Not homogenous aggregates of spherical nanoparticles

As far as the antibacterial activities of NsZnO -2 and NsZnO -3 are concerned, the enumeration of viable microorganism' method suggested that NsZnO-2 and NsZnO-3 possess an equivalent antibacterial activity, despite of the different MIC values. Since their physicochemical parameters are much different, the similar activity could be ascribed to the similar morphologies of NsZnO-2 and NsZnO-3, both composed by ovoidal assembled nanoparticles (Figure 5.4).

Moreover, as described in the introduction of this thesis, among the key mechanisms influencing the antibacterial activity of nanostructured ZnO, it is important to consider the release of Zn^{2+} ions. In this investigation, a simple experiment was carried out to study the Zinc ions release from NsZnO-1, NsZnO-2 and NsZnO-3, using vertical Franz diffusion cells equipped with synthetic skin. The results drawn from the Zinc ion quantification are shown in Figure 5.5. The higher amount of Zn^{2+} ions was released from NsZnO-1 and NsZnO-3, confirming the predominant role of the crystallite sizes affecting the antibacterial activity. Furthermore, the *in vitro* Zn^{2+} release study demonstrated the ability of all the three investigated NsZnOs in releasing $Zn^{2+,}$ highlighting their potential use as multitasking antimicrobial drug carriers. Furthermore, it is well-established in the the literature that also the ROS release into the medium by the photocatalytic effect dependes on the crystallinity of the ZnO nanostructure [18]. Consequently, it is logic to consider that the higher activity of NsZnO-1 could also be ascribed to the higher amount of ROS released.

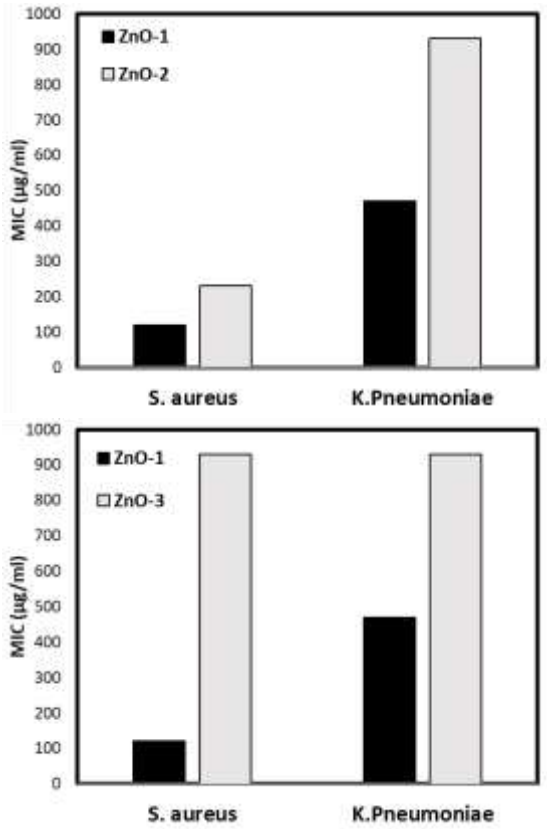

Figure 5.3 The antibacterial activity of NsZnO-1, NsZnO-2 and NsZnO-3 against *S. aureus* and *K. pneumoniae* expressed as MIC (µg/ml).

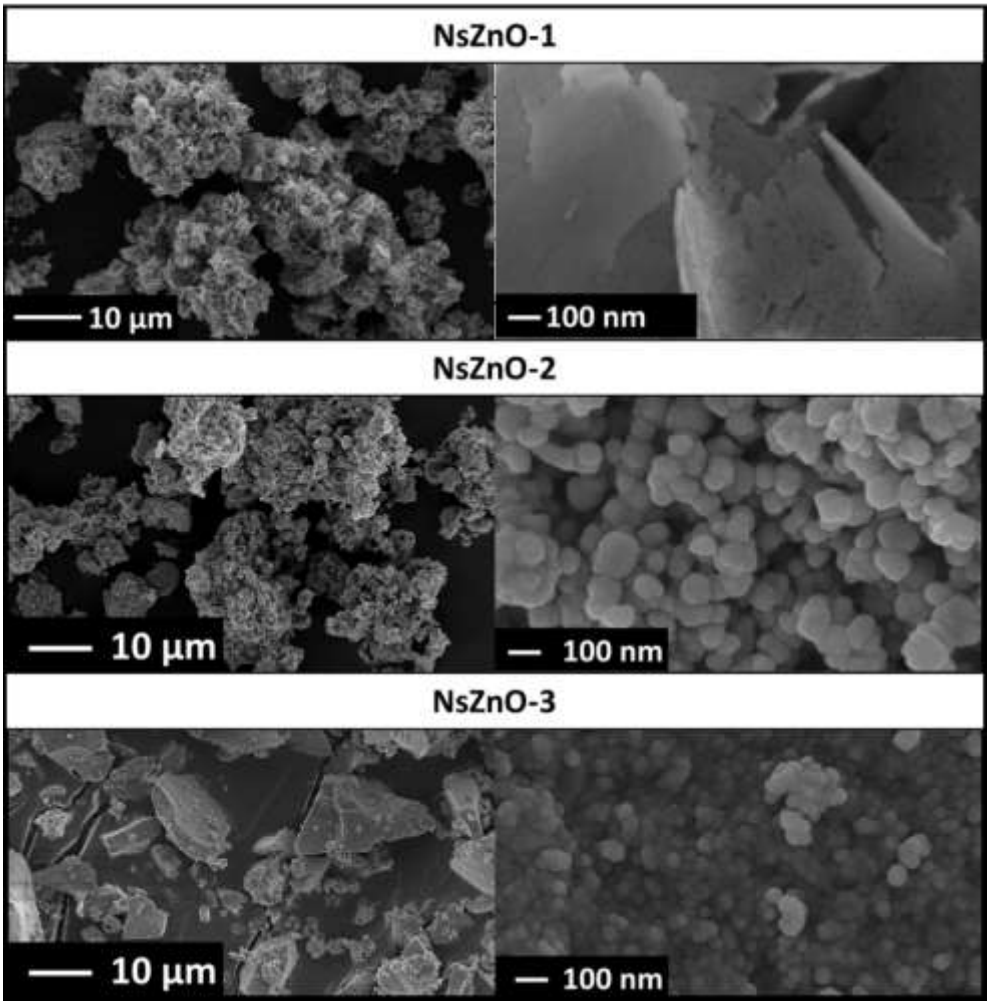

Figure 5.4 Fesem pictures of NsZnO-1 (uppest panels), NsznO-2 (middle panels) and NsZnO-3 (lowest panels).

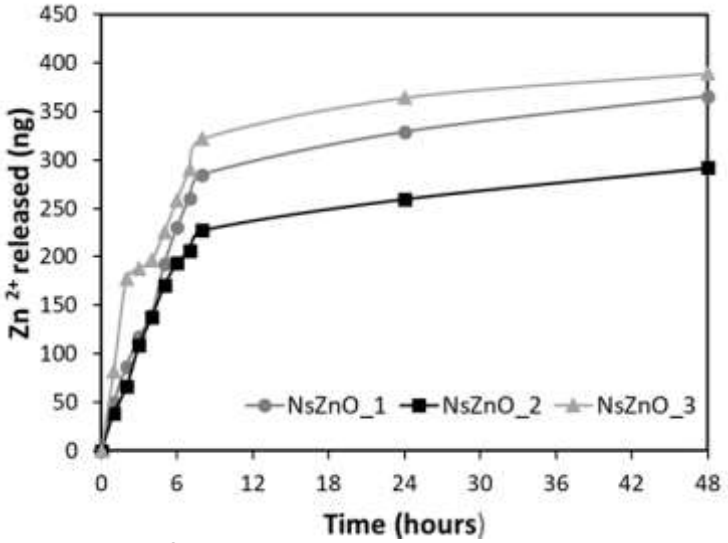

Figure 5.5 *In vitro* Zn^{2+} ion release study from NsZnO-1, NsZnO-2 and NsZnO-3

5.4 Conclusions

This chapter was focused on the evaluation of the antimicrobial activity of the three NsZnOs developed in this thesis project. Both the antibacterial and antifungal activity of NsZnO-1, NsZnO-2 and NsZnO-3 samples was tested against two bacterial strains, *Staphylococcus aureus* and *Klebsiella pneumoniae*, and against *Candida albicans*, the most common opportunistic fungal pathogen of humans. In order to investigate the antimicrobial activities of the NsZnO samples, two different experimental techniques were adopted: broth microdilution method and the enumeration of viable organisms' method. The results of this investigation revealed that the three ZnO nanostructures exhibited a stronger microbicidal activity towards the Gram-positive *S. aureus* than the Gram-negative *K. pneumoniae* and yeast *C. albicans*, in accordance to the literature. Morevoer, the sample NsZnO-1, characterized by the smallest crystallite sizes, the highest SSA and pore volume and by the largest pore sizes possessed the best antibacterial activity against all the investigated strains, *S. aureus*, *K. pneumoniae* and *C.albicans.* The *in vitro* release of Zn^{2+} ions from the three NsZnOs was also studied. The results drawn from the Zinc ion quantification showed that the higher amount of Zn^{2+} ions was released from

NsZnO-1 and NsZnO-3, confirming the predominant role of the crystallite sizes in the enhancement of the antibacterial activity.

The antimicrobial activity of the three NsZnOs was successful determined in this study, highlighting their potential use as multitasking antimicrobial drug carriers. The results of this scientific investigation build up the fundamentals for the next steps of this research project. In fact, innovative dermatological formulations are going to be develop, including in their composition these multitasking NsZnO-based drug carriers.

5.5 References

(1) Kołodziejczak-Radzimska, A.; Jesionowski, T. Zinc Oxide—From Synthesis to Application: A Review. *Materials (Basel).* **2014**, *7* (4), 2833–2881.

(2) Djurišić, A. B.; Chen, X.; Leung, Y. H.; Man Ching Ng, A. ZnO Nanostructures: Growth, Properties and Applications. *J. Mater. Chem.* **2012**, *22* (14), 6526.

(3) Mirzaei, H.; Darroudi, M. Zinc Oxide Nanoparticles: Biological Synthesis and Biomedical Applications. *Ceram. Int.* **2017**, *43* (1), 907–914.

(4) Aula, S.; Lakkireddy, S.; AVN, S.; Kapley, A.; Jamil, K.; Tata, N. R.; Hembram, K. Biological Interactions *in Vitro* of Zinc Oxide Nanoparticles of Different Characteristics. *Mater. Res. Express* **2014**, *1* (3), 35041.

(5) Kumar, R.; Umar, A.; Kumar, G.; Nalwa, H. S. Antimicrobial Properties of ZnO Nanomaterials: A Review. *Ceram. Int.* **2017**, *43* (5), 3940–3961.

(6) Jones, N.; Ray, B.; Ranjit, K. T.; Manna, A. C. Antibacterial Activity of ZnO Nanoparticle Suspensions on a Broad Spectrum of Microorganisms. *FEMS Microbiol. Lett.* **2008**, *279* (1), 71–76.

(7) Pasquet, J.; Chevalier, Y.; Couval, E.; Bouvier, D.; Noizet, G.; Morli??re, C.; Bolzinger, M. A. Antimicrobial Activity of Zinc Oxide Particles on Five Micro-Organisms of the Challenge Tests Related to Their Physicochemical Properties. *Int. J. Pharm.* **2014**, *460* (1–2), 92–100.

(8) Xiong, H. M. ZnO Nanoparticles Applied to Bioimaging and Drug Delivery. *Adv. Mater.* **2013**, *25* (37), 5329–5335.

(9) Pasquet, J.; Chevalier, Y.; Couval, E.; Bouvier, D.; Bolzinger, M. A. Zinc Oxide as a New Antimicrobial Preservative of Topical Products: Interactions with Common Formulation Ingredients. *Int. J. Pharm.* **2015**, *479* (1), 88–95.

(10) Gupta, M.; Mahajan, V. K.; Mehta, K. S.; Chauhan, P. S. Zinc Therapy in Dermatology: A Review. *Dermatol. Res. Pract.* **2014**, *2014*, 709152.

(11) Pasquet, J.; Chevalier, Y.; Pelletier, J.; Couval, E.; Bouvier, D.; Bolzinger, M. A. The Contribution of Zinc Ions to the Antimicrobial Activity of Zinc Oxide. *Colloids Surfaces A Physicochem. Eng. Asp.* **2014**, *457*, 263–274.

(12) Holmes, A. M.; Song, Z.; Moghimi, H. R.; Roberts, M. S. Relative Penetration of Zinc Oxide and Zinc Ions into Human Skin after Application of Different Zinc Oxide Formulations. *ACS Nano* **2016**, *10* (2), 1810–1819.

(13) Rex, J. H.; Alexander, B. D.; Andes, D.; Arthington-Skaggs, B.; Brown, S. D.; Chaturvedi, V.; Ghannoum, M. A.; Espinel-Ingroff, A.; Knapp, C. C.; Ostrosky-Zeichner, L.; Pfaller, M. A.; Sheehan, D. J.; Walsh, T. J. Reference Method for Broth Dilution Antifungal Susceptibility Testing of Yeasts: Approved Standard - Third Edition. *Clin. Lab. Stand. Inst.* **2008**, No. April, 1–25.

(14) Wahid, F.; Yin, J. J.; Xue, D. D.; Xue, H.; Lu, Y. S.; Zhong, C.; Chu, L. Q. Synthesis and Characterization of Antibacterial Carboxymethyl Chitosan/ZnO Nanocomposite Hydrogels. *Int. J. Biol. Macromol.* **2016**, *88*, 273–279.

(15) Reddy, K. M.; Feris, K.; Bell, J.; Hanley, C.; Punnoose, A. Selective Toxicity of Zinc Oxide Nanoparticles to Prokaryotic and Eukaryotic Systems. *Appl Phys Lett.* **2007**, *24* (90), 213902–1–213902–213903.

(16) Tayel, A. A.; El-Tras, W. F.; Moussa, S.; El-Baz, A. F.; Mahrous, H.; Salem, M. F.; Brimer, L. Antibacterial Action of Zinc Oxide Nanoparticles against Foodborne Pathogens. *J. Food Saf.* **2011**, *31* (2), 211–218.

(17) Lipovsky, A.; Nitzan, Y.; Gedanken, A.; Lubart, R. Antifungal Activity of ZnO Nanoparticles-the Role of ROS Mediated Cell Injury. *Nanotechnology* **2011**, *22* (10).

(18) Li, D.; Haneda, H. Morphologies of Zinc Oxide Particles and Their E Ff Ects on Photocatalysis. **2003**, *51*, 129–137.

Chapter 6

Composite materials for wound healing: preparation and characterization of in situ cross-linking bionanocomposite hydrogels.

This chapter deals with research carried out in the Department of Chemistry and Materials Science Institute at Lancaster University (United Kingdom), under the supervision of Dr. John Hardy, for a 6-month period as a visiting PhD student. This highly interdisciplinary collaborative project aimed to develop composite materials for wound healing. The final result of the project will be a multifunctional wound dressing, based on the combination of different classes of materials and their properties, to address important public health issues (i.e. microbial infection in wound healing). The choice of the collaboration topic was driven by the will to combine polymer-based biomaterials (the expertise of Dr Hardy), with the ZnO nanostructures studied in this PhD thesis. Briefly, the main objectives of the project are:

1. To develop robust bionanocomposite hydrogels based on chitosan, zinc oxide and conducting polymers.
2. To characterize the chemical, electrical and mechanical properties of the hydrogels.
3. To carry out *in vitro* drug delivery studies (e.g. painkiller, anti-inflammatory, antimicrobial) and *in vitro* cell culture experiments of a wound healing paradigm with/without electrical stimulation.

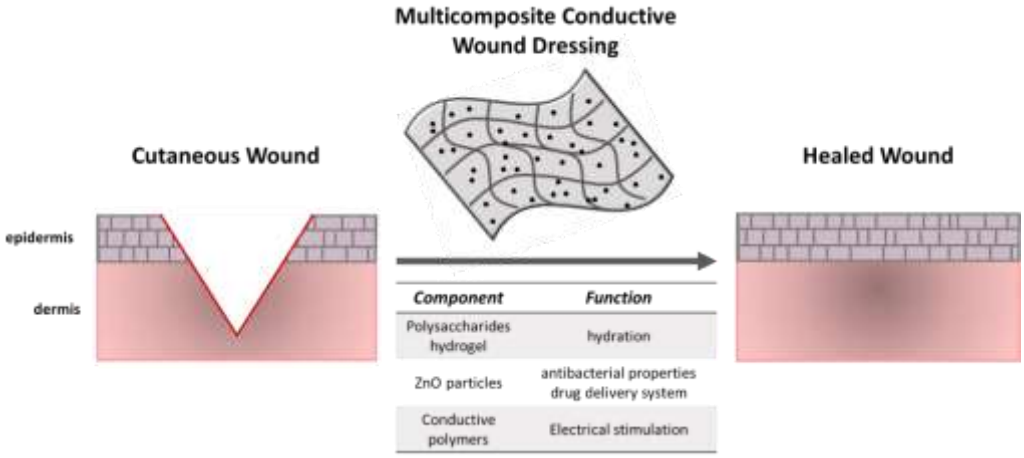

Figure 6.1. Schematic illustration of the multicomposite conductive material and its peculiar properties, which play a key role in wound healing process.

The research work reported in this chapter represents a preliminary investigation, inherent to the first objective of the main project. In particular, during my research visit at the Lancaster University, the possibility to obtain materials with hydrogel-like properties based on modified polysaccharides able to assist the wound healing process was investigated. Moreover, preliminary composite hydrogels were prepared, by the dispersion of NsZnO, developed at Politecnico di Torino, with the purpose to obtain antibacterial biomaterials. We gratefully acknowledge financial support from the UK Biotechnology and Biological Sciences Research Council BBSRC and a Researcher Mobility Grant from the Royal Society of Chemistry (RSC) which facilitated the research to be undertaken.

6.1 Introduction

Wound dressings are materials designed to cover wounds, prevent infection and help injured tissues to repair and regenerate[1]. A variety of different materials have been investigated for application as wound dressings designed to improve the healing process and thereby the rate of healing when compared to traditional systems. Consequently, wound dressings are generally composed of materials that are hydrophilic, porous and swellable, in different morphologies such as fibers, films, foams and hydrogels; and the materials may be degradable and/or loaded with therapeutically active molecules (e.g. drugs and antimicrobials).

Among the different classes of materials, hydrogels have gained much attention in the field of wound treatment, because of their outstanding properties. Hydrogels are a polymeric network filled with water, that when are applied to a wound site are effective in absorbing exudates and protecting wounds from secondary infection [2–4].

In recent years, several methods have been investigated for the preparation of *in situ* forming hydrogels, such as the use of chemical crosslinking agents and the photopolymerization of precursor monomers [5–8]. However, both these approaches present several drawbacks, concerning toxicity issues and limiting their applications.

To overcome the limitations related to the preparation of *in situ* forming biodegradable hydrogels, innovative approaches, not employing any external crosslinking agents, are under investigation. In this chapter, the possibility to obtain two different hydrogels matrices, based on the self-crosslinking of chitosan and oxidized polysaccharides, is reported. The use of natural materials was taken into consideration, due to the enormous interest they have gained as biomaterials for human healthcare systems [9]. Chitosan, a partially deacetylated derivative from chitin composed of glucosamine and N-acetylglucosamine, is structurally similar to glycosaminoglycan (GAG) and its analogs. It is of significant interest for industrial and biomedical applications because it is a cheap abundant waste product of the food industry, with excellent biocompatibility, degradability and antimicrobial as well as unique structural and physicochemical characteristics. Furthermore, chitosan is involved in wound healing and regeneration processes [10,11].

Hyaluronic acid is a linear polysaccharide (high-molecular weight), composed of repeating disaccharide units of N-acetyl-D-glucosamine and D-glucuronic acid. It represents the main component of the GAG structures, in association with other polysaccharides such as chondroitin sulfate. Due to its good biocompatibility, biodegradability, as well as excellent gel-forming properties, hyaluronic acid shows potential in biomedically-relevant hydrogel systems [12].

Pectin is a natural polysaccharide, poly (1,4-galacturonic acid), which derives from the cell walls of terrestrial plants [9]. Thanks to its attractive hydrocolloid nature, pectin has been employed in a wide range of traditional applications, such as in food industry as a gelling agent, and as component in several wound dressings on the market. Both hyaluronic acid and pectin can be both oxidized, and the generating in their structures reactive aldehyde functions, which can chemically crosslink with amino functions via Schiff's base linkage formation [13–18].

Thanks to this self-crosslinking method, in this research work the properties of chitosan and oxidized hyaluronic acid on one hand, and chitosan and oxidized pectin on the other hand, were combined fabricating hydrogels with advantages from the different biomaterials. Moreover, the possibility to improve these *in situ* forming hydrogels by the addition of nanostructured ZnO was also investigated. Bionanocomposites represent an emerging group of advanced materials resulting from the combination of biopolymers with inorganic components [19]. Particularly, the addition of NsZnO in the polymeric matrix aims to impart novel functionality, such as antibacterial activity which is attractive for wound dressings [20]. In conclusion, the objectives of this work were to prepare biocompatible *in situ* forming composite hydrogels based on natural polysaccharides and to characterize them. Their crosslinking mechanism, structure, morphology and swelling behavior were studied. *In vitro* zinc ion release was simulated on synthetic skin. Cytotoxicity of the different component was carried out on HaCat cell line.

6.2 Experimental

6.2.1. Materials

All the reagents for chemical synthesis were purchased from Sigma-Aldrich and used as received without further purification. For cell culture, all reagents were purchased from Thermo Fisher Scientific. HaCaT cells (immortalized human keratinocytes) were purchased from Lonza.

6.2.2. Synthesis

Synthesis of Hyaluronic Acids Displaying Aldehydes

Oxidized hyaluronic acid (HA-ALD) was synthesized following a procedure previously described by Hardy and colleagues [13]. In order to obtain a solution of hyaluronic acid (HA) (MW ca. 2 MDa) at a concentration of 10 mg/ml, 1.0 g of HA was dissolved in ultrapure (Millipore) water (100 mL). Sodium periodate (0.535 g, 2.5 mM) was added and the reaction was stirred for 24 h at room temperature in the dark. At the end of the oxidizing phase, the unreacted periodate was eliminated by the addition of ethylene glycol (140 μL, 2.5 mM) and stirring the reaction for 1 h at room temperature in the dark. Then, dialysis was performed in order to remove low molecular weight contaminants, using ultrapure water in dialysis tubing cellulose membrane (MWCO 3500), for four days with water exchange every 2 hours during the day time. HA-ALD was then freeze-dried.

Synthesis of Pectine Displaying Aldehydes

Pectin from citrus peel (poly-D-galacturonic acid methyl ester) (21000 - 70000 Da) has been oxidized to introduce aldehyde groups using the experimental procedure described in the previous paragraph. The reagents and their amounts were not modified, except for the use of 1.0 g of Pectin from citrus peel (MW ca. 2 MDa) as starting material. The final product, consisting of Pectin displaying aldehydes, PEC-ALD, was isolated by dialysis followed by freeze-drying.

Synthesis and characterization of NsZnO

In this investigation, nanostructured ZnO is proposed as the inorganic filler for hydrogel matrices. The synthesis procedure of the NsZnO was reported in the first chapter of this thesis, with an exhaustive characterization (NsZnO-2).

6.2.3. Preparation of chitosan stock solution

Commercial chitosan with medium molecular weight (190,000-310,000 Da, 75-85% deacetylated) was used. A chitosan (CS) stock solution at 2% was prepared adding the polysaccharide powder into an acetic acid aqueous solution (at 1 vol% acetic acid in water) at ambient temperature. After complete dissolution, the pH was adjusted to 5.5 by drop-wise addition of 1M sodium hydroxide. The formulation was stirred for 24 h.

6.2.4. Hydrogel Preparation

Stock solutions of HA-ALD (1 wt% in PBS), PEC-ALD (1 wt% in PBS) and CS (2 wt%) were prepared. In this research work two different hydrogels were fabricated: one based on HA-ALD and CS (HA-ALD/CS) and another one based on PEC-ALDs and CS (PEC-ALD/CS). Different volume ratios were tested, mixing either HA-ALD or PEC-ALD with CS.

6.2.5. Bionanocomposite Hydrogel Preparation

To obtain bionanocomposite hydrogels, NsZnO powder was suspended in PBS and sonicated for 5 minutes at room temperature to disperse the particles. Then the NsZnO suspension was injected into the CS stock solution (NsZnO-CS), and gently stirred until complete homogenization. All the previous formulations were tailored in order to get a final concentration of 1% wt of NsZnO in the various hydrogels.

6.2.6. *In vitro* swelling test

The freeze-dried hydrogels were weighed and immersed in PBS solutions (pH = 7.4) at 33 °C. After certain times, the swollen hydrogels were removed and immediately weighed after the excess of water lying on the surfaces was blotted away with filter paper, and until the weight of hydrogels reached an equilibrium value. The swelling ratio (SR) was calculated as follows:

Eq. 6.1 $$SR\ (\%) = (W_t - W_0) / W_0 \times 100\%$$

where, W_t and W_0 are the weights of the hydrogels in the swollen state and dry state.

6.2.7. Characterization

FTIR analysis

Infrared spectroscopy was carried out on a Thermo Scientific FTIR Spectrometer (Thermo Fisher Scientific Inc., USA). Spectra were recorded for 16 scans in ATR mode at room temperature, with a 1 cm^{-1} resolution. Spectra were corrected for background and atmosphere using OMNIC software provided with the spectrometer.

X Ray Diffraction

The pattern of X-ray diffraction of the samples was obtained by using a PANalytical X'Pert (Cu Kα radiation) diffractometer. Data were collected with a 2D solid state detector (PIXcel) from 10 to 80 2θ with a step size of 0.001 2θ and a wavelength of 1.54187 Å.

FESEM measurements

The surface morphologies of the hydrogelswere analyzed by using a FESEM (Zeiss Supra 40) (Carl Zeiss AG, Jena, Germany), equipped with Oxford detector for Energy Dispersive X-ray analysis (EDX).

6.2.8 *In vitro* Zin Ion release

Zinc ion release from the bionanocomposite hydrogels was studied using vertical Franz diffusion cells and synthetic skin (Dow Corning, 7-4107, Silicone Elastomer Membrane). HA-ALD/CS/ZnO and PEC-ALD/CS/ZnO were employed as a donor phases. The receiving phase consisted of PBS buffer, at pH 7.4. The apparatus was maintained at 33°C with stirring, and at scheduled times the receiving phase was withdrawn and entirely substituted with fresh receiving phase. Zinc ion quantification was performed for each sample using inductively coupled plasma mass spectrometry (ICP-MS).

6.2.9. Cytotoxicity of CS, HA Derivatives, PEC Derivatives and NsZnO

The cytotoxicity of the CS, HA-ALD and PEC-ALD was determined using a cell viability assay, based on the metabolic activity of cells and their proliferation. 96-well plates were set up dispensing 100 µL of each compound at a starting concentration of 1 mg ml^{-1}. A set of control media (100 µL of medium with serum) and control cells (100 µL of suspended cells in medium) was also included. Then 10^4 cells were injected in each well, except the control

cells wells and control medium wells. The 96-well plates were incubated at 72 hours in a humidified CO_2 incubator air atmosphere (5%) at 33°C, to allow cells to grow. After the incubation time, the PrestoBlue assay were performed. Precisely, 10μL of PrestoBlue solution (ThermoFisher) was added to all wells and incubated for at least 30 minutes. Then, the absorbance was read using a Magellan plate reader at the required wavelength/s.

6.3. Results and discussion

In situ crosslinking hydrogels preparation and physicochemical characterization

The preparation of *in situ* crosslinking hydrogels proposed in this investigation is based on the Schiff base reaction. This reaction takes place when the electrophilic carbon atoms of aldehydes and ketones undergo nucleophilic attack by amines. The result of this reaction is a compound in which the C=O double bond is replaced by a C=N double bond. This type of compound is known as an imine, or Schiff base. In recent years many research papers have focused on the preparation of *in situ* forming hydrogels using the Shiff base linkage, because of the simplicity of the mechanism and the possibility to involve only the polymeric building blocks without the addition of a chemical crosslinking agent. In this project the mechanism of formation of the hydrogels was based on the possibility to link the terminal amine groups of chitosan with the aldehyde groups displayed on the oxidized HA and PEC, through the Shiff base reaction (Figure 6.2).

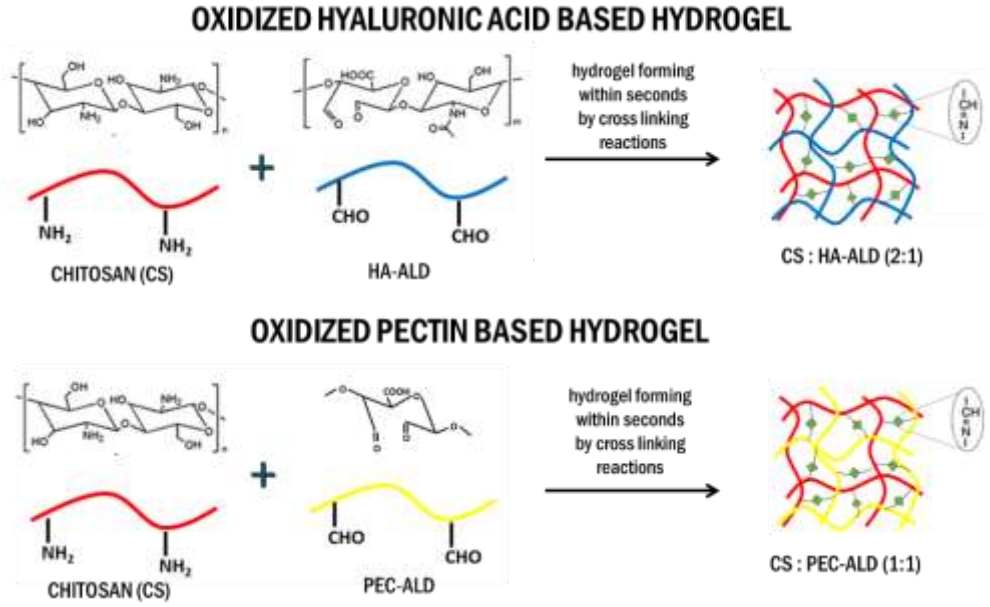

Figure 6.2 Schematic illustration of the Shiff base reaction on the basis of the hydrogels formation

To prepare the *in situ* cross linking hydrogels, stock solutions of the various components were prepared. A chitosan (CS) stock solution at 2% was prepared, obtaining a viscous polysaccharide solution, with a pH of 5.5. HA-ALD and PEC-ALD were dissolved in phosphate buffered saline (PBS, pH 7.4) at 1 wt%, obtaining clear solutions.

Hydrogels were prepared mixing polymers stock solutions of HA-ALD (1 wt% in PBS), PEC-ALD (1 wt% in PBS) and CS (2 wt%). Precisely, two different gels were obtained by mixing in different volume ratios HA-ALD with CS (HA-ALD:CS) and PEC-ALDs with CS (PEC-ALD:CS). The cross-linking time and consistency of the gels were visually determined. The best results were represented by the hydrogels obtained by mixing HA-ALD and CS in the volume ratio of HA-ALD:CS = 1:2, while in the case of hydrogels based on modified pectin the best formulation resulted from the volume ratio PEC-ALD:CS =1:1. Crosslinking was observed to occur within seconds of mixing the building blocks polymers, forming a transparent and homogenous, semi-solid polymeric matrix in both cases (Fig.6.3). The results obtained were in agreement with those previously demonstrated by other researchers [21,22].

The selected hydrogels were used in the development of the bionanocomposite materials. In particular two different composite hydrogels

with a NsZnO final concentration of 1% were prepared, starting from HA-ALD:CS (1:2)-based gel and PEC-ALD:CS (1:1)-based gel. After the dispersion of NsZnO, the polymeric matrices appeared more translucent, due to the presence of the colloidal particles (Figure 6.3).

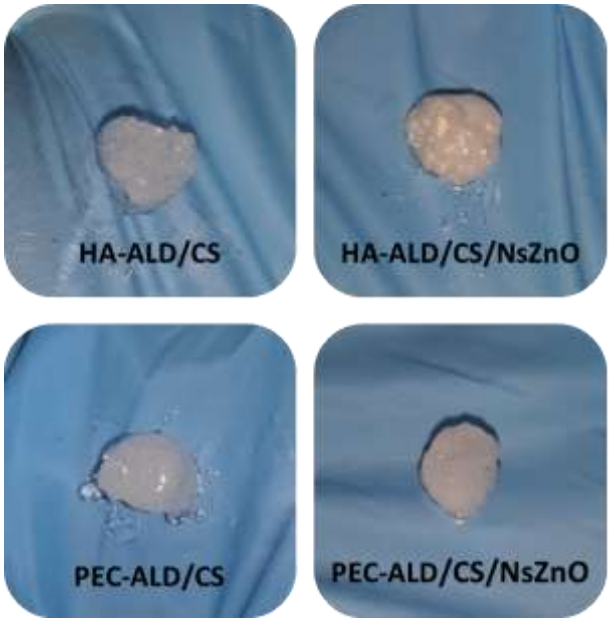

Figure 6.3 Representative picture showing the aspect of the HA-ALD/CS based hydrogel before and after the dispersion of NsZnO.

In particular, HA-based composite gels were prepared by mixing HA-ALD and NsZnO-CS in the volume ratio HA-ALD:CS = 1:2. The same method was applied in the preparation of composite gels based on modified pectin. For this purpose, PEC-ALD and the suspesion NsZnO-CS were mixed in the volume ratio PEC-ALD:CS =1:1.

FTIR analysis

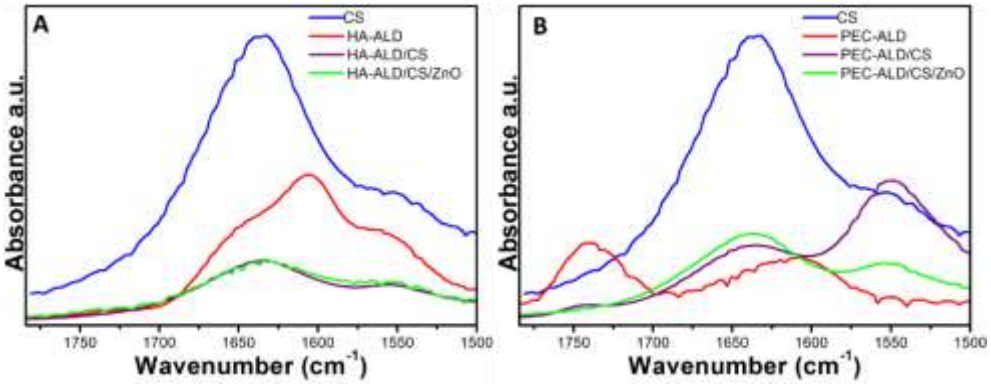

Figure 6.4 Panel A) FTIR spectra of chitosan and HA-ALD as single component, in comparison with the neat hydrogels and the composite one. Panel B) FTIR spectra of chitosan and PEC-ALD as single component, in comparison with the neat hydrogels and the composite one.

The FTIR spectra of both the bionanocomposite hydrogels are presented in Fig. 6.4, aiming to show the formation of the crosslinked hydrogels after the Shiff base reaction. Panel 6A shows the spectra of the chitosan, of the hyaluronic acid derivative and of the composite hydrogel HA-ALD/CS, with and without the NsZnO. Simultaneously, in panel 6B are shown the spectra of the chitosan, of the pectin derivative and of the composite hydrogel PEC-ALD/CS, with and without the NsZnO. Successful crosslinking of the chitosan with the aldehyde-functionalized polysaccharides derivatives was confirmed by the appearance of a peak at around 1550 cm^{-1} in the infrared absorption spectrum of lyophilized hydrogels, which corresponds to the imine bonds that crosslink the hydrogels. This peak is masked by the amide II peaks for the acetylated amines present on HA and Chitosan (75-85% deacetylated).

XRD analysis

X-ray diffraction analysis was performed to determine the structure of chitosan, the oxidized polymers derivatives and of the neat hydrogels in comparison with the bionanocomposite materials. The results are displayed in figure 6.5, where panel A is related to the HA-ALD/CS based hydrogels and the panel B to the PEC-ALD/CS based hydrogels.

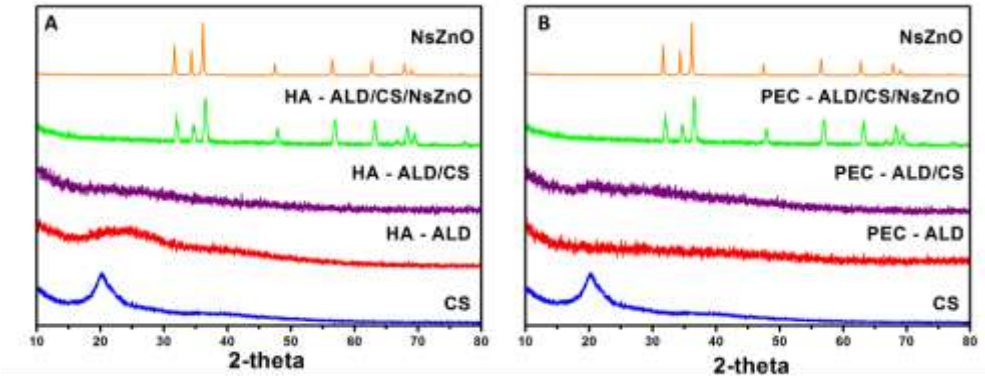

Figure 6.5 Panel A) XRD patterns of chitosan, HA-ALD and NsZnO as single component, in comparison with the neat hydrogels and the composite one. Panel B) XRD patterns of chitosan, PEC-ALD and NsZnO as single component, in comparison with the neat hydrogels and the composite one.

The main aim was to identify ZnO nanoparticles loaded in the polymer matrix. The diffractogram showing the chitosan structure were typical of a partially crystalline structure, exhibiting very broad peaks at $2\theta = 10°$ and $2\theta = 20°$ [23]. Moreover, XRD analyses show the predominantly amorphous character of the building blocks polymers and the of the neat hydrogels. On the contrary, the crystalline wurtizitic structure of the NsZnO was clearly highlighted by the XRD patterns of the bionanocomposite hydrogels. The preservation of the ZnO crystalline structure after its dispersion in the polymeric matrix was a significant result, considering the strict link between ZnO structural properties and its functionalities. The detailed description of the XRD analysis of the nanostructured ZnO has been discussed in the first chapter of this thesis.

FESEM analysis

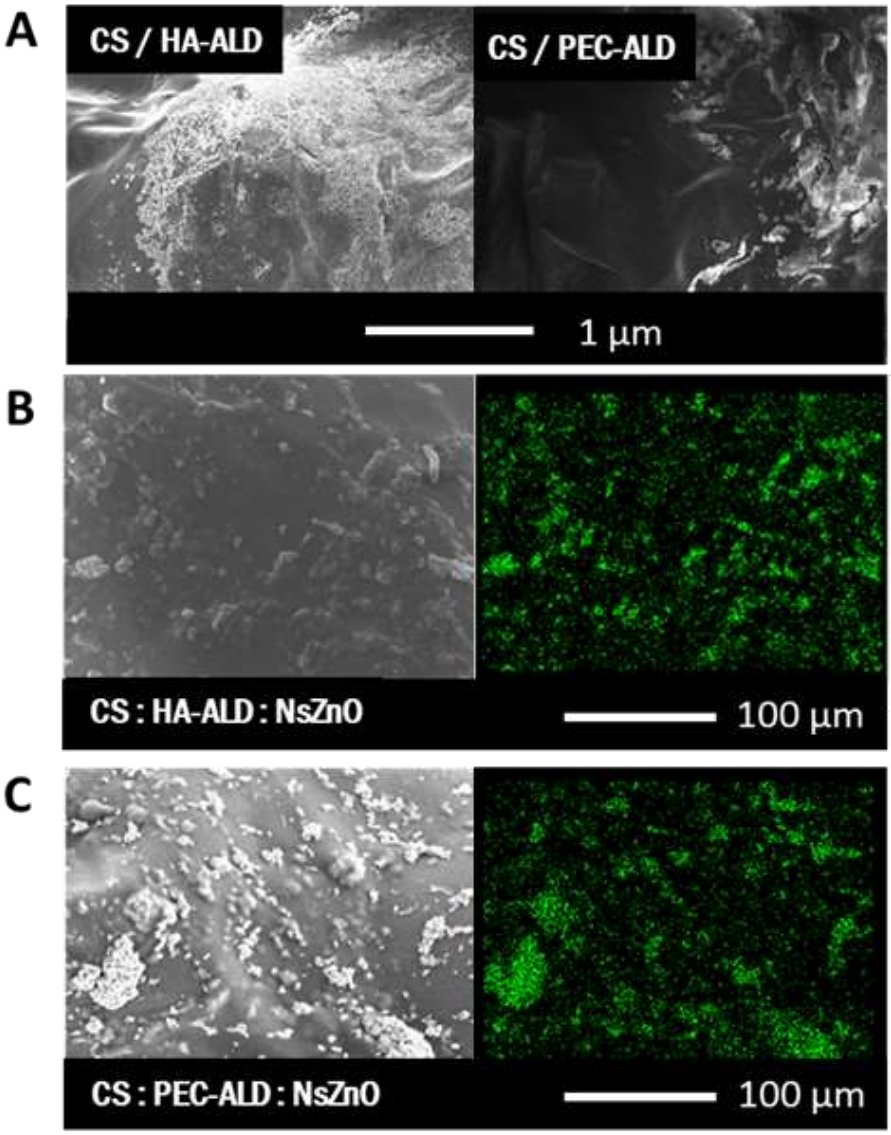

Figure 6.6 Panel A shows the FESEM images of both the neat hydrogels, HA-ALD/CS and PEC-ALD/CS. Panel B and panel C present the FESEM image of the bionanocomposite hydrogel HA-ALD/CS/NsZnO and of the bionanocomposite hydrogel PEC-ALD/CS/NsZnO, respectively. Moreover, the EDS elemental mapping directly associated with the FESEM images is reported for the bionanocomposite materials.

FESEM analyses were carried out to evaluate the morphology of the neat hydrogels matrix in comparison with the bionanocomposite hydrogels. The principal goal was the determination of the degree of dispersion of the NsZnO particles inside the polymeric matrix. Figure 6.6A shows the FESEM images of both the neat hydrogels, HA-ALD/CS and PEC-ALD/CS. Panel 4.6B and panel 6.6C present the FESEM image of the bionanocomposite hydrogel HA-ALD/CS/NsZnO and of the bionanocomposite hydrogel PEC-ALD/CS/NsZnO, respectively. Moreover, the EDS elemental mapping directly associated with the FESEM images is reported for the bionanocomposite materials. A uniform and smooth surface morphology can be observed for the neat hydrogels (Fig. 6.6A), while ZnO nanostructures can be identified in the bionanocomposite hydrogels (Fig. 6.6B and 6.6C). FESEM analyses associated with EDS mapping also show that the ZnO particles are uniformly dispersed in crosslinked polymeric matrices. The homogenous dispersion of the NsZnO is an important factor, playing a key role in the antibacterial activity of these multicomposite materials. In fact, a higher ZnO surface area might be exposed to the bacteria, enhancing its killing activity.

Swelling behavior

The swelling behavior was studied soaking the freeze-dried hydrogels in PBS at pH = 7.4 comparing the neat hydrogels with the bionanocomposite hydrogels. As shown in figure 6.7, the hydrogels have excellent swelling properties for both the polymeric matrices.

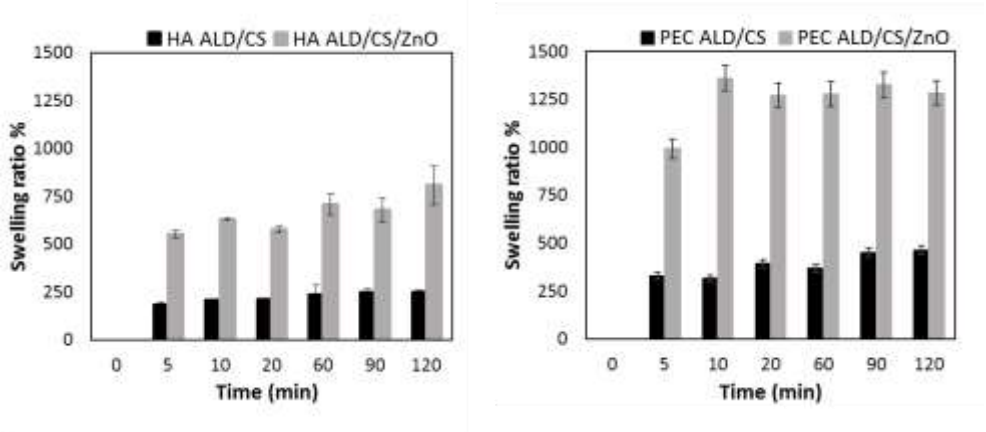

Figure 6.7 Swelling behaviour of the neat hydrogels in comparison with the nanocomposite hydrogels in PBS buffer at pH 7.4. Panel A shows the swelling profiles of HA-ALD/CS (purple curve) and of HA-ALD/CS/NsZnO (green curve) based hydrogels. Panel B shows the swelling profiles of PEC-ALD/CS (purple curve) and of PEC-ALD/CS/NsZnO (green curve) based hydrogels.

It is evident that in both cases the bionanocomposite hydrogels exhibit a higher swelling capability in comparison to neat hydrogels. NsZnO may cause the expansion of hydrogel network either by diminishing the number of Schiff base crosslinks that form or repelling the polymer chains due to electrostatic interactions, thereby increasing the pore sizes within the hydrogel, which accounts for the absorbance of more water [24]. The bionanocomposite hydrogel based on the crosslinking between oxidized pectin and chitosan seems to be more effective in absorbing water than the composite hydrogel based on oxidized hyaluronic acid and chitosan. Since the percentage of NsZnO is the same in both the composite matrices, this behaviour is ascribed to a combination of diminished number of Schiff base crosslinks that form and repelling the polymer chains due to electrostatic interactions. This outstanding swelling behaviour can be successfully exploited in a real application in wound

healing treatments, where hydrogels able to absorb consistent degree of wound exudate are required. In fact, hydrogels absorbing wound exudates, would be able to protect wounds from secondary infection.

In vitro zinc release from bionanocomposite hydrogels

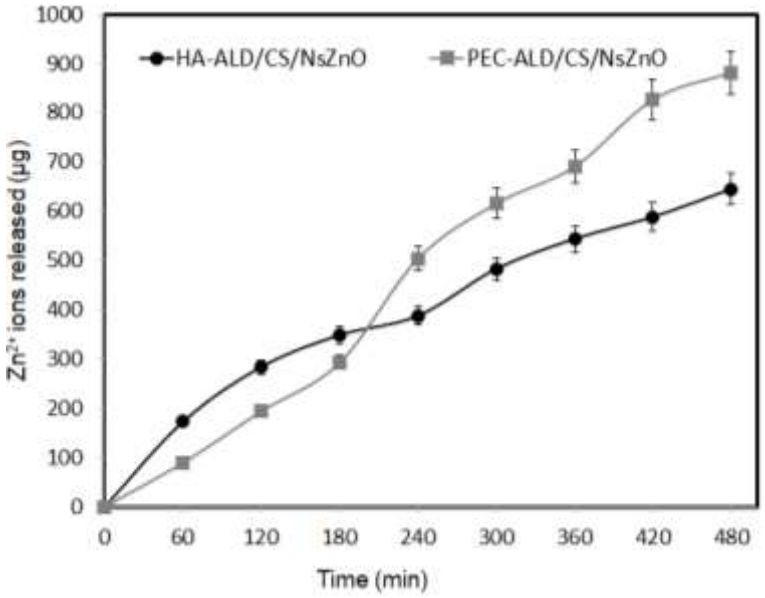

Figure 6.8 Zinc release of bionanocomposite hydrogels as a function of time, at pH 7.4. HA-ALD/CS/NsZnO and PEC-ALD/CS/NsZnO are represented by the purple curve and green curve, respectively.

The release profiles of zinc ions at pH 7.4 from the bionanocomposite hydrogels is shown in Figure 6.8. Exudate pH in wounds normally ranges between 4.8–9.8, consequently the PBS buffer was chosen in order to simulate the wound environment [25]. Both the bionanocomposite hydrogels, based on HA-ALD/CS and PEC-ALD/CS matrices, showed zinc ion release constant over time. This behaviour is a promising result, which may endow the hydrogels with efficient antibacterial activity. It is well known in fact that the main mechanism of ZnO antibacterial activity would be ascribed to the Zinc ions (Zn^{2+}) released from the surface of the particles. As described in the introduction section of this thesis, the released Zn^{2+} has significant effect on bacterial metabolism and enzyme system disruption [20].

Cytotoxicity of CS, HA-ALD, PEC-ALD and NsZnO

Since this investigation aim at developing of *in situ* crosslinking hydrogels for wound treatment, immortalized human keratinocyte (HaCat) cell line was chosen in order to test the cytotoxicity of the various components. HaCaT cells have been extensively investigated as model to evaluate the epidermal homeostasis and its pathophysiology [26]. The HaCaT cells, were maintained in Dulbecco's modified Eagle's medium (DMEM) with 10% fetal bovine serum at 33 °C with 5% CO_2. The cells were cultured until 100% confluence was reached, and then the cytotoxicity tests were performed. In order to test their cytotoxicity HA-ALD, PEC-ALD and NsZnO were dissolved in PBS solution and conveniently sterilized. HaCat cells were incubated with different concentrations of HA-ALD-24 and PEC-ALD-24 for 24 hours, after which the cells viability were tested using the PrestoBlue™ Cell Viability method. This protocol was adopted due to the possibility to rapidly obtain an evaluation of the cell viability and proliferation after their contact with the polymers. PrestoBlue™ reagent is quickly reduced by metabolically active cells, providing a quantitative measure of viability and cytotoxicity. After an incubation time of 1 hours, the absorbance was read using a plate-reader at the required avelength (570 nm) associated with Magellan software.

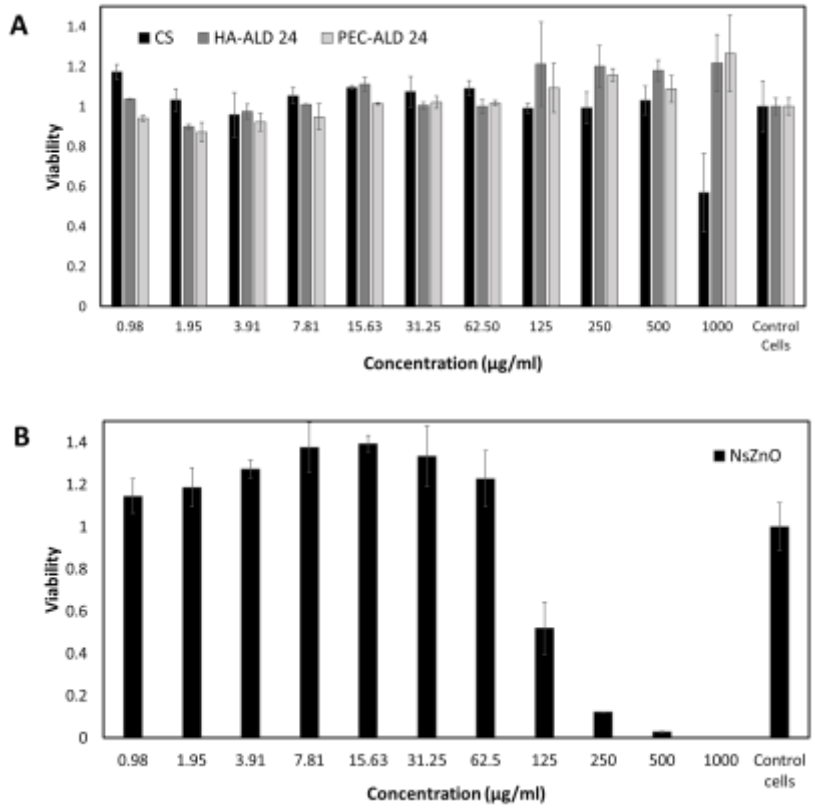

Figure 6.9 Panel A: Hacat cell viability after incubation with different polymers: chitosan m.m.w. (dark grey), HA-ALD-24 (grey) and PEG-ALD-24 (light grey). Panel B: HaCaT cell viability after incubation with NsZnO. The viability was assessed using a PrestoBlu Cell Viability Assay(ThermoFisher Scientific).

As it is possible to see in figure 6.9A, in all the evaluated polymers concentrations, a high cell viability was observed. The significant results suggest that all the polymers in this investigation are promising starting materials for *in situ* crosslinking hydrogels for application in wound healing.

The viability of HaCaT cells treated with ZnO has already been studied [27–29], and the results achieved in this investigation are perfectly consistent with the previous considerations (Fig. 6.9, panel B). As expected, the NsZnO material showed a dose-dependent effect. Interestingly, a recent study concluded that the use of nanostructured ZnO on dermatological applications would not have any concern since it shows a similar or less pronounced effect on keratinocytes than the corresponding bulk form [29].

6.4. Conclusions

In this study a facile synthesis of bionanocomposite hydrogels, able to act as multifunctional materials in wound healing applications was demonstrated. Future work will include the completion of mechanical testing and cell culture studies (with an *in vitro* wound healing model). Moreover the possibility to develop a conductive prototype of these composite hydrogels will be investigated.

Acknowledgements

I wish to thank Dr John Hardy and Dr Karen Wright for their support and teaching during my research experience at Lancaster University. I gratefully acknowledge financial support from the UK Biotechnology and Biological Sciences Research Council (BBSRC) and Royal Society of Chemistry (RSC) (specifically for a Researcher Mobility Grant) which facilitated the research to be undertaken.

6.5 References

(1) Boateng, G.; Matthews, J.; Stevens, K.; Eccleston, H. Wound Healing Dressings and Drug Delivery Systems: A Review. *J. Pharm. Sci.* **2010**, *99* (10), 4215–4227.

(2) Du, L.; Tong, L.; Jin, Y.; Jia, J.; Liu, Y.; Su, C.; Yu, S.; Li, X. A Multifunctional in Situforming Hydrogel for Wound Healing. *Wound Repair Regen.* **2012**, *20* (6), 904–910.

(3) Varghese, S.; Jamora, C. Hydrogels: A Versatile Tool with a Myriad of Biomedical and Research Applications for the Skin. *Expert Rev. Dermatol.* **2012**, *7* (4), 315–317.

(4) Jones, A.; Vaughan, D. Hydrogel Dressings in the Management of a Variety of Wound Types: A Review. *J. Orthop. Nurs.* **2005**, *9* (SUPPL. 1).

(5) Deligkaris, K.; Tadele, T. S.; Olthuis, W.; Berg, A. Van Den. Sensors and Actuators B : Chemical Hydrogel-Based Devices for Biomedical Applications. *Sensors Actuators B. Chem.* **2010**, *147* (2), 765–774.

(6) Chai, Q.; Jiao, Y.; Yu, X. Hydrogels for Biomedical Applications : Their. **2017**.

(7) Ahmed, E. M. Hydrogel : Preparation , Characterization , and Applications : A Review. *J. Adv. Res.* **2015**, *6* (2), 105–121.

(8) Li, Y.; Rodrigues, J.; Tomás, H. Injectable and Biodegradable Hydrogels: Gelation, Biodegradation and Biomedical Applications. *Chem. Soc. Rev.* **2012**, *41* (6), 2193–2221.
(9) Gupta, B.; Tummalapalli, M.; Deopura, B. L.; Alam, M. S. Functionalization of Pectin by Periodate Oxidation. *Carbohydr. Polym.* **2013**, *98* (1), 1160–1165.
(10) Patrulea, V.; Ostafe, V.; Borchard, G.; Jordan, O. European Journal of Pharmaceutics and Biopharmaceutics Chitosan as a Starting Material for Wound Healing Applications. **2015**, *97*, 417–426.
(11) Oryan, A.; Sahvieh, S. Effectiveness of Chitosan Scaffold in Skin, Bone and Cartilage Healing. *Int. J. Biol. Macromol.* **2017**, *104*, 1003–1011.
(12) Hussain, Z.; Thu, H. E.; Katas, H.; Bukhari, S. N. A. Hyaluronic Acid-Based Biomaterials: A Versatile and Smart Approach to Tissue Regeneration and Treating Traumatic, Surgical, and Chronic Wounds. *Polym. Rev.* **2017**, *57* (4), 594–630.
(13) Hardy, J. G.; Lin, P.; Schmidt, C. E. Biodegradable Hydrogels Composed of Oxime Crosslinked Poly(ethylene Glycol), Hyaluronic Acid and Collagen: A Tunable Platform for Soft Tissue Engineering. *J. Biomater. Sci. Polym. Ed.* **2015**, *26* (3), 143–161.
(14) Kim, D. Y.; Park, H.; Kim, S. W.; Lee, J. W.; Lee, K. Y. Injectable Hydrogels Prepared from Partially Oxidized Hyaluronate and Glycol Chitosan for Chondrocyte Encapsulation. *Carbohydr. Polym.* **2017**, *157*, 1281–1287.
(15) Zhang, R.; Li, X.; He, K.; Sheng, X.; Deng, S.; Shen, Y.; Chang, G.; Ye, X. Preparation and Properties of Redox Responsive Modified Hyaluronic Acid Hydrogels for Drug Release. *Polym. Adv. Technol.* **2017**, No. January.
(16) Gupta, M.; Mahajan, V. K.; Mehta, K. S.; Chauhan, P. S. Zinc Therapy in Dermatology: A Review. *Dermatol. Res. Pract.* **2014**, *2014*, 709152.
(17) Chetouani, A.; Elkolli, M.; Bounekhel, M.; Benachour, D. Synthesis and Properties of Novel Hydrogels from Oxidized Pectin Crosslinked Gelatin for Biomedical Applications. *Polym. Bull.* **2014**, *71* (9), 2303–2316.
(18) Fan, L.; Sun, Y.; Xie, W.; Zheng, H.; Liu, S. Oxidized Pectin Cross-Linked Carboxymethyl Chitosan: A New Class of Hydrogels. *J. Biomater. Sci. Polym. Ed.* **2012**, *ahead-of-p* (ahead-of-print), 1–14.
(19) Zafar, R.; Zia, K. M.; Tabasum, S.; Jabeen, F.; Noreen, A.; Zuber, M. Polysaccharide Based Bionanocomposites, Properties and Applications: A Review. *Int. J. Biol. Macromol.* **2016**, *92*, 1012–1024.
(20) Sirelkhatim, A.; Mahmud, S.; Seeni, A. Review on Zinc Oxide Nanoparticles : Antibacterial Activity and Toxicity Mechanism. *Nano-Micro Lett.* **2015**, *7*, 219–242.

(21) Neethu, M.; Pv, M.; Sabareeswaran, A.; Prabha, N. Chitosan-Hyaluronic Acid Hydrogel for Cartilage Repair. *Int. J. Biol. Macromol.* **2017**.

(22) Chetouani, A.; Elkolli, M.; Bounekhel, M.; Benachour, D. Chitosan/oxidized pectin/PVA Blend Film: Mechanical and Biological Properties. *Polym. Bull.* **2017**, *74* (10), 4297–4310.

(23) Rumengan, I. F. M.; Suryanto, E.; Modaso, R.; Wullur, S.; Tallei, T. E.; Limbong, D. Structural Characteristics of Chitin and Chitosan Isolated from the Biomass of Cultivated Rotifer, Brachionus Rotundiformis. *Int. J. Fish. Aquat. Sci.* **2014**, *3* (1), 12–18.

(24) Wahid, F.; Yin, J. J.; Xue, D. D.; Xue, H.; Lu, Y. S.; Zhong, C.; Chu, L. Q. Synthesis and Characterization of Antibacterial Carboxymethyl Chitosan/ZnO Nanocomposite Hydrogels. *Int. J. Biol. Macromol.* **2016**, *88*, 273–279.

(25) Britland, S.; Smith, A.; Finter, W.; Eagland, D.; Vowden, K.; Vowden, P.; Telford, G.; Brown, A.; Pritchard, D. Recombinant Lucilia Sericata Chymotrypsin in a Topical Hydrogel Formulation Degrades Human Wound Eschar Ex Vivo. *Biotechnol. Prog.* **2011**, *27* (3), 870–874.

(26) Seo, M.; Kang, T.; Lee, C.; Lee, A.; Noh, M. HaCaT Keratinocytes and Primary Epidermal Keratinocytes Have Different Transcriptional Profiles of Cornified Envelope-Associated Genes to T Helper Cell Cytokines. *Biomol Ther (Seoul).* **2012**, *20* (2), 171–176.

(27) N., S.; H.A., J. Comparison of Calcium Phosphate and Zinc Oxide Nanoparticles as Dermal Penetration Enhancers for Albumin. *Indian J. Pharm. Sci.* **2015**, *77* (6), 694–704.

(28) Huang, X.; Wang, X.; Wang, S.; Yang, J.; Zhong, L.; Pan, J. UV and Dark-Triggered Repetitive Release and Encapsulation of Benzophenone-3 from Biocompatible ZnO Nanoparticles Potential for Skin Protection. *Nanoscale* **2013**, *5*, 5596–5601.

(29) Vinardell, M.; Llanas, H.; Marics, L.; Mitjans, M. In Vitro Comparative Skin Irritation Induced by Nano and Non-Nano Zinc Oxide. *Nanomaterials* **2017**, *7* (3), 56.

Conclusions and Outlooks

In Material Science, ZnO nanostructures (NsZnO) have been attracted much interest in many fields of application, included the biomedical one, due to its outstanding intrinsic properties. Nevertheless, the study of NsZnO as drug delivery system is still in its nascent stage, particularly considering the administration to the skin.

In this PhD thesis nanostructured ZnO was selected as material to develop innovative drug carriers for future dermatological applications.

In particular, three different NsZnOs have been investigated: NsZnO-1, NsZnO-2 and NsZnO-3. Starting from different synthesis approaches, three different ZnO nanostructures were obtained, with different morphologies and physicochemical parameters. In this stage, particular attention was focused on obtaining materials potentially able to host drug molecules into their structure. For this purpose, the morphologies of NsZnO-1, NsZnO-2 and NsZnO-3 were tailored for the biomedical applications. Moreover, the investigated NsZnO were characterized by significative SSA and pore volume values, both important parameters for the role of drug carrier.

In this PhD project, the supercritical CO_2 ($scCO_2$) technology was selected to perform the drug loading of the obtained NsZnOs. The choice was driven by the need to study innovative method to obtain drug delivery systems, focusing on the possibility to use greener technologies, such as the $scCO_2$, able to replace organic solvents, toxic for the environment and for the health. In addition, at the end of the the $scCO_2$ process, ready-to-use drug carriers are obtained, without any further purification process.

Clotrimazole (CTZ) and Ibuprofen (IBU) were selected as drug models in this study, because of their poorly-water soluble profiles and their traditional role in dermatological formulations.

To the best of my knowledge, this was the first attempt of study the $scCO_2$ assisted drug impregnation of ZnO nanostructures and interesting conclusions were drawn. Firstly, the possibility to use $scCO_2$ as solvent to load NsZnO was successfully demonstrated. In fact, any structure modification of the ZnO

structures was observed after $scCO_2$ process, excluding the transformation in $ZnCO_3$. Secondly, both the drugs were successfully incorporated into the NsZnOs, reporting significative drug loaded amount. Furthermore, the drugs were found to be in their amorphous status, indicating a potential improved dissolution profile, suitable for biomedical purposes. Preliminary *in vitro* release studies confirmed that the APIs were not irreversibily confined in the NsZnO structures and that they could be released over time.

The antimicrobial activity of the three NsZnOs was successful confirmed in this research project, highlighting their potential use as multitasking antimicrobial drug carriers. The study revealed that the three ZnO nanostructures exhibited a stronger microbicidal activity towards the Gram-positive *S. aureus* than the Gram-negative *K. pneumoniae* and yeast *C. albicans*, in accordance to the literature. Morevoer, the sample NsZnO-1, characterized by the smallest crystallite sizes, the highest SSA and pore volume and by the largest pore sizes possessed the best antibacterial activity against all the investigated strains. The *in vitro* release of Zn^{2+} ions from the three NsZnOs showed that the higher amount of Zn^{2+} ions was released from NsZnO-1 and NsZnO-3, confirming the predominant role of the crystallite sizes in the enhancement of the antibacterial activity.

Part of this PhD thesis was dedicated to the study of innovative materials for wound healing. In this framework, the development of biocompatible *in situ* forming composite hydrogels was investigated. In particular, the use of NsZnO-2 as inorganic nanofiller in the hydrogel matrix was studied, as strategy to add antibacterial properties to the material. This successful combination led to an enhanced swelling behaviour of hydrogels, indicating a possible improved capacity in absorbing exudates from the wound compartment. Moreover, the bionanocomposite hydrogels were able to release Zn^{2+} ions over time, suggesting the enhanced antimicrobial activity of the materials.

In conclusion, the overall results of this PhD thesis build up the fundamentals for the future outlooks of the research project. The next stages will consider:

- a more accurate study of the *in vitro* release properties of the samples NsZnO-1 and NsZnO-3, selected for their advantageous phicochemical and biological parameters compared to NsZnO-2;

- the impregnation of new APIs in the NsZnO-1 and NsZnO-3 with the assistance of $scCO_2$;
- the development of formulations able to deliver these multitasking NsZnO
  to the skin;
- the addition of IBU@NsZnO into the bionanocomposite hydrogels and the study of its ability in enhancing the wound healing process with suitable cellular models.

APPENDIX

From the fundamental research to the Proof of Concept: an innovative dermatological formulation containing Ordered Mesoporous Silica for the administration of active pharmaceutical ingredients.

The publication of the patent "*Eudermic compositions*" (WO 2012007906 A2) in 2012 [1], by Prof. Barbara Onida e Dr Renato Mortera, represents the starting point of the research work described in this chapter. From the birth of this invention, many efforts have been dedicated by Onida's group to the development of innovative dermatological formulations, containing mesoporous silica, able to act as skin surface drug reservoir in topical applications [2]. In the last years, this scientific project has implemented many activities and involved different research groups, creating new fruitful collaborations and new promising horizons. Within my PhD research project, I have taken actively part to the advance of this scientific investigation. The most important activity has been represented by the possibility to develop the "*Proof of Concept*" of this innovative dermatological product, thanks to a 40k€-budget funded by *Compagnia di San Paolo* in collaboration with *Politecnico di Torino*. It has been an important opportunity for the overall progress of the project, assessing outstanding results and opening new research

perspectives for the future. In the next chapter, I chose to report a part of this activity, which involved me in first person, in order to highlight that the Proof of Concept of this research proposal is possible and it is a real prospect. Moreover, this successful outcome inspired me and my team in starting a new research line focused on the application of the technology proposed in the patent to other materials. For this purpose, nanostructured ZnO was selected as test material and the possibility to use it as *drug reservoir platform* in dermatological application was mainly investigated during PhD.

We gratefully acknowledge financial support from *Compagnia di San paolo* and *Politecnico di Torino*, which facilitated the research to be undertaken.

7.1. Introduction

In the dermatology field, the administration of topical antibiotics embodies a crucial issue and there is significant controversy about their use [3]. Generally topical antibiotics represent the first choice in several skin infectious diseases, due to several advantages, such as the high concentration at the specific site, limited systemic absorption and easy application of semisolid formulations (i.e. gels, ointments, creams). Despite of all these benefits, there is an open debate related to the use of topical antibiotics due to its critical drawbacks, such as the need of frequent administrations [4] and the lack of dose accuracy. Firstly, it is commonly known that traditional topical antibiotics require at least 2-3 applications/day in order to ensure the efficacy of the treatment. Unfortunately, this high number of applications often affect the patient adherence to the therapy, hindering the healing process. Generally, patients in treatment with topical antibiotics follow a self-medication regime, where the lack of administrations could frequently occur, due to forgetfulness or voluntary interruption of the treatment caused by the painful applications. Moreover, it has been reported that the administration of topical antibiotic should be restricted to no more than 7-14 days, in order to avoid tissue damage, systemic toxicity, or even contact sensitivity and allergic reactions [5]. Secondly, a more important limitation in the use of topical antibiotic is represented by the occurrence of bacterial resistance in some bacteria strains [6]. As consequence, in the last decade several protocols and guidelines have been produced,

claiming that topical antibiotics should be avoided because they may cause several adverse phenomena, such as hypersensitivity reactions, super-infections and resistant bacteria [7]. As alternative to topical antibiotics, the use of systemic antibiotics could be considered, but it is generally avoided due to systemic side effects and bacterial resistance issues. A preferred substitute therapy is represented by the use of topical antimicrobial agents, such as silver, iodine and honey [4], which are frequently recommended in the international guidelines for wound treatments. Nevertheless, also this alternative approach presents limiting drawbacks in common with the topical antibiotics, such as the scarce number of effective agents, the appearance of local hypersensitivity, difficult to accurately dose and most significant, the need of frequent reapplications.

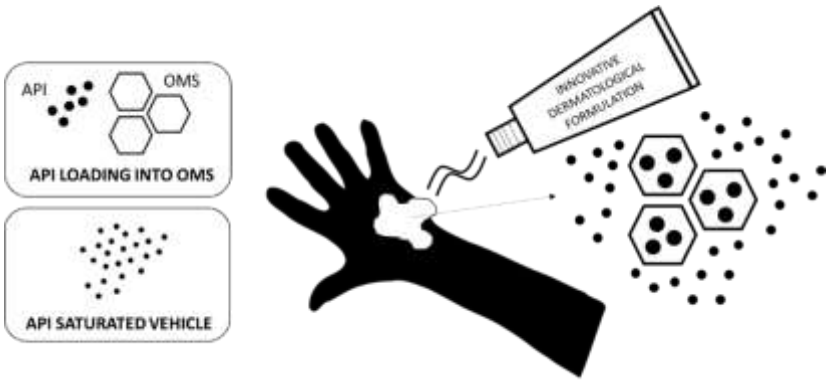

Figure 7.1 Schematic representation of the composition of the innovative dermatological formulation

In this context, the present research work offers a promising solution developing the proof of concept of an innovative eudermic formulation, potentially able to act as skin surface reservoir of an antibiotic molecule. This new technology is based on the use of ordered mesoporous silica (OMS), loaded with an active pharmaceutical ingredient (API), delivered by a saturated solution of the API. The main aim of OMS loaded with the API, is ensuring a reservoir of drug. Briefly, the basic mechanism of this innovative dermatological formulation can be sum up in 3 main steps: 1) after the administration on the skin site, the API dissolved in the saturated solution is released from the vehicle following a traditional release profile, as all the commercial creams; 2) then, the concentration of the dissolved API begins to

decrease; 3) simultaneously, the API incorporated in OMS start dissolving, due to the API lower concentration in the vehicle; in this way, the API released from the OMS-based reserve preserves the saturated concentration inside the vehicle until the OMS is empty. Consequently, the concentration of the API in the site of administration is kept constant for a longer and controlled time.

In order to test the proof of concept of this technology, OMS was adopted as model material due to its wide and proven application as drug delivery systems in these last years [8–11]. OMS has outstanding properties, such as high surface area, high pore volume and significant pore sizes, which make it able to host molecules and to release them efficiently. Exploring the literature, it is evident that many research works have been addressed to investigate OMS as drug delivery system in several administration routes. However, to the best of our knowledge, only few papers have been published about the possibility to use OMS for drug delivery in dermatological application [12–14].

In this study, Amikacin Sulfate (AKS) was selected as model antibiotic drug. AKS is a semisynthetic aminoglycoside [15], with a broad spectrum of activity against the most gram-negative infections. It contains a unique structure able to bind the bacterial 30S ribosomal subunit, causing misreading of mRNA. These leave bacteria unable to synthesize proteins vital to its growth. Since the treatment with parenteral aminoglycosides, to which AKS belongs, could cause potential ototoxicity and nephrotoxicity, the topical use of AKS has always been preferred in the ulcer and wound treatments. Nevertheless, the spreading of news guidelines discouraging the use of topical antibiotics has also limited the use of topical amikacin in the clinical practice.

This research work describes the development of an innovative dermatological formulation, containing OMS for the prolonged release of AKS, which could represent a promising solution to the current limitations in the use of topical antibiotics.

7.2 Material and methods

Ordered Mesoporous Silica of MSU-H type, Amikacin sulfate (AKS) (6-O-(3-amino-3-deoxy-α-D-glucopyranosyl)-4-O-(6-amino-6-deoxy-α-D-lucopyranosyl)-1-N-[(2S)-4-amino-2-hydroxybutanoyl]-2-deoxy-D-streptamine sulfate) (MW = 781.76 g·mol-1) (Ph.Eur 8.2), the derivatizing agent 1-fluoro-2,4-dinitrobenzene (FDNB), , glycerol, acetonitrile CHROMASOLV® gradient grade (≥99.9%) and hydroxyethyl cellulose (Natrosol MR) were purchased from Sigma Aldrich (Italy). A commercial

formulation of AKS (5% by mass) was purchased from a community pharmacy. Bidistilled water has been used throughout this investigation.

7.3 Experimental

7.3.1. Drug loading into OMS

The drug loading was performed by a traditional approach consisting In the Incipient Wetness Impregnation (IWI) procedure, based on the capillary action [16]. Typically, 1 ml of a water saturated solution AKS was added drop by drop to one gram of OMS (0.898 $cm^3 \cdot g^{-1}$) during mechanical agitation. The homogeneous slurry was vacuum dried for 24 hours to 0.1 Pa, in order to obtain a dry powder (AKS-loaded OMS).

7.3.2. Characterization of the AKS-loaded OMS

AKS-loaded OMS were characterized by means of X-Ray diffraction (XRD), Fourier transform infrared spectroscopy (FTIR), thermogravimetry (TG) analysis, differential scanning calorimetry (DSC), nitrogen adsorption isotherms, field emission scanning electron microscopy (FESEM), dynamic light scattering (DLS) and zeta potential. XRD patterns were obtained using a Philips X'Pert Powder (Cu Kα radiation) diffractometer. For FTIR measurements, powders were pressed in self-supporting wafers and spectra were recorded at room temperature with a Bruker Tensor 27 spectrometer operating at 2 cm^{-1} resolution, after outgassing the sample at 100°C for one hour (residual pressure equal to 0.1 Pa). FTIR spectrum of crystalline AKS was recorded on the powder dispersed in potassium bromide (KBr). TG analyses were carried out between 25°C and 800°C in air (flow rate 100 $mL \cdot min^{-1}$ with a heating rate of 10 K·min-1) using a SETARAM 92 instrument to evaluate the quantity of loaded drug. DSC measurements were performed with a DSC1 STARe (Mettler Toledo) System apparatus of TA Instruments equipped with a low temperature probe between 25°C and 800°C under nitrogen flux (flow rate 60 $mL \cdot min^{-1}$ with a heating rate of 10 $K \cdot min^{-1}$). Nitrogen adsorption isotherms were measured using a Quantachrome AUTOSORB instrument after degassing the sample at 100°C for 2 hours. Brauner-Emmet-Teller (BET) specific surface areas (SSA) were calculated in the relative pressure range 0.04-0.1 and the pore size distribution (PSD) was determined through the non-linear density functional theory method (NLDFT). FESEM image were recorded with a FESEM ZEISS MERLIN. DLS and Zeta

Potential analysis were performed with 90 Plus Instrument (Brookhaven) on a suspended water mixture of OMS after homogenization with a high shear homogenizer (Ultraturrax, Ika) for 5 min at maximum velocity.

Derivatization and Analytical method

The analytical method for AKS was taken by [17]. Particularly, AKS derivatized by mixing 100 µl of aqueous solution of the drug with 300 µl of methanol, 40 µl of NaOH (0.05 M) and 50 µl of a methanolic solution of the derivatizing agent (FDNB) (180 mg/ml). The obtained mixture was heated at 90 °C in an air-circulating oven for 10 min, then cooled and injected in HPLC. Each solution was separately derivatized prior to injection. The HPLC apparatus consisted of an isocratic pump (Series 200, Perkin-Elmer instrument, Norwalk, CT, USA) equipped with a µBondapack C18 300 mm × 4.6 mm column (particle size: 10 µm; pore size: 125 Å; endcapped) (Waters, Milford, MA, USA). The mobile phase was a mixture of acetonitrile–water–acetic acid (47:53:0.1 v/v/v) pumped at 1.5 ml/min. A spectrophotometric detector (LC 290, Perkin-Elmer) working at 365 nm was used.

7.3.3. Preparation and characterization of the AKS-OMS reservoir vehicle

In order to obtain a saturated solution of AKS at the therapeutic concentration of commercially available creams (5%), a solution of glycerol and water was selected, investigating different volume ratios between the two solvents, until a drug saturated solution at 5% wt was achieved. The reservoir effect of saturated solution with OMS-API have been evaluated. In the saturated solution of API was then dispersed the API-OMS reservoir, containing an amount of drug equal to that of the free drug in the saturated solution. At regular intervals (1h) small amounts of solution were withdrawn and replaced with the same quantity of pure solvent. The extracted solutions were then diluted and analysed through UV–Vis spectrophotometry to assess the API concentration. The addition of pure solvent causes a dilution of the solution and allow us to evaluate the reservoir effect of incorporated OMS.

7.3.4 Preparation of the topical semisolid dosage form

In order to deliver AKS-loaded OMS to the skin, a suitable semisolid formulation was developed. Among all the possible semisolid preparations, a hydrophilic gel was selected, consisting of a liquid phase within a polymeric

matrix composed by a suitable gelling agent. Firstly, AKS was added in a solution of glycerol and water under magnetic stirring obtaining a saturated solution of the drug (5% wt). When AKS was completely dissolved, OMS-AKS powder was added to the medium, having the same amount of the free drug in the reservoir. Then the liquid dispersion was purposely homogenized with a high shear homogenizer for 5 min at maximum velocity. Hydroxyethyl cellulose was selected as gelling agent, because it is primarily used in topical pharmaceutical formulations and it is generally considered as an essentially non-toxic and non-irritant material [18]. With this purpose, 2% by mass of hydroxyethyl cellulose was added to the homogeneous dispersion and it was gently stirred for one hour at room temperature. In the next paragraphs, the topical gel containing OMS-AKS and free AKS at therapeutic saturated concentration will be indicated as AKS-OMS@GEL.

7.3.5. Characterization of AKS-OMS@GEL

A complete and detailed evaluation of AKS-OMS@GEL properties was assessed comparing it with a commercial gel containing 5% of Amikacin by mass, over a period of 30 days. The AKS-OMS@GEL macroscopic properties were examined by visual inspection of clarity, colour, homogeneity and phase separation. The pH of both gels were measured using a digital pHmeter (GLP 21 of Crison). The measures were replicated three times. Rheological properties were evaluated using a rotational Brookfield viscometer (Rheometer Model LVDV-III+). About 10 ml of the gels were introduced to the cylinder. Readings were taken over a large range of shearing rates (from 0.75 to 1875 s^{-1}) corresponding to 0.1 to 250 rpm. Viscosity and degree of pseudoplasticity (Farrow's constant) were determined.

7.3.6. In-vitro Release studies using vertical diffusion cells

AKS release from different formulations was studied using vertical glass diffusion cells (Franz cell) equipped by a Spectra/Por (12000-14000 Dalton MWCO) hydrophilic cellulose membrane (Spectrum Lab). In particular, AKS-OMS@GEL and the commercial formulation were employed as donor phases. The receiving phase was acetate buffer at pH 5.0. The apparatus was maintained under stirring for 72 h at 33°C, during which at scheduled times the receiving phase was withdrawn and entirely substituted

with fresh receiving phase. Each withdrawn aliquot was analysed using high performance liquid chromatography (HPLC) analysis. Each sample was prepared and analysed in triplicate.

7.3.7. In-vitro permeation studies using vertical diffusion cells

AKS transepidermal permeation from the two different gels was also studied using vertical diffusion cells equipped by porcine ear skin. Skin slices were isolated using an Acculan dermatome (Aesculap) from the outer side of pig ears freshly obtained from a local slaughterhouse and then stored for at least 24 h at -18°C. Prior to each experiment, the excised skin was rinsed with normal saline solution and pre-hydrated by floating it in 0.002% (w/v) sodium azide aqueous solution. The skin was then sandwiched between the two cell compartments with the stratum corneum side upwards. Both AKS-OMS@GEL and the commercial formulation were employed as a donor phase. The receiving phase consisted of acetate buffer at pH 5.0. The apparatus was maintained under stirring for 72 hours at 34°C, during which at scheduled times the receiving phase was withdrawn and entirely substituted with fresh receiving phase. Each withdrawn was analysed using HPLC. Each sample was prepared and analysed in triplicate. Moreover, parallel Franz experiments with AKS-OMS@GEL were performed, stopping the procedure after 6, 24, 48 and 72 hours, in order to analyse the *ex-vivo* skin tissues extracted from the cells through FESEM microscopy. For this purpose, the pig skin was gently washed, deep-freezed with liquid nitrogen, broken in different pieces and analysed with FESEM, after the deposition of a chromium coating by electron sputtering.

7.3.8. Microbiological activity studies

The antibacterial tests were performed by the research group of Prof. Vivian Tullio at the Department of Public Health and Pediatrics of the University of Turin. In order to determine the antibacterial activity of the innovative AKS-OMS@GEL proposed in this research work, different microbiological activity tests were carry on.

Antibacterial susceptibility tests

Firstly, the determination of the MIC and the MIB was carried out through the broth microdilution method, according to the Clinical and Laboratory Standards Institute (CLSI) guidelines [19]. The essay was performed on different bacterial strains: *Escherichia coli*, *Klebsiella pneumoniae* and *Pseudomonas aeruginosa*. Each component of the formulation was singularly evaluated, investigating the antimicrobial activity on the free AKS, on the commercial product and on the glycerol/water vehicle with and without OMS as such.

Microbiological determination of the AKS released from the AKS-OMS@GEL

A second test was performed, evaluating the microbiological activity of the drug amount released over time, during the *in vitro* release studies performed with Franz Cells. The test was carried out comparing the AKS-OMS@GEL with the commercial Amikacin gel. During the *in vitro* release studies, an aliquot of each samples withdrawn from the Franz cell at predetermined times, was used to determine its microbiological activity, using the disk diffusion method. Agar plates (*Brain Heart Agar*) were inoculated with a standardized inoculum of the test microorganism, consisting in 10^8 UFC/ml of *K. pneumoniae*. In order to determine the antibacterial activity, the diameters of inhibition growth zones were measured, after the incubation of each AKS-containing samples at 37 ° C for 24 hours. In order to determine the AKS concentrations, the same experiment was previously performed using known concentration of drug.

Determination of the time-kill curves

The bactericidal effect of AKS-OMS@GEL was investigated using the time-kill test. Aliquots of samples withdrawn at predetermined times during the in vitro release study were incubated (37°C) with the microbial strain, *K. pneumoniae 28024*. The bactericidal effect was determined performing the colony count of different aliquots, removed at predetermined times.

7.4 Results and discussion

7.4.1 Characterization of the AKS-loaded OMS

In order to assess the physicochemical properties of the AKS-loaded OMS, a complete characterization has been done. The wide angle XRD diffraction pattern of the OMS as-such presented the typical (100), (110) and (200) peaks, related to the hexagonal (P6mm) 2D symmetry of the ordered mesopores materials (Figure 7.2.A). The XRD patterns of AKS-OMS showed a complete amorphization of the API (Figure 7.2.B); the lack of crystallization in these materials is a very well reported and crucial phenomenon [20–22]. The pattern of the sample containing AKS after the IWI process, shows the same reflections, confirming that the drug loading does not affect the mesostructure.

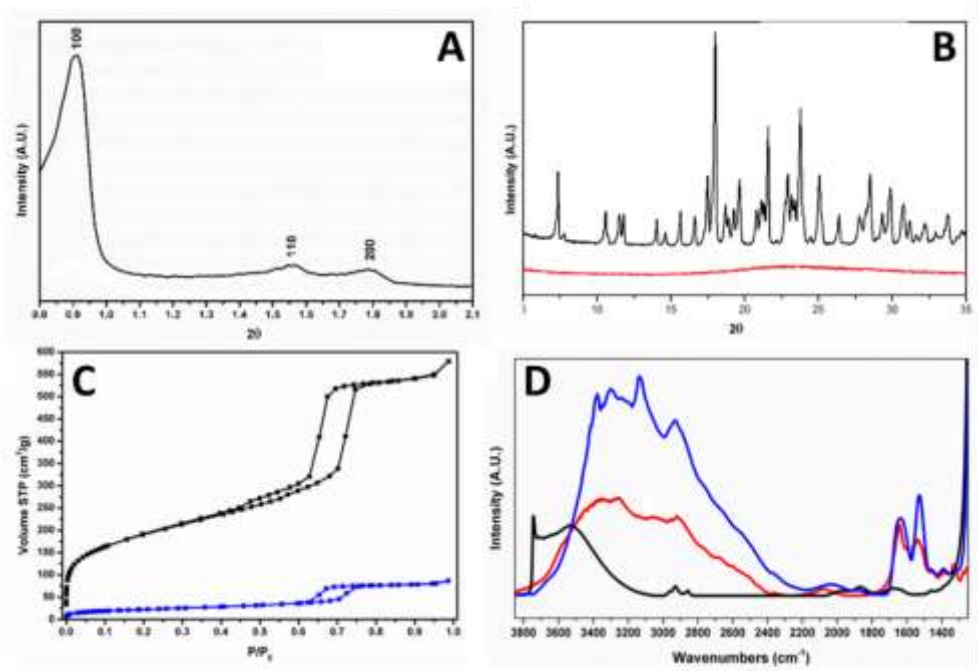

Figure 7.2: Panel A) XRD pattern of OMS as-such. Panel B) XRD spectra of AKS powder (black) and OMS-AKS (red). Panel C) N_2 isotherms of OMS (black) and OMS-AKS (blue) Panel D) FTIR spectra of OMS (black), AKS in KBr (red) and OMS-AKS (blue).

FT-IR spectra (Fig. 7.2.B) reveal that AKS interacts with the silica surface through hydrogen bonds with silanols. In fact, the OMS as such shows two main band: a narrow one due to free silanols at 3742 cm^{-1} and a broader one at

3520 cm^{-1}due to H-bonded silanols. In the spectrum OMS-AKS sample no free silanols are observable (3742 cm^{-1}) suggesting a direct interaction between surface silanols and AKS frequency. The spectrum of AKS in KBr shows a broad envelope in the range 3600-2400 cm^{-1}

. This results from the absorptions due to free and H-bonded -NH_2, -NH and -OH groups. In the same spectrum absorption at about 2900 cm^{-1} are due to -CH stretching mode of the molecule. At lower frequency narrow bands are present at 1640 and 1550 cm^{-1} due to -CONH- groups [15]. As clearly showed in in Fig.7.2B, these AKS characteristic peaks are present also in the AKS-OMS spectrum. The TG analysis was used to evaluate the amount of API loaded into OMS and the result was 47% by mass. This percentage was further confirmed by HPLC analyses carried on the total AKS amount released from the reservoir carrier.

Figure 7.2C shows nitrogen adsorption isotherms of OMS as-such and of AKS-OMS, from which the specific surface area, the specific pore volume and the pore size distribution can be evaluated. Passing from OMS to OMS-AKS, BET specific surface area decreased from 625 m^2/g to 69 m^2/g, while the pore volume decreased from 0.898 cm^3/g to 0,121 cm^3/g. In addition to this, the NLDFT PSD shows a reduction of the volume without any significant change in pore diameter. These evidences, compared to other literature results [20], strongly suggest that AKS molecules are hosted inside the mesopores but not uniformly distributed on the OMS surface.

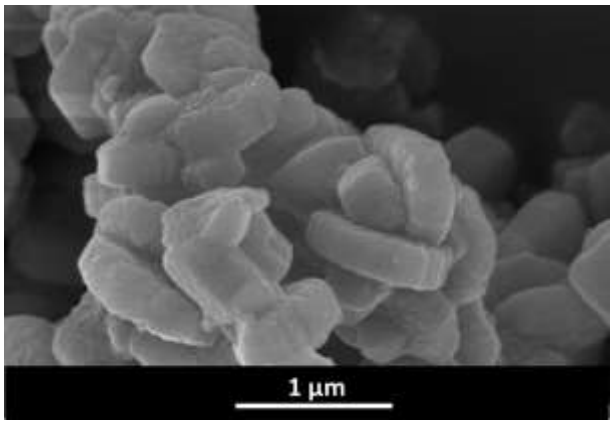

Figure 7.3 FESEM image of OMS aggregates (Mag =100.00 KX)

Figure 7.3 reports the scanning electron microscopy picture of OMS showing aggregates of microns composed by particles of about 500-600 nm. The primary particles resemble short prism of hexagonal base with striping along the height recalling the ordered hexagonal (P6mm) network of mesopores. After IWI, FESEM images exhibit no change in morphologies or API crystals outside the mesopores (data not shown). The DLS measurements of OMS as such agree with the FESEM image, resulting in aggregates of 1300 nm mean value. Indeed, after high shear homogenization (5 min at 30 krpm), OMS particles result completely disaggregates, giving a mean value of 569±16 nm.

7.4.2. Characterization of the AKS-loaded OMS reservoir formulation

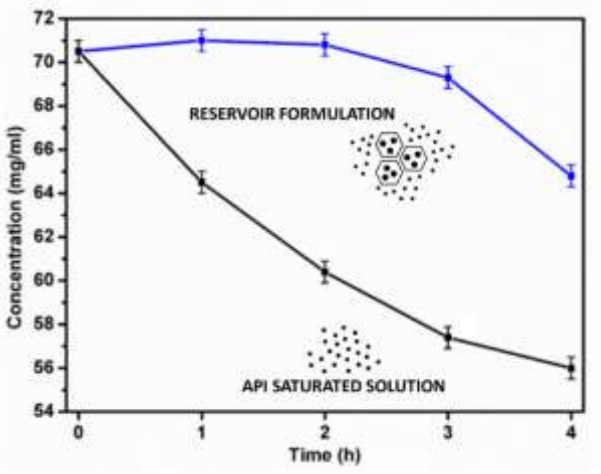

Figure 7.4 AKS sustained release from the reservoir formulation and from the API saturated solution without reservoir

The reservoir effect of the AKS-loaded OMS in a AKS saturated solution was successfully confirmed by a simple *in vitro* release study (Fig.7.4). Generally, amikacin is available on the market as hydrophilic topical gel, at 5% by mass of API, corresponding to 6,67% by mass of AKS. In this research work, a mixture of water and glycerol was investigated, in order to obtain a solvent saturated with AKS at the therapeutic concentration. The solvent composition was 45:55 = water: glycerol (by weight). In order to confirm the reservoir effect of the formulation, the AKS in vitro release profile was determined over

time, withdrawing an aliquot every hour from the combined system and replacing it with the same amount of pure solvent. Figure 7.4 reports the AKS in vitro release profile from the reservoir formulation and from the API saturated solutions. It is evident that the reservoir formulation is able to provide a more sustained and constant release of drug, preserving the saturated concentration as long as there is drug that can be released and solubilized from the OMS.

7.4.3. Characterization of AKS-OMS@GEL

The type of formulation in which a drug delivery system is dispersed represents an important aspect to take into consideration during the development of an effective skin product. For this purpose, a hydrophilic gel was selected as dosage form in order to administer the reservoir system, based on the combination of AKS-loaded OMS and the AKS saturated solution, to the skin. This semisolid formulation was selected considering the hydrophilic profile of the API and its well-established role in delivering drug carriers to the skin [23]. The choice of excipients was driven by the will of using only admitted materials able to assure the physico-chemical stability of the preparation. Table 7.1 reports the qualitative composition of the AKS-OMS@GEL in comparison with that of the marketed gel.

Table 7.1. Comparison between the qualitative composition of the Amikacin commercial gel and the AKS-OMS@GEL (reservoir system)

COMMERCIAL GEL	***AKS-OMS@GEL***
Amikacin 5%	Amikacin 5%
Hydroxyethylcellulose	Hydroxyethylcellulose
Glycerine (E 422);	Glycerine
Water	Water
Methyl parahydroxybenzoate (E 218); Propyl parahydroxybenzoate (E 216);	AKS-loaded OMS (reservoir system)

Hydrophilic gels have been reported as an effective and inert environment for drug carriers, assessing their role in the improvement of the drug delivery to the skin [23,24]. This semisolid dosage form allows a uniform dispersion of the particles in the matrix, a longer contact time of the drug carrier with the skin and a resultant enhanced drug delivery. After the identification of the

qualitative composition, a preparation method was also developed, able to assure an easy incorporation of the reservoir system (AKS-loaded OMS) and based on technologies traditionally used for the preparation of topical pharmaceutical dosage forms. This method is based on the use of a high speed homogenisation (Ultraturrax) to mix the excipients, the active ingredient and the amikacin-silica reserve, followed by a stirring phase to achieve the correct viscosity. The physico-chemical stability of the AKS-OMS@GEL was performed over time (30 days) particularly investigating the pH and the viscosity through rheological measurements. Moreover, a visual evaluation was carried out to highlight any macroscopic alterations in the preparation. As results, the characterization of AKS-OMS@GEL confirmed a physico-chemical profile comparable to the commercially available product. Particularly the results showed that the pH value was stable at 4.7 over time, resulting compatible with the skin [25]. The viscosity of the AKS-OMS@GEL resulted compatible with the administration on the skin, as shown in Figure 7.5. No macroscopic alterations of the preparation was observed. The gel shows rheological characteristic of shear-thinning fluid (data not reported), with the same profile of the commercial products.

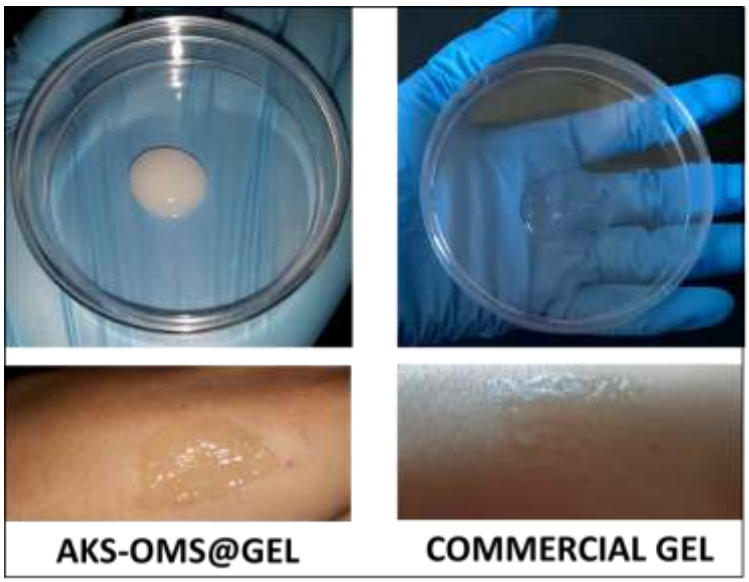

Figure 7.5. Pictures of the innovative formulation (left side) containing the reservoir system (AKS-OMS@GEL) in comparison with the commercial gel (right side). The aspect of the gels, before and after administration to the skin, is illustrated.

7.4.4. In-vitro Release studies using vertical diffusion cells

In order to test the ability of the AKS-OMS in acting as reservoir system on the skin surface, the AKS release profile from the semisolid formulation containing the reserve technology was evaluated. For this purpose, *in vitro* Franz diffusion experiments were selected for its crucial importance in the field (Figure 7.6) [26].

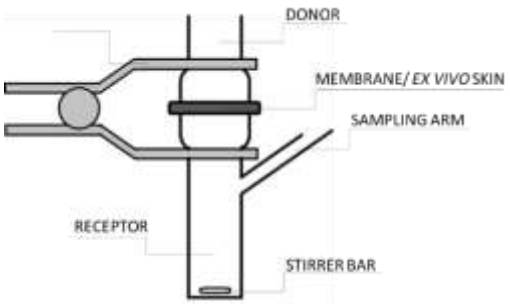

Figure 7.6 Schematic representation of a vertical diffusion cell (Franz Cell)

The Franz cells were equipped with a synthetic membrane to model real skin. Even though artificial membranes are not able to simulate completely a biological system, they are generally preferred to skin tissue, because of their cheaper cost and simpler structure. Moreover, synthetic membranes offer more reproducibility, eliminating many *in vivo* variables such as sex, race, skin age and anatomical site [26]. In these Franz experiments, both the AKS-OMS and the commercial gel were used as donor samples. The receiving compartments was filled with acetate buffer at pH 5.0, under stirring at 33°C, mimicking the skin conditions [27]. At predetermined times, the receiving receptor was sampled and analyzed to know the amount of amikacin released from the formulations. Figure 7.7 reports the AKS release profiles obtained. In the first 100 minutes, AKS-OMS and the commercial formulation presented the same AKS release behaviour. During this first phase, the AKS-OMS released the free drug molecules contained in the saturated vehicle. However, after about 120 minutes, some differences are evident. While the release rate of the marketed gel decreased due to the depletion of API in the formulation, the release rate of AKS-OMS remained constant for a doubled time, demonstrating the efficacy of the proposed reservoir effect. In fact, the AKS delivered by the

OMS particles started replacing the free drug molecules inside the vehicle, playing a key role in assuring a constant administration of drug to the skin. Moreover, it is worth of noting that at the end of the experiment the amount of API released from the AKS-OMS@GEL was double in comparison with the commercial gel, confirming that the AKS-OMS is able to totally release the incorporated drug. The Franz experiments furtherly demonstrated the proof of concept of this technology, as a possible strategy to reduce the number of applications during the day.

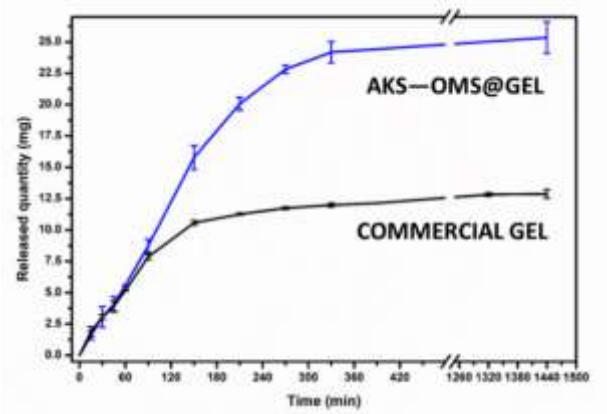

Figure 7.7 Franz experiments for the *in-vitro* determination of AKS release from AKS-OMS@GEL and from the commercial formulation. Each point is the mean value of three different release tests.

7.4.5. *In-vitro* permeation studies using vertical diffusion cells

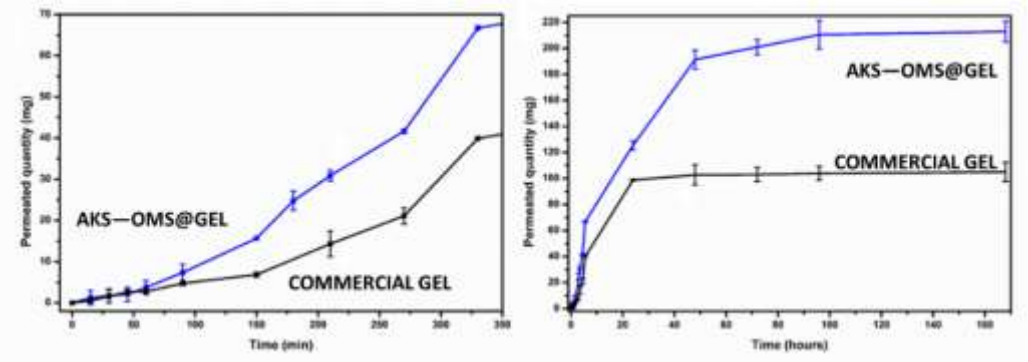

Figure 7.8. Franz experiments for the evaluation of the *in-vitro* permeation of AKS release from AKS-OMS@GEL and from the commercial formulation, using *ex vivo* skin tissues. On the left panel, the AKS permeation profiles during the first 6 hours; on the right panel the overall results over 170 hours. Each point is the mean value of three different release tests.

In order to obtain preliminary information about the behaviour of the reservoir technology through an *ex-vivo* skin site, Franz experiments were carried out using the same previous procedure, but equipping them with pig ear skin. Figure 7.8 reports the resulting AKS release profiles, from the AKS-OMS GEL in comparison with the commercial formulation. On the left panel of the Fig. 7.8 is showed in detailed the API release profiles during the first 6 hours. It is evident that the permeated AKS profiles during the first 100 minutes from both the formulations, confirm the trend of the *in vitro* release studies and the two formulations behaved in a similar way. Nevertheless, after the first 100 minutes significant differences arose and the AKS permeated amount from the reserve formulation exceeded that from the commercial gel. This was caused by the depletion of API in the semisolid matrix of the commercial gel, in which the concentration gradient decreases gradually overtime. On the contrary, in the AKS-OMS gel matrix the API concentration gradient is kept constant due to the release of the drug from the OMS, which replaces the drug depleted in the saturated vehicle. Despite of the commercial formulation completed its

drug release in 24 hours, the experiment furtherly demonstrated the ability of the AKS-OMS@GEL of keep releasing the API for at least a doubled time, around 48 hours (Panel left, Figure 7.8). These results showed that assuring a constant concentration on the skin site for a prolonged time could be a promising strategy to extend and enhance the permeation of API. Two different interpretations might be drawn from these outstanding results. On one hand, the enhancement of the AKS permeation profile could endow to an overdose during the treatment, causing some toxicity issues, as described in the introduction of this chapter. On the other hand, the constant amount of API supplied thanks to the reservoir system of the proposed technology, could lead to a decrease of the starting therapeutic amount of API, play a key role in the reduction of those skin irritating phenomena and, most important aspect among all, to the limitation of bacterial resistance insurgence.

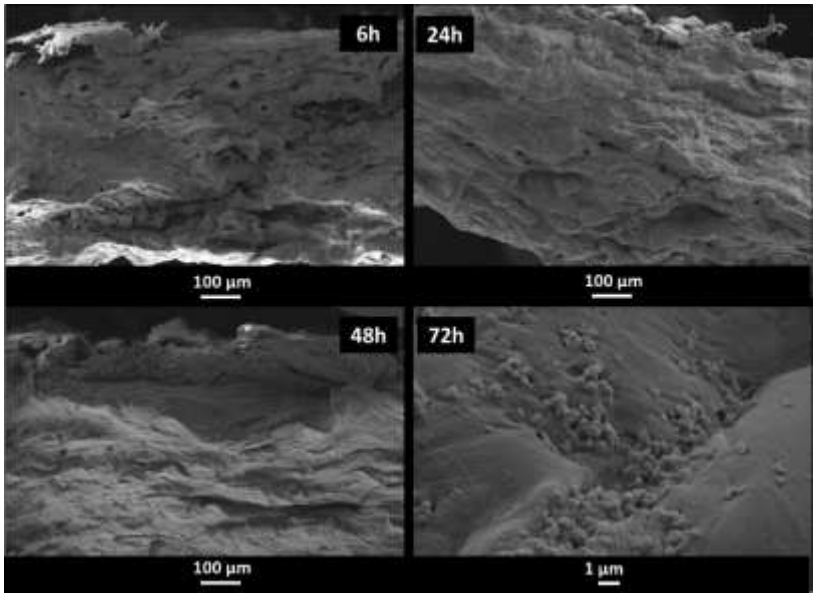

Figure 7.9 FESEM images of the *ex vivo* skin after the in-vitro permeation test through Franz experiments, after 6, 24, 48 and 72h.

Figure 7.9 reports the results obtained monitoring the *ex vivo* skin tissues during the Franz permeation experiments at different time intervals. The aim of this study was to perform a preliminary investigation of the interaction between the innovative reservoir gel and the skin. In particular, the behaviour of the contained OMS was tracked. For this purpose, four Franz cells were

equipped with *ex vivo* ear pig skin and filled with AKS-OMS@GEL as donor samples. After 6, 24, 48 and 72 hours the permeation experiment was interrupted in one Franz cell per time, extracting the ex vivo skin for the FESEM analysis. In literature, several research works have been dedicated to the evaluation of the possible permeation of OMS through the skin site of application [27–29]. After a careful study, to the best of our knowledge, none of these papers reports a direct permeation of particles greater than 10 nm. On the contrary, as already described in this chapter, it is well known the possibility for these particles to enter skin pores and hair follicles, enhancing the drug release [27]. The FESEM results confirmed the literature conclusions, evidencing the present of the OMS particles on the skin surface. It is evident that from 6 to 48 hours, the OMS particles are organized in aggregated platforms on the skin, acting as surface drug reservoir. Probably, some of these aggregates might be formed during the samples preparation for the FESEM analysis. However, after 72 hours, the image shows a higher OMS dispersion on the skin surface, confirming the supporting role of the gel in the dispersion of carrier to the skin surface. However, skin penetration the OMS particles can be excluded. In fact, it is well-established in the literature and also reported in the EU regulation on nanomaterials that no skin penetration has been demonstrated for particles with larger size that 10 μm [30,31]. In conclusion, no risk of toxicity from the use of this innovative drug reservoir formulation is present, also considering that amorphous silica is listed in the inactive ingredient guide of the FDA as a safe excipient for topical drug products and is compatible with a broad range of APIs [32].

7.4.6. Microbiological activity studies

In order to determine the antibacterial activity of the innovative AKS-OMS@GEL proposed in this research work, different microbiological activity tests were carried out.

Antibacterial susceptibility tests

The antibacterial susceptibility test was performed on different bacterial strains: *Escherichia coli*, *Klebsiella pneumoniae* and *Pseudomonas aeruginosa*. The essay confirmed that all the tested strains are susceptible to amikacin, according to the limits established by CLSI. Moreover, each component of the formulation was singularly evaluated, investigating the antimicrobial activity of the commercial product and of the glycerol/water vehicle with and without OMS as-such. The results showed that the vehicles

of the two formulations do not have any self-antibacterial activity and that they do not affect the activity of the drug.

Microbiological determination of the AKS released from the AKS-OMS@GEL

This test was carried out comparing the AKS-OMS@GEL with the commercial Amikacin gel. During the *in vitro* release studies, an aliquot of each samples withdrawn from the Franz cell at predetermined times, was used to determine its microbiological activity, using the disk diffusion method. Table 7.2 reports the diameters of inhibition growth zones measured after the incubation of each AKS-containing samples at 37 ° C for 24 hours. Pictures of the experiments are reported in Figure 7.10.

Table 7.2. Inhibition zone diameters

	Commercial gel		***AKS-OMS@GEL***	
Time (h)	Diameter of inhibition growth zone (mm)	Concentration (µg/ml)	Diameter of inhibition growth zone (mm)	Concentration (µg/ml)
1	21	177.36	22	246.13
2	21	177.36	22	246.13
3	18	72.85	20	137.78
4	16	40.25	18	77.13
5	13	16.53	15	32.30
6	14	22.24	12	13.53
24	7	2.79	13	18.08
48	7	2.79	16	43.17

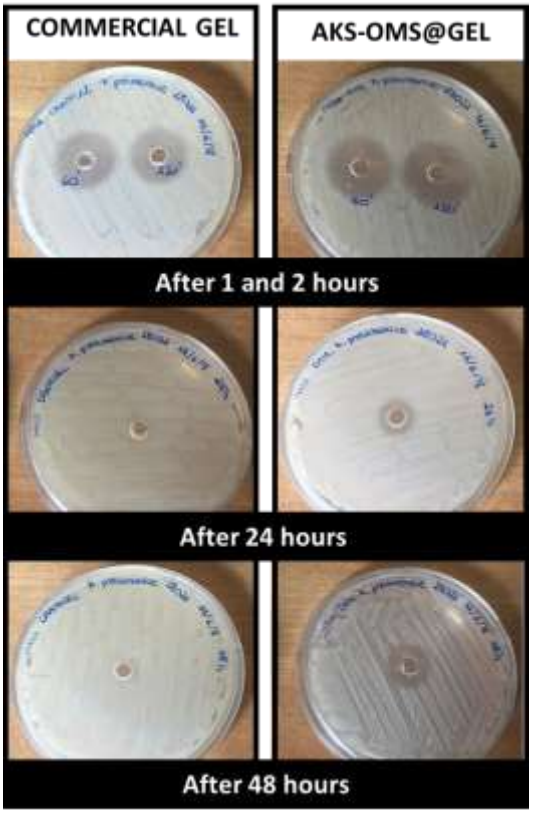

Figure 7.10 Disk-diffusion method of the AKS-OMS@GEL in comparison with the amikacin-based commercial gel with using *K. Pneumoniae* as test microorganism.

From the evaluation of the results, it is evident that the two gel formulations possess a similar bacterial inhibition activity in the first hours of administration. In fact, the diameters of the inhibition growth zone are very similar in both cases. Nevertheless, after 24 and 48 hours AKS-OMS@GEL is still able in inhibiting the bacterial growth in comparison with the commercial gel, not more surrounded from any inhibited zone.

Determination of the time-kill curves

The bactericidal effect of AKS-OMS@GEL and of the amikacin-based commercial gel was investigated using the time-kill test. Aliquots of samples withdrawn at predetermined times during the *in vitro* release study were incubated (37°C) with the microbial strain, *K. pneumoniae 28024*. Figure 7.11 reports the results obtained performing the colony count of different aliquots, removed at predetermined times.

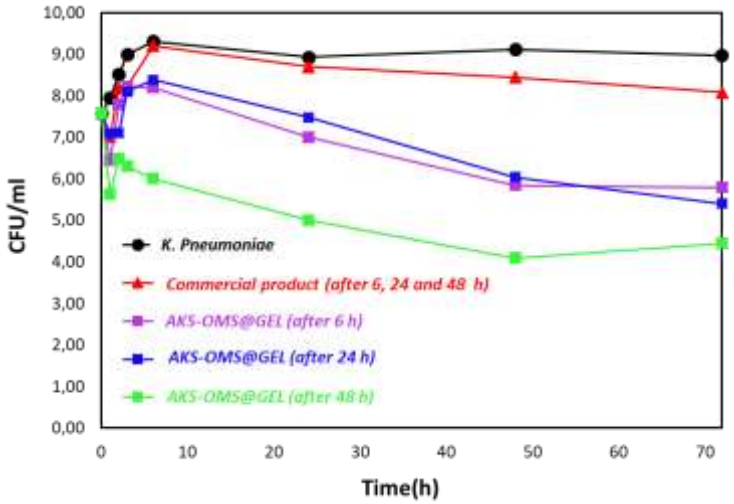

Figure 7.11 Time-kill plot of Amikacin released from AKS-OMS@GEL and from the commercial gel after different time. The test microorganism was *K. Pneumoniae*.

It is evident that the amikacin amounts released from the AKS-OMS@GEL at 6, 24 and 48 hours from the *in vitro* application were significantly more effective in contrasting the bacterial growth than the commercial formulation. On the other hand, blue is the trend of bacterial growth without antibiotic interference. In fact, at the end of the test the microbial population decreases by about one logarithmic unit with the commercial gel, while the reduction induced by the formulation containing the reservoir system was about 4.5 logarithmic units. This essay successfully confirmed the efficacy of the innovative dermatological formulation, demonstrating its reservoir function also from an antibacterial activity point of view.

7.5 Conclusions

The proof of concept of an innovative dermatological formulation containing ordered mesoporous silica was successfully demonstrated. The possibility to obtain a drug reservoir system, combining API-loaded OMS with a saturated solution of the same API was investigated obtaining outstanding results from both a physical-chemical and biological points of views. The innovative formulation demonstrated a drug sustained release for twice the

time of the commercial gel, opening the possibility to reduce the daily number of administrations during a real treatment. Moreover, the new reservoir technology, maintaining a constant concentration of the API for a longer period, might be able to enhance the antibacterial activity in a shorter time reducing the insurgence of bacterial resistance.

7.6. References

(1) Onida, B.; Mortera, R. Eudermic Compositions. WO2012-007906 A2, 2012.
(2) Gignone, A. Ordered Mesoporous Silica for Drug Delivery in Topical Applications. PhD Thesis, 2016.
(3) Drucker, C. R. Update on Topical Antibiotics in Dermatology. *Dermatol. Ther.* **2012**, *25* (1), 6–11.
(4) Lipsky, B. A.; Hoey, C. Topical Antimicrobial Therapy for Treating Chronic Wounds. *Clin. Infect. Dis.* **2009**, *49* (10), 1541–1549.
(5) Carla Wells, Lynn Power. Skin and Wound Care Manual Newfoundland Labrador Skin and Wound Care Manual. **2008**, 1–3.
(6) Bowler, P. G.; Duerden, B. I.; Armstrong, D. G. Wound Microbiology and Associated Approaches to Wound Management. *Clin. Microbiol. Rev.* **2001**, *14* (2), 244–269.
(7) European Wound Management Association. Position Document: Management of Wound Infection. London:MEP Ltd 2006, pp 1–19.
(8) Vallet-Regí, M.; Balas, F.; Arcos, D. Mesoporous Materials for Drug Delivery. *Angew. Chemie Int. Ed.* **2007**, *46* (40), 7548–7558.
(9) Manzano, M.; Colilla, M.; Vallet-Regí, M. Drug Delivery from Ordered Mesoporous Matrices. *Expert Opin. Drug Deliv.* **2009**, *6* (12), 1383–1400.
(10) Vallet-Regí, M. Ordered Mesoporous Materials in the Context of Drug Delivery Systems and Bone Tissue Engineering. *Chem. - A Eur. J.* **2006**, *12* (23), 5934–5943.
(11) Slowing, I.; Viveroescoto, J.; Wu, C.; Lin, V. Mesoporous Silica Nanoparticles as Controlled Release Drug Delivery and Gene Transfection Carriers☆. *Adv. Drug Deliv. Rev.* **2008**, *60* (11), 1278–1288.
(12) Pilloni, M.; Ennas, G.; Casu, M.; Fadda, A. M.; Frongia, F.; Marongiu, F.; Sanna, R.; Scano, A.; Valenti, D.; Sinico, C. Drug Silica Nanocomposite: Preparation, Characterization and Skin Permeation Studies. *Pharm. Dev. Technol.* **2013**, *18* (3), 626–633.
(13) Gastaldi, L.; Ugazio, E.; Sapino, S.; Iliade, P.; Miletto, I.; Berlier, G. Mesoporous Silica as a Carrier for Topical Application: The Trolox

Case Study. *Phys. Chem. Chem. Phys.* **2012**, *14* (32), 11318.

(14) Berlier, G.; Gastaldi, L.; Ugazio, E.; Miletto, I.; Iliade, P.; Sapino, S. Stabilization of Quercetin Flavonoid in MCM-41 Mesoporous Silica: Positive Effect of Surface Functionalization. *J. Colloid Interface Sci.* **2013**, *393* (1), 109–118.

(15) Monteleone, P. M.; Muhammad, N.; Brown, R. D.; McGrory, J. P.; Hanna, S. A. Amikacin Sulfate. In *Analytical Profiles of Drug Substances*; Florey, K., Ed.; Academic Press, 1983; Vol. 12, pp 37–71.

(16) Haber, J.; Block, J. H.; Delmon, B. Manual of Methods and Procedures for Catalyst Characterization (Technical Report). *Pure Appl. Chem.* **1995**, *67* (8–9), 1257–1306.

(17) Nicoli, S.; Santi, P. Assay of Amikacin in the Skin by High-Performance Liquid Chromatography. *J. Pharm. Biomed. Anal.* **2006**, *41* (3), 994–997.

(18) Rowe, R. C.; Sheskey, P. J.; Quinn, M. E.; Association, A. P. *Handbook of Pharmaceutical Excipients*, 6th ed. /.; London ; Chicago : Washington, DC : Pharmaceutical Press ; American Pharmacists Association, 2009: London, 2012.

(19) Weinstein, M. P.; Zimmer, B. L.; Cockerill, F. R.; Wiker, M. A.; Alder, J.; Dudley, M. N.; Eliopoulos, G. M.; Ferraro, M. J.; Hardy, D. J.; Hecht, D. W.; Hindler, J. A.; Patel, J. B.; Powell, M.; Swenson, J. M.; Thomson, R. B.; Traczewski, M. M.; Turnidge, J. D. *Methods for Dilution Antimicrobial Susceptibility Tests for Bacteria That Grow Aerobically ; Approved Standard — Ninth Edition*; 2012; Vol. 32.

(20) Gignone, A.; Piane, M. D.; Corno, M.; Ugliengo, P.; Onida, B. Simulation and Experiment Reveal a Complex Scenario for the Adsorption of an Antifungal Drug in Ordered Mesoporous Silica. *J. Phys. Chem. C* **2015**, *119*, 13068−13079.

(21) Mellaerts, R.; Aerts, C. A.; Van Humbeeck, J.; Augustijns, P.; Van den Mooter, G.; Martens, J. A. Enhanced Release of Itraconazole from Ordered Mesoporous SBA-15 Silica Materials. *Chem. Commun.* **2007**, *d* (13), 1375–1377.

(22) Qian, K. K.; Bogner, R. H. Application of Mesoporous Silicon Dioxide and Silicate in Oral Amorphous Drug Delivery Systems. *J. Pharm. Sci.* **2012**, *101* (2), 444–463.

(23) Liang, X. W.; Xu, Z. P.; Grice, J.; Zvyagin, A.; Roberts, M.; Liu, X. Penetration of Nanoparticles into Human Skin. *Curret Pharm. Des.* **2013**, *19*, 6353–6366.

(24) Batheja, P.; Sheihet, L.; Kohn, J.; Singer, A. J.; Michniak-Kohna, B. Topical Drug Delivery by a Polymeric Nanosphere Gel: Formulation Optimization and in Vitro and in Vivo Skin Distribution Studies. *J. Control. Release* **2011**, *149* (2), 159–167.

(25) Lambers, H.; Piessens, S.; Bloem, A.; Pronk, H.; Finkel, P. Natural Skin Surface pH Is on Average below 5, Which Is Beneficial for Its Resident Flora. *Int. J. Cosmet. Sci.* **2006**, *28* (5), 359–370.

(26) Ng, S.-F.; Rouse, J. J.; Sanderson, F. D.; Meidan, V.; Eccleston, G. M. Validation of a Static Franz Diffusion Cell System for In Vitro Permeation Studies. *AAPS PharmSciTech* **2010**, *11* (3), 1432–1441.

(27) Prow, T. W.; Grice, J. E.; Lin, L. L.; Faye, R.; Butler, M.; Becker, W.; Wurm, E. M. T.; Yoong, C.; Robertson, T. A.; Soyer, H. P.; Roberts, M. S. Nanoparticles and Microparticles for Skin Drug Delivery. *Adv. Drug Deliv. Rev.* **2011**, *63* (6), 470–491.

(28) Campbell, C. S. J.; Contreras-Rojas, R.; Delgado-Charro, M. B.; Guy, R. H. Objective Assessment of Nanoparticle Disposition in Mammalian Skin after Topical Exposure. *J. Control. Release* **2012**, *162* (1), 201–207.

(29) Watkinson, A. C.; Bunge, A. L.; Hadgraft, J.; Lane, M. E. Nanoparticles Do Not Penetrate Human Skin - A Theoretical Perspective. *Pharm. Res.* **2013**, *30* (8), 1943–1946.

(30) SCCS, S. C. on C. S. Guidance on the Safety Assessment of Nanomaterials in Cosmetics. *Eur. Comm.* **2012**, No. March, 0–136.

(31) Roberts, M. S.; Mohammed, Y.; Pastore, M. N.; Namjoshi, S.; Yousef, S.; Alinaghi, A.; Haridass, I. N.; Abd, E.; Leite-Silva, V. R.; Benson, H. A. E.; Grice, J. E. Topical and Cutaneous Delivery Using Nanosystems. *J. Control. Release* **2017**, *247*, 86–105.

(32) Fireman, S.; Toledano, O.; Neimann, K.; Loboda, N.; Dayan, N. A Look at Emerging Delivery Systems for Topical Drug Products. *Dermatol. Ther.* **2011**, *24* (5), 477–488.